NASA Contractor Report 4068

Preliminary Design, Analysis, and Costing of a Dynamic Scale Model of the NASA Space Station

M. J. Gronet, E. D. Pinson, H. L. Voqui,
E. F. Crawley, and M. R. Everman

CONTRACT NAS1-18229
JULY 1987

NASA

NASA Contractor Report 4068

Preliminary Design, Analysis, and Costing of a Dynamic Scale Model of the NASA Space Station

M. J. Gronet, E. D. Pinson, and H. L. Voqui
Lockheed Missiles & Space Company, Inc.
Sunnyvale, California

E. F. Crawley
Massachusetts Institute of Technology
Cambridge, Massachusetts

M. R. Everman
AEC-ABLE Engineering Company, Inc.
Goleta, California

Prepared for
Langley Research Center
under Contract NAS1-18229

National Aeronautics
and Space Administration

**Scientific and Technical
Information Office**

1987

TABLE OF CONTENTS

ACKNOWLEDGEMENTS

The authors wish to acknowledge the valuable contributions of Domenic Sicoli of LMSC (study manager) and Max Benton of AEC-ABLE in the design, manufacturing, and costing exercises. In addition, the authors wish to thank Paul McGowan, Robert Letchworth, and Jerrold Housner of NASA/LaRC for their assistance. The support of Dan Durante and Charles Shih in the preparation of this report is sincerely appreciated.

LIST OF SYMBOLS

A	Area
β	Angle or cable strain
C_d	Drag Coefficient
D	Characteristic length
d	Deadband gap distance
δ	Deflection
E	Young's modulus
e	Coefficient of restitution
ϵ	Strain
F	Force
f	Frequency (Hz)
F_b	Bifilar pendulum mode frequency
F_n	Normal force
F_x	Force or pendular frequency
g	Damping loss factor or gravitational constant
I	Mass moment of inertia
K,k	Stiffness
L,l	Length
λ	Scale factor
M,m	Mass or mass per unit length
M_a	Mach number
MAC	Modal assurance criterion matrix or value
μ	Coefficient of friction
ν	Kinematic viscosity
P_g	Gravity preload
P_{cr}	Critical buckling load
r	Radius
R_e	Reynolds number
ρ	Density
σ	Stress
T	Tensile load
t	Thickness
U	Strain energy
u	Deflection
Ω,ω	Circular frequency
x	Deflection
XO	Cross-orthogonality matrix or value
ζ	Critical damping ratio

Subscripts

j	Joint quanity
M	Macro-slip quantity
p	Preloaded quantity
t	Tube or strut quantity

1.0 INTRODUCTION

Aerospace structural dynamicists have traditionally relied upon ground testing as a basis for correcting analyses. Hands-on experience with flight hardware has proven invaluable in gaining a better understanding of complex dynamic phenomena and in developing confidence in analytical models. The difficulty of testing the next generation of large flexible space structures on the ground places an emphasis on other means of validating the predicted on-orbit dynamic behavior. Often, the large size of proposed space structures, such as the NASA Space Station, prohibits testing the full-size spacecraft. In many cases, the static preloads and deflections caused by gravity are greater than those expected on orbit.

Scale model technology represents one way of verifying analytical predictions obtained through math modeling with ground test data. Scale models can be used to investigate the dynamic behavior of a particular design at a fraction of the cost of testing the fully assembled, full-scale article. In the past, dynamic models of various scales have been employed in the Titan III, Apollo/Saturn V, and Space Shuttle programs [1,2]. Scale model testing has also been used to investigate the behavior of highly nonlinear systems [3]. Suspension systems and the effects of gravity on scale model testing have been studied in detail [4-7].

In addition to its primary function of verifying math models, a Space Station scale model could also be used to: reveal potential design problems which influence the design, assess the impact of changes and/or growth in the configuration on overall dynamic performance, evaluate the location and servicing of payloads, and aid in the investigation of flight anomalies [2,4]. The Space Station scale model could serve as a testbed for on-orbit construction, assembly and evaluation; for flight instrumentation of the Space Station, and for associated ground and space-based dynamics and control experiments.

This report documents the preliminary design, scaling, and cost trades for a Space Station Scale Model. The work presented here was supported by

the NASA/Langley Research Center under contract number NAS1-18229.

1.1 SCOPE OF STUDY

The purpose of this study is to investigate the preliminary design, scaling and cost trades for a dynamic scale model of the NASA Space Station. The work conducted during the study involved the following principal tasks:

- Select and construct math models of a baseline Space Station configuration for the study

- Conduct replica scaling analyses for the Space Station model. Assess the effects of scale (e.g., manufacturing tolerances) and the ground test environment (e.g., gravity and air) on the fidelity of the dynamic behavior of the replica scale model.

- Examine the issue of replication vs. simulation for the scale model.

- Investigate the ability of the scale model to simulate free-free dynamic behavior while suspended by cables in the proposed NASA/LaRC Large Spacecraft Laboratory (LSL).

- Investigate the design and manufacturing of scale model components, including an articulation capability for the rotary joints.

- Provide a cost estimate for fabricating the components of a Space Station scale model.

- Recommend a model scale factor and suggest further studies.

The main thrust of this task is to assess the impact of the choice of scale factor on the cost of manufacturing the scale model and on the feasibility of obtaining accurate, relevant, test data. Regarding the latter, the extrapolation from ground test data to flight vehicle dynamic behavior requires the knowledge of three processes. The first is the prediction of full-scale component behavior from subscale component

behavior, or scaling. The second is the prediction of dynamic behavior in zero-g from data taken in 1-g. The third is the prediction of the behavior of the assembled vehicle based on the behavior of its components. This study concentrates on the issues associated with the first two extrapolations and indirectly addresses the third. Scaling laws are applied to the current Space Station configuration to ascertain their implications on the way the model is manufactured, suspended, and prepared for testing. Key issues addressed are scaling laws, replication vs. simulation of components, manufacturing, joint behavior, suspension interactions, damping, articulation capability, and cost. These issues are the subject of parametric trades versus the model scale factor. The results of these detailed analyses are used to recommend scale factors for four different scale model options, each with varying degrees of replication.

This report is divided into five major sections. Chapter 1 describes the configurations selected for the study and the proposed LSL test facility. Chapter 2 introduces the fundamental replica scaling laws and derives theoretical scaling relationships for joint stiffness and damping behavior. The relative practical importance of the effects of scale and the ground test environment are analyzed. Chapter 3 documents the dynamic analyses including the finite element modeling and the suspension system analyses. Chapter 4 details the preliminary design, fabrication, and costing of the scale model components on an individual basis. Finally, Chapter 5 presents a system-level summary of the results of the trade studies in the previous sections. These are combined to form a rationale for the selection of the model scale factor. Potential problems in constructing and testing the scale model are identified, and recommendations for further study are outlined.

1.2 SELECTION OF STUDY CONFIGURATIONS

The initiation of this study coincided with the release of the latest DR-02 document by the Space Station Work Package 2 Phase B prime contractors to NASA. The MDAC Team DR-02 document dated June 5, 1986 contains a detailed database of the Hybrid Power, Dual Keel configuration at that time, including mass properties, payload locations and attachments, and build-up

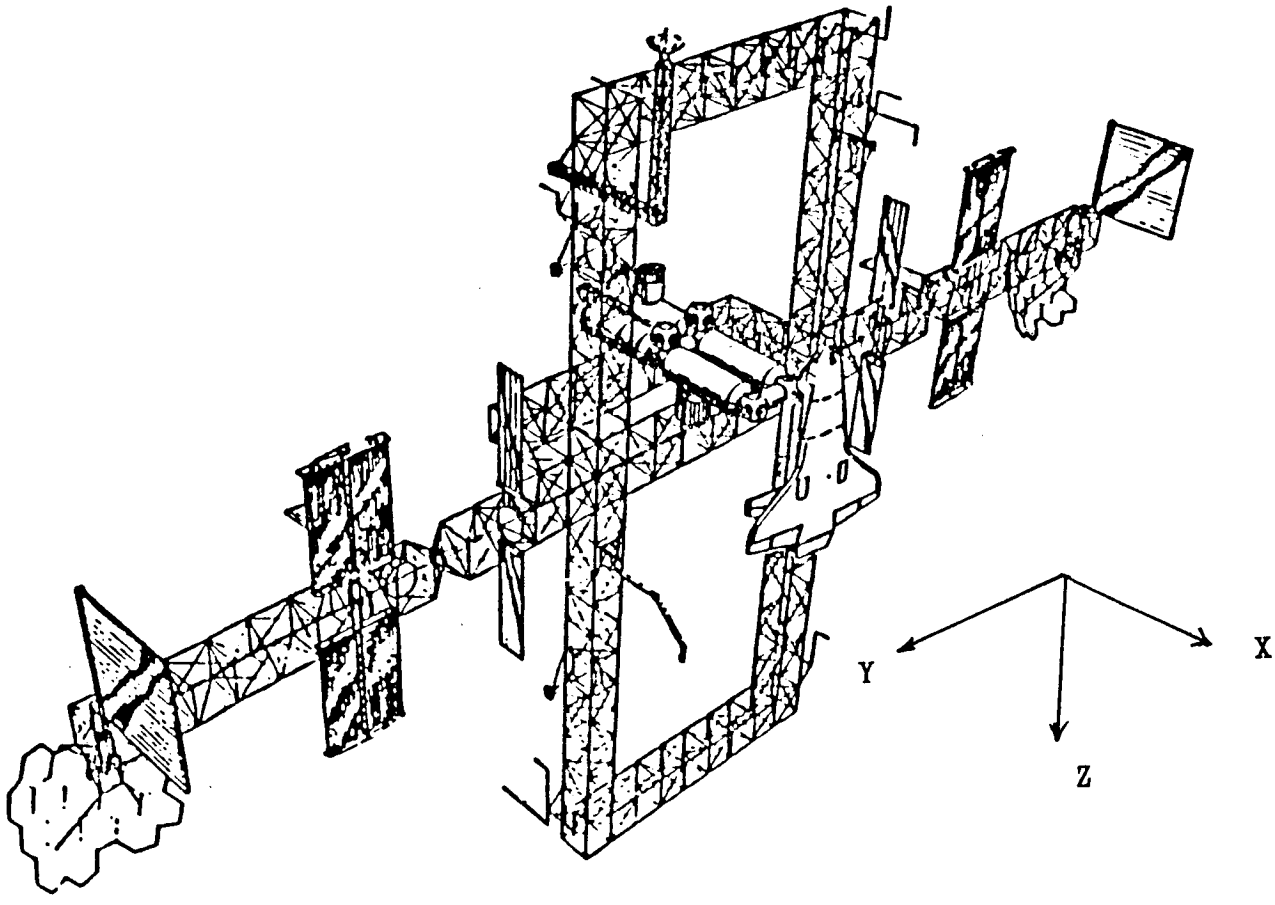

FIGURE 1.2-1: ISS CONFIGURATION

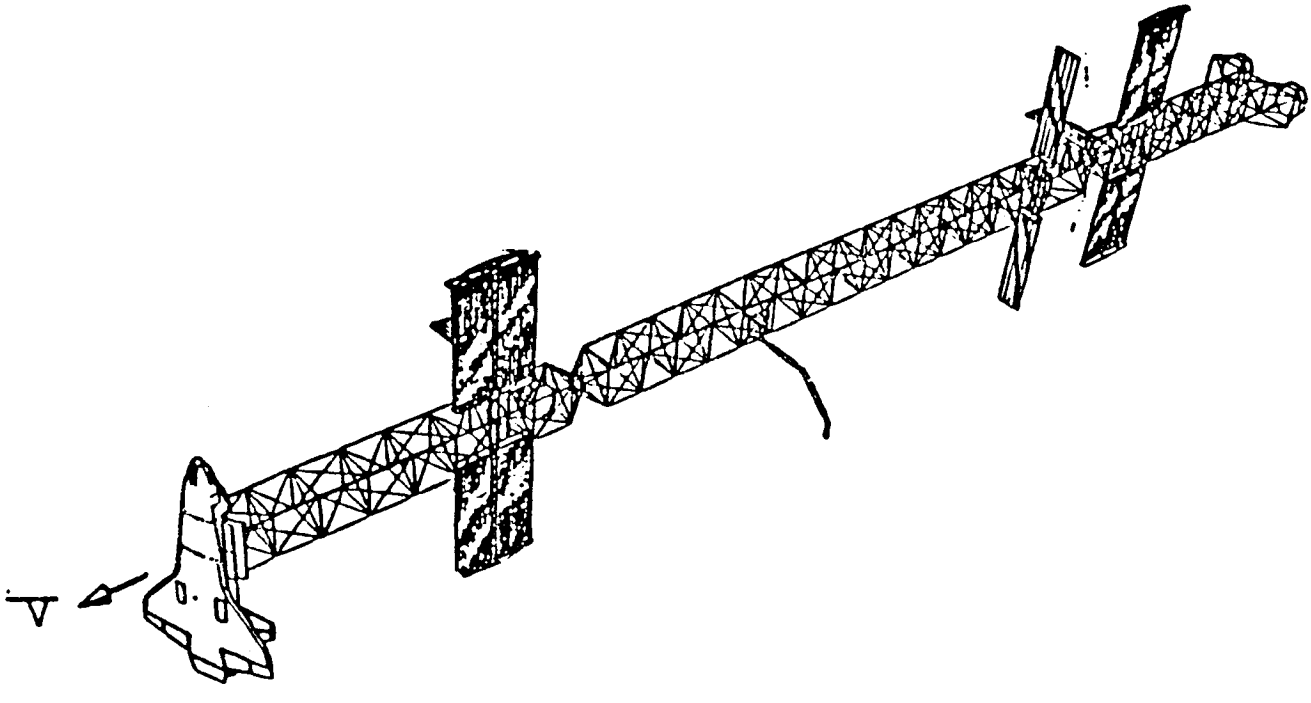

FIGURE 1.2-2: STEP-2 BUILD-UP STAGE CONFIGURATION

(construction) stages. This document served as the basic source of consistent baseline design data for the study. Figure 1.2-1 illustrates the fully operational International Space Station (ISS) configuration along with the Space Station reference coordinates (the configuration sketches in this section are excerpted from the MDAC DR-02). The Space Station is erected in a series of build-up stages defined to a large extent by Orbiter payload bay mass and volume constraints. It is expected that the Space Station scale model ground test program will follow the same build-up sequence in order to permit the correlation of subscale ground test data with full-scale flight data. However, the scaling issues associated with the build-up stages may be different from the fully operational ISS configuration (for example, the build-up stages are characterized by a much smaller fraction of non-structural weight than the ISS with its modules and payloads). Therefore, it was decided to include one of the build-up stages in the parametric scaling analyses in this study.

The step-1 build-up configuration is quite different from the fully-mated ISS, but was considered too simplistic for this study. Tests of various trusses which have been performed in the past have provided information similar to that which would be obtained from a test of this configuration. Beginning with the fourth STS flight, most of the elements of the completed ISS have been incorporated into the station. The structure which remains in orbit after the second STS flight is basically limited to the completed transverse boom, whereas the third flight adds a significant amount of truss structure. From these candidates, the step-2 build-up stage was chosen for study because it represents the greatest departure from the ISS configuration in terms of geometry and mass properties (Figure 1.2-2). In addition, many large space structures are expected to utilize booms composed of such a truss structure. Thus, the results from tests of the step-2 build-up stage may find fairly general applicability in the aerospace community. An additional benefit derived from the analysis of this particular build-up stage was not realized until late in the contract term, when revised plans were made available by the Space Station program office. These plans indicate that the habitation modules are being added to the truss early in the build-up sequence in order to achieve an operational station at an earlier date. This version of the station is similar to the

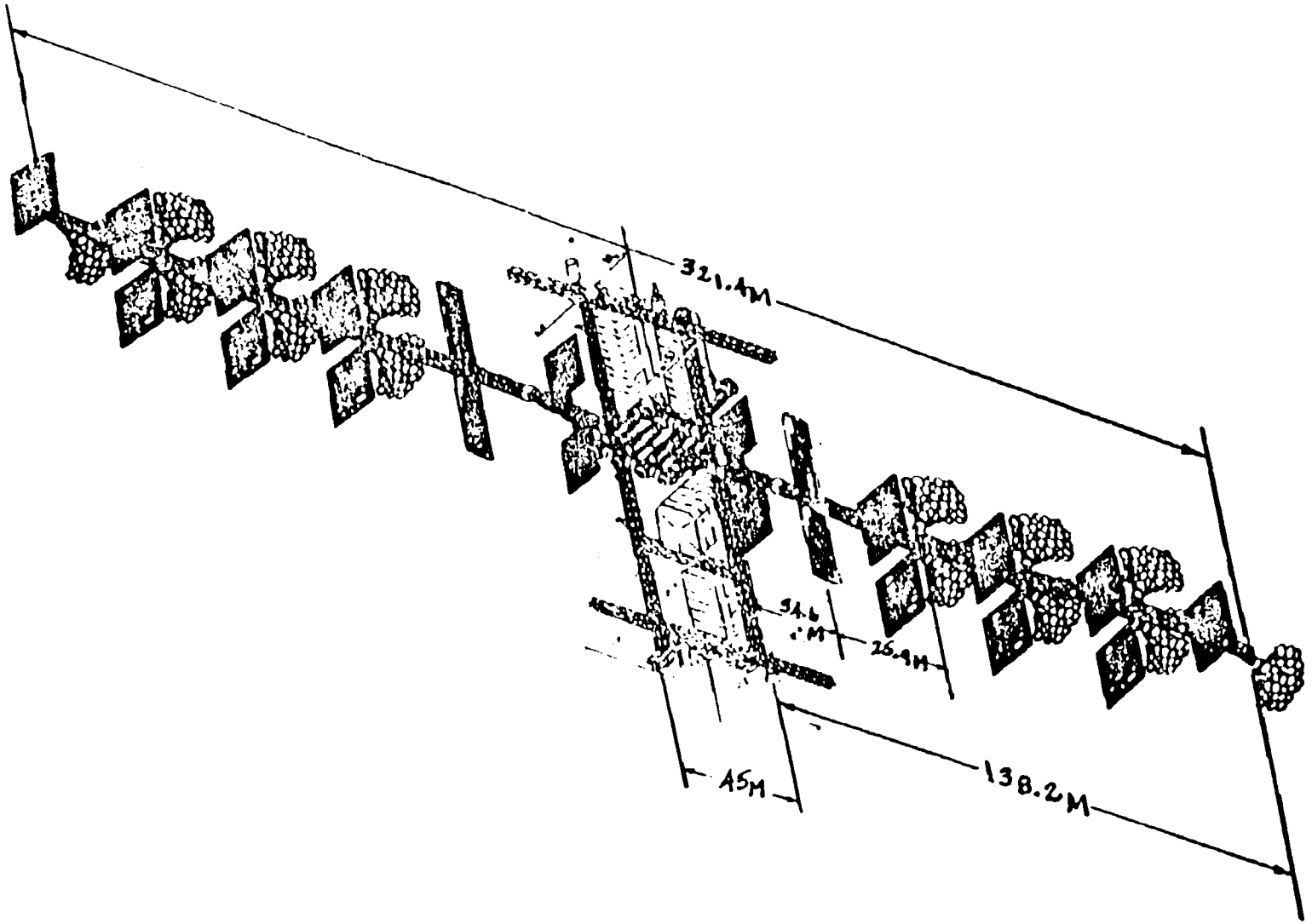

FIGURE 1.2-3: SPACE STATION HYBRID POWER GROWTH CONFIGURATION

Step-2 build-up stage with the modules added.

Figure (1.2-3) depicts the Growth version of the Space Station as of June 5, 1986. Twelve solar concentrator power generation systems are added across the transverse boom along with additional trusses for payload support. The growth configuration is discussed in the next section in terms of scale factor constraints imposed by the size of the proposed LSL test facility.

1.3 TEST FACILITY

The task statement baselines the proposed Large Spacecraft Laboratory (LSL) as the facility for dynamic testing of the scale models under consideration in this study. The paragraphs to follow contain a discussion of the facility and the limits on the scale factor for the model imposed by the size of the LSL test chamber.

1.3.1 General Description

The LSL, illustrated in Figure 1.3.1-1, is a hemispherical structure that provides a large, environmentally controlled volume in which various tests may be performed. This building has a maximum radius of 156 feet from the planform center at ground level to the domed ceiling. Six catwalks are mounted at the ceiling level of the structure accessing the perimeter of the dome at several heights. These catwalks reduce the radius of the building available for testing purposes to 145 feet, although the volume between the catwalks could be utilized, if necessary. A single, square elevator shaft (12' X 12') is located at floor level 40 feet from the side of the building, imposing only minor constraints on the usable test volume.

1.3.2 Facility Limitations on Scale Model Size

In this analysis, the LSL was assumed to have a hemispherical usable volume with a radius of 145 feet. Two models were examined: the ISS and Growth configurations as defined in the MDAC DR-02. These dual keel

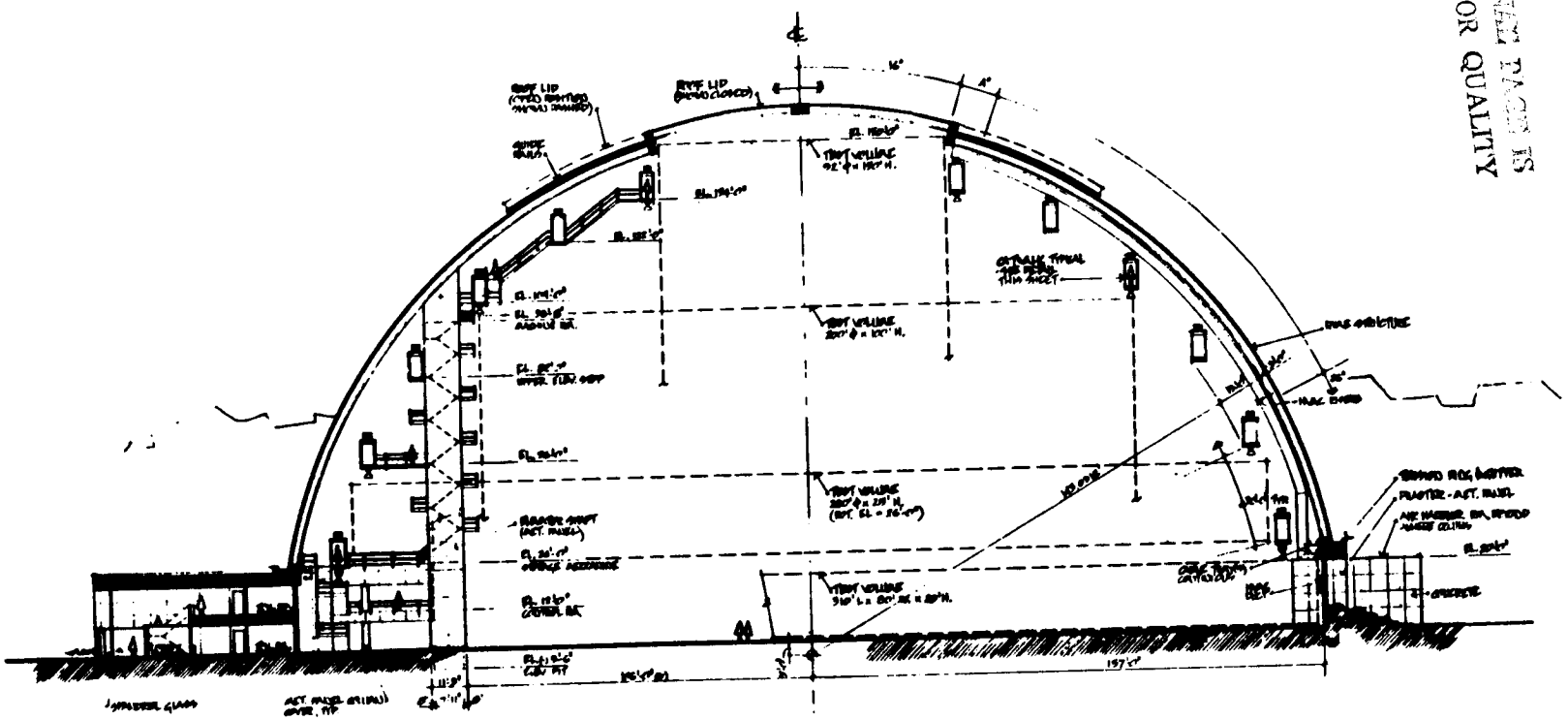

FIGURE 1.3.1-1 LARC LARGE SPACECRAFT LABORATORY

configurations are basically planar structures. Thus, the most practical suspension configuration in terms of access and usable area places the plane of the dual keel parallel to the LSL floor (x-axis vertical). However, the dynamic constraints of a cable-type suspension system may require that the model be tested in all three planar orientations. The other two orientations place the plane of the dual keel perpendicular to the LSL floor, with the transverse boom either vertical or horizontal (y-axis vertical and z-axis vertical, respectively). These latter two suspension configurations delineate the upper bounds for the sizes of the ISS and Growth scale models.

Figures 1.3.2-1 and 1.3.2-2 show the quarter scale ISS Space Station model inside the LSL. This is the largest model which can be located in the building (with little allowance for structural assembly activities). The envelope for this model is 155' X 90', in the boom and keel directions, respectively). Figures 1.3.2-3 and 1.3.2-4 present the maximum scale growth configuration model which can be tested in the LSL (1/8 scale). The envelope dimensions of this structure are 132' X 45'. Figures 1.3.2-5 and 1.3.2-6 show the fifth scale version of the growth configuration (211' X 72'), which can be tested in the LSL only in "transverse boom horizontal" orientations. The latter figure also indicates that interference with the elevator shaft mentioned above can be easily avoided. Other diagrams of the ISS and Growth configurations at various scale factors are shown in Appendix A.

Due to these physical constraints on the size of the scale model, a scale factor range of 1/10 to 1/4 was chosen for the parametric trades in the remainder of this study. If the testing of the growth configuration is important, a 1/5 scale model would fit in two of the three possible orientations. This may be adequate if an active suspension system is used.

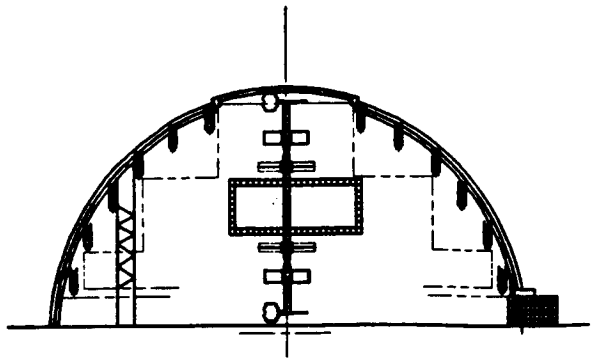

FIGURE 1.3.2-1
QUARTER SCALE ISS MODEL
IN VERTICAL ORIENTATION

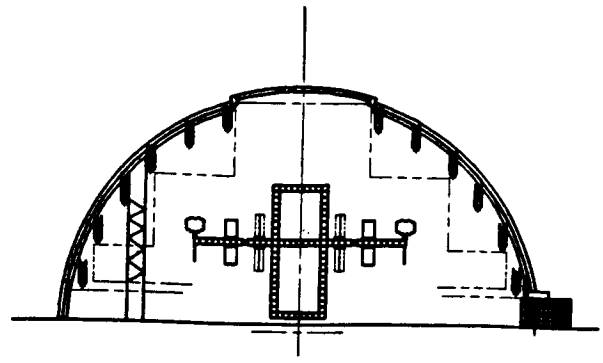

FIGURE 1.3.2-2
QUARTER SCALE ISS MODEL
IN HORIZONTAL ORIENTATION

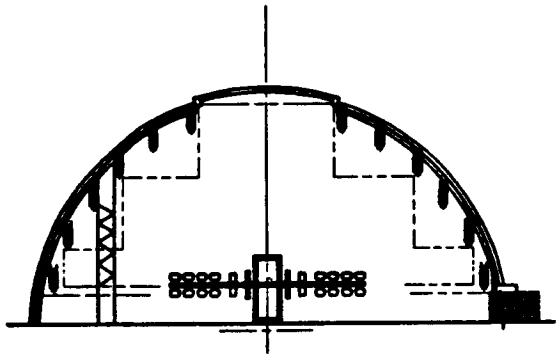

FIGURE 1.3.2-3
EIGHTH SCALE GROWTH MODEL
IN HORIZONTAL ORIENTATION

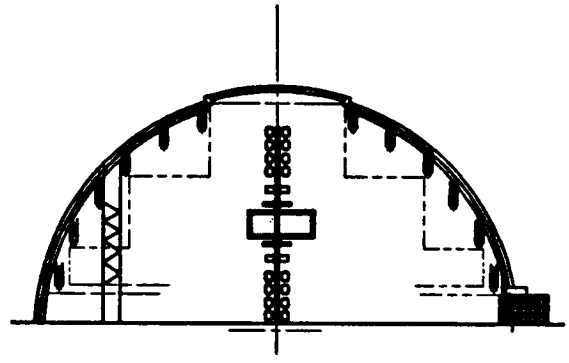

FIGURE 1.3.2-4
EIGHTH SCALE GROWTH MODEL
IN VERTICAL ORIENTATION

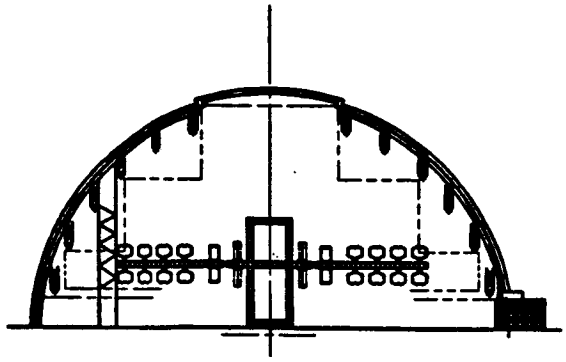

FIGURE 1.3.2-5
FIFTH SCALE GROWTH MODEL
IN HORIZONTAL ORIENTATION

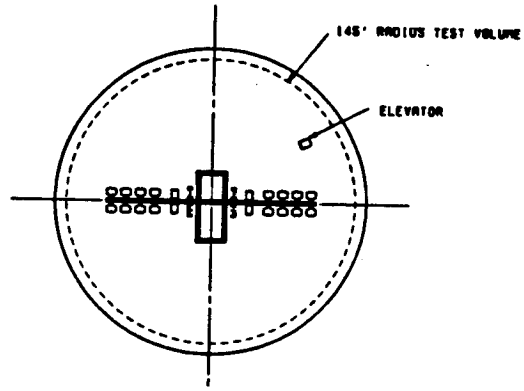

FIGURE 1.3.2-6
FIFTH SCALE GROWTH MODEL
IN HORIZONTAL ORIENTATION,
PLANFORM VIEW

2.0 SCALING ANALYSES

This chapter develops and reviews the scaling laws pertinent to the design and construction of a scale model space station. In Section 2.1 the fundamental scaling relationships associated with the linear undamped dynamics of the free-free space station model will be summarized. Based on the assumptions of matched model density and replica scaling, these scaling laws provide guidance as to how the fundamental quantities of mass and frequency, as well as derived quantities such as stress, displacement, and accelerations, scale. Section 2.2 details the manner in which the truss members and joints must be scaled in order to meet the replica scaling requirements, and where these requirements might be relaxed. Section 2.3 investigates the adverse interactions resulting from the necessity of conducting the test in 1-g and air. In this chapter, the following questions are addressed:

- How do the phenomena in question scale in principle? That is, what are the inherent scaling relationships of the linear or nonlinear mechanism?

- How important are the phenomena in practice? That is, for the specific scale range under consideration (1/10 to 1/4 scale), is the influence of the phenomena important to the dynamics of the model? Note that this is an entirely different question from the first. A given phenomenon can scale well, but be totally irrelevant to the final dynamics. Conversely, the phenomenon may not scale, and be critical to the dynamics.

- In view of the answers to these two questions, what are the design implications of the phenomena? How do they influence the choice of scale, and the specification of tolerances?

The approach to the resolution of these questions is straightforward. For each phenomenon, a simple dynamic model which captures the essential physics is developed. From the model equations for this phenomenon, the scaling relationship is derived. The scaling influence on both the stiffness and the damping of the structure is then evaluated. These scaling

PROTOTYPE JOINT (STAR-NET)

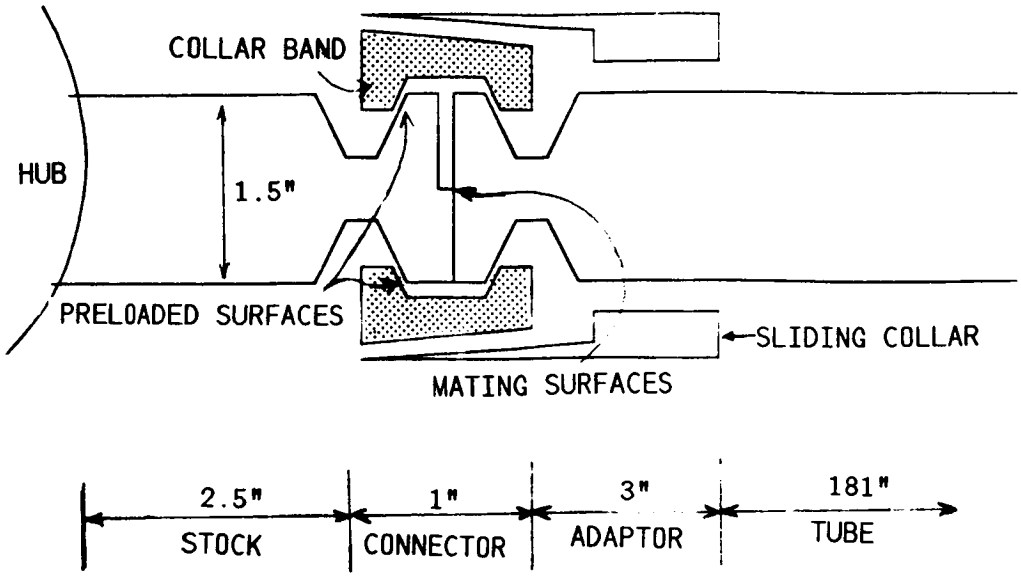

TRUSS TUBES

Radius = 1.0"
Thickness = 0.1"
Gr/Ep Unidirectional
Modulus E = 36 X 10^6 psi.
Density = 0.055 lb/in^3
Material Damping ζ = 0.0006

TRUSS JOINTS

Material: Aluminum
Modulus E = 10 X 10^6 psi.
Density = 0.1 lb/in^3
Material Damping ζ = .001

FIGURE 2.0-1 REFERENCE JOINT DESIGN AND TRUSS PARAMETERS FOR SCALING DISCUSSION IN CHAPTER 2

relationships are generic and applicable to all scaled models. Next, the importance of the phenomenon is evaluated for the current baseline space station, making the problem specific to the current design. Figure 2.0-1 lists some of the important parameters for the baseline design and defines the joint nomenclature. These assumptions are used to ascertain the specific importance of the phenomenon and to understand the associated design implications. At the outset, it should be noted that the task of modeling the damping in a structure is inherently more difficult than modeling its stiffness or mass. If the stiffness and inertial forces acting on a structure are considered of order unity at resonance, then the damping forces are of order 2ς. Thus if the critical damping ratio ς is expected to be 1%, and all of the features of the dynamics are replicated in scale to 1%, the errors in the stiffness and mass can be expected to be of order 1%, in frequency 1%, but in damping up to the order of 50%. Therefore, extreme care must be taken in the replication of components to accurately reproduce the structural damping in comparison with the mass or stiffness. The analyses in this chapter evaluate the practicality of reproducing both the structural stiffness and damping of the Space Station scale model.

2.1 REVIEW OF REPLICA SCALING LAWS

This section introduces the fundamental replica scaling laws for the scale model. Replica scaling can be considered a subset of the more general technique of similarity scaling. Similarity scaling is classically used to design wind tunnel models for investigating aerodynamic and aeroelastic behavior. In similarity scaling, the equations of motion are non-dimensionalized and the characteristics which are to be scaled are expressed in terms of non-dimensional parameters. The dimensionless parameter of interest can be properly scaled, given that the other non-dimensional ratios are preserved. For example, in aeroelastically scaling a cantilever wing with a tip mass [6], the frequencies and mode shapes can be scaled if the mass distribution, inertia distribution and stiffness distribution are preserved. In this similarity scaling example, the scale factors for time, length, and mass may be selected independently, while the rest of the model properties are derived from these three primary scale factors. By way of contrast, in replica scaling only one of these scale factors may be chosen

- INTRODUCE PRIMARY SCALE FACTORS (VM = λ * VF)

LENGTH λ MASS ($\rho_m = \rho_f$) λ^3 TIME λ

- DERIVED SCALE FACTORS

AREA	λ^2	FORCE	λ^2	LINEAR ACCEL	λ^{-1}
VOLUME	λ^3	TORQUE	λ^3	DAMPING	1.
DISPLACEMENT	λ	STRESS	1.	AREA INERTIA	λ^4
VELOCITY	1.	FREQUENCY	λ^{-1}	MASS INERTIA	λ^5

- UNSCALED EFFECTS

GRAVITY PRELOAD λ HANDLING λ^2 SUSPENSION ? AIR ?

FIGURE 2.1.1-1 REPLICA SCALING LAWS

independently, and all of the other model properties are derived from dimensionless ratios. The advantage gained in using replica scaling is that much of the nonlinear behavior of the full-scale spacecraft will also scale (see Sections 2.2 and 2.3).

2.1.1 Theoretical Replica Scaling Laws

In replica scaling, the nondimensional ratio that is typically selected is the length scale factor, λ. The other two primary scale factors are mass and time, which cannot be selected independent of the length scale factor. Following this convention, Figure 2.1.1-1 lists the other pertinent scale factors as a function of the length scale factor. These replica scale factors are derived from the nondimensional equations of motion using energy techniques [6]. In this formulation, it is assumed that the same materials are used in the scale model as in the full-scale Station.

In order to obtain correct scale model data, the scale model must be tested at force levels which are a scaled fraction of the forces on the full-scale Space Station. As an example, select a scale factor of 1/4. Figure 2.1.1-1 shows that the scale factor for force is λ^2. Thus, a 500 lb force on the full-scale station would be a 31.25 lb force on a 1/4 scale model. Ideally, testing the 1/4 scale model at this force level would result in displacements that were one-fourth of the full-scale displacements. Referring to the figure, the same test would yield velocities, stresses, strains, and damping that were the same as those in the full-scale, but the frequencies and accelerations would be four times as great as those in the full-scale Space Station.

2.1.2 Application of Replica Scaling Laws in Practice

The replica scaling laws make up a consistent set of rules which must be followed in order to be able to correlate scale model dynamic results with full scale spacecraft dynamic behavior. However, proper implementation of the replica scaling laws would dictate that the scale model be tested in zero-g and in vacuum, the same environment as the full-scale Space Station. The bottom of Figure 2.1.1-1 lists a few of the effects which cannot be

properly scaled because the model is being tested on earth. These include gravity, handling loads, suspension effects, and air effects. Gravity effects scale by the structural Froude number which scales as λ. The Froude number can be considered a measure of the relative importance of gravity when compared with the inertial accelerations of the model. One way to interpret this number is that if the 1/4 scale model is tested in 1-g, the influence of the gravity forces is equivalent to testing the full scale model in 1/4-g. Thus, the desire to minimize gravity effects drives the scale factor lower, and in the limit, an infinitely small scale model would have the same gravitational influence as the full-scale model in zero g. Other gravity effects, such as the buckling margin of safety for the model struts, scale linearly as well. For example, assume that the ratio of the gravity load to the buckling load in a strut for the full-scale model in 1-g (Pg/Pcr) is 0.8. A 1/4 scale model suspended by cables at the same locations as the full-scale model would have a ratio of Pg/Pcr of 0.2. Because smaller scale models are more robust, fewer cables may be needed to support them, saving time and complexity (the cable location trade studies are discussed in Section 3.3.5.2). Another unscaled effect is the handling loads. The overall size and weight of the model is reduced at smaller scales, easing the task of handling the assembled model. However, the fragility of the components and sensitivity to accidental forces increases by a factor of λ^{-2}.

When considering the effects of transportation and handling loads on the selection of the model scale factor, it is usually assumed that these loads vary with the mass of the model in a way which usually results in more robust models as scale decreases. However, it is important to note that certain types of loadings are independent of model size and will remain constant at all scale factors (i.e., accidental loads and impacts, machining loads, etc.). For these scale-invariant loads, special allowances must be made to protect components with very thin sections which could be bent or fractured (i.e., a thin lip on a joint or a thin-walled graphite-epoxy tube). Considering that the model is likely to be assembled and disassembled a number of times and suspended in different orientations, the issue of handling loads drives the choice of the scale factor up, toward larger scale models. Some of the handling problems can be mitigated by

employing more robust simulated components in the place of fragile replicated components. One example of this would be the use of P-55 graphite tubes with thicker walls (and a reduced modulus to match the EA) instead of the delicate P-75 tubes. The relative importance of the other unscaled effects and their influence on the selection of the model scale factor and the replication or simulation of components is discussed further in Sections 5.1.3 and 5.4.

Figure 2.1.2-1 outlines the trade space for the physical characteristics of the scale model, defined by the range of scale factors chosen (1/10 to 1/4 scale). This figure illustrates the large range of sizes for the ISS and the Step-2 build-up stage models, as well as their weights, which are a cubic function of the scale factor. Figure 2.1.2-2 depicts actual size drawings of the subscale joint for different scale factors, along with a drawing of the full-scale joint node. This figure illustrates the minute sizes of the components in a replica scale model joint. The issues associated with scaling and manufacturing subscale replica joints are discussed in subsequent sections.

2.2 STRUCTURAL SCALING

Now that the replica scaling laws have been summarized, it is necessary to examine the application of these scaling laws to the detailed elements, both linear and nonlinear. Section 2.2.1 discusses the scaling of the truss material and geometry, with particular emphasis on the interconnecting tubes in the truss. Section 2.2.2 details the scaling of the more complicated joint elements of the truss. Both sections address the question of the whether it is necessary to use replica scaling or if less costly simulations can be employed.

2.2.1 Truss Material, Geometry, and Stiffness Scaling

In this section, the requirements for the design of the scaled truss will be derived, in order to assure that the stiffness is properly modeled. In order to scale the stiffness in a structure, the proper load paths and strain energy distribution must be maintained. Therefore the analysis begins

	FULL SIZE	1/4 SCALE	1/6 SCALE	1/10 SCALE
HEIGHT (Z) (FT)				
ISS	360.9	90.2	60.2	36.1
STEP-2	148.0	37.0	24.7	14.8
WIDTH (Y)				
ISS	621.2	155.3	103.5	62.1
STEP-2	582.0	145.5	97.0	58.2
DEPTH (X)				
ISS	114.8	28.7	19.1	11.5
STEP-2	75.0	18.8	12.5	7.5
WEIGHT (LBS)				
ISS	518,400	8,100	2,400	518
STEP-2	73,600	1,150	340	74
WEIGHT W/ORBITER				
ISS	769,000	12,000	3,560	769
STEP-2	324,200	5,070	1,500	324
BAY SIZE (FT)	16.4	4.1	2.7	1.6

FIGURE 2.1.2-1 SCALE MODEL DATA

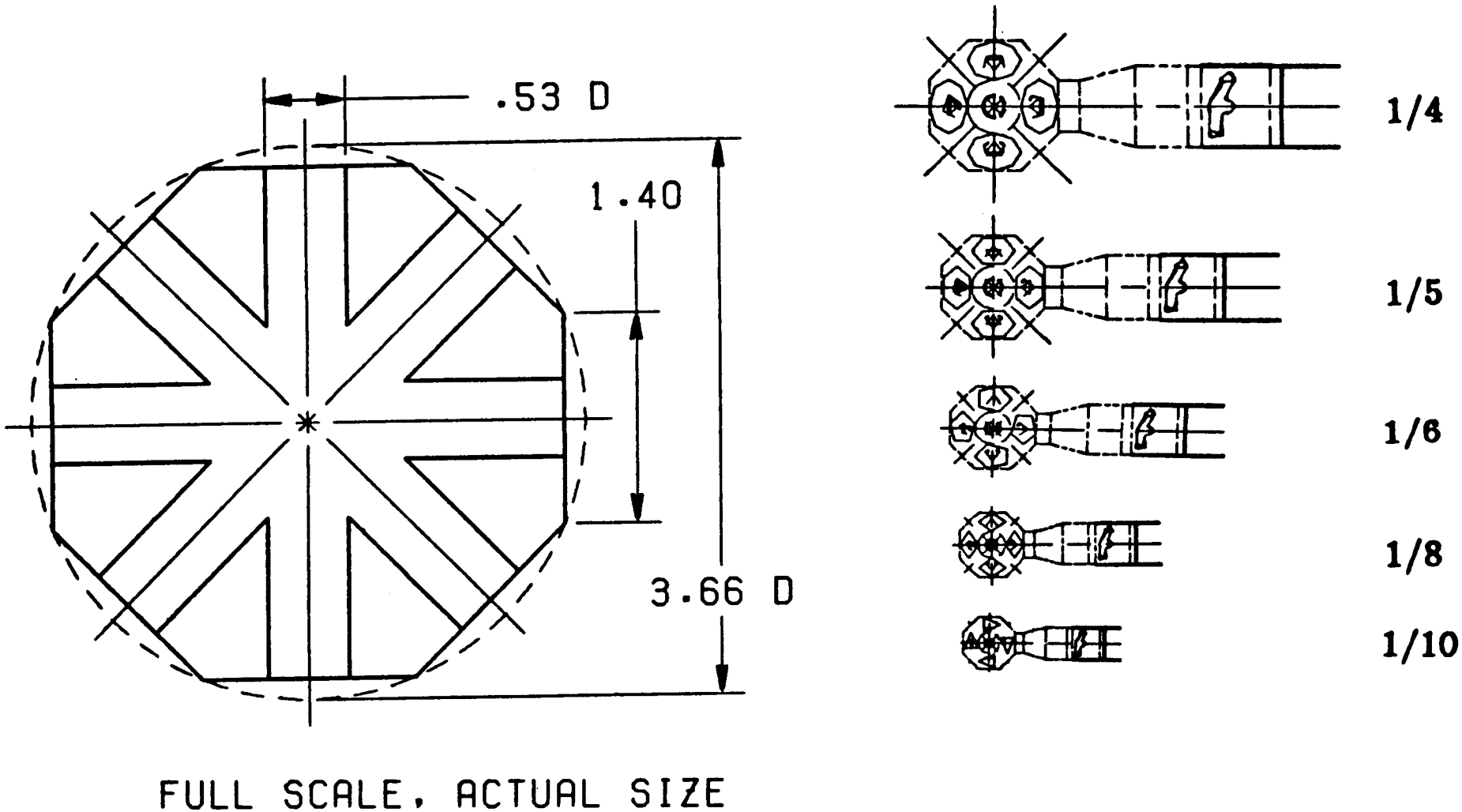

FIGURE 2.1.2-2 ACTUAL SIZE DRAWINGS OF SCALED SPACE STATION JOINTS

with a model for the strain energy in a tube in an imperfect truss (i.e., a truss in which the joints are not free to rotate). In this case both extension and bending can be carried by the truss element.

2.2.1.1 Theoretical Scaling Model

For a joint/tube/joint truss element located off the bending axis of the truss, the total strain energy is stored in four mechanisms: tube extension, tube bending, joint extension, and joint bending

$$U_{Tot} \approx \underbrace{E_t t_t r_t l_t}_{\text{Tube Extension}} + \underbrace{E_t t_t r_t^3 l_t l^{-2}}_{\text{Tube Bending}} + \underbrace{E_j r_j^2 l_j}_{\text{Joint Extension}} + \underbrace{E_j r_j^4 l_j l^{-2}}_{\text{Joint Bending}} \qquad (2.2.1.1\text{-}1)$$

Normalizing by the strain energy stored in the tube in extension (which is expected to be the largest contributor)

$$\frac{U_{tot}}{U_{tube-ext}} \approx 1 + \frac{r_t^2}{l^2} + \frac{E_j}{E_t}\frac{r_j^2}{t_t r_t}\frac{l_j}{l_t} + \frac{E_j}{E_t}\frac{r_j^4}{t_t r_t l^2}\frac{l_j}{l_t} \approx \lambda^0 \qquad (2.2.1.1\text{-}2)$$

The ratios represented by the second, third, and fourth terms on the right hand side must be matched in order to obtain the correct strain energy distribution. If perfect replica scaling is employed and the same materials are used in the subscale model as in the full-scale model, none of the terms depend on the scale factor, (λ) and the strain energy distribution is preserved. If other than perfect replication is used (i.e., similarity scaling), the ratios of the strain energy distribution should be matched.

2.2.1.2 Importance and Design Implications

Substitution into Eq. (2.2.1.1-2) above for the baseline truss parameters yields

$$\frac{U_{tot}}{U_{tube-ext}} \approx 1 + 10^{-5} + 10^{-1} + 10^{-6} \qquad (2.2.1.2\text{-}1)$$

This implies that the slenderness ratio r_t/l is so small for the tubes in the truss that even though the joints are fixed rather than pinned, most of

the energy is stored in the extension of the tube, not in bending. Likewise, the relative size of the third and fourth terms reveal that the strain energy stored in bending in the joints is insignificant, but the strain energy stored in extension in the joints is relatively important. Since the bending strains in the tube and joint are not important, it is only necessary in practice to reproduce the extensional stiffness. This can be done by simulation rather than replication. The quantity (EA/l) for the joint and tube must be scaled properly, and their ratio maintained, but details such as the wall thickness and the radius need not be replicated. This allows, for example, the substitution of lower modulus graphite in the scale model tubes as opposed to the high modulus graphite in the actual structure. It also permits the simulation of the load path in the joint, so long as the extensional stiffness is maintained. The joints will be discussed further in Sections 2.2.3 and 2.2.4.

2.2.2 Scaling of Truss Material Damping

Material damping is the underlying energy dissipation mechanism present in all structures and, in principle, should be replicated. The material at any point in a structure dissipates a fraction of the local strain energy stored in it during each cycle. In order to scale the damping correctly, it is necessary to simulate both the material dissipation characteristics and the strain energy distribution.

2.2.2.1 Theoretical Scaling Model

For a single structural element, the loss factor is defined as

$$g = \frac{\Delta U}{2 \pi U} \approx 2 \zeta \qquad (2.2.2.1\text{-}1)$$

where: ΔU = energy dissipated per cycle
U_i = peak strain energy in the cycle

For a lightly damped structure,

$$\eta \simeq 2\zeta \qquad (2.2.2.1\text{-}2)$$

For a built-up structure, the total loss factor is the sum of all the energy dissipated per cycle divided by the sum of all the strain energy stored in the various structural elements

$$g_{tot} \approx \frac{\sum \Delta U}{2\pi \sum \Delta U} \approx \frac{\frac{\Delta U_1}{2\pi U_1} + \frac{\Delta U_2}{2\pi U_2}\left[\frac{U_2}{U_1}\right] + \ldots}{1 + \frac{U_2}{U_1} + \ldots} \qquad (2.2.2.1\text{-}3)$$

For material damping, the terms in brackets can be considered just the material damping constant g, a property which may depend on frequency and stress level. Employing the notation of the joint/tube/joint truss model described in Section 2.2.1, the total material damping in the truss is functionally dependent on

$$2\zeta \approx g \approx \frac{g_{tube}\left[1 + \frac{U_{t\text{-}bend}}{U_{t\text{-}ext}}\right] + g_{joint}\left[\frac{U_{j\text{-}ext}}{U_{t\text{-}ext}} + \frac{U_{j\text{-}bend}}{U_{t\text{-}ext}}\right]}{1 + \frac{U_{t\text{-}bend}}{U_{t\text{-}ext}} + \frac{U_{j\text{-}ext}}{U_{t\text{-}ext}} + \frac{U_{j\text{-}bend}}{U_{t\text{-}ext}}} \qquad (2.2.2.1\text{-}4)$$

where the g's are the material damping constants, and the strain energy ratios are as given in Section 2.2.1. If replica scaling laws are employed (i.e., the strain energy distribution is scaled, the materials are matched), the material damping of the structure is matched in the scale model.

2.2.2.2 Importance and Design Implication

Subsituting the material damping values for the materials baselined for the ISS into Equation (2.2.2.1-4), and assuming the strain energy distribution computed in Section 2.2.1, the estimated material damping for the space station scale model is

$$\zeta \approx \frac{0.6 \times 10^{-3}[\,1 + 10^{-5}\,] + 1 \times 10^{-3}[\,10^{-1} + 10^{-6}\,]}{1 + 10^{-5} + 10^{-1} + 10^{-6}} \qquad (2.2.2.2\text{-}1)$$

$$\approx 10^{-3}$$

The expected dissipation will be due almost entirely to the extensional

straining of the graphite/epoxy material in the tube. The extensional damping of the aluminum in the joint plays a smaller role. Given that the total material critical damping ratio expected for the ISS Space Station is on the order of .001, it must be decided whether it is desirable to replicate such a low level of damping at all. Subsequent analyses investigate the relative order of magnitude of other sources of damping (including those in the scale model test environment) such as joints, air, cables, etc. Regarding specific design implications, if the material damping must be matched, it is most important to match the extensional damping in the tubes. All unidirectional graphite/epoxy systems and aluminum have approximately the same material damping in extension. Therefore, this consideration would not strongly affect the choice of tube material.

2.2.3 Joint Stiffness Scaling

The joints in a space structure truss are potential sites for stiffness nonlinearities in the structure. Design steps can be taken to preload the joints, which modifies their behavior so that in principle they operate in a linear regime. The current baseline Space Station joint designs embrace this philosophy. Two models of possible nonlinear mechanisms were developed to assess the needs for preload, tolerance control and replication of the joint.

2.2.3.1 Theoretical Scaling Models

The LaRC and Star-Net joints proposed as candidates for the Space Station may have deadbands due to manufacturing tolerances as well as friction at the contact surfaces. Two models were made of this joint, as shown in Figure 2.2.3.1-1. In Figure (a) the stiffness of the joint has three components, k_p, the stiffness of the preloading element, k_1, the stiffness of the part of the mating faces which are initially in contact, and k_2, the stiffness of that part of the mating surfaces which may not be in initial contact due to machining tolerances. In the absence of a preload, the elements represented by k_1 lift off the face at the right end, due to tensile loading. In the presence of the preload

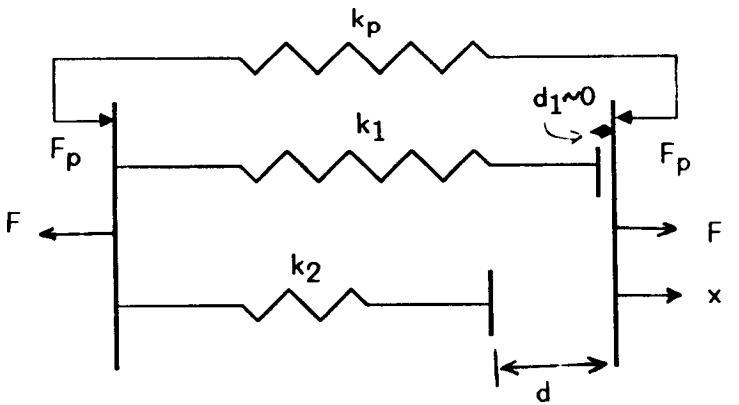

a) dead-band model

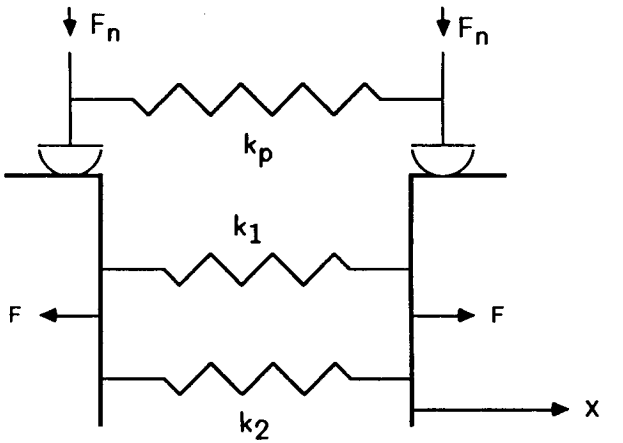

b) friction model

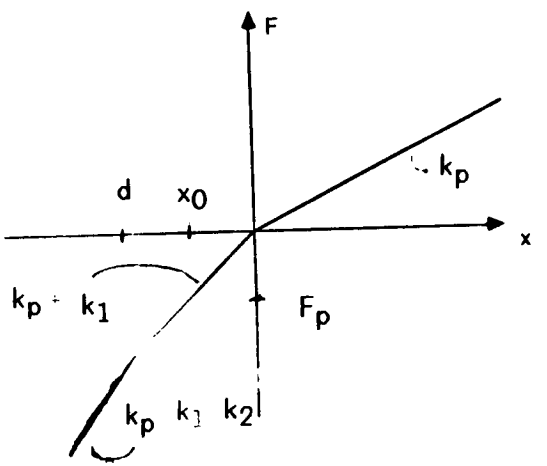

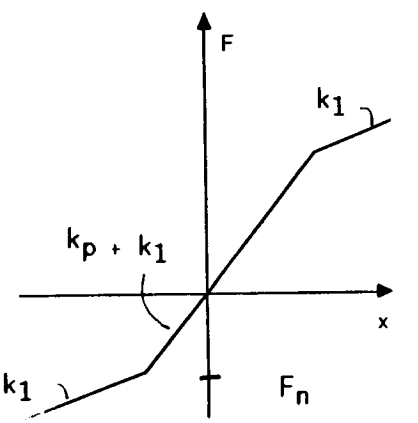

FIGURE 2.2.3.1-1 JOINT STIFFNESS MODELS

$$F_p = (k_1 + k_p)d \qquad (2.2.3.1\text{-}1)$$

the deadband gap closes and three springs contribute to the joint stiffness.

In order to scale the stiffness characteristics of this nonlinear joint correctly, the ratio of the strain energy stored in the joint to the strain energy in the tube must remain constant

$$\frac{U_j}{U_t} \approx \frac{E_jA_pl_p + E_jA_1l_1 + E_jA_2l_2}{E_tA_tl_t} \approx \lambda^0 \qquad (2.2.3.1\text{-}2)$$

These three ratios should be matched in principle, requiring that the material and the detailed geometry of the joint, including tolerances, be scaled. If all aspects of the joint are replicated, the fractional strain energy content of the structure is also scaled.

For a nonlinear element, the operating point must also be scaled. The operating point depends on the load/preload ratio and the deadband. Thus, the operating load/preload ratio is

$$\frac{F}{F_p} \approx \frac{E_tA_t\epsilon_t}{E_jA_p\delta_p/l_p} \approx \lambda^0 \qquad (2.2.3.1\text{-}3)$$

The force level at which the model operates depends on the axial stiffness (EA) and the strain level. If the tests are conducted at a constant strain level, and the joint is replicated such that the stiffness, preload, and displacement are scaled, the load-to-preload ratio remains constant. The deadband is

$$d \approx \lambda \qquad (2.2.3.1\text{-}4)$$

Thus, the deadband must be scaled in a replicated joint.

The scaling of the the friction model shown in Figure 2.2.3.1(b) is similar to that in the deadband model. The ratio of the stiffnesses must remain constant, and the ratio of operating load to frictional load at the

interface must be constant

$$\frac{F}{F_F} = \frac{F}{F_N \mu} \approx \frac{E_t A_t \epsilon_t}{E_p A_p \delta_p \mu / l_p} \approx \lambda^0 \qquad (2.2.3.1\text{-}5)$$

Thus, the ratio of the operating load to the slipping load stays constant if the joint is replicated and the coefficient of friction is maintained.

In summary, the nonlinear stiffness characteristics of a deadband/friction joint can be reproduced in scale if:

- the parts are replicated in scale
- the preload mechanism is replicated in scale
- the tolerances are scaled as λ
- the coefficient of friction is held constant

The required scaling of the tolerances drives the design of the joint to larger scale factors, thereby easing the manufacturing of the joint.

2.2.3.2 Importance and Design Implications

In order to assess the practical importance of replicating the detailed load paths and tolerances of the joint, it is necessary to establish where on the stiffness curve it operates, and how large a change in the effective stiffness is expected. In order to evaluate the constants in the models, it was assumed that the collar has an effective area of 0.5 square inches, that the mating surfaces have an area of 1.0 square inches, that half of the mating surfaces are in contact, and that the other half of the surface is separated by the manufacturing tolerance (full-scale) of 3 mils. The stiffnesses of the three springs are then

$$k_p = k_1 = k_2 = 10^7 \times 0.5 / 1 = 5 \times 10^6 \ \text{lb/in} \qquad (2.2.3.2\text{-}1)$$

The level of preload on the surfaces at the collar (see Figure 2.0.1) depends on the geometry and coefficient of friction of the contact surfaces. It is estimated to be

$$F_p = \begin{cases} 1300 \text{ lbs} & \text{for } \mu = .2 \\ 200 \text{ lbs} & \text{for } \mu = .5 \end{cases} \qquad (2.2.3.2\text{-}2)$$

Under this preload, the deflection of the joint is

$$X = \frac{F_p}{k_p + k_1} = \begin{cases} .00013" & \text{for } \mu = .2 \\ .00002" & \text{for } \mu = .5 \end{cases} \qquad (2.2.3.2\text{-}3)$$

which places it on the characteristic of Figure 2.2.3.1 at the point labelled X_o, (i.e., with some preload but not enough to close the deadband gap). The preload F_p is much larger than the expected operating load (10 lbs full-scale) so that the joint will exhibit at worst only a slight change in stiffness.

The frictional slipping load for macro-slip at the preloaded surfaces is

$$\mu F_N = \begin{cases} 330 \text{ lbs} & \text{for } \mu = .2 \\ 150 \text{ lbs} & \text{for } \mu = .5 \end{cases} \qquad (2.2.3.2\text{-}4)$$

Since these forces are also well above the operating load level, it is unlikely that any macro-slip friction will occur.

It is also instructive to analyze the sensitivity of the stiffness of the joint/tube/joint truss member to the worst-case changes in the stiffness of the joint. The total stiffness is composed of several stiffnesses in series

$$\frac{1}{k_{tot}} = 2 \underbrace{\left[\frac{1}{k_{stock}} + \frac{1}{k_{connector}} + \frac{1}{k_{adaptor}} \right]}_{1/k_j} + \frac{1}{k_{tube}} \qquad (2.2.3.2\text{-}5)$$

Reasonable estimates of these properties are

$$k_{stock} = 0.7 \times 10^7 \quad \text{lb/in}$$

$$k_{connector} = 1 \pm .5 \times 10^7 \quad \text{lb/in}$$

$$k_{adaptor} = 0.8 \times 10^7 \quad \text{lb/in}$$

$$k_{tube} = 0.012 \times 10^7 \quad lb/in$$

$$k_{tot} = 0.0110 \left\{ \begin{matrix} -.0002 \\ \\ +.0001 \end{matrix} \right\} \times 10^7 \quad lb/in$$

The results show that the connector mechanism in the joint is so stiff in comparison with the tube that moderate changes in the joint stiffness are reflected as only small changes in the truss stiffness. The practical implication is that the overall stiffness of the truss is virtually insensitive to small changes in the tolerances of the joint. As a note of caution, however, the mode shapes of modes closely spaced in frequency can be significantly altered by small changes in the stiffness distribution. A more complete assessment of this sensitivity is warranted prior to the final design of the scale model joints.

2.2.4 Scaling of Joint Damping

The loss mechanisms in the joints of a structure depend on the details of the load path and the interactions between the contacting surfaces. A detailed calculation of the losses in a real joint is impossible, but several simplified models can be derived in order to infer the scaling laws for these nonlinear loss mechanisms. In this section, three loss mechanisms are analyzed, two due to friction and one due to impact.

2.2.4.1 Theoretical Scaling Models

The constraining band/collar-type joint (of which the NASA/LaRC interim Space Station joint is an example), creates frictional fits at the contacting surfaces. If there is either macroscopic motion (i.e. the whole surface slips) or microscopic motion (i.e. parts of the surface strain and slip) at the interface, then frictional energy loss will take place. In Section 2.2.3, it was predicted that under normal operating loads, macro-slip of the interfaces would not occur. However, the mechanisms of macro-slip and micro-slip are sufficiently similar that two macro-slip models are developed.

The first model (shown in Figure 2.2.4.1-1a) represents a joint in

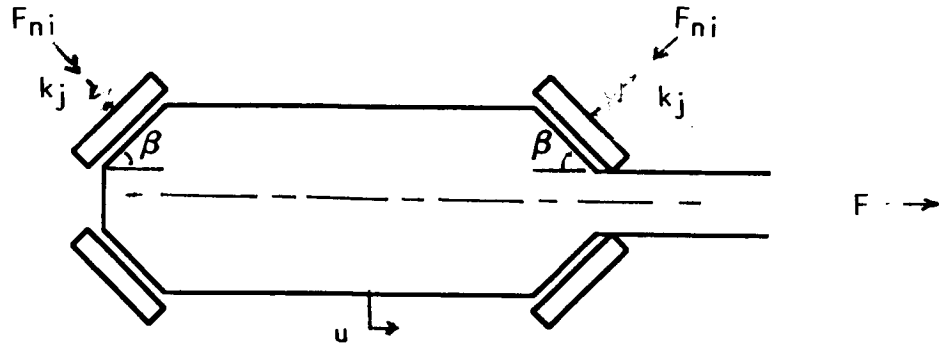

(a) friction at a joint in extension

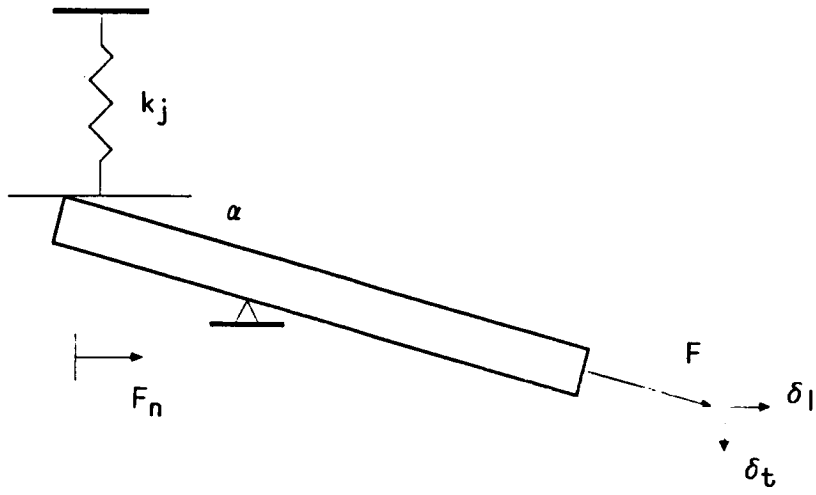

(b) friction at a joint in bending

FIGURE 2.2.4.1-1 JOINT DAMPING MODELS

extension, restrained by the preload Fn acting on frictional surfaces with finite stiffness properties. The model assumes that the joint tolerances are scaled properly. The loss factor for the bar, due to this joint, is estimated to be

$$g = \frac{\Delta U}{2\pi U} = \left[\frac{4\mu}{\pi}\frac{F_N}{F}\right]\frac{\cos\beta}{[\mu\sin\beta\cos\beta + \sin^2\beta]}\left[\frac{F - F_N\mu\cos\beta}{F}\right]\frac{(EA/l)_t}{k_j} +$$

$$+\left[\frac{2\mu}{\pi}\right]\frac{\sin\beta\cos\beta}{[\mu\sin\beta\cos\beta + \sin^2\beta]^2}\left[\frac{F - F_N\mu\cos\beta}{F}\right]^2\frac{[EA/l]_t^2}{k_j^2} \approx \lambda^o \qquad (2.2.4.1\text{-}1)$$

where F is the maximum expected load in the bar. A similar model of the friction in a preloaded surface is derived from the system shown in Figure 2.2.4.1-1b which shows local bending occuring at the joint. In this case

$$g = \frac{4\mu}{\pi}\frac{F_N}{F}\frac{l_j}{l}\tan\alpha + \frac{2\mu}{\pi}\left[\frac{l_j}{l}\right]^2\frac{k_j}{[EA/l]_t}\tan\alpha \approx \lambda^o \qquad (2.2.4.1\text{-}2)$$

A second potential loss mechanism in built-up joints is due to the impacting of contacting surfaces. If during one period, the joints open and close either macroscopically or microscopically, impacting will occur. In the simplest possible coefficient of restitution model of a joint undergoing periodic impacting of surfaces not initially in contact (due, for example, for manufacturing tolerances), the loss factor can be estimated as

$$g = \frac{1}{2\pi}\left[\frac{k_t}{k_j}\right]^2(1-e^2) \approx \lambda^o \qquad (2.2.4.1\text{-}3)$$

where e is the coefficient of restitution (1 for a perfectly elastic impact, 0 for a perfectly inelastic impact).

Examination of the above three relationships for damping in the truss due to losses at the joints yields the following parameters which must be maintained in a replica scale model to match the joint damping:

- The material constants μ, the coefficient of friction and e, the coefficient of restitution

- The geometric constants l_j/l, the nondimensional scale $k_j/(EA/l)$, the ratio of the joint and tube stiffnesses, and α, β the geometry of the contacting surface

- The load/preload ratio F/F_n

If the same material is used in the subscale joints as in the full-scale joints, the material constants are identically matched. If the joints are built in perfect replica scale (including tolerances), the geometric constants are matched. If the test is conducted at the correct scaled loading condition (consistant strain level), then the load/preload ratio is correct (as shown in Section 2.2.3). These three statements imply that if perfect replica scaling can be achieved, the structural damping in the joints can probably be matched, and the structural damping can be determined from a scale model. The need to scale the tolerances and surface conditions favors a large scale factor for the model.

2.2.4.2 Importance and Design Implications

Unlike Sections 2.2.1 thru 2.2.3, it is impossible to make realistic scaling estimates of the joint damping from the models presented above. However, two general statements can be made:

1) If the dominant source of damping in the structure is at the joints, and if the objective of the scale model test is to determine damping, then it is possible, by precise replication, to reproduce the joint damping.

2) If joints are not the dominant source of damping, or if the damping measurement is not a prime objective, then there is no need to replicate the joints, and a simulation of the joint may suffice. This is because the structural stiffness is relatively less sensitive to the details of the joint stiffness (as shown in Section 2.2.3), than the damping.

2.3 CONVENTIONAL TEST CONSTRAINTS

The previous section examined the theoretical and design issues associated with the replica scaling of the model joints and truss elements.

This section investigates some of the practical effects of the 1-g gravity and air of the test environment and their implications on the ability of the scale model to simulate on-orbit dynamic behavior.

2.3.1 Aerodynamic Mass Effects

The presence of air around a test article has two effects: it increases the apparent mass of the test article, and it provides a path for the transmission of energy out of the test article. This creates apparent damping in the test article. The mass effects will be examined first.

2.3.1.1 Theoretical Scaling Models

The increase in apparent mass, the so-called virtual mass effect, is simply due to the fact that as a structure moves, the air around the structure must be accelerated with it. For a circular cross-section in an incompressible medium, the virtual mass is one-half the mass of the displaced air

$$\frac{m_{air}}{m_{tube}} \approx \frac{\pi \rho_{air} r^2}{2m} \approx \frac{\pi \rho_{air} r_t^2}{4\pi \rho r_t t_t} \approx \lambda^0 \qquad (2.3.1.1\text{-}1)$$

so that provided the mass per unit length of the structure is scaled properly, the virtual mass effect is independent of the scale factor.

2.3.1.2 Importance and Design Influences

For air at standard atmospheric conditions and the proposed graphite/epoxy structure, the virtual mass of the air in comparison with the tubes is

$$\frac{m_{air}}{m_{tube}} \approx 0.002 \qquad (2.3.1.2\text{-}1)$$

which is independent of scale. The influence this will have on the measured frequencies is

$$\frac{\omega}{\omega_{ref}} \approx \left(1 + m_{air}/m_{tube} \right)^{-1/2} = .999 \qquad (2.3.1.2\text{-}2)$$

or one part in one thousand change in frequency. This level of change is practically undetectable. Since this change in mass is uniform over the entire structure, there is little chance that even closely spaced modes would be affected.

2.3.2 Aerodynamic Damping

The presence of air also provides an energy pathway out of the structure. Structures radiate energy to the air by three mechanisms: conventional dynamic pressure-related drag losses, viscous losses, and acoustic radiation. The nondimensional group indicating the relative importance of acoustic radiation is the Mach number based on frequency and diameter

$$M_a \approx \frac{\omega D}{c} \approx \lambda^0 \qquad (2.3.2\text{-}1)$$

which is independent of scale. If this number is of the order unity or greater, acoustic radiation is important. For the full-scale space station

$$M_a \approx 10^{-4} \qquad (2.3.2\text{-}2)$$

thus, acoustic radiation is not an important factor. The ratio of viscous to inertial effects is indicated by the Reynolds number based on diameter and frequency

$$R_e \approx \frac{\omega D^2}{\upsilon} \approx \lambda^1 \qquad (2.3.2\text{-}3)$$

which scales linearly with the scale factor. For a full-scale test

$$R_e \approx 218 \qquad (2.3.2\text{-}4)$$

Thus, a sub-scaled test will operate at a fraction of this Reynolds number. The practical significance of this result is that the viscous dissipation terms may be important, and thus must be retained in the scaling analysis.

2.3.2.1 Theoretical Scaling Model

The conventional model of aerodynamic drag allows the force per unit length of the tube to depend on the dynamic pressure caused by the motion

$$F' = \frac{1}{2}\rho_{air} D C_d \left|\frac{dy}{dt}\right| \frac{dy}{dt} \qquad (2.3.2.1\text{-}1)$$

Low Reynolds number effects are included by allowing the drag coefficient to depend on the Reynolds number. For a cylinder

$$C_d = b_1 + b_2/R_e \qquad b_1 = 1.3 \quad b_2 = 10 \qquad (2.3.2.1\text{-}2)$$

Calculating the equivalent viscous damping of such a force yields

$$\zeta \approx \frac{1}{2\pi} \frac{\rho_{air} D^2}{2m} \left[\frac{8}{3} a b_1 \left[\frac{A_y}{D}\right] + \pi b_2 \left[\frac{\nu}{\omega D^2} \right] \right] \qquad (2.3.2.1\text{-}3)$$

where the first term in brackets depends on the amplitude of the motion, and includes a nondimensional shape factor

$$a = \frac{\int \varphi^3 \, dx}{\int \varphi^2 \, dx} \qquad (2.3.2.1\text{-}4)$$

to account for non-uniform velocity over the structure. The aerodynamic losses scale as

$$\zeta \approx \left[1 + \frac{1}{\lambda} \right] \qquad (2.3.2.1\text{-}5)$$

Thus, as the scale factor decreases, the second (or viscous) term becomes more important.

2.3.2.2 Importance and Design Influences

For the scale model structure, the aerodynamic damping depends on both the choice of scale factor and the peak amplitude of vibration. Estimates of the aerodynamic damping for the Space Station truss structure are:

	A/D = 1	A/D = 0.1
full-scale	.0004	.00005
1/4 scale	.0005	.0002

These levels are insignificant, unless the material and the joint damping are extremely low. The contribution to the aerodynamic damping by the large, heavy attached masses, such as the modules and the solar dynamic power systems, will be even less, due to their smaller mass ratio. Aerodynamic damping will only be an important effect for those modes which are characterized by large motions of the lighter components. Otherwise, the aerodynamic damping can be considered a relatively inconsequential effect and relatively independent of scale.

2.3.3 Gravity Effects

The gravitational forces acting on the structure will have several effects. In general, the linear deflections due to gravity scale by the structural Froude number. The nondimensional deflection or strain level is

$$\delta/l \approx \rho g l/E \approx \lambda \qquad (2.3.3\text{-}1)$$

and the nondimensional stress is governed by the same parameter

$$\sigma/E \approx \rho g l/E \approx \lambda \qquad (2.3.3\text{-}2)$$

Thus, these gravitational influences on the structure will diminish with decreasing scale.

For a completely linear structure, gravitational forces would simply impose a steady load on the structure which would not significantly affect the dynamic tests results. However, if the structure or components of the structure are sufficiently flexible, gravity loads can stiffen members, cause excessive deflection, or induce buckling. These problems can be mitigated with a properly designed suspension system. The suspension system concept presented in Chapter 3 offloads most of the large masses in the Space Station, requiring the truss to support only its own weight. Even the

full-scale truss can support its own weight in 1-g. The structural Froude number argument above showed that the gravity-induced stresses and deflections diminish at smaller scales.

On the other hand, the gravity-induced forces will create a preload on the joints. The analyses in Sections 2.2.3 and 2.2.4 demonstrated the necessity of properly scaling the preload. The ratio of gravity preload to the internal joint preload is

$$\frac{F_g}{F_p} = \frac{\rho l^3}{\frac{E_p A_p \delta_p}{l_p}} \approx \lambda \qquad (2.3.3\text{-}3)$$

which diminishes with scale as expected. Therefore, it is theoretically impossible to match the 0-g joint preload exactly in a 1-g test of the scale model.

2.3.3.1 Importance and Design Implications

In practice, the gravity preload is small compared to the mechanically induced preload in the joints. In Section 2.2.3 it was estimated that the preload ranged from 200 to 1300 lbs depending on the coefficient of friction assumed for the joint components. If the truss is supported at every other bay by cables, the maximum load that will be induced at any joint due to the gravity loading will be on the order of the weight of 12 truss members or approximately 96 lbs. The ratio of the gravity preload to the internal joint preload can be calculated

$$F_g/F_p = (12\ m_t l_t g)/F_p \qquad (2.3.3.1\text{-}1)$$

substituting,

	F_p = 200	1300
$\lambda = 1.0$	.48	.074
$\lambda = .25$	.12	.018

These results imply that the worst case gravity load would be 10% of the preload. Although significant moments could be developed, the analysis in Section 2.2.3 showed that the truss stiffness is virtually insensitive to

the joint stiffness. Thus the overall stiffness effect would be minimal provided that there is no "slop" in the joints. The influence on the joint damping could be more significant, however, since small changes in the load path can cause changes in the behavior of the frictional interfaces.

As a final caution, it should be noted that if the truss is not properly suspended, or the truss is required to carry more than its own weight, then the gravity induced loads could increase by an order of magnitude. This would be the case if the truss directly carried the weight of the utility trays. In this case, the gravity loads could reach the order of the preload, possibly causing changes in the joint stiffness and certain changes in the joint damping.

2.3.4 Suspension Damping Effects

A detailed analysis of the suspension interactions with the mode shapes and frequencies is the subject of Chapter 3. This section documents a subtle, yet important interaction between the suspension system and the model damping which must be considered. If the transverse vibration frequencies of the suspension wires are close to the structural frequencies, they will participate in the model dynamics as coupled oscillators. These coupled oscillators are damped due to their vibration in air. This creates a condition that the test structure is coupled to a number of tuned mass dampers. Tuned mass dampers are extremely efficient absorbers of energy, and a considerable increase in the apparent damping of the structure could take place.

The maximum damping ratio which can be achieved in a structure with a single tuned mass damper depends on the mass ratio of the damper to the structure, but is of the order

$$\zeta \approx \frac{1}{2\sqrt{2}} \sqrt{\frac{m_{damper}}{m_{structure}}} \qquad (2.3.4\text{-}1)$$

where in this case, the damper is the suspension strings.

This theoretical damping ratio is achieved only if the damper is

precisely tuned. However, if the damper is tuned to within 10% of one of the resonant frequencies of the structure (particularly below the resonance), up to 1/3 of this value can be achieved. The easiest way to avoid this resonant damper phenomenon is to place in the transverse modes of the suspension wires well above those of the test article (see Section 3.3.5). The ratio of the frequencies of the wires and the truss is

$$\frac{\omega_{susp}}{\omega_{struct}} \approx \frac{\frac{\pi}{l}\sqrt{\sigma/\rho}}{\frac{k}{l^2}\sqrt{EI/m}} \approx \lambda \qquad (2.3.4\text{-}2)$$

which is desired to be high. Preliminary calculations based on these equations yielded damping values for the cables that were almost an order of magnitude higher than the material damping of the structure.

A summary of the scaling analysis results that impact the choice of the model scale factor is presented in Section 5.1.

3.0 DYNAMIC ANALYSES

This chapter documents dynamic analyses that were conducted to evaluate the relationship between the model scale factor and the ability of the suspended model to emulate the free-free dynamic behavior of the Space Station. Sections 3.1 and 3.2 document finite-element analyses of the full-scale Step-2 and ISS configurations. These analyses were conducted to determine the full-scale dynamic characteristics of the baseline configurations. In Section 3.2.3, criteria for comparing the suspended and free-free modes of the models are developed. Sections 3.3.1 - 3.3.4 describe preliminary analyses that were conducted to examine the effects of the suspension system on the free-free dynamics of the scale model. These include trades with respect to the model scale factor of soft and hard suspension systems, boundary condition effects, and shadow structure interactions. Section 3.3.5.1 outlines the development and validation of techniques used in the detailed analysis of the suspension system pendulum modes, cable string modes, and other interactions with the flexible modes of the structure. Sections 3.3.5.2 and 3.3.5.3 present the detailed analysis results for the scale models suspended in the LSL, including trade studies of cable location, size, and weight. In Sections 3.3.5.4 and 3.3.5.5 the criteria developed in Section 3.2.3 are applied to the results obtained from these detailed analyses to estimate, at the system level, the ability of the suspended model to emulate the dynamic characteristics of the full-scale Space Station. Finally, Section 3.4 summarizes the conclusions of the dynamic analyses and discusses some of the potential difficulties in testing the scale models.

3.1 FINITE-ELEMENT MODELING

The general purpose finite-element program EAL312 was used in this study. EAL version 312 is a database oriented collection of processors that can be used to generate thermal, mechanical, and pressure loading functions, in association with vibration, buckling, or stress analyses of a model described in the database [8]. EAL312 also has the capability of analyzing geometrically nonlinear systems. EAL usage is described in Section 3.1.1.

Section 3.1.2 contains a description of the configurations which were modeled and analyzed and Section 3.1.3 relates details of these models and their execution. A comparison between the mass properties of the models and the corresponding estimates contained in the DR-02 is presented in Section 3.1.4.

3.1.1 Facilities and Computer Program Description

EAL runstreams, or command sequences, were created and validated on a VAX-11/785. However, all mathematically intensive analyses were performed using the LMSC Cray-1S computer. Aside from the greatly decreased execution times experienced using the Cray, 64-bit arithmetic was found to be necessary for the relatively large models being analyzed. The EAL program, executed using all available VAX double precision options, provides insufficient numerical accuracy for the suspension system analysis. This is due to the fact that the modeling of the suspension system adds low stiffness springs to the model stiffness matrix. When the range of values in the stiffness matrix spans several orders of magnitude, increased accuracy is needed to prevent significant roundoff errors. It is therefore recommended that the suspension system analysis runstreams be executed on computers possessing at least 64-bit accuracy.

3.1.2 Descriptions of the Configurations Studied

The Space Station is erected in a series of build-up stages defined primarily by STS payload bay mass and volume constraints. Two of these Space Station flight configurations were selected for analysis in this study: the Step-2 build-up configuration and the fully operational ISS. These stages were chosen because of their geometric and mass properties differences, since the scaling issues associated with the smaller build-up stages may be different from those associated with the fully operational ISS. Descriptions of each of these configurations are contained in the McDonnell Douglas DR-02 Mass Properties Report, which is based on the ISS construction plans and flight schedules for the Space Station as of June 5, 1986.

The Step-2 build-up stage configuration, shown in Figure 3.1.2-1,

consists of the cumulative construction after two STS flights. This phase incorporates the full transverse boom, several modules, arrays, and radiators. At this stage of construction, two RCS modules are positioned at one end of the transverse boom, a temporary location where they are stored until permanent locations are established during a later STS flight. Many of the other payloads and modules are fixed in their permanent locations at this time.

The ISS configuration, shown in Figure 3.1.2-2, represents the fully constructed station, with all the modules, payloads, solar dynamic generators, etc., properly located. The ISS configuration represents the cumulative construction at the end of the fourteenth STS flight. A large servicing hangar (not shown in the figure) is situated inside the dual keel beneath the upper payload boom.

Table 3.1.2-1 presents the component weight breakdowns for the Step-2 build-up stage and the ISS Space Station. The five categories are the truss structure, utility trays, rotary joints and appendages (appendages include solar arrays, and all radiators), habitable modules, and rigid masses (payloads, servicing bay, resource modules, etc.). Note that the truss structure itself makes up a rather small fraction of the total mass. The dominant portion of the total mass is in the form of lumped masses attached to the truss at discrete points. This classification of the type of large space structure that the Space Station represents characterizes the relative importance of exactly matching the weight of different components and influences the design of the suspension system.

3.1.3 Runstream Description

EAL runstreams were constructed for each of the two configurations analyzed. In these models, each joint in the trusswork is represented by a single node. Longerons, battens, and diagonals are modeled as single beam elements which connect the proper nodes. Reductions in the graphite modulus and flexibilities in the truss joints are incorporated into the model by decreasing the stiffness of the truss elements by 15%. Solar arrays are modeled as beams, possessing bending stiffnesses and mass properties which

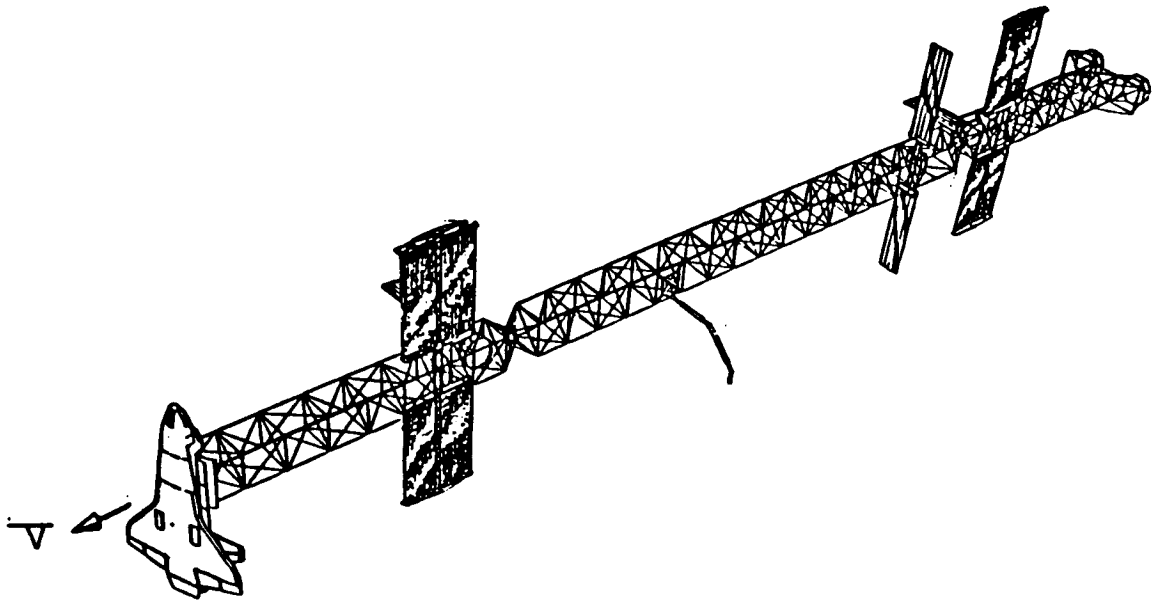

FIGURE 3.1.2-1: STEP-2 BUILD-UP STAGE CONFIGURATION

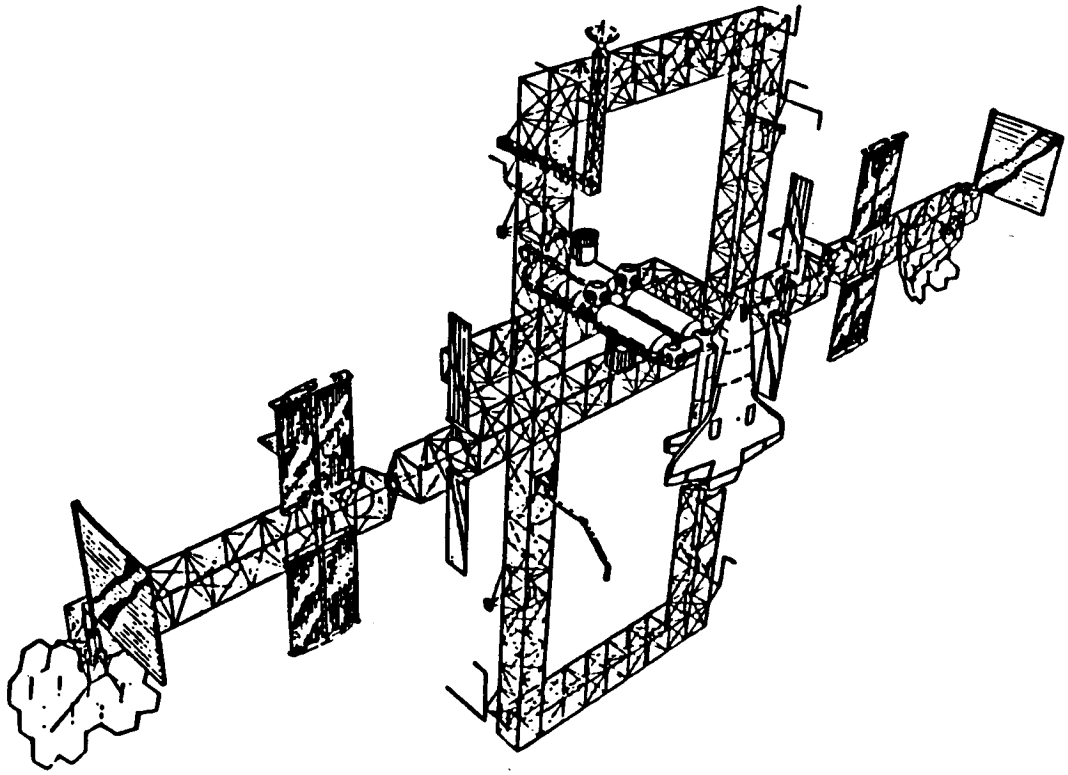

FIGURE 3.1.2-2: ISS CONFIGURATION

TABLE 3.1.2-1 SCALE MODEL WEIGHT BREAKDOWN (%)

	STRUCTURE	UTILITY TRAYS	APPENDAGES /R. JOINTS	MODULES	RIGID MASSES
STEP-2	2.6	23.5	18.9	-	55.0
ISS	1.3	10.0	9.7	57.0	22.0

CONCLUSION: MAJORITY OF WEIGHT IS IN THE FORM OF LARGE RIGID MASSES ATTACHED TO THE TRUSS STRUCTURE

* VALUES DO NOT INCLUDE SHUTTLE WEIGHT

produce a fundamental bending frequency of 0.1 Hz at full-scale. Thermal and ESS radiators are also modeled as beams having a fundamental bending frequency of 0.11 Hz at full-scale. Modules, payloads, and other accessories are modeled as lumped masses. Most of the rigid masses are input exactly as they appear in the DR-02, with the units converted to the lb-in-sec system using the CM command within the EAL TAB processor.

Two of these runstreams are designed to create and analyze models of the unconstrained (free-free) versions of the two configurations based on several user-input parameters. One important variable is the model scale factor, λ. Model data is input for the full-scale Space Station. To construct replica scale finite-element models, the replica scale factor is set to a value less than unity. Software in the finite-element runstream is then executed to scale all of the geometric and inertial model properties according to the replica scaling laws presented in Section 2.1 (Table 2.1-1). Following the construction of a finite-element model, a modal analysis is performed resulting in flexible and rigid-body modes and frequencies. A component modal kinetic energy table is constructed based on the results, showing the relative distribution of energy between the components of the structure for each mode. The modal component kinetic energy rankings were useful in identifying the primary system modes.

Two other runstreams are designed to create and analyze a scaled model of the respective configurations suspended by cables from the domed ceiling of the LaRC LSL facility. Both of these runstreams automatically create nodes on the assumed LSL ceiling directly above user-specified nodes on the structure (discussed in the following paragraphs). Following this, axial elements representing cables are created to suspend the structure at these locations. The cross-sectional areas of each of these cables is calculated internally based on the constraints of maximum working stress and uniform sag at the cable/structure interfaces under the influence of gravity. A table containing summary information regarding the cables is also produced. Columns in this table indicate the nodes at each end, tension, length, area, and fundamental frequency of each cable in the test environment. In addition, the modal kinetic energy table discussed above is produced following the solution of the eigenvalue problem. Figure 3.1.3-1 presents a

flow chart outlining the procedure to size the cable areas and the EAL processors that are used. This procedure is discussed further in Sections 3.3.5.1 and 3.3.5.2.

Listings of the EAL runstreams are provided in Appendix B. Each runstream is designed to accept several parameters from the user, in addition to the processor resets currently available in EAL. These additional resets are conveniently placed at the beginning of the runstreams and should be checked prior to each execution. In the unconstrained models, the only reset available is the scale factor (SL), but in the models simulating possible test configurations, several other parameters may be varied: The distance above the LSL floor (AFD) may be set to any feasible value, however, caution should be exercised when adjusting this parameter because no internal checks are performed to alert the user when the model exceeds the size of the LSL. NVA denotes the model axis pointing toward the ceiling of the LSL, and may assume a positive or negative value depending on the desired test configuration. The maximum allowable stress in the cables, input as SIGW, should be based on the working stress of the cable material in the test environment. Cable density and elastic modulus are input as RHOC and ECAB, respectively.

The user is required to determine and input the number of cables (NHN) used during each execution of the runstream. The locations of the cables should also be determined by the user prior to execution. Node numbers corresponding to the cable attachment points on the structure are input in the SUSP NODS table. These numbers must be integers and input according to EAL TABLE formatting instructions (i.e., one value per line or multiple values on a single line separated by colons). The runstreams automatically calculate the total number of nodes in the model as well as the coordinates of the suspension points on the LSL based on this input.

3.1.4 Model Verificiation

The mass properties for the two configurations are documented in the DR-02, with only a few minor exceptions. Tabular comparisons of several parameters are presented in Tables 3.1.4-1 and 3.1.4-2 for the Step-2 build-

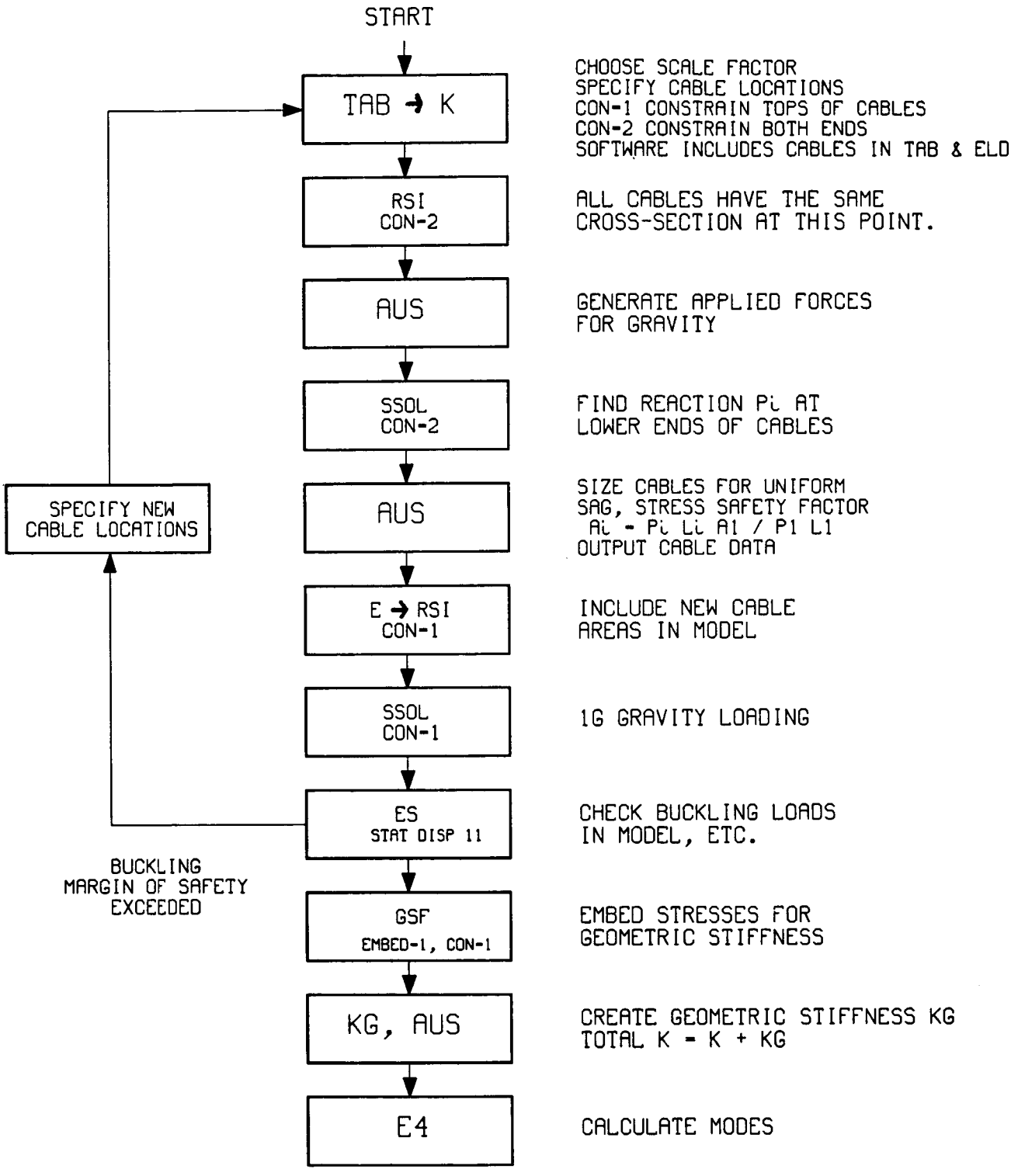

FIGURE 3.1.3-1 EAL RUNSTREAM FLOW DIAGRAM FOR SUSPENDED MODEL ANALYSES

TABLE 3.1.4-1. STEP-2 BUILD-UP STAGE MASS PROPERTIES COMPARISON

Item	Step-2 Build-up Stage FE Model	DR-02	% Diff.
Weight [lbs]	73654	67450	8.4
C.G. Location			
X [in]	12.68	12.63	0.4
Y [in]	-583.23	-586.46	0.6
Z [in]	0.00	0.00	0.0
Mass Moments of Inertia			
I_{xx} [sl-ft^2]	5.6E+08	5.0E+08	8.0
I_{yy} [sl-ft^2]	6.0E+05	5.0E+05	17.0
I_{zz} [sl-ft^2]	5.5E+07	5.0E+07	8.0

TABLE 3.1.4-2. ISS MASS PROPERTIES COMPARISON

Item	ISS Configuration FE Model	DR-02	% Diff.
Weight [lbs]	518,398	512,087	1.2
C.G. Location			
X [in]	-203.88	-176.76	13.3
Y [in]	-97.98	-107.16	8.6
Z [in]	-229.56	-231.24	0.7
Mass Moments of Inertia			
I_{xx} [sl-ft^2]	1.8E+08	1.7E+08	5.6
I_{yy} [sl-ft^2]	7.9E+07	7.6E+07	3.8
I_{zz} [sl-ft^2]	1.3E+08	1.1E+08	15.4

up stage and the ISS configuration, respectively. These tables reveal small discrepancies in the total mass and certain inertia values, but the centroids and other inertia values agree well. The differences in total mass (and the Iyy inertia term, to a lesser extent) between the models and the DR-02 estimates are attributed to the weight of the utility trays on the transverse boom, outboard of the alpha joints. The DR-02 assumes that the utility trays span only the region between the alpha joints along the transverse boom. However, the weight of the trays is present in the finite-element models along the entire length of the boom. The cross-product of inertia errors, most noticeable in the Ixz term of the build-up stage configuration, are attributed to the unidirectionality of the internal truss diagonals. The DR-02 assumes a uniform mass distribution in the cross-section of a symmetric truss, whereas the models accurately represent the diagonal bias in the distribution. Table 3.1.4-3 in this report, and Tables 5.0-1 to 5.0-7 in the DR-02 list the inertial properties of components modeled as rigid masses in the build-up and ISS configurations, respectively.

3.2 FULL-SCALE MODEL ANALYSES

In order to determine the baseline modal characteristics of the two configurations, full-scale models (one for each configuration) were analyzed, resulting in vibrational modes and frequencies of the flight articles. From the results, primary system modes were selected. The results of these analyses are described in the following subsections.

3.2.1 Step-2 Build-up Stage Configuration

Results from the modal analysis of the full-scale Step-2 build-up stage are presented in Table 3.2.1-1. System modes, indicated by some level of participation in all components, are described in this table and the corresponding natural frequencies are listed. Plots of these eleven modes are provided in Appendix C. These modes were targeted for testing in this study because of their global influence on several structural components and subsystems. Primary modes are easily detected through an examination of the component modal kinetic energy table. Interspersed among the system modes

TABLE 3.1.4-3. CONCENTRATED MASSES (STEP-2 BUILD-UP STAGE FE MODEL)

Item	Center of Mass [in] X	Y	Z	Inertia [sl-ft^2] X	Y	Z
Navigation Base (723 lbs)	-150.0	-1181.0	0.0	532.9	266.6	266.6
Port GN&C/DMS Module (5040 lbs)	0.0	-984.0	0.0	3715.3	1857.5	1857.5
Port ESS Module (4442 lbs)	0.0	-1968.0	0.0	3274.3	1637.1	1637.1
Port Alpha Joint (1450 lbs)	0.0	-1772.0	0.0	534.2	1068.8	534.4
Port S/A Beta Gimbal (1830 lbs)	0.0	-2205.0	0.0	674.5	1349.0	674.5
Fore RCS Module (3088 lbs)	197.0	-3543.0	0.0	1138.1	2276.3	1138.1
Aft RCS Module (3088 lbs)	-197.0	-3543.0	0.0	1138.1	2276.3	1138.1
Assembly Fixture (FSE) (2500 lbs)	0.0	164.0	0.0	9293.0	3490.1	9293.0
Thermal Rad. Beta Joint (1191 lbs)	0.0	-1310.0	0.0	439.0	877.8	439.0
Stbd. ESS Module (4429 lbs)	0.0	1968.0	0.0	3274.3	1637.1	1637.1
HR&T Bay (2230 lbs)	0.0	-787.0	0.0	821.9	1643.8	821.9
Stbd. Alpha Joint (1450 lbs)	0.0	1772.0	0.0	534.4	1068.8	534.4
Stbd. S/A Beta Joint (1830 lbs)	0.0	2205.0	0.0	674.5	1349.0	674.5
Berthing Mechanism (1055 lbs)	138.0	0.0	0.0	332.4	179.0	179.0
Mobile Service Center (8000 lbs)	143.0	-984.0	0.0	11151.8	5575.8	5575.8

TABLE 3.2.1-1. FULL-SCALE MODAL CHARACTERISTICS (SYSTEM MODES, STEP-2 BUILD-UP STAGE)

STEP-2 BUILD-UP STAGE

MODE	FREQ.	DESCRIPTION
22	0.16	1-T TBOOM
23	0.35	1-B TBOOM (Y-Z)
24	0.35	1-B TBOOM (X-Y)
41	0.96	2-B TBOOM (Y-Z)
42	0.97	2-B TBOOM (X-Y)
51	1.68	3-B TBOOM (Y-Z)
52	1.70	3-B TBOOM (X-Y)
61	1.83	2-T TBOOM
62	2.61	4-B TBOOM (Y-Z)
63	2.71	4-B TBOOM (X-Y)
72	3.06	3-T TBOOM

TBOOM - TRANSVERSE BOOM
PRCH - MODULE PORCH

C - CANTILEVER
T - TORSION
B - BENDING

(ALL FREQUENCIES ARE IN HZ.)

TABLE 3.2.2-1. FULL-SCALE MODAL CHARACTERISTICS (SYSTEM MODES, ISS)

ISS

MODE	FREQ.	DESCRIPTION
27	0.22	1-B TBOOM (Y-Z)
28	0.23	1-B TBOOM (X-Y)
29	0.32	2-B TBOOM (Y-Z)
30	0.36	1-B KEELS (X-Z)
31	0.44	2-B TBOOM (X-Y)
32	0.50	2-B KEELS, C PRCH (X-Z)
42	0.63	1-B KEELS (Y-Z)
55	0.66	1-B KEELS (Y-Z), 1-T TBOOM
56	0.70	1-T TBOOM, KEELS
57	0.87	1-T (Y-Z)
58	1.05	3-B TBOOM (Y-Z)

TBOOM - TRANSVERSE BOOM
PRCH - MODULE PORCH

C - CANTILEVER
T - TORSION
B - BENDING

(ALL FREQUENCIES ARE IN HZ.)

are various solar array, thermal radiator, and other appendage modes of local extent and low modal mass. System modes for this configuration are a subset of the 75 modes below 3.25 Hz.

3.2.2 ISS Configuration

The system mode descriptions for the full-scale ISS configuration are presented in Table 3.2.2-1. Plots of these eleven modes are given in Appendix C. These modes were chosen from the 58 modes below 1.0 Hz using component modal kinetic energy rankings. The mode shapes and frequencies shown here are in agreement with the results of simpler continuum beam models given in the DR-02.

3.2.3 Modal Comparison Criteria

The high modal density of the Space Station severely complicates the comparison of the free-free modes obtained by analysis with the "distorted" modes obtained from analytical models. The comparison of a large number of mode shape plots is both time consuming and highly subjective. Conseqently, two figures of merit (typically used to compare test data with analytical model data) are employed. They are the Cross-Orthogonality and the Modal Assurance Criterion. These parameters measure the similarity between two modes in slightly different ways.

The Cross-Orthogonality Matrix is defined as follows:

$$[\phi_a]^T\ [M]\ [\phi_b] = [XO] \qquad (3.2.3\text{-}1)$$

where: $[\phi_a]$ = Free-Free Modes
$[\phi_b]$ = Modes of the Suspended Structure

This matrix is rectangular with the number of rows equal to the number of modes in $[\phi_a]$ and the number of columns equal to the number of modes in $[\phi_b]$. It represents the kinetic energy or modal mass distribution similarities between the modes in question. If the mode shape matrices are identical, the XO matrix becomes the identity matrix. Since the free-free

modes and suspended modes are not guaranteed to be paired one-to-one in the same order, the scalar XO(i,j) represents the degree of correlation between free-free mode i and the suspended mode j. Differences in the mode shapes (more specifically the modal mass distribution over the mode shapes) result in XO entries in the range of $-1 < XO(i,j) < +1$, where a value of zero indicates that the two modes are mass-orthogonal, and a value of unity (either positive or negative) indicates that the modes are identical. Typically, modes with Cross-Orthogonality values greater than .85 are considered to be similar.

The Modal Assurance Criterion matrix is defined entry-by-entry as follows

$$[MAC(i,j)] = \left\{ \frac{([\phi_{ai}]^T [\phi_{bj}])^2}{[\phi_{ai}]^T [\phi_{ai}] \cdot [\phi_{bj}]^T [\phi_{bj}]} \right\}^{\frac{1}{2}} \qquad (3.2.3\text{-}2)$$

This matrix is also rectangular having the same dimensions as the corresponding XO matrix. Perfectly correlated modes produce entries of one (always positive), whereas uncorrelated modes yield zero entries. Since this measure of modal similarity is independent of the mass matrix, it measures only the geometric similarities between the two modes shapes. Thus, a value of zero indicates that the two modes are shape-orthogonal and a value of unity indicates that the modes have the same shape.

Overall trends in the XO and MAC matrices are usually similar, but corresponding entries in the arrays seldom match exactly. This is due to the weighting effect of the mass matrix on the XO values. High XO entries corresponding to significantly lower MAC entries indicate that the heaviest parts of the structure are moving in a consistent manner in both modes, but that the overall shapes of the two modes are not similar.

The MAC formulation may also be used when the two mode shape matrices are derived from different models (i.e., different mass or stiffness matrices). In this situation, the XO matrix will contain erroneous entries because the two mode shape matrices are, by definition, orthogonal to

different mass matrices.

3.2.4 Utility Tray Location Study

In an effort to determine the level of fidelity required in the scale model with respect to the mass distribution of the utility trays, EAL finite-element models were constructed with different mass properties for the utility trays. Another goal of this analysis was to evaluate the implications of using heavier aluminum tubes in the truss as a cost- saving alternative to graphite/epoxy. If the heavier aluminum tubes were employed, the weight of the utility trays could be thought of as "smeared" uniformly over the truss, as opposed to the baseline graphite/epoxy design where the utility trays are located near the diagonally opposite corners of the truss. The extra weight of the aluminum is nearly equal to the weight of the utility trays, so that the utility trays would not have to be added to the test model. Since the build-up configuration is influenced more than the ISS configuration by changes in the truss, the EAL model constructed for this trade study was obtained by modifying the full-scale Step-2 build-up stage model. The model was modified to include the two utility trays (for redundancy) at diagonally opposite corners of the truss. This represents the highest practical non-uniformity in redundant tray assembly placement and therefore the largest departure from uniformly distributed mass effects.

Modal characteristics of the original and modified build-up stage models are compared in Tables 3.2.4-1 and 3.2.4-2. The data in Table 3.2.4-1 was obtained by locating the utility trays in the corners which lie along the axis of the interior diagonal. This placement is probably not desirable, but yields the worst-case cross-product of inertia. The data in Table 3.2.4-2 was obtained by positioning the trays in the other two diagonally opposite corners along the axis of the truss. Comparing these tables, no appreciable differences between the two possible locations are noted. Based on this, the discussions to follow make no distinction between the two tray placement schemes.

The tables referenced above indicate that several small differences are introduced by the distributed mass assumption, but the effects of these

TABLE 3.2.4-1. UTILITY TRAY PLACEMENT TRADE STUDIES
(STEP-2 BUILD-UP STAGE, ON DIAGONAL AXIS PLACEMENT)

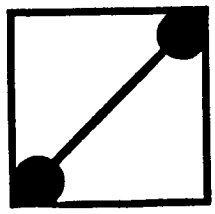

● Denotes Utility Trays

For 75 modes below 3.25 Hz	Freq. Change [%]	MAC	Max(MAC)
Maximum	7.69260	1.00000	1.00000
Minimum	0.00000	0.00000	0.44728
Mean	0.98776	0.82491	0.94170
Standard Deviation	2.01050	0.33666	0.12088
For the system modes			
Maximum	7.69260	0.99549	0.99549
Minimum	2.87555	0.59880	0.59880
Mean	5.56050	0.88684	0.88684
Standard Deviation	1.47316	0.17127	0.17127

TABLE 3.2.4-2. UTILITY TRAY PLACEMENT TRADE STUDIES
(STEP-2 BUILD-UP STAGE, OFF DIAGONAL AXIS PLACEMENT)

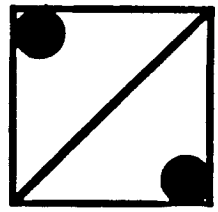

● Denotes Utility Trays

For 75 modes below 3.25 Hz.:	Freq. Change [%]	MAC	Max(MAC)
Maximum	7.69517	1.00000	1.00000
Minimum	0.00000	0.00002	0.44921
Mean	0.98766	0.82601	0.94074
Standard Deviation	2.01032	0.33408	0.12039
For the system modes			
Maximum	7.69517	0.99747	0.99747
Minimum	2.87517	0.55073	0.60004
Mean	5.39726	0.85997	0.86698
Standard Deviation	1.50328	0.18914	0.17760

changes on the overall representation of the structure (referring to statistics involving all 75 modes below 3.25 Hz.) are quite small. The largest shift in any natural frequency is less than 8% (modes 41 and 42) and the lowest MAC value is 0.45 (mode 53). However, these two data points are anomalous and infer less overall correlation than is actually present. The mean frequency shift and MAC value for the 75 modes considered are quite acceptable (approximately 1.0 Hz. and 0.942, respectively), as are the standard deviations of the two values (2.0 Hz. and 0.121, respectively).

For the eleven system modes, statistics are presented which indicate less correlation than observed for system and non-system modes considered together. This is because each of the system modes involves the transverse boom of the structure, the subject of this trade, to a larger extent than the other modes. Examining the statistics of a population containing only these modes, it is noted that the frequency error bandwidth no longer encompasses the zero value in the +/- 3σ band. Further, there is no longer any perfect modal shape correlation (indicated by a 1.00 in either of the Modal Assurance criteria columns). It is also noted that the order of the system modes is unchanged by the assumptions regarding utility tray mass distribution.

One puzzling aspect of this analysis is the lack of correlation found for mode 61. This mode, shown in Figure 3.2.4-1, is a mass-weighted, second torsional mode of the truss which weakly correlates to mode 55, a non-system mode. The low correlation of mode 72, a mass-weighted third torsional mode of the truss, suggests that the mass distribution of the utility trays influences torsional motions of the truss more than bending motions. The other slightly uncorrelated mode (51), the W-bending mode of the transverse boom with more torsional coupling than any of the other bending modes, also supports this assertion.

In summary, when considering torsional motions of the transverse boom as opposed to bending motions, there will be more correlation between the model and the flight article if the locations of the utility trays are carefully replicated. However, it should be noted that the Step-2 build-up stage is dominated by the presence of the transverse boom, the weight of

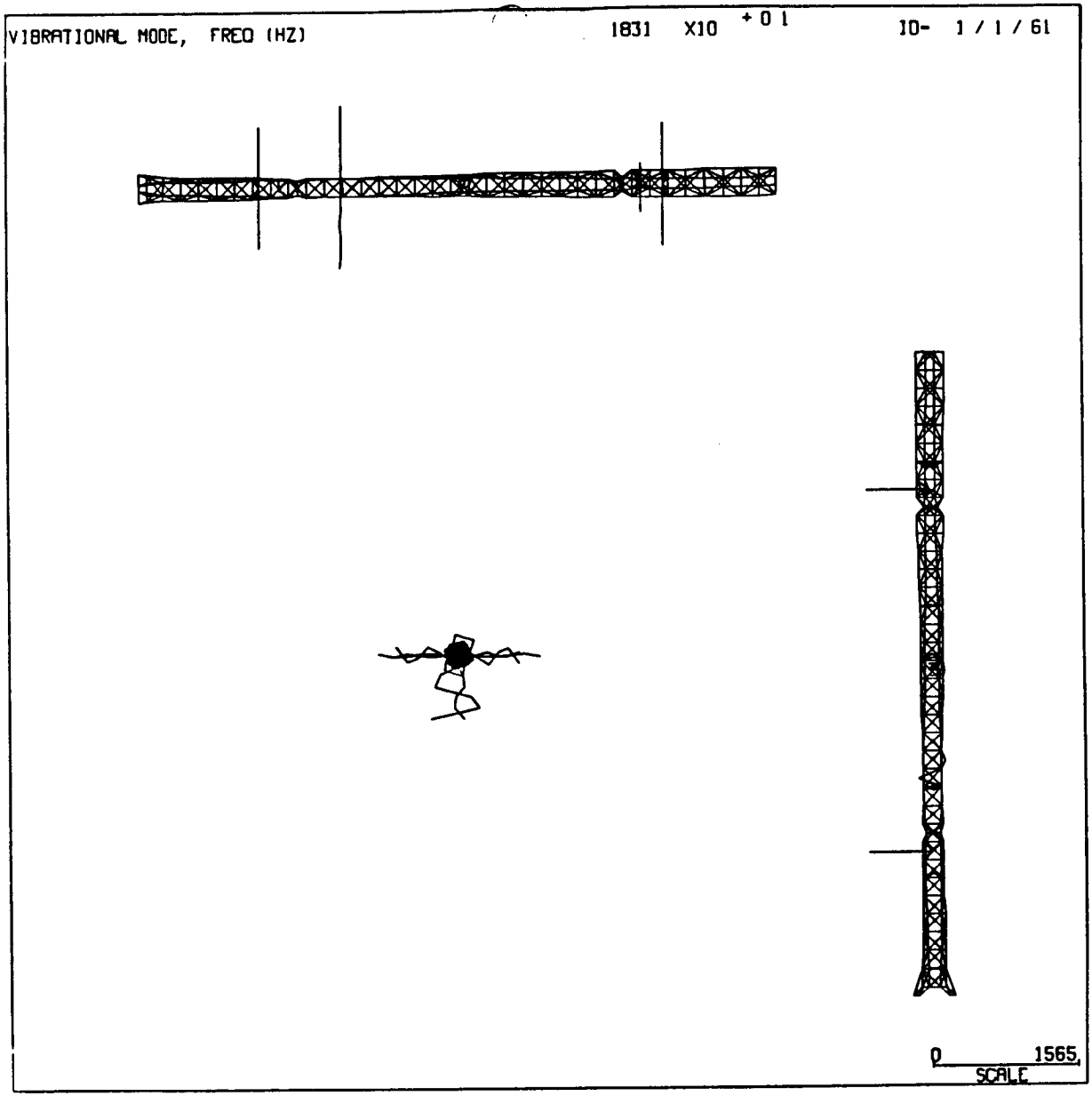

FIGURE 3.2.4-1: MODE 61, STEP-2 BUILD-UP STAGE

which is dominated by the utility trays. For the ISS configuration, the utility trays dominate the structural weight to a much lesser degree. Therefore, their placement will not influence the resulting modal characteristics to the extent indicated above. Overall, the results of this analysis show that there is a compromise in model fidelity associated with the use of aluminum tubes which must be traded against the potential cost savings.

3.3 SUSPENSION ANALYSES

The suspension system for the model serves two primary functions. The first is to support the scale model in a way which permits rigid-body motion by simulating free-free boundary conditions. The second is to off-load the gravity forces on the structure and minimize the amount of gravity-induced stresses in the model. The ideal suspension system for the scale model would allow unrestrained motion in all six rigid degrees of freedom and would support the structure in such a way that all the internal stresses are zero.

The cable-type suspension system baselined for this study permits small rigid-body motions only in the plane parallel to the floor. Cable-type suspension systems depart from the ideal suspension system in four ways:

1) The stiffness of the cable restrains the vertical motion of the model. With stiff cables, the vertical motion of the model could be completely constrained. With softer cables, cable "plunge" modes could occur at frequencies which couple with the structural modes of the model. This effect is comparable to a set of vertical ground springs attached to the model.

2) The pendulum modes in the plane parallel to the floor have a non-zero frequency. These system and subsystem pendulum modes may couple with the structural modes of the model or its appendages, distorting the test results. This effect is comparable to a set of horizontal ground springs attached to the model.

3) Taut cables have violin or "string" modes where the cable itself vibrates in the transverse direction at a particular fundamental frequency and its harmonics. These cable string modes may couple with the structural modes of the model in the same frequency range.

4) The cables, cable connectors, and other suspension equipment add weight to the model, changing the modal mass.

This section of the report describes preliminary analyses that examine these undesirable suspension system effects as a function of the scale factor. Subsequent sections document more detailed analyses of the suspension system interactions with the structure at various scale factors, including all of the effects mentioned in items (1) thru (4).

3.3.1 High versus Low Strain-Rate Cable Suspension Systems

One way to minimize the constraints imposed by the suspension system on the vertical motion of the model (item 1 above) is to use a soft (low stiffness) cable material such as rubber or bungee cord. The candidate material must be capable of sustaining large strains because the combination of soft cables supporting large masses in gravity results in large displacements. The amount of strain induced in the cable material can be reduced by using longer cables. Large structures tested in confined spaces (such as the Space Station in the LSL) typically require soft cables that are both long and highly strained to minimize the coupling between cable plunge modes and structural modes of the model.

Based on a simple lumped-mass model, the equation for the frequency ratio of the lowest structural mode to the cable plunge mode can be written:

$$\frac{f_1}{f_p} = \frac{2\pi f_1}{\lambda}\sqrt{\frac{\beta L}{g(1+\beta)}} \qquad (3.3.1\text{-}1)$$

where: β = strain in the cable, λ = scale factor, f_p = plunge-mode frequency, and f_1 = full-scale frequency.

Figure 3.3.1-1 shows the results of a trade study comparing the ratio of the structural and plunge mode frequencies with the strain in the cable material. This analysis accounts for the usable cable length at a given scale factor for the ISS scale model hanging with the x-axis vertical in the LSL. These curves show that, as the scale factor is increased from .10 to .25, the amount of cable strain required increases greatly. Typically, a minimum value for f_1/f_p of 5 is desirable. The results show that, at 1/10 scale, a value of 5 can be achieved with the cable material strained 5%. At 1/4 scale, a material capable of withstanding greater than 28% strain is required, limiting the selection of available soft cable materials. The second axis in Figure 3.3.1-1 presents similar information for the case where f_1/f_p is the ratio of the solar array mode frequency (.1 Hz) to the plunge mode frequency.

A similar trade study can be conducted by plotting the length of cable required to achieve a frequency ratio of 5 versus the cable strain. Equation 3.3.1-1 above can be rewritten:

$$L = \frac{\lambda^2 g}{4\pi^2 f_1^2}\left(\frac{f_1}{f_p}\right)^2 \frac{(1+\beta)}{\beta} \qquad (3.3.1\text{-}2)$$

According to this equation, the length of cable required increases as the square of the scale factor. Figure 3.3.1-2 shows the trade results for the first primary structural mode (.222 Hz full-scale) and for the solar array modes (.1 Hz full-scale).

In summary, the LSL is not large enough to permit the use of a soft suspension system in conjunction with a large (fourth or fifth scale) model without incurring high strain rates in the cables. Candidate materials capable of such high strain rates (i.e. rubber surgical tubing) typically exhibit high damping and nonlinear stiffness characteristics, further complicating the problem. In addition, safety becomes a concern because of the large amount of stored energy in the cables.

By way of contrast, the primary drawback of a "hard" or stiff cable

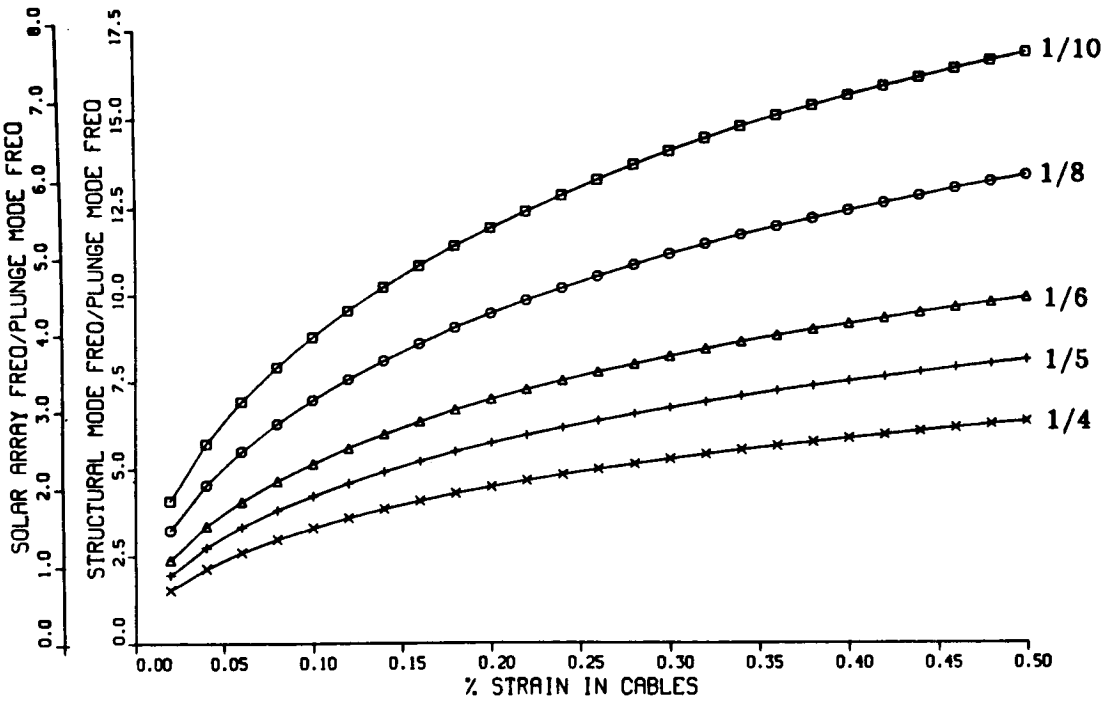

FIGURE 3.3.1-1: FREQUENCY RATIOS VERSUS CABLE STRAIN RATE (ISS) MODEL IN FIXED-SIZE LSL

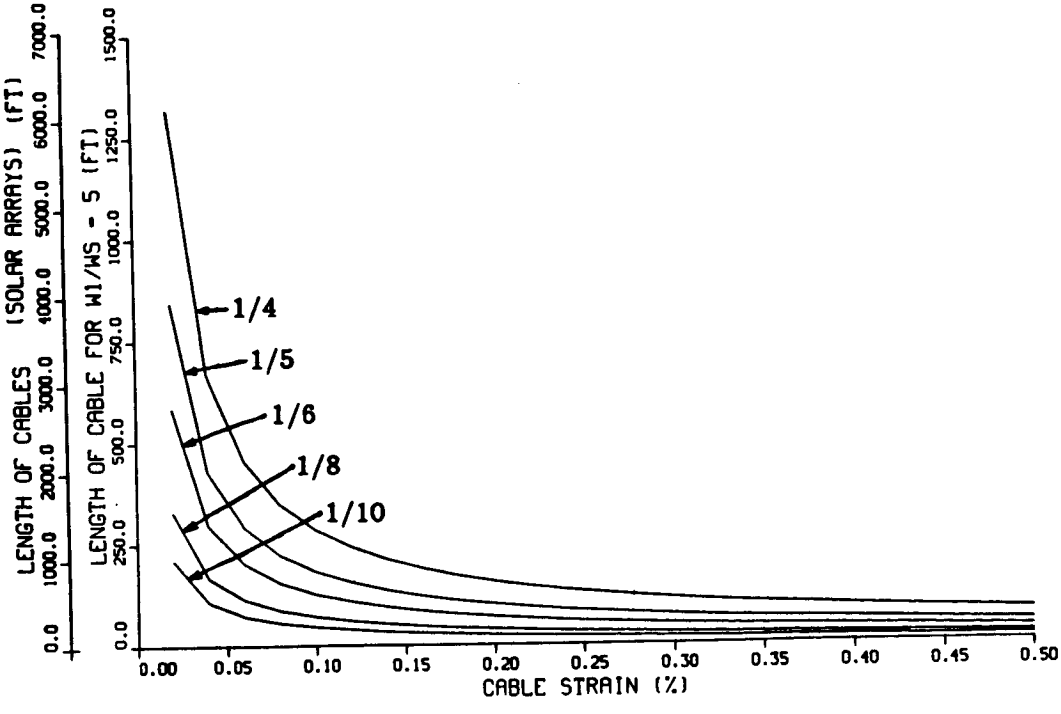

FIGURE 3.3.1-2: LENGTH OF CABLE VERSUS CABLE STRAIN RATE (ISS) FOR A FREQUENCY RATIO OF 5.0

suspension system is that the motion of the model in the vertical direction is restrained. This does not pose a problem for planar modes which only involve motion in the plane parallel to the floor. If the model was characterized by mostly planar modes, the model could be suspended in three orientations (x-vertical, y-vertical, and z-vertical) and tested for all of the possible modes. Modes which would be difficult to test, under these circumstances, are modes with significant motion in all three orthogonal directions.

Because of the aforementioned problems with soft cable suspensions, the remainder of this study assumes a relatively hard suspension system. The effect of a hard suspension system on the non-planar modes of the Space Station is examined in later sections. Later results show, for the most part, that the majority of the Space Station modes are planar.

3.3.2 Shadow Structure Analyses

It is envisioned that the Space Station scale model will be suspended by cables from a supporting "shadow structure" in the LSL, which is attached to the domed ceiling of the building (see Figure 3.3.2-1). The shadow structure allows the test article to be hoisted evenly from the floor as sections of the model are constructed. It also accomodates many suspension cables while remaining connected to the LSL ceiling at fixed attachment points. Previous studies [1,4] have suggested two types of shadow structures: one which is fixable to the ceiling, and one which is suspended from the ceiling by cables. Figure 3.3.2-2 summarizes the results of a trade study encompassing both of these alternatives. It was performed to determine the relationship between the vertical location of the shadow structure and the rigid-body pendulum modes of the suspended model.

The simple rigid-body model shown in the figure includes the mass and the inertia of a 1/4 scale model of the ISS lumped at the c.g. The shadow structure is assumed to have a mass equal to 2% of the total scale model mass, equivalent to four times the mass of the scale model structure. This configuration was analyzed as a triple-pendulum problem using closed form equations to produce the curves shown. At the extreme values of Ls/Lm

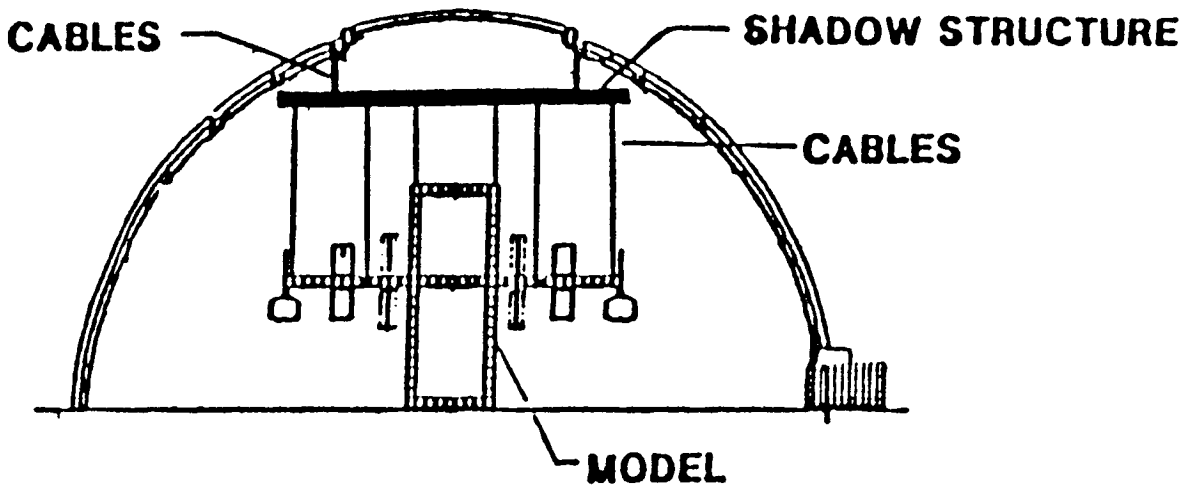

FIGURE 3.3.2-1: SHADOW STRUCTURE SUSPENSION CONCEPT

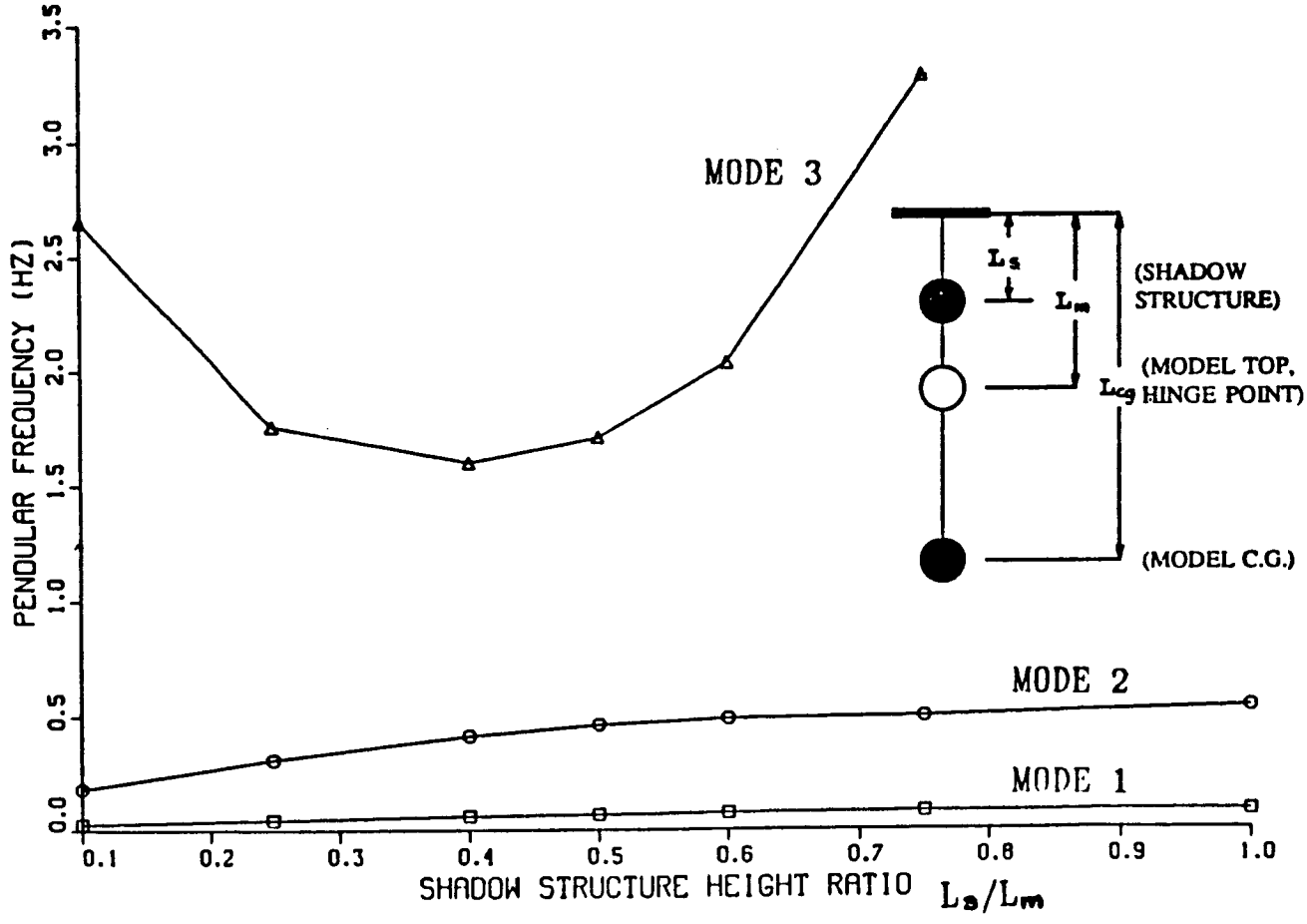

FIGURE 3.3.2-2: PENDULAR FREQUENCIES OF SUSPENSION SYSTEM INCORPORATING A SHADOW STRUCTURE

(0 or 1), no shadow structure exists and there are only two pendulum modes. Between these two values, a triple pendulum mode exists, which could interfere with the dynamics of the structural modes being tested. Other analyses, using both larger and smaller shadow structure masses, produced similar results with slight variations in the frequency of the triple pendulum mode. This result suggests that the problem is governed by the test geometry rather than the relative masses of the test article and the shadow structure. Because of the possibility of dynamically coupling the shadow structure pendulum modes with the structural modes of the model, the shadow structure was assumed to be rigidly attached to the LSL ceiling for the remainder of the study.

3.3.3 Articulation Capabilities

The option of rotary joint articulation was considered from the viewpoint of both manual and automated articulation. Manual articulation would provide the model with a capability to be tested with the solar arrays and radiators locked in any orientation. Automated articulation would provide the additional capability of testing the model while the solar arrays, radiators, and the outer transverse boom are tracking. Due to suspension system constraints in the vertical direction, automated articulation of most of these joints is not feasible. This is exhibited in a graphic way by considering the "transverse boom horizontal" suspension configuration, where cables are attached to the model at several locations in a horizontal plane. If the outer transverse boom is continuously rotated by a motor in the alpha joint, the tips of the solar arrays and radiators attached to the transverse boom will displace vertically, causing the cables to slacken, and redistributing the gravity load in the scale model.

If the cable locations and tension levels are adjusted at each joint rotation desired, the joints can be manually articulated to the desired position and locked. Although it does not simulate the noise source of a continuously tracking alpha joint, this type of joint articulation could be useful, and is recommended as a scale model requirement. A sufficient number of "lock positions" should be provided, possibly by introducing clamps on a continuous interface rather than using discrete lock points around the

joint. Motors and drive mechanisms could be simulated by concentrated masses.

The universal (beta and radiator) joints which "step" the solar arrays and radiators could be articulated during the test, but with uncertain results due to the flexibilities of the appendages. Wire mesh, simulating the surface of these structures, could (and probably will) be removed during dynamic testing. In this configuration, the appendages in question are simply tuned beams extending radially outward from the truss. Bearing races, fitted around these beams and serving as "slip rings", will allow the rotation of these appendages. However, it is anticipated that even small amounts of friction in the bearing surfaces could introduce an undesirable "stick-slip" behavior as the joint is rotated. Caution would have to be exercised to insure that the excitation supplied to the structure is scaled properly, and that this stick-slip behavior does not cause "unscaled" excitation of the low frequency lateral bending modes of the solar arrays and radiators. Because of this complexity, automated rotation of the beta and radiator joints is not recommended for the initial test phases of the model.

Articulations which are not related to joint rotations, such as motion of the MRMS, introduce the same gravity loading problems discussed above if the articulated masses are not off-loaded by the suspension system as they move. A suspension system capable of providing such support would be quite complicated and expensive, but should be considered because of the potential usefulness of the capability to model atypical and/or unanticipated configurations during construction and operation, and servicing.

Another important consideration which should be noted with respect to component articulation is the necessity of constructing a FE model of each configuration tested. Analyses of such models typically provide the basis for a test plan indicating target modes and cable tension levels.

3.3.4 Suspension System Boundary Condition Analysis

Preliminary analyses were conducted to investigate the ability of the

suspended Step-2 build-up and ISS models to emulate the free-free dynamic behavior of the full-scale structures. Modified versions of the unconstrained full-scale FE models were used to determine the effects of an infinitely stiff suspension system. This condition is simulated by constraining the translational degree-of-freedom in the vertical direction and the rotational degrees-of-freedom in the other two orthogonal directions at every node in the model. This preliminary analysis does not include dynamic interactions with the vertical or "plunge" modes in the cables, the pendulum modes, nor the cable string modes. The analysis independently addresses the effects of an infinitely "hard" suspension system (item 1 in Section 3.3). Since the cables in the actual suspension system will have less than infinite stiffness, this analysis yields an upper bound for the effects of the suspension system vertical constraints.

The analyses discussed in the paragraphs to follow were conducted by applying the above-mentioned contraints to the full-scale model in each of the three orthogonal test configurations (see Figure 3.3.4-1). The resulting mode shapes are compared with the free-free mode shapes for the Step-2 build-up stage and ISS configurations of the Space Station using the Cross-Orthogonality and Modal Assurance criteria measures. Given that all of the vertical degrees of freedom are constrained and that the mode shapes scale as unity, the Modal Assurance and Cross-Orthogonality results of this analysis are independent of the model scale factor. The same Cross-Orthogonality values would result from a 1/4 scale model analysis as for the full-scale model analysis.

3.3.4.1 Results for Step-2 Build-up Stage Model

The results from the boundary condition analysis of the full-scale Step-2 build-up stage model are shown in Table 3.3.4.1-1. In all cases, the frequencies of the constrained modes are higher than those of the corresponding unconstrained case because of the stiffness added to the system. In order to determine the feasibility of identifying any particular mode, the Modal Assurance and Cross-Orthogonality values are examined. Normally, testable modes are indicated by values above 0.75 and 0.85, respectively, but due to the conservativeness of the model, modes may be

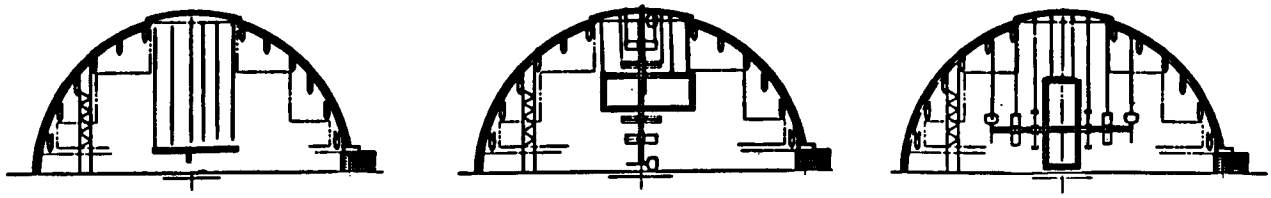

X-VERTICAL Y-VERTICAL Z-VERTICAL

CROSS-ORTHOGONALITY

$$XO = [\phi_A]^T [M] [\phi_B]$$

XO = 1.00, MODES ARE IDENTICAL
XO = 0.00, MODES ARE MASS-ORTHOGONAL

MODAL ASSURANCE CRITERION

$$MAC = \left[\frac{[\phi_A^T \phi_B]^2}{[\phi_A^T \phi_A] \cdot [\phi_B^T \phi_B]} \right]^{1/2}$$

MAC = 1.00, MODES ARE IDENTICAL
MAC = 0.00, MODES ARE SHAPE-ORTHOGONAL

A = FREE FREE B = SUSPENDED

FIGURE 3.3.4-1: ORTHOGONAL SUSPENSION CONFIGURATIONS (ISS)

TABLE 3.3.4.1-1. BOUNDARY CONDITION ANALYSIS RESULTS (STEP-2 BUILD-UP STAGE)

STEP 2 BUILD-UP STAGE				
MODE	FREQ.	X	Y	Z
22	0.16	-	1.00	-
23	0.35	-	0.77	0.93
24	0.36	0.94	-	-
41	0.96	0.93	-	-
42	0.97	0.72	-	-
51	1.67	0.79	-	-
52	1.70	-	-	0.81
61	1.83	-	0.99	-
62	2.61	0.87	-	-
63	2.71	-	-	0.90
72	3.06	-	0.73	-

testable at lower values. The information given in this table (only XO values are presented) indicates a reasonable probability that all of the system modes can be detected with the possible exception of modes 47, 51, 52 and 72.

3.3.4.2 Results for ISS Space Station Model

The Cross-Orthogonality results for the ISS Space Station scale model are shown in Table 3.3.4.2-1 for the system modes below 1 Hz full-scale. The data show that in order to obtain the system modes of the ISS Space Station, the model must be tested in all three test configurations. The seven modes with XO values greater than .85 are essentially planar and somewhat unaffected by the vertical constraints of the suspension system. Many of the modes had higher Cross-Orthogonality values than Modal Assurance values. This indicates that the movement of the large masses (or the modal mass distribution) in each mode is nearly the same, and that the motions of the lighter appendages (i.e. solar arrays and radiators) are different. Overall, the results indicate a high probability of acquiring test data for system modes 27 thru 31, 57, and 58. Modes 32, 42, 55, and 56 may be distorted by the effects of the suspension system vertical constraint. Figure 3.3.4.2-1 summarizes the results for all the modes below 1 Hz and illustrates mode 32, which involves motion in all three translational degrees of freedom, making it difficult to simulate in the LSL.

3.3.5 Detailed Suspension System Analysis

This section documents the more detailed analyses that were performed to evaluate the relationship between the model scale factor and the ability of the suspended scale model to emulate the free-free dynamic behavior of the Space Station. These analyses include the effects of the suspension vertical stiffness and the interaction of the pendulum modes while the model is hung in the LSL. The cable sizes, weights, and "string" mode frequencies are calculated independently using closed-form equations. Trade studies are conducted to determine the minimum number of cables required and the location of the cable attachments on the model. The analyses are conducted

TABLE 3.3.4.2-1. BOUNDARY CONDITION ANALYSIS RESULTS (ISS)

		ISS		
MODE	FREQ.	X	Y	Z
27	0.22	0.99	-	-
28	0.23	-	-	0.98
29	0.32	0.99	-	-
30	0.36	-	0.96	-
31	0.44	-	-	0.93
32	0.50	-	0.80	-
42	0.63	0.71	-	-
55	0.66	-	-	-
56	0.70	-	-	-
57	0.87	0.93	-	-
58	1.05	0.93	-	-

- M.A.C. GREATER THAN 70% FOR 32 OF ALL 58 MODES < 1 HZ
- M.A.C. GREATER THAN 70% FOR 6 OF 11 PRIMARY STRUCTURAL MODES < 1 HZ
- M.A.C. GREATER THAN 70% FOR: 13 OF THE X-VERTICAL MODES
  14 OF THE Y-VERTICAL MODES
  5 OF THE Z-VERTICAL MODES
- FREE-FREE MODES WHICH COUPLE INTO ALL THREE TRANSLATIONAL DOF (SUCH AS MODE 32 PICTURED) CANNOT BE SIMULATED

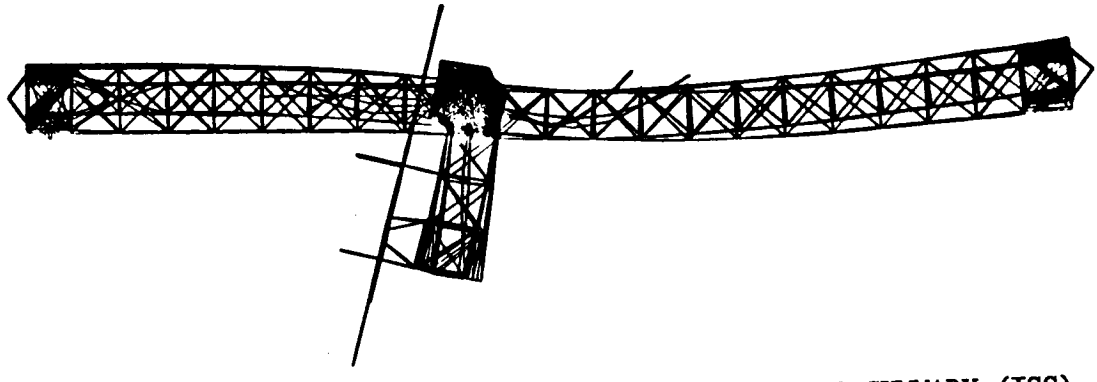

FIGURE 3.3.4.2-1: BOUNDARY CONDITION ANALYSIS RESULTS SUMMARY (ISS)

in all three suspension orientations in the LSL.

3.3.5.1 Development of Detailed Suspension Analysis Techniques

The calculation of frequencies and mode shapes for simple pendulums is straight-forward and well understood. However, the correct analysis of a large flexible structure suspended by numerous cables is more difficult. This section briefly presents some of the dynamic characteristics of more complex pendular systems and outlines the procedure used to calculate the pendulum modes and frequencies. Also included in this section are descriptions of the equations used to describe the "string" modes of the cable.

3.3.5.1.1 Pendulum Mode Analysis

The pendulum analysis methods used in this study were carefully verified prior to implementation. This was accomplished by starting out with simple textbook pendulum models and gradually progressing to more complex structures. At each step, the answers resulting from closed-form equations were compared to the results of finite-element geometric stiffness models. The knowledge gained in this exercise was used to validate the understanding of the fundamental physical concepts before complex models such as the ISS Space Station were analyzed. In addition, several tests were conducted on stick models in order to observe, understand, and check more complex pendular dynamic behavior.

Analytical expressions for simple pendulum models are typically written in terms of masses, inertias and angular coordinates

$$mgl^2\ddot{\phi} + mgl\phi = 0 \qquad (3.3.5.1.1\text{-}1)$$

More complex systems, such as the double pendulum (Figure 3.3.5.1.1-1), are similarly described by matrix equations in the same coordinates. In this case, there are off-diagonal coupling terms in the mass matrix.

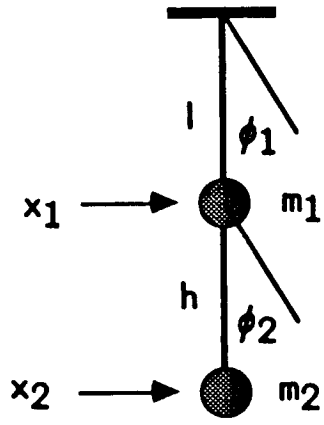

ϕ model: $\quad [M]\ddot{\phi} + [K]\phi = 0$

$$M = \begin{bmatrix} (m_1 + m_2)l^2 & m_2 lh \\ m_2 lh & m_2 h^2 \end{bmatrix} \qquad K = \begin{bmatrix} (m_1 + m_2)lg & 0 \\ 0 & m_2 hg \end{bmatrix}$$

x model: $\quad [M]\ddot{x} + [K]x = 0$

Transformation $\phi_1 = x_1/l$, $\phi_2 = (x_2 - x_1)/h$

$$M = \begin{bmatrix} m_1 & 0 \\ 0 & m_2 \end{bmatrix} \qquad K = \begin{bmatrix} (m_1+m_2)g/l + m_2 g/h & -m_2 g/h \\ -m_2 g/h & m_2 g/h \end{bmatrix}$$

FIGURE 3.3.5.1.1-1 Analytical and Finite-Element Geometric-Stiffness Descriptions of the Linearized Double-Pendulum Model. Both yield equivalent frequencies and mode shapes.

Linear finite-element analyses of pendulum models are based on the dynamic equation

$$m\ddot{x} + kx = 0 \qquad (3.3.5.1.1\text{-}2)$$

The cables may be modeled as axial elements, and the gravity-induced pre-stress in the cables contributes to the formation of a geometric stiffness matrix. The geometric stiffness terms correspond to the displacement coordinates, as opposed to the rotational coordinates in Equation 3.3.5.1.1-1. In the double pendulum example, the FE mass matrix is diagonal and the geometric stiffness matrix is fully populated. This indicates static, rather than dynamic, coupling in the characteristic equation in the FE representation of this configuration. However, both equations in Figure 3.3.5.1.1-1 lead to the same eigenvalues and eigenvectors, though the physical motions are described in different coordinate systems.

During the series of analytical and finite-element comparisons, the FE geometric stiffness method was validated for more complex models involving flexible systems. In this method, the geometric stiffness matrix is created based on the gravity-induced stiffness effects using the entire model and then added to the structural stiffness matrix. The results of FE analyses of large, three dimensional structures with distributed flexibility indicate that the pendulum frequencies and mode shapes are dependent on the mass distribution of the structure, the location, stiffness, and number of cables; and the load distribution among the cables.

Rather than detail all of the analyses here, some representative examples, based on a simple rigid-body finite-element models of the ISS station, are presented in the following paragraphs. Many of these models have the proper mass and inertia properties lumped at the c.g. and serve only as examples. All final results presented later in this report are derived from complete FE models of the appropriate flexible structures.

Figure 3.3.5.1.1-2 depicts the four pendulum mode shapes which may be expected from the Space Station suspended with the z-axis vertical in the

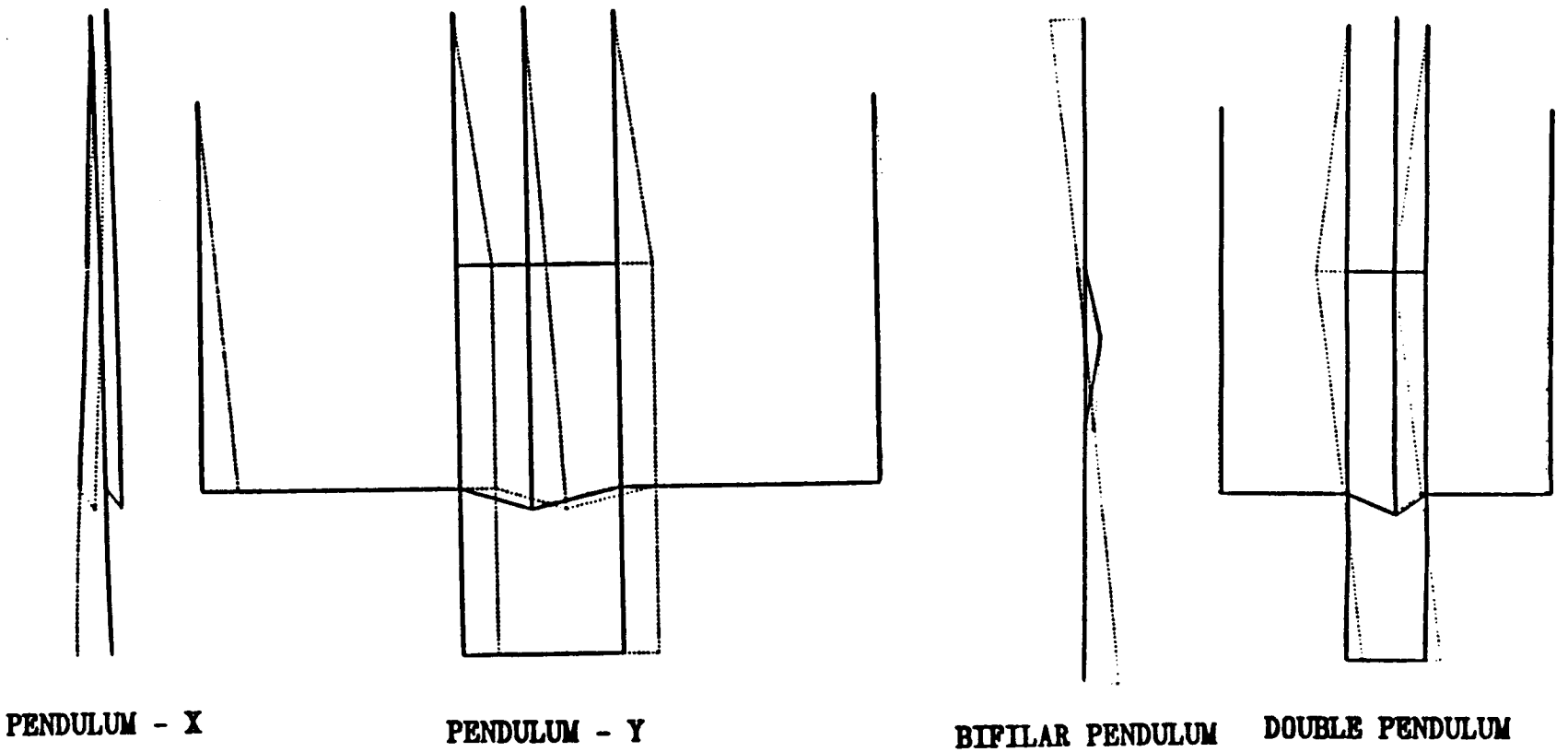

FIGURE 3.3.5.1.1-2: FOUR POSSIBLE PENDULUM MODES (ISS)

LSL. There are two transverse pendulum modes, one bifilar (torsional) pendulum mode, and one double pendulum mode. Figure 3.3.5.1.1-3 illustrates the dependence of the pendulum frequencies on cable location. The solid curve represents the first three pendulum modes (all equal for the x, y, and bifilar modes) for the case where the Station is suspended with cables attached to all of the large rigid masses. The three curves marked by symbols represent the same modes for the case where the Station is suspended by four cables attached to the truss at the locations shown.

Figure 3.3.5.1.1-4 presents the results of an analysis which shows the effect of cable placement on the bifilar (torsional) pendulum mode of a beam. The sloping curve shows the effect of cable placement on the bifilar mode where the beam is modeled using the beam inertia

$$Izz = ml^2/12 \qquad (3.3.5.1.1\text{-}3)$$

The flat curve shows that the pendular frequency does not change for the case where the mass of the beam is lumped entirely at the cable attachment points, regardless of the distance between the cables. This same result applies to the case where there are more than two lumped masses, provided each lumped mass is off-loaded by a separate cable.

Figure 3.3.5.1.1-5 compares the in-plane pendulum mode frequencies for a rigid ISS model supported by two cables, attached to the model at different locations. In this example, the ISS model (z-vertical) is suspended from a flat ceiling rather than the domed LSL, for simplicity. The c.g. of the Space Station is located in the module area, along with the bulk of the total Space Station mass. The plot shows that when the model is suspended only by the two shorter cables, a higher in-plane pendular frequency results, even though the distance to the c.g. has not changed. Further analyses revealed that when the model is supported by a combination of long and short cables, it is the amount of load carried by the long and short cables which characterizes the pendular frequency. The greater the percentage of the load carried by the longer cables, the lower the in-plane pendular frequency. In an analagous manner, the bifilar mode frequency for a distributed structure may vary according to the moment arm and length of

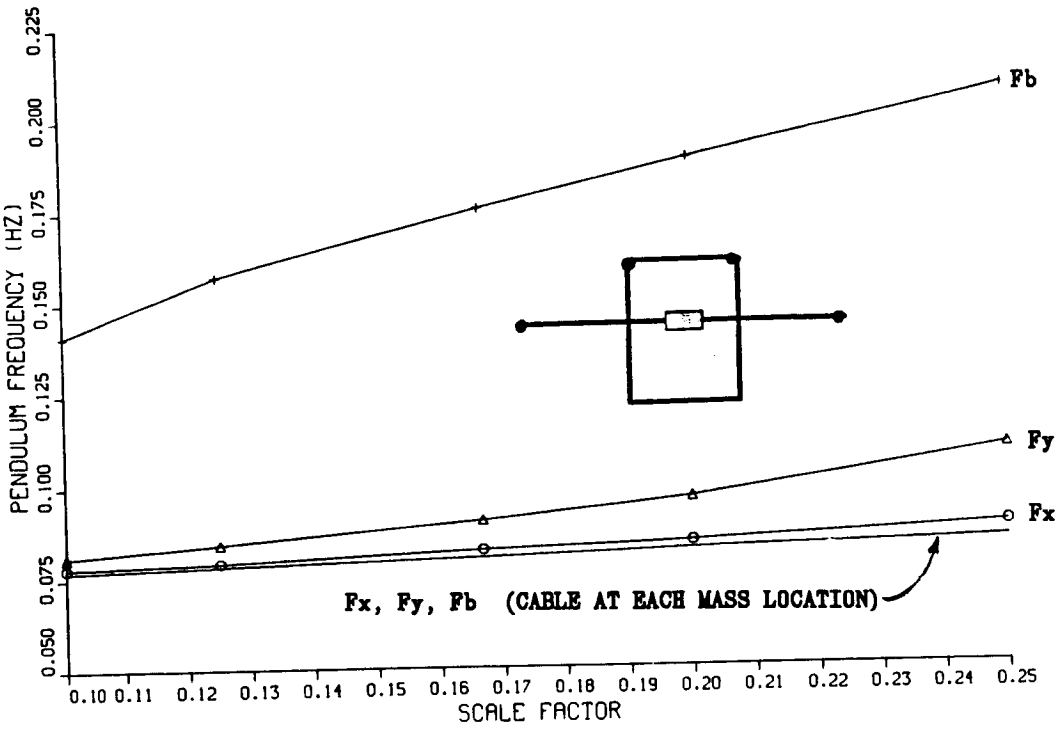

FIGURE 3.3.5.1.1-3: SIMPLE PENDULUM MODE FREQUENCY DEPENDENCE ON CABLE LOCATION

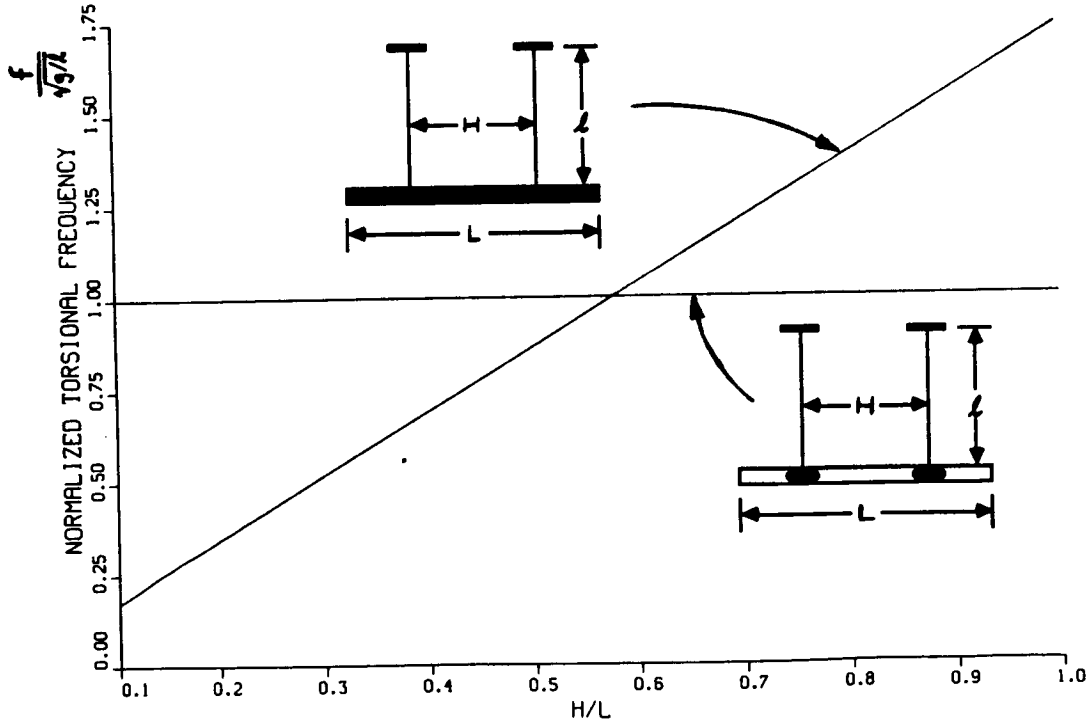

FIGURE 3.3.5.1.1-4: BIFILAR PENDULUM MODE FREQUENCY DEPENDENCE ON CABLE LOCATION

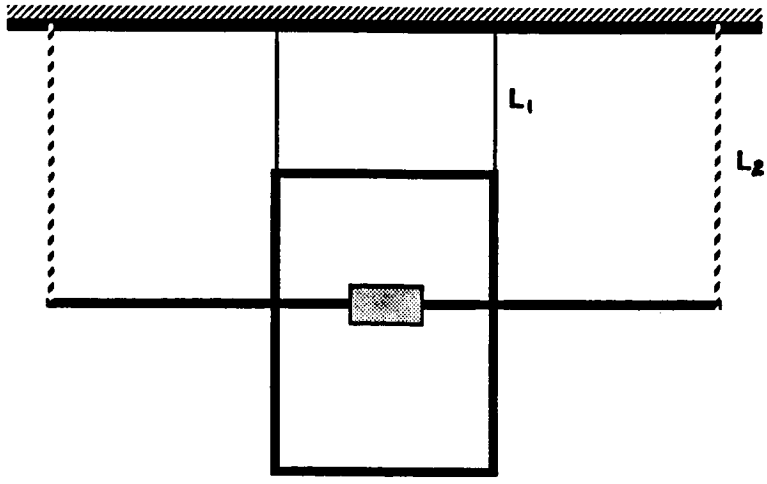

Suspended by ——— Cables, $\Omega = \sqrt{g/L_1}$

Suspended by - - - - Cables, $\Omega = \sqrt{g/L_2}$

(Ω = In-Plane Simple Pendulum Mode Frequency in rad/sec)

FIGURE 3.3.5.1.1-5: PENDULUM MODE FREQUENCY DEPENDENCE ON CABLE LENGTH AND PLACEMENT

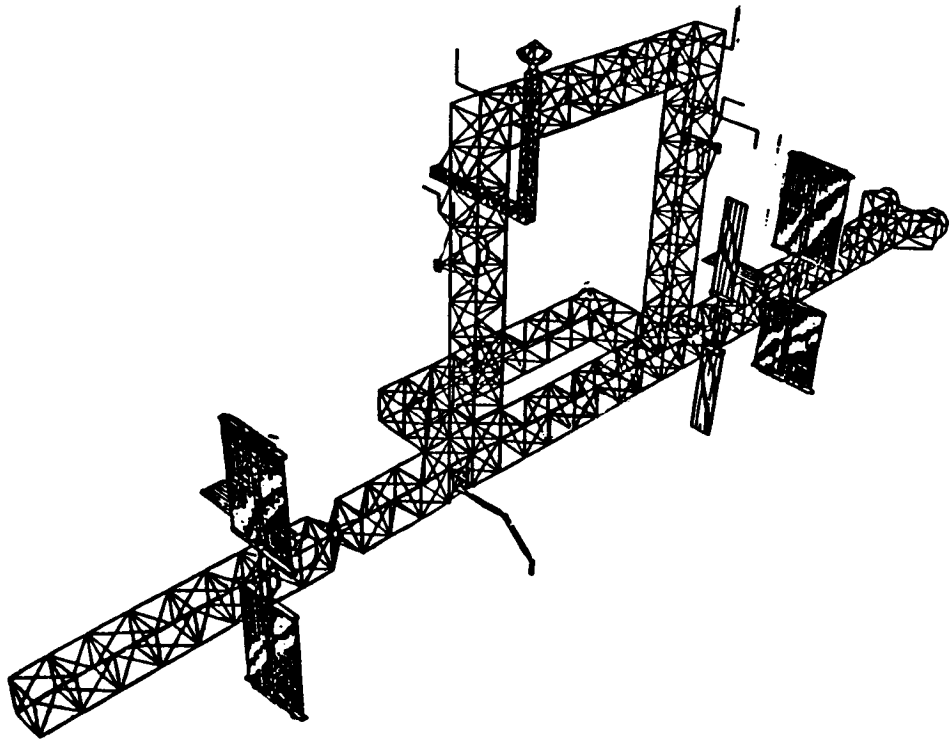

FIGURE 3.3.5.1.1-6: STEP-3 BUILD-UP STAGE CONFIGURATION

the cables carrying the most load. Note, however, that in this case the out-of- plane pendular frequency is always the same because the model is planar. These results were also corroborated by simple experiments. Note that if the structure does not sag evenly at all the cable attach points while in the LSL (i.e., the static deflections at opposite ends of the horizontal booms are not equal) coupling may occur between the out-of-plane and bifilar pendulum modes

Applying these observations to the case of the ISS Space Station, it should be noted that a large fraction of the total weight is located in the module area. The length of the cables attached to the module area will characterize the pendular frequency to first order, while the length of the cables attached to the upper boom and other booms will have a secondary effect. Thus, the pendular frequency of the ISS model may be lower than one would expect when looking at the limited clearance between the domed LSL ceiling and the top of the ISS Space Station model.

By way of contrast, consider the Step-3 build-up stage, a structure characterized by even mass distribution throughout the structure (Figure 3.3.5.1.1-6). The in-plane, out-of-plane, and bifilar pendulum mode frequencies of this test configuration are very sensitive to the lengths of the cables. The in-plane and bifilar frequencies remain dependent on the approximate length of the most heavily loaded cables, as discussed earlier. However, for the Step-3 build-up stage, all of the cables are important because they all carry a significant amount of the total load. Thus, the pendular frequencies are higher because the effect of the short cables is significant.

In summary, the closed-form frequency equations used for simple pendulum models have limited application to more complex models. In this context, more complex models include multiple cables, curved suspension structures, and non-rigid test articles. The suspension system interaction depends in a complex way on the mass distribution of the structure, the number and location of the cables, and the load distribution among the cables. These suspension effects and pendulum modes can be modeled in detail using geometric stiffness finite-element methods, following the procedure

outlined in Figure 3.1.3-1, using the EAL312 code [8].

3.3.5.1.2 Cable Mode Analysis

Another type of possible suspension system interaction with the model dynamics is the coupling of the cable or "string" modes with the primary structural modes of interest. These cable modes are analagous to the vibration of strings on a guitar, and their frequency is given by

$$f = 1/2l\sqrt{T_0/m} \qquad (3.3.5.1.2\text{-}1)$$

where T_0 = tension in the cable, m = mass/unit length, and l = length of cable.

If the cable is sized to have a maximum stress of σ psi, the preceding equation may be rewritten as

$$f = 1/2l\sqrt{\sigma/\rho} \qquad (3.3.5.1.2\text{-}2)$$

where σ = allowable stress in the cable, and ρ = cable material density.

Here, the frequency depends only on the cable length, and the cable material, with the corresponding allowable stress and density. Equation 3.3.5.1.2-2 is used to calculate the frequencies of the cable modes in subsequent analyses.

3.3.5.2 Suspension Cable Trade Studies

As shown in Section 3.3.5.1.1, the pendulum mode frequencies depend on the location of the cable attachments, the load carried by each cable, and the size of each cable. Hence, considerable knowledge of the details of the suspension system is required to conduct a valid suspension interaction trade study. Accordingly, cable location trade studies were conducted to minimize the number of cables and the complexity of the suspension system.

In order to conduct the trade study, several assumptions are made regarding the suspension system. Early results indicate that the asymmetrical mass distributions of the ISS Space Station and the Step-2 build-up stage cause the models to hang at a tilted attitude in the LSL. Consequently, the first assumption is that the tension in the cables is adjusted so that the scale models hang level. For this trade study it is also assumed that the cables are made of stranded steel wire-rope with a maximum stress of 10 ksi, yielding a factor of safety of 3.3. Other cable materials are examined as part of a separate investigation that is detailed later in this report. The cable placement trades are conducted to minimize the number of cables, subject to the conditions that: 1) a minimum factor of safety of two exists for all buckling loads, and 2) that the elastic deflections of the structure do not exceed the cable elongation distance. Each radiator or solar array is supported by two cables. Figure 3.3.5.2-1 illustrates the results of a closed-form analysis that shows that two cables are sufficient to ensure that the solar array or radiator beams do not statically deflect more than 1.0% of their length over the range of scale factors investigated.

All of these assumptions were incorporated into the FE models of the Step-2 build-up stage and the ISS configurations through the addition of supplemental software. The software routines automatically tension the cables so that the model deflects evenly under the influence of gravity, with no rigid body rotations. Several iterations of the software may need to be run to satisfy conditions (1) and (2) above, as shown in Figure 3.1.3-1. The cable location analysis was conducted for each of the three suspension orientations and at 5 different scale factors ranging from 1/4 to 1/10 scale. The top part of the flow chart in Figure 3.3.5.3-2 illustrates this procedure.

The results of the cable location trade study show that, at 1/4 scale, a minimum of 35 and 65 cables are required to support the Step-2 build-up Stage and ISS models, respectively. At smaller scales and different orientations, five to ten cables could be removed from the models. Fewer cables are needed at smaller scales because the ratio of P/Pcr for buckling in the gravity field decreases as linear function of the scale

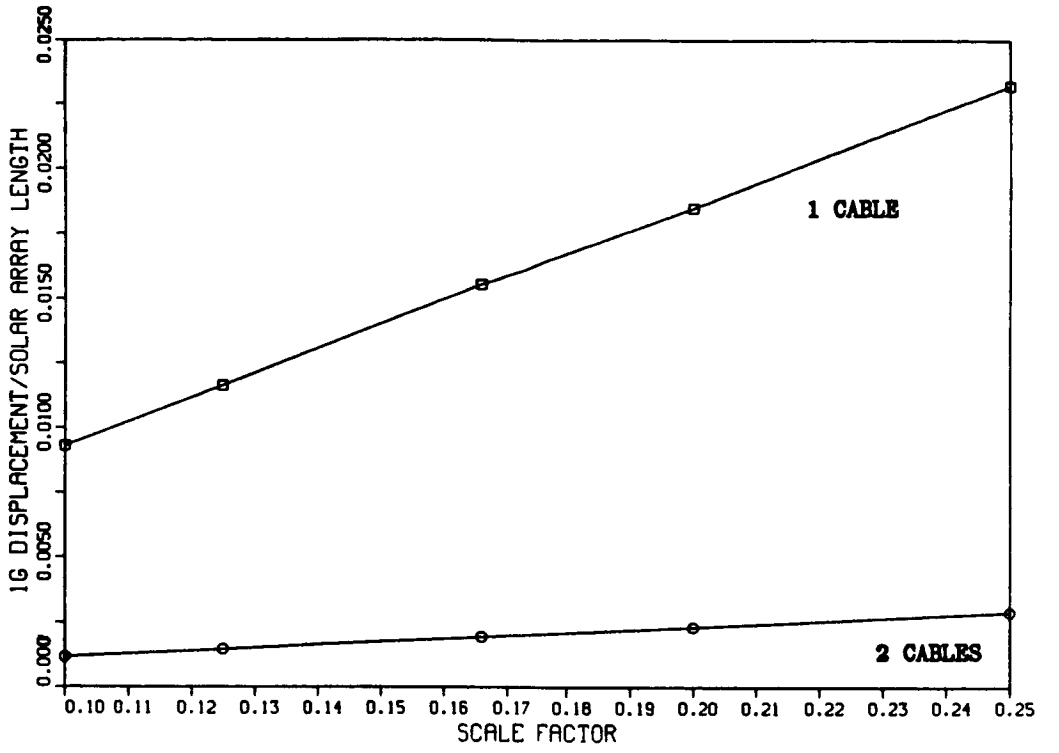

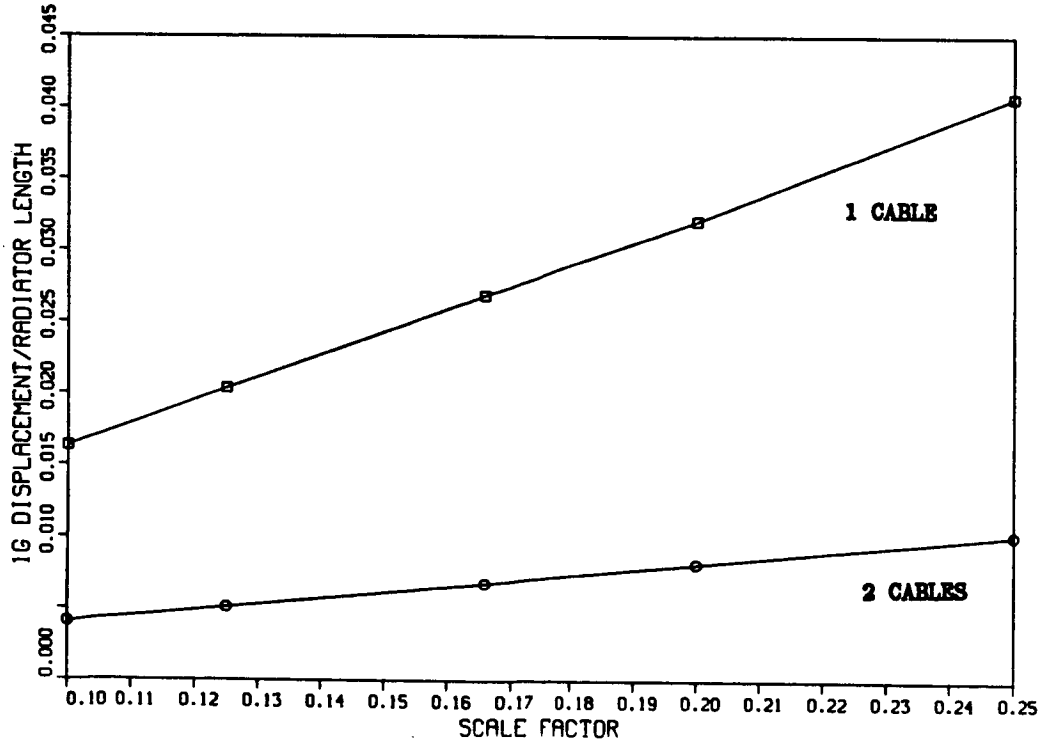

FIGURE 3.3.5.2-1.

SOLAR ARRAY AND THERMAL RADIATOR DEFLECTIONS IN GRAVITY

factor. After relatively few iterations, it became apparent that the most efficient way to support the models was to attach cables to all of the rigid masses (i.e., modules, module nodes, payloads, resource modules, alpha drives, etc.), adding additional cables to support the truss only where necessary. This approach minimizes the preload induced in the truss by the heavy masses of the station since the weight is off-loaded from the truss by individual cables. The goal is to provide a direct load path to the cables without involving the truss structure. The truss then functions as a lightweight connection between what would otherwise be a set of simple pendulums. Figure 3.3.5.2-2 shows the resulting cable attachment locations for a 1/4 scale ISS Station hanging in the x-vertical direction in the LSL.

Table 3.3.5.2-1 is an example of some of the information output by the software. The column for the vertical displacement of the model at the suspension locations serves to check that the model is suspended in a level attitude. In the process of conducting the cable location analysis, it was noted that the static adjustment of the cables may be a very complicated task, as the adjustment of one cable affects the load carried by all of the others. The tension in each cable must be properly tuned in order to be able to correlate the analytical and test results.

Tables 3.3.5.2-2 and 3.3.5.2-3 were produced using the results from the cable trade study. The results shown pertain to the ISS Space Station suspended with the x-axis vertical in the LSL. Since the results presented are largely a function of the height of the LSL, they are representative of the other suspension orientations as well. Table 3.3.5.2-2 lists the largest and smallest cable diameters (attached to the U. S. Lab and Avionics modules, respectively) as a function of scale factor for four different cable types: 1) Steel loaded to 10 ksi, 2) Steel loaded to 30 ksi, 3) Kevlar loaded to 20 ksi, and 4) Kevlar loaded to 55 ksi. These materials and stress levels were chosen in order to facilitate trades between the cable diameter, cable weight, and in subsequent sections, the cable mode frequencies.

Table 3.3.5.2-2 indicates that, in many cases, the cable diameters

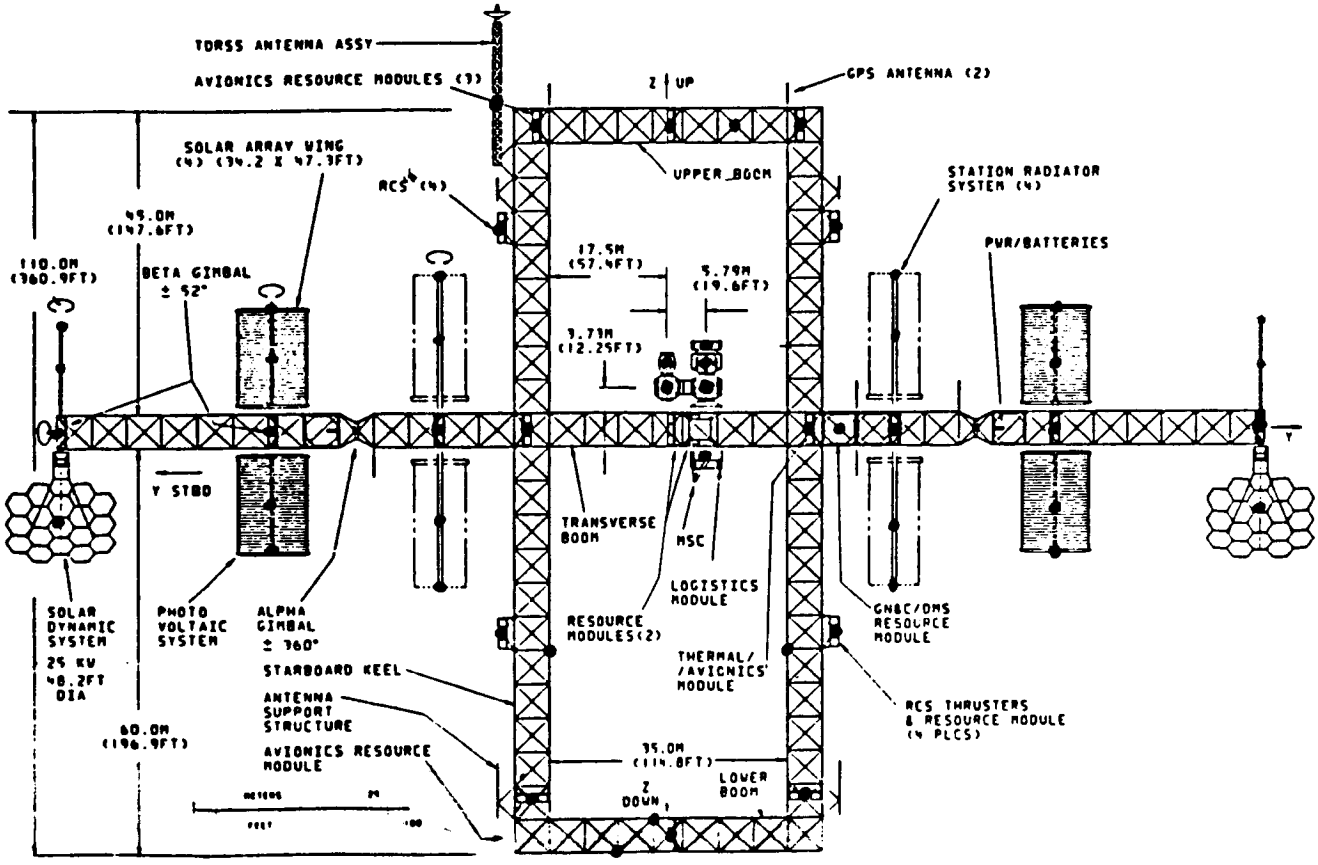

FIGURE 3.3.5.2-2. MINIMUM CABLE ATTACHMENT LOCATIONS (QUARTER-SCALE ISS CONFIGURATION, X-VERTICAL)

TABLE 3.3.5.2-1. TYPICAL OUTPUT FROM FE RUNSTREAMS UNDER THIS STUDY

DATE 860922

SUMMARY OF CABLE DATA

Node Numbers On Mod.	Node Numbers On LSL	Length [in]	Area [in^2]	Cable Force [lb]	Freq. [Hz]	Vert. Disp. [in]
440	568	1529.797	0.0002	0.2029E+01	1.10	1.34
452	569	1529.797	0.0002	0.2031E+01	1.10	1.34
445	570	1532.329	0.0007	0.6510E+01	1.10	1.34
458	571	1529.797	0.0003	0.2274E+01	1.10	1.34
466	572	1580.441	0.0004	0.3574E+01	1.05	1.34
472	573	1580.441	0.0008	0.6892E+01	1.05	1.34
530	574	1342.130	0.0062	0.6198E+02	1.34	1.34
533	575	1440.630	0.0067	0.6198E+02	1.20	1.34
538	576	1607.504	0.0099	0.8265E+02	1.02	1.34
539	577	1613.608	0.0074	0.6141E+02	1.01	1.34
535	578	1623.927	0.0138	0.1138E+03	1.00	1.34
536	579	1589.894	0.0021	0.1743E+02	1.04	1.34
537	580	1571.754	0.0151	0.1289E+03	1.05	1.34
554	581	1637.514	0.0022	0.1803E+02	0.99	1.34
459	582	1594.350	0.0055	0.4608E+02	1.03	1.34
433	583	1537.906	0.0107	0.9353E+02	1.09	1.34
558	584	1555.849	0.0116	0.1003E+03	1.07	1.34
550	585	1569.029	0.0016	0.1376E+02	1.06	1.34
434	586	1537.906	0.0216	0.1882E+03	1.09	1.34
561	587	1555.849	0.0092	0.7966E+02	1.07	1.34
438	588	1534.388	0.0009	0.8300E+01	1.09	1.34
443	589	1535.973	0.0005	0.4363E+01	1.09	1.34
450	590	1534.388	0.0009	0.8293E+01	1.09	1.34
456	591	1534.388	0.0009	0.7491E+01	1.09	1.34
464	592	1588.586	0.0018	0.1546E+02	1.04	1.34
469	593	1591.330	0.0017	0.1465E+02	1.04	1.34

TABLE 3.3.5.2-2. CABLE DIAMETERS FOR VARIOUS CANDIDATE CABLE MATERIALS (QUARTER-SCALE ISS CONFIGURATION, X-VERTICAL)

	CABLE DIAMETER (IN)				
	1/10 SCALE	1/8 SCALE	1/6 SCALE	1/5 SCALE	1/4 SCALE
STEEL 10,000 PSI					
U.S. LAB	0.0469	0.0656	0.1010	0.1327	0.1855
AVIONICS	0.0063	0.0089	0.0136	0.0179	0.0251
STEEL 30,000 PSI					
U.S. LAB	0.0271	0.0379	0.0583	0.0766	0.1071
AVIONICS	0.0037	0.0051	0.0079	0.0104	0.0145
KEVLAR 20,000 PSI					
U.S. LAB	0.0332	0.0464	0.0714	0.0939	0.1312
AVIONICS	0.0045	0.0063	0.0097	0.0127	0.0177
KEVLAR 55,000 PSI					
U.S. LAB	0.0200	0.0280	0.0431	0.0566	0.0791
AVIONICS	0.0027	0.0038	0.0058	0.0077	0.0107

TABLE 3.3.5.2-3. CABLE WEIGHT AS A PERCENTAGE OF TOTAL ISS WEIGHT (QUARTER-SCALE ISS CONFIGURATION, X-VERTICAL)

	CABLE MASS/ISS MASS (%)				
	1/10 SCALE	1/8 SCALE	1/6 SCALE	1/5 SCALE	1/4 SCALE
STEEL 10,000 PSI	5.040	4.950	4.800	4.650	4.440
STEEL 30,000 PSI	1.680	1.650	1.600	1.550	1.480
KEVLAR 20,000 PSI	0.437	0.429	0.416	0.403	0.385
KEVLAR 55,000 PSI	0.159	0.156	0.151	0.147	0.140

specified by the software are too small to be purchased in wire-rope, especially at smaller scales. Stranded rope is recommended because it does not have a single point-of-failure. However, the smallest diameter of wire-rope available is 0.009 inches. Therefore, some of the cables for the smaller scale models must be oversized (i. e., stressed lower than the prescribed levels), which adds unnecessary weight to the suspension system. Kevlar yarn is lighter, composed of smaller strands, and available in smaller diameters. However, Kevlar yarn has a tendency to creep, which may further complicate the tuning of the cables to their specified stress level.

Table 3.3.5.2-3 lists the minimum total cable weight as a percentage of the model weight for each scale factor. Values contained in this table are minimum weight percentages because they are calculated under the assumption that all of the cables are loaded to the maximum allowable stress value. Thus, the weight percentages for the cables supporting the smaller scale models are expected to increase. The weight percentages in this table also do not include attachment fittings or turnbuckles. Based on these considerations, the weight of the suspension sytem is a potential problem.

3.3.5.3 Dynamic Suspension Interaction Analysis and Assumptions

The detailed dynamic suspension interaction analysis was carried out using the analysis techniques described in Section 3.3.5.1. Each cable is modeled as a single rod element. Thus, the interactions between the pendulum modes and the structural modes are included in the analysis. Also included are realistic cable stiffnesses. It is important to note that although the cable string mode frequencies are calculated, their interaction with the structural modes of the model is not included. In addition, the masses of the cables are not included in the model. Both of these assumptions would require a much more detailed model with at least five nodes per cable. Since both effects are examined outside this analysis, the forthcoming results are viewed as more dependent on the LSL geometry than the selection of the cable material.

In the FE modeling process, certain assumptions were made concerning the LaRC LSL. In all models involving this facility, the ceiling of the

structure is assumed to be a hemisphere with a radius of 150 feet. As mentioned in Section 3.3.2, the shadow structure is assumed to be fixed to the ceiling while the dynamic testing is being conducted. As a matter of convenience, attachment points at the ceiling level were assumed to exist as necessary to fulfill cable location requirements.

As an example of the output of the dynamic analysis, Table 3.3.5.3-1 shows the modal kinetic energy table for a 1/4 scale model of the ISS Space Station suspended with the x-axis vertical. The column labelled PKPE represents the strain energy in the structure only (not the cables). Thus, pendulum modes will be indicated by strain energies near zero (in this case, the first three modes are pendulum modes). The other modes can be compared with their free-free counterparts. Figure 3.3.5.3-1 shows a top view of three example pendulum modes for the 1/4 scale ISS model suspended in the LSL with the z-axis vertical.

Table 3.3.5.3-2 presents a summary of the resulting pendulum mode frequencies for the two subject configurations suspended in the LSL in all three orientations. The 1/4 scale results shown in this table are typical of results from analyses at other scales. As shown in the table, the double pendulum mode appears below the cutoff frequency in only one of the cases presented. Most of the pendulum modes are closely spaced in frequency.

The process of correlating suspended mode shapes with those of the unconstrained structure was performed in similar fashion to the boundary condition analysis. However, in this analysis, the results are dependent on the scale factor. Thus, unconstrained models had to be analyzed at each scale factor. As shown in Figure 3.3.5.3-2, modal information from these free-free models is compared with the suspended model modes and frequencies. At a given scale factor, both the ISS and the Step-2 build-up stage models are analyzed with the models oriented in the LSL with the x, y, and z axes vertical. Data from each of these analyses is compared with the respective free-free model modal information by calculating the Cross-Orthogonality (XO) values, Modal Assurance values (MAC), and frequency errors.

TABLE 3.3.5.3-1 COMPONENT MODEL KINETIC ENERGY

Mode No.	Freq (HZ)	Modal K.E.,	Percent Modal Kinetic Energy TBOM	UPBK	LPBK	MODS	RMAS	SOLA	RADI	PKPE
1	0.082	0.1952E+02	4.8	3.2	4.1	58.0	26.5	1.4	1.9	0.
2	0.082	0.1842E+02	4.8	3.3	4.0	58.0	26.6	1.4	1.9	0.
3	0.085	0.2776E+01	11.6	3.7	10.2	2.0	65.7	4.4	2.5	0.
4	0.396	0.3384E-01	0.0	0.0	0.0	0.0	0.0	100.0	0.0	592.
5	0.396	0.3763E-01	0.0	0.0	0.0	0.0	0.0	100.0	0.0	593.
6	0.396	0.2849E-01	0.0	0.0	0.0	0.0	0.0	99.9	0.0	593.
7	0.397	0.3338E-01	0.0	0.0	0.0	0.2	0.1	99.5	0.1	596.
8	0.439	0.5755E-01	0.0	0.0	0.0	0.0	0.0	0.0	100.0	735.
9	0.439	0.6900E-01	0.0	0.0	0.0	0.0	0.0	0.0	100.0	736.
10	0.440	0.4758E-01	0.0	0.0	0.0	0.0	0.1	0.0	99.8	737.
11	0.441	0.5721E-01	0.0	0.0	0.1	0.5	0.2	0.1	99.1	742.
12	0.534	0.6497E-02	0.0	0.0	0.0	0.0	0.0	0.0	100.0	737.
13	0.534	0.8407E-02	0.0	0.0	0.0	0.1	0.0	0.0	99.9	737.
14	0.534	0.6958E-02	0.0	0.0	0.0	0.0	0.0	0.0	99.9	738.
15	0.534	0.7009E-02	0.0	0.0	0.0	0.0	0.1	0.0	99.8	738.
16	0.898	0.1022E+01	14.3	0.4	1.0	7.3	74.0	2.9	0.2	3153.
17	1.294	0.1321E+01	7.7	2.8	13.6	1.8	73.2	0.6	0.4	6585.
18	2.318	0.2440E-01	0.0	0.1	0.4	0.1	0.8	98.6	0.0	21178.
19	2.319	0.3492E-01	0.0	0.0	0.0	0.0	0.0	100.0	0.0	21198.
20	2.319	0.3072E-01	0.0	0.0	0.0	0.0	0.1	99.8	0.0	21203.
21	2.319	0.2318E-01	0.0	0.0	0.0	0.0	0.1	99.9	0.0	21207.
22	2.383	0.7488E+00	3.0	0.1	0.3	3.6	91.7	0.5	0.7	22376.
23	2.491	0.9206E+00	2.2	4.2	20.9	14.5	47.0	1.7	9.5	24439.
24	2.590	0.4549E-01	0.0	0.0	0.0	0.0	0.1	0.0	99.9	26441.
25	2.590	0.4584E-01	0.0	0.0	0.0	0.0	0.2	0.0	99.8	26456.

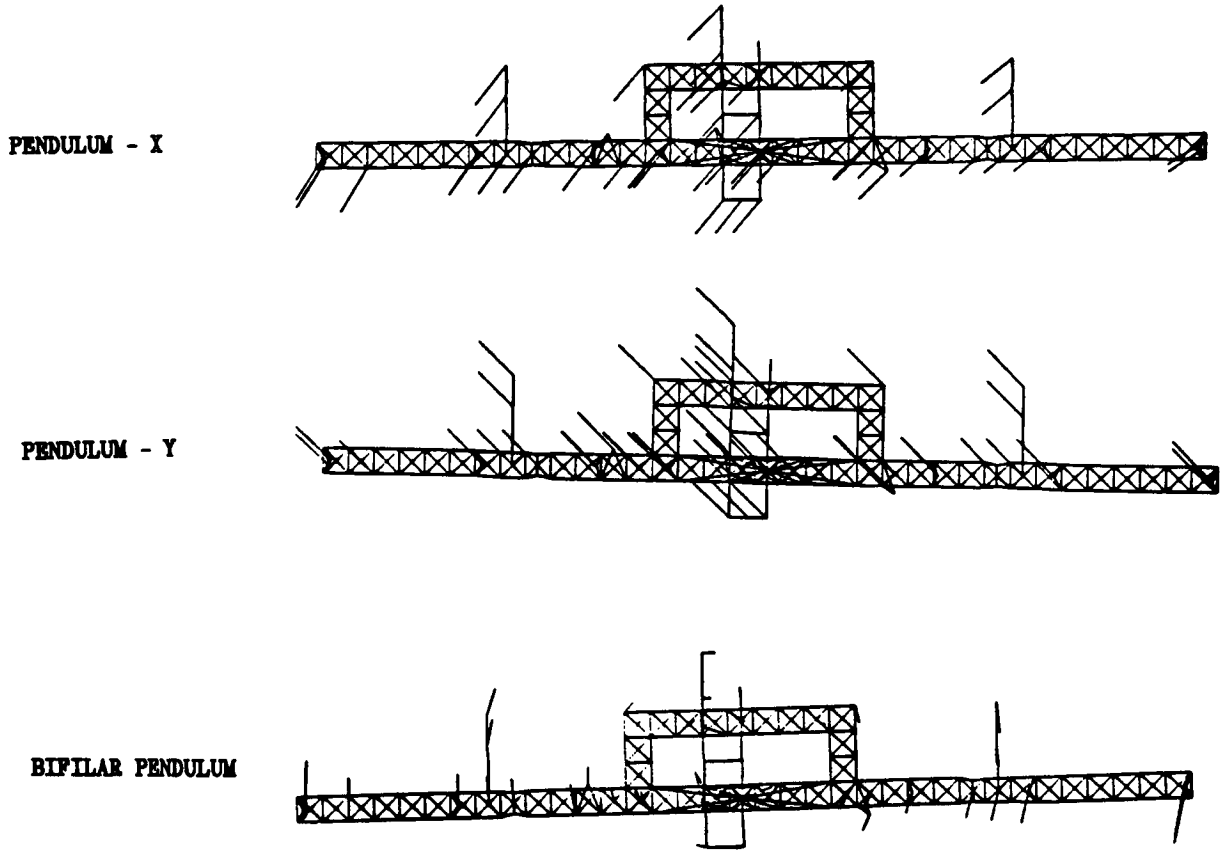

FIGURE 3.3.5.3-1. TOP VIEW OF PENDULUM MODES (QUARTER-SCALE ISS CONFIGURATION, Z-VERTICAL)

TABLE 3.3.5.3-2. DETECTED PENDULUM MODE FREQUENCIES (QUARTER-SCALE CONFIGURATIONS)

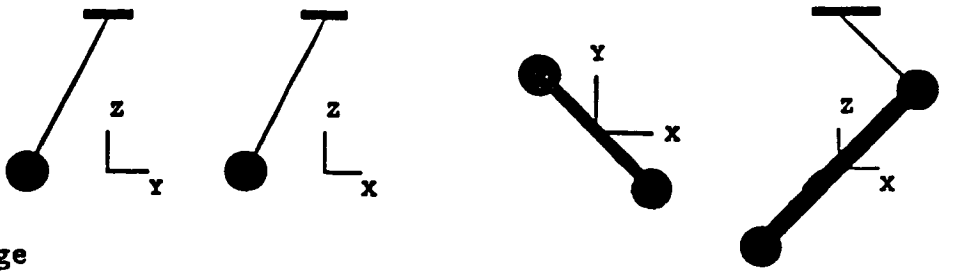

Step-2 Build-up Stage Suspended in the ... Direction				
X	0.081	0.081	0.084	N/A
Y	0.138	0.176	0.150	0.325
Z	0.082	0.082	0.084	N/A
ISS Configuration Suspended in the ... Direction				
X	0.082	0.082	0.085	N/A
Y	0.113	0.115	0.105	N/A
Z	0.087	0.087	0.091	N/A

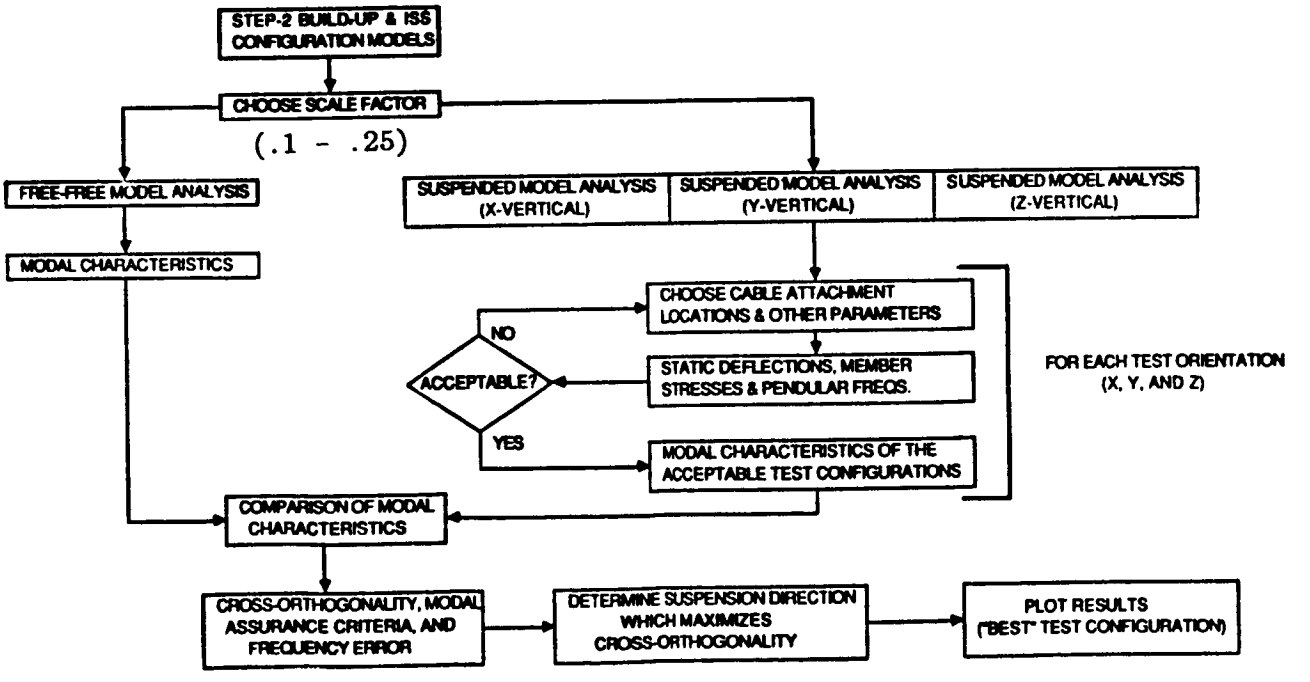

FIGURE 3.3.5.3-2. SUSPENSION SYSTEM ANALYSIS FLOW CHART

3.3.5.4 Results of Step-2 Configuration Analysis

For the Step-2 build-up stage, most of the correlation values suggest that all the system modes may be excited if the model is suspended in only one direction - negative y-axis towards the LSL ceiling. Figures 3.3.5.4-1 and 3.3.5.4-2 display the XO and MAC results, respectively, and indicate problems in correlating modes 41 and 42. All the other system modes have XO and MAC values greater than 0.85 and 0.80, respectively. Figure 3.3.5.4-3 shows the effect of the suspension system on the frequencies of the model as a function of scale factor. This graph indicates that the frequency error increases rapidly with scale factor and that the modes most affected by this trend are those having a bending mode anti-node at the end of the transverse boom (i. e., modes 23, 24, and 52). This is logical in view of the short, cables attached near the end of the boom, adding a significant amount of constraint stiffness in that area.

Figures 3.3.5.4-4 and 3.3.5.4-5 present the XO and MAC data representing the best correlation between the suspended and free-free modes out of all three suspension orientations. Figure 3.3.5.4-6 presents the accompanying frequency error values. These figures reveal acceptable values for all three figures-of-merit for most mode and scale factor combinations. The cable directions used in obtaining these results are also given in Figure 3.3.5.4-6 as a function of the mode number and scale factor. The frequency error exhibits a decreasing trend as the scale factor decreases. The higher frequency errors at 1/4 scale are attributed to the fact that the 1/4 scale model required more cables. The data at 1/4 scale suggest that this scale factor is an upper limit where significant suspension interactions occur.

Figure 3.3.5.4-7 presents a summary of the suspension system interactions with the system modes of the structure. This figure contains graphs of the frequencies of the system modes based on the scaling laws presented in Section 2.1 (monotonically decreasing functions), and the ranges of pendulum and cable sway mode frequency interactions. As seen in this figure, the pendulum mode frequencies are well separated from the

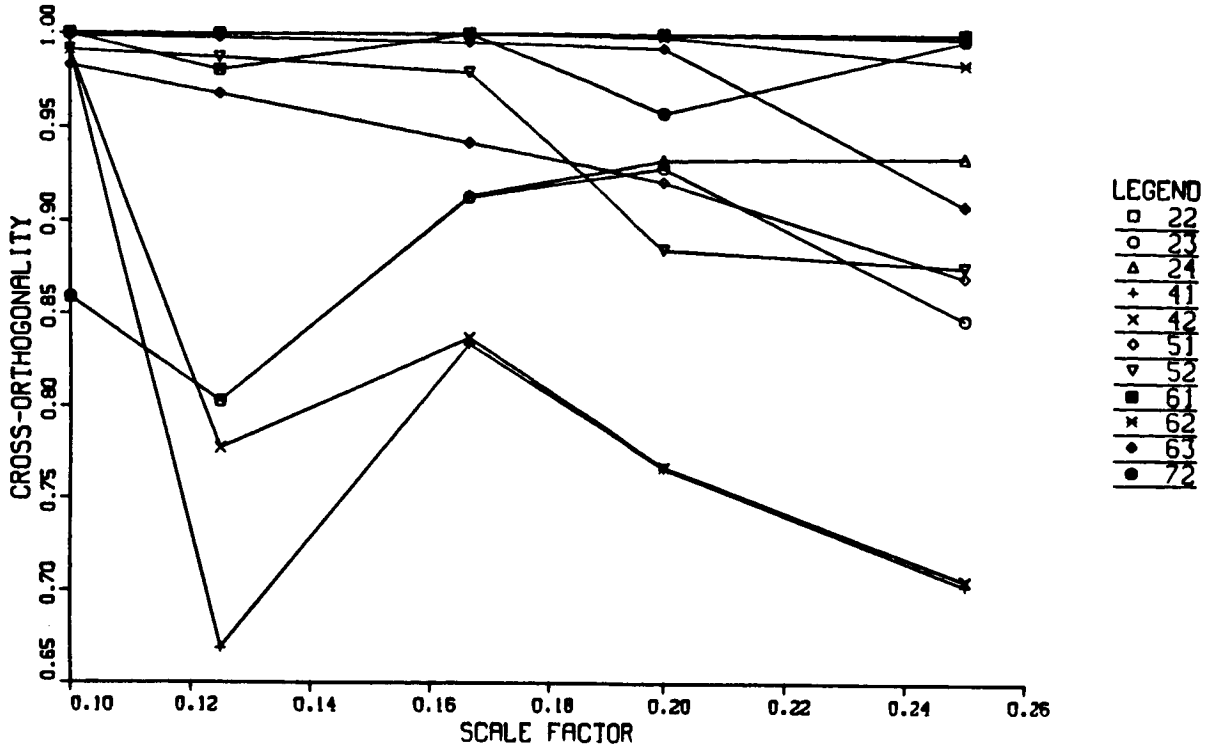

FIGURE 3.3.5.4-1. CROSS-ORTHOGONALITY FOR STEP-2 BUILD-UP STAGE (Y-VERTICAL)

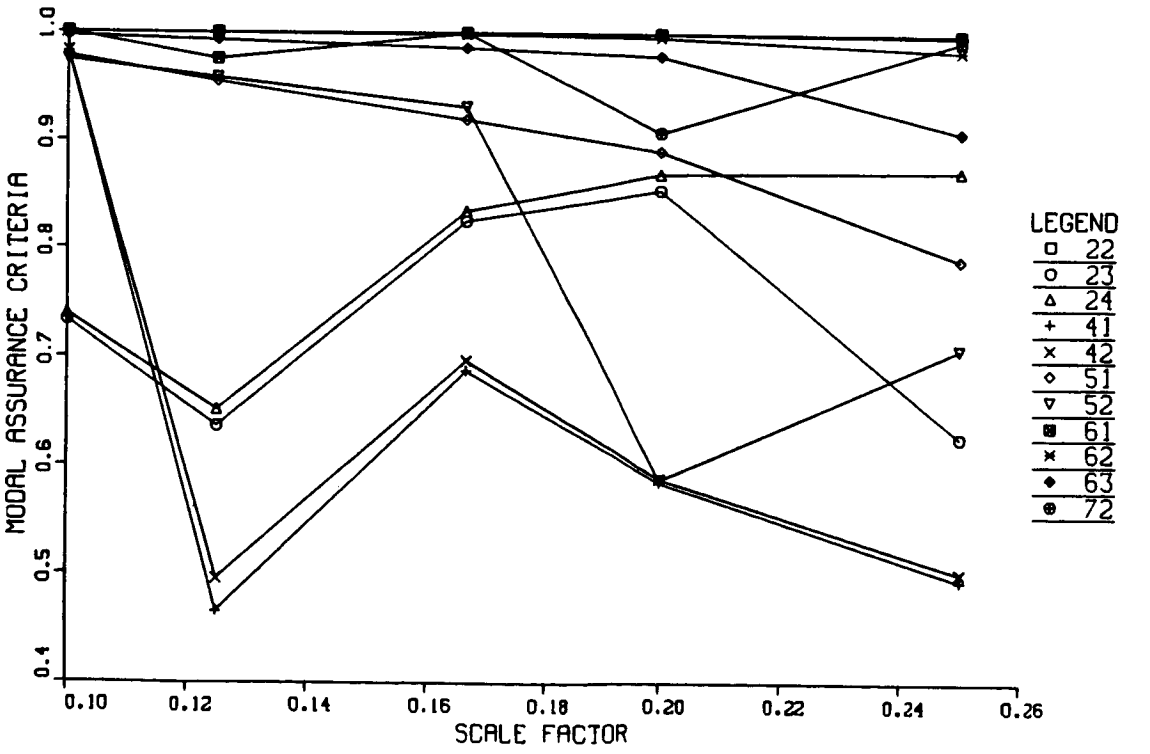

FIGURE 3.3.5.4-2. MODAL ASSURANCE CRITERIA FOR STEP-2 BUILD-UP STAGE (Y-VERTICAL)

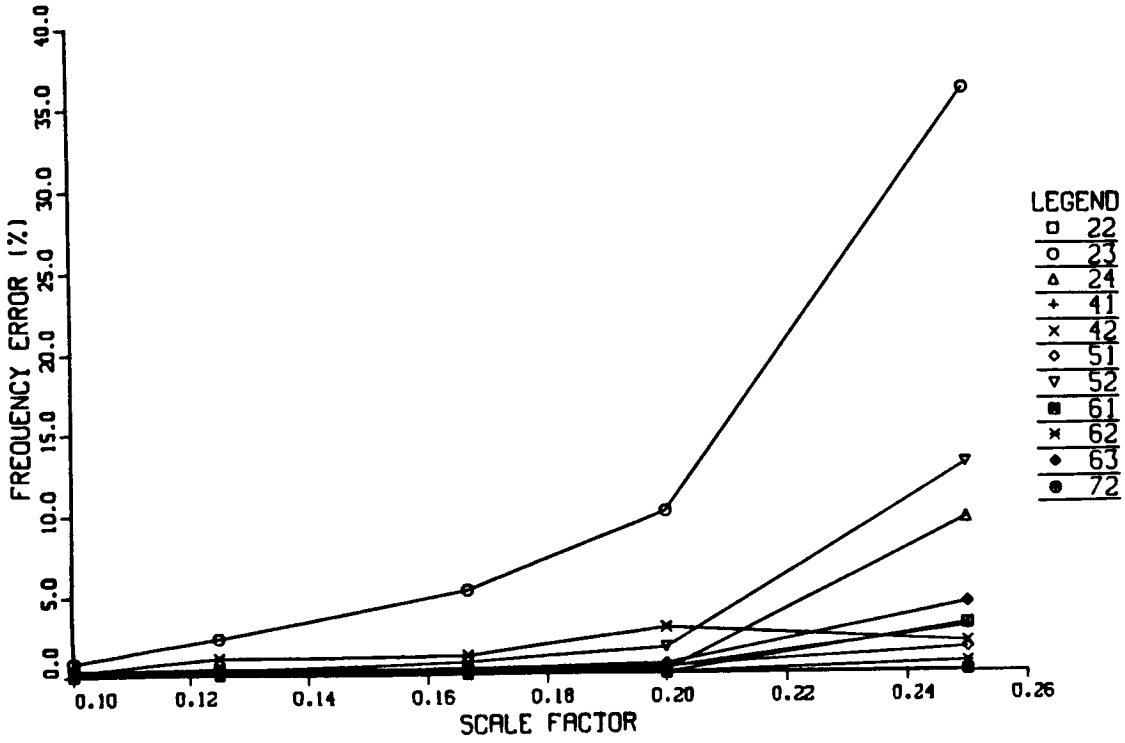

FIGURE 3.3.5.4-3. FREQUENCY ERROR FOR STEP-2 BUILD-UP STAGE (Y-VERTICAL)

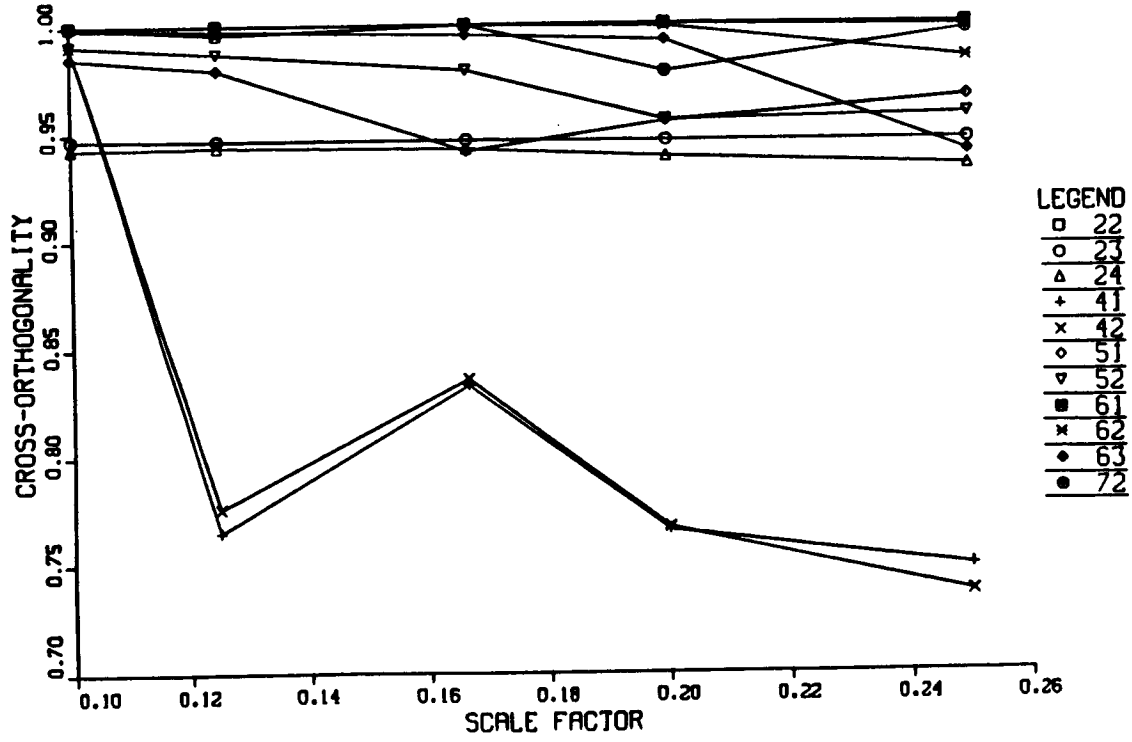

FIGURE 3.3.5.4-4. CROSS-ORTHOGONALITY FOR STEP-2 BUILD-UP STAGE (OPTIMUM TEST CONFIGURATIONS)

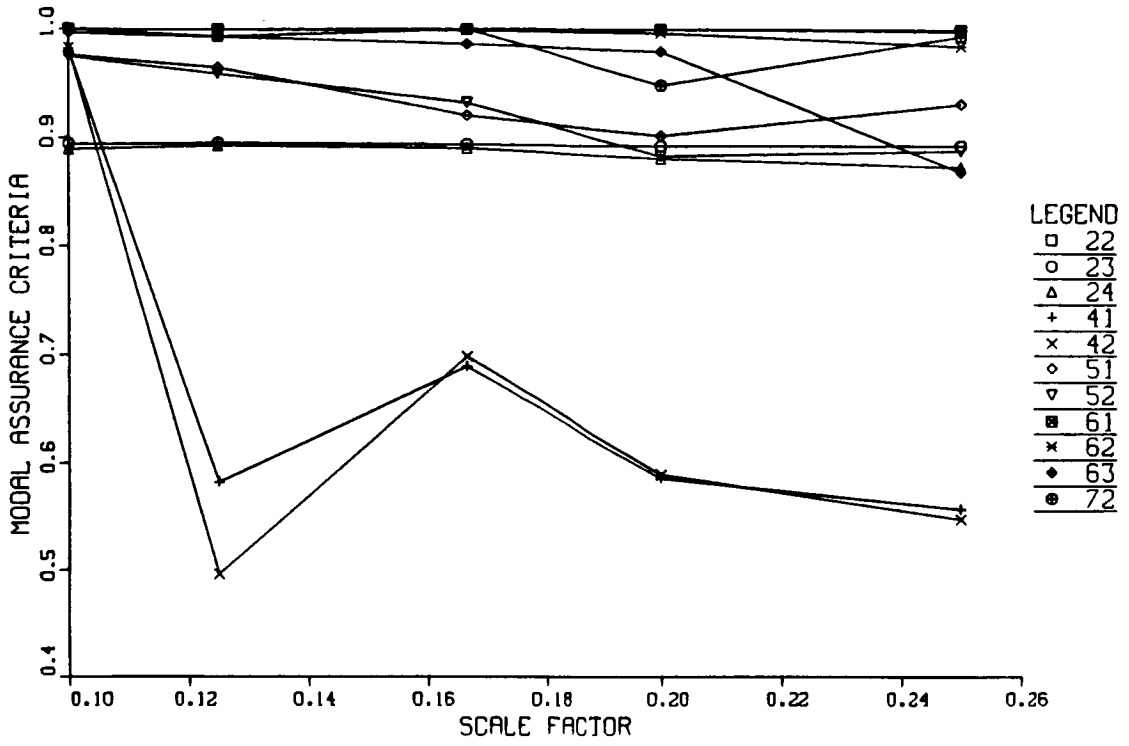

FIGURE 3.3.5.4-5. MODAL ASSURANCE CRITERIA FOR STEP-2 BUILD-UP STAGE (OPTIMUM TEST CONFIGURATIONS)

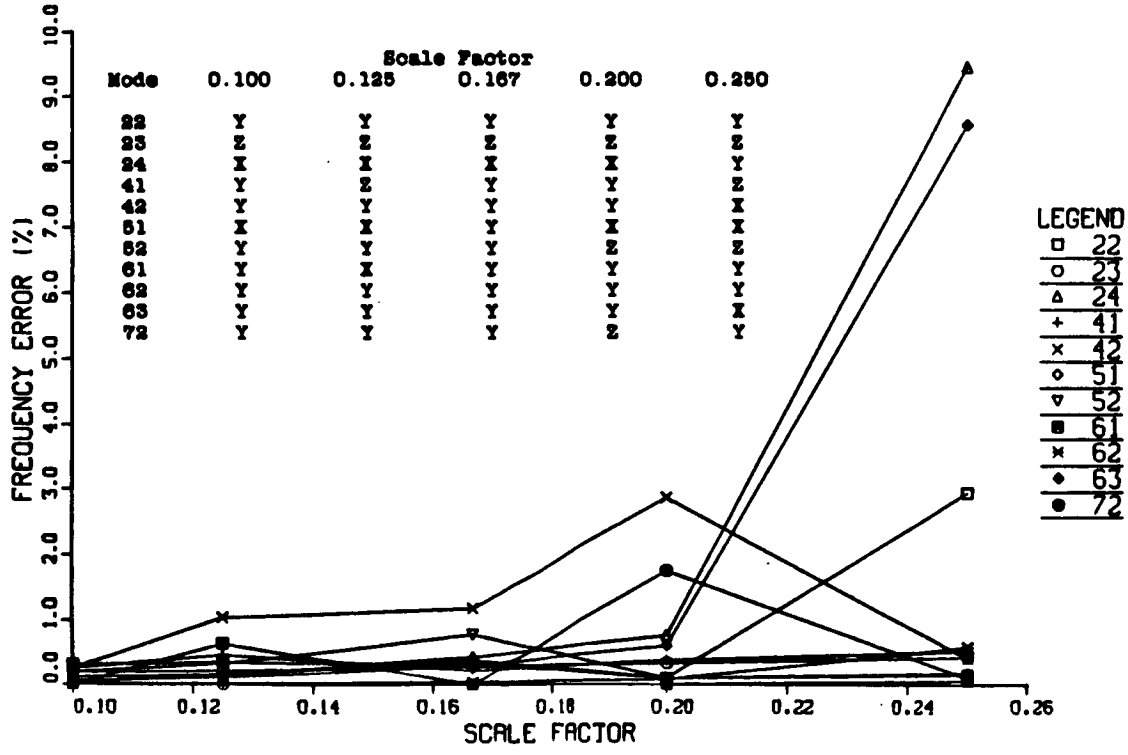

FIGURE 3.3.5.4-6. FREQUENCY ERROR AND CABLE DIRECTIONS FOR STEP-2 BUILD-UP STAGE (OPTIMUM TEST CONFIGURATIONS)

C-2

structural mode frequencies, but this is not the case for the cable sway modes. The frequencies corresponding to the cable string modes envelope the structural mode frequencies at 1/4 scale and gradually decrease in extent at smaller scales. These results indicate a strong possibility of interaction between the structural modes of interest and the cable modes. The harmonics of the cable string mode frequencies are not shown on the graph. However, these harmonics more or less blanket the frequency range above the shaded cable mode region. In previous tests, these higher frequency cable modes have been excited. As mentioned in Section 2.3.4, the interaction of the cable modes may increase the apparent model damping of the test model and/or interfere with the dynamics of the system modes. Possible solutions to this problem are discussed later.

Figure 3.3.5.4-8 is a summary of the observable modes (XO > 0.85) for the Step-2 build-up stage suspended in the "best" test orientations described above. If a mode qualifies as "testable" in multiple suspension directions, the direction yielding the highest XO value is plotted in this figure. Based on this data, if the model is suspended in all three directions, very little variation in the number of observable modes (system, sub-system, and total) with respect to scale factor is noted. Of the eleven system modes, nine can be resolved at 1/4 scale and all are detectable at 1/10 scale. Sixty non-system modes are resolvable at 1/4 scale and 1/10 scale alike, yielding a total of 69 and 71 observable modes (of the 75 below 3.25 Hz.) at 1/4 and 1/10 scale, respectively.

3.3.5.5 Results of ISS Configuration Analysis

Figures 3.3.5.5-1 and 3.3.5.5-2 show the XO and MAC data as a function of the scale factor for 10 of the 11 ISS Space Station primary system modes. One mode (mode 55) is not shown because the data did not indicate a positive correlation. Lower XO and MAC values indicate a greater amount of suspension system interaction. The data presented in this section represent the best correlations between the suspended and free-free modes from all three suspension orientations. Unlike the Step-2 build-up stage, the ISS model must be suspended in all three orientations to test for the primary system modes. The data show that theoretically, most of the modes are only mildly

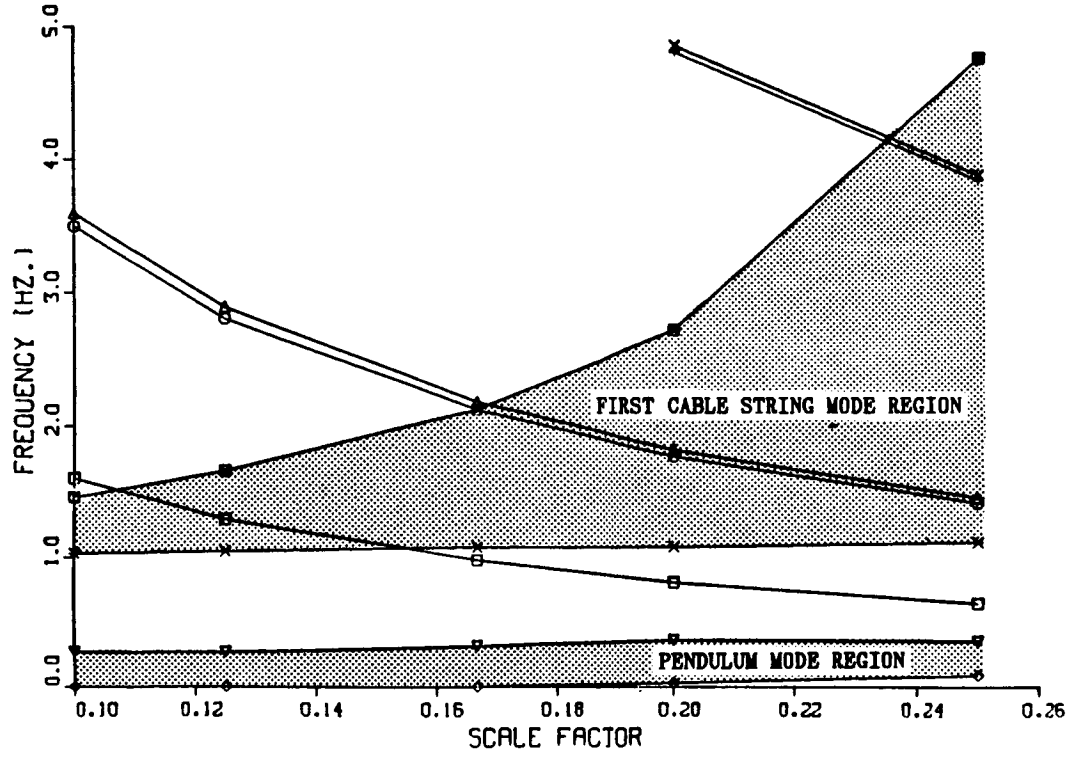

FIGURE 3.3.5.4-7. SUSPENSION INTERACTION SUMMARY (STEP-2 BUILD-UP STAGE)

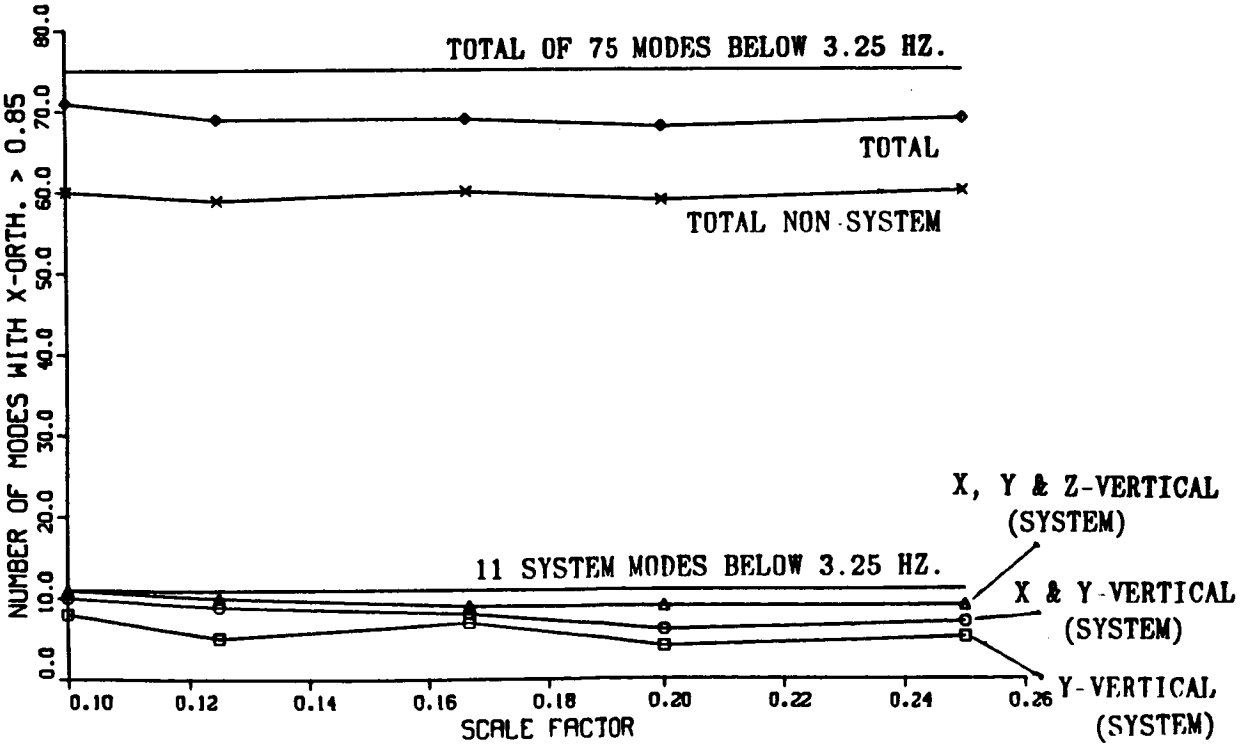

FIGURE 3.3.5.4-8. TESTABLE MODE SUMMARY (STEP-2 BUILD-UP STAGE)

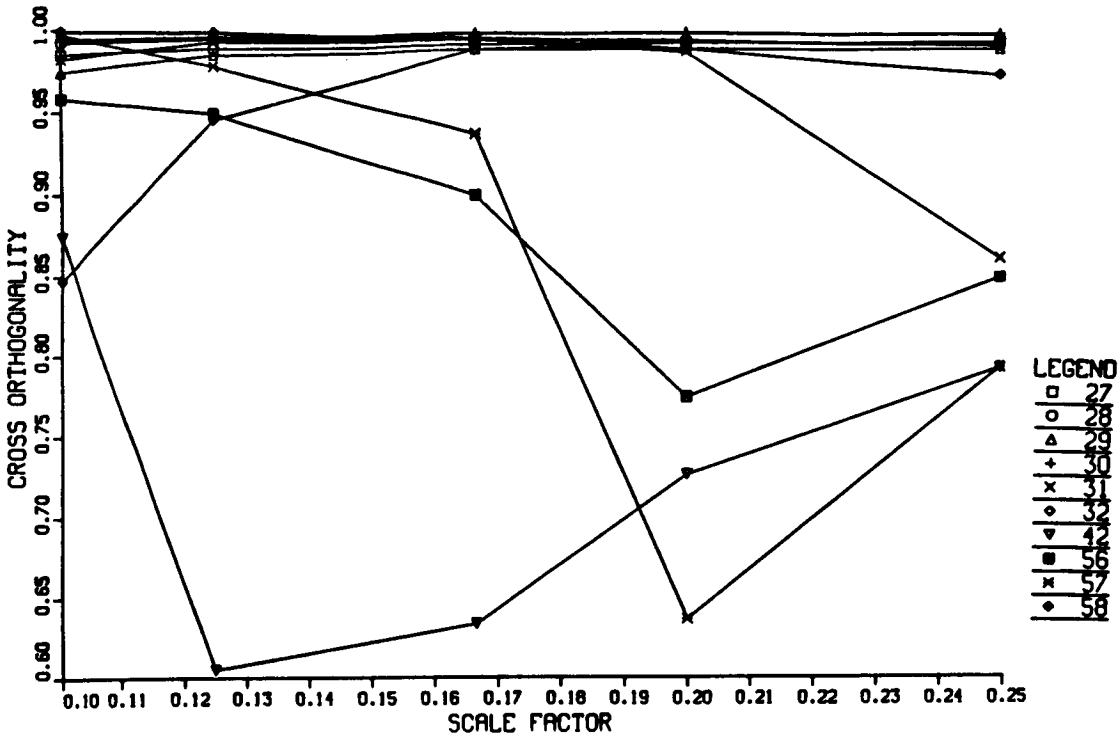

FIGURE 3.3.5.5-1. CROSS-ORTHOGONALITY FOR ISS (OPTIMUM TEST CONFIGURATIONS)

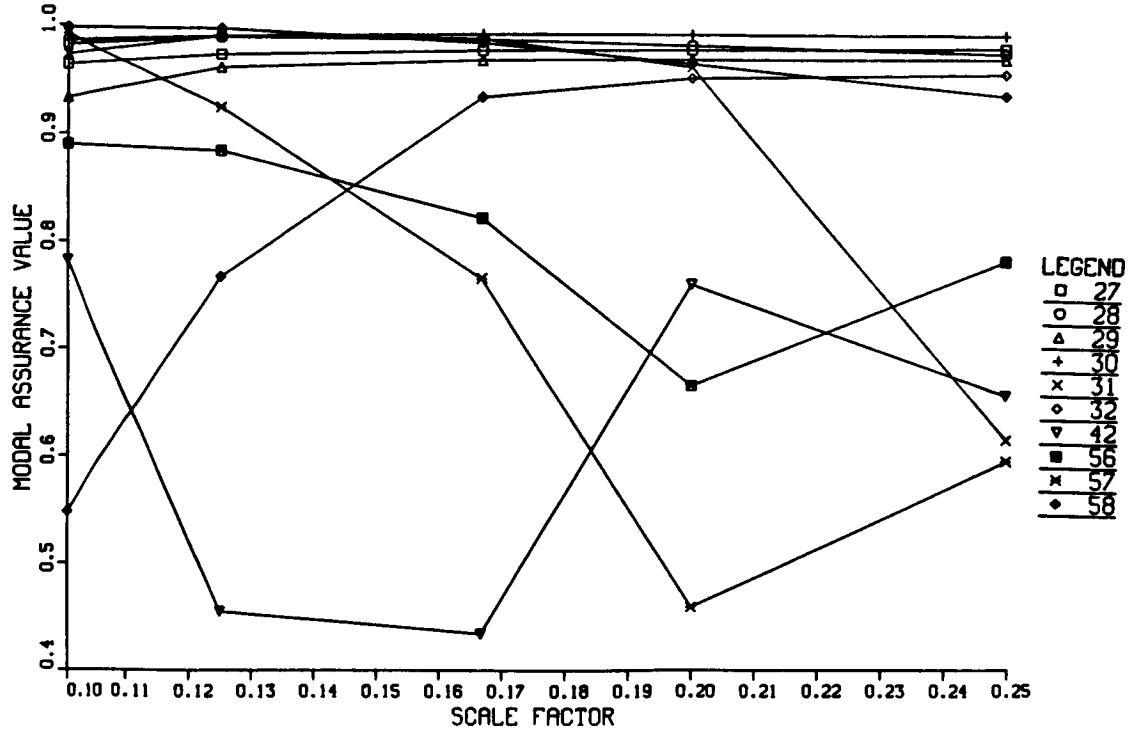

FIGURE 3.3.5.5-2. MODAL ASSURANCE CRITERIA FOR ISS (OPTIMUM TEST CONFIGURATIONS)

affected by the suspension system. However, at each scale factor, there are a few suspended model modes which exhibit a low correlation with their free-free counterparts.

Figure 3.3.5.5-3 presents the frequency error as a function of the scale factor for the ISS Space Station. The results show that overall, the frequency error is less than 3% and that there is a slight trend toward smaller errors at lower scale factors. The cable directions corresponding to the "best" test configurations are also shown.

Figure 3.3.5.5-4 is a system-level chart of the suspension system interactions. Plotted on the chart are the idealized scale model system mode frequencies, the range of pendulum mode frequencies, and the range of cable (string) mode frequencies over all three suspension orientations. The results show that the pendulum mode frequencies are well separated from the primary system modes and that the relative separation increases with decreasing scale factor. This result is encouraging, but there is an implied challenge to the designer to be able to reach all of the rigid masses with cables in any suspension configuration. The results also show that there is a strong potential for coupling of the approximately 180 cable modes with the model system modes. Again, the higher cable modes are not shown, but do blanket the area above the first cable modes. As mentioned earlier, the interaction of the cable modes involved too much detail for a trade-study analysis. However, the strong potential for coupling indicates that the cable modes may be a test problem. To further examine this issue, Figures 3.3.5.5-5 thru 3.3.5.5-7 present the results of studies using different cable materials and stress levels (margins of safety). The use of different materials may worsen the problem, depending on the scale factor. However, Kevlar cables stressed at 55 ksi seem to be an alternative.

Figure 3.3.5.5-8 presents an overall summary of the XO data as a function of the scale factor for the ISS configuration. The chart represents a count of the modes with a Cross-Orthogonality value greater than .85 versus scale factor. Of the 11 system modes, 8 can be resolved at 1/4 scale and 10 at 1/10 scale. The model must be suspended in all three orientations in order to do this. Of the 47 subsystem modes (appendage

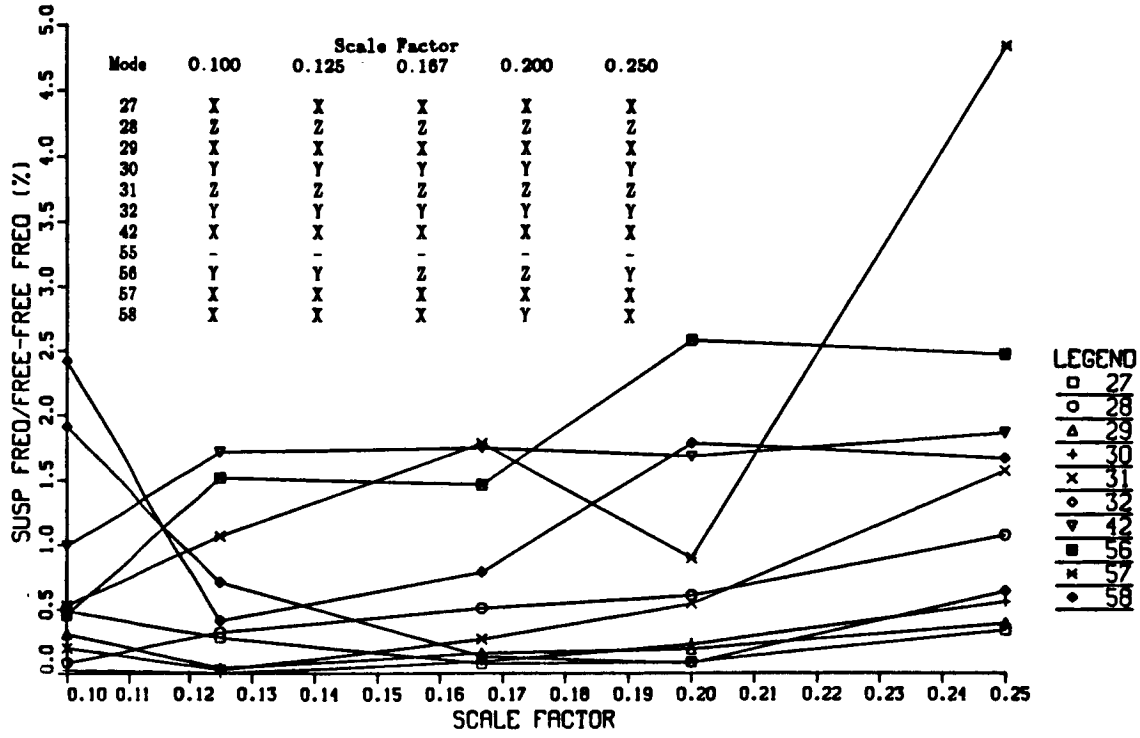

FIGURE 3.3.5.5-3. FREQUENCY ERROR AND CABLE DIRECTIONS FOR ISS (OPTIMUM TEST CONFIGURATIONS)

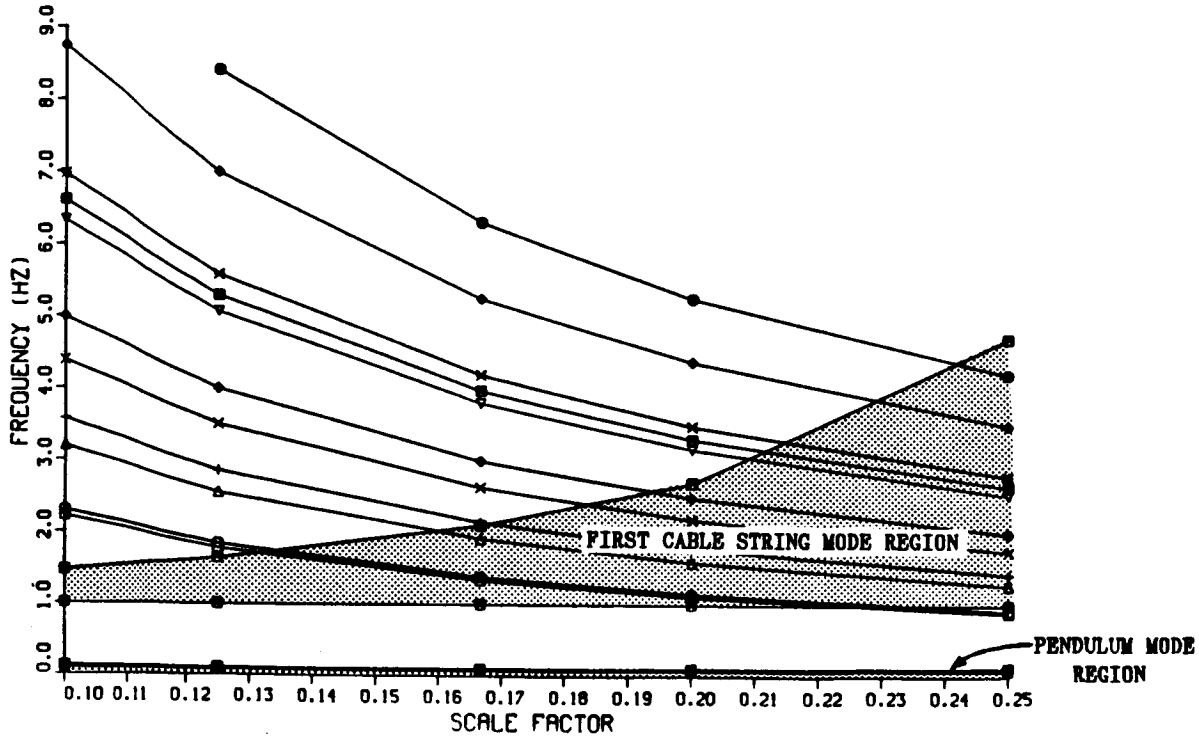

FIGURE 3.3.5.5-4.
SUSPENSION INTERACTION SUMMARY (ISS, STEEL CABLES, 10 KSI ALLOWABLE STRESS)

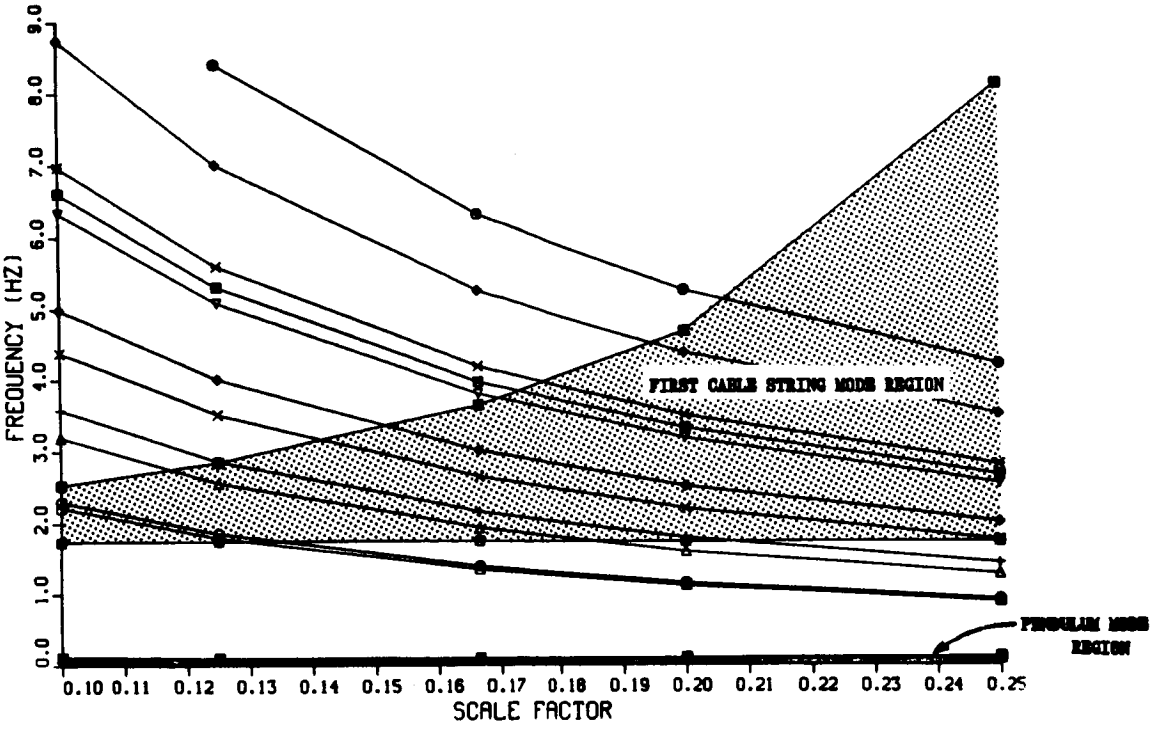

FIGURE 3.3.5.5-5. SUSPENSION INTERACTION SUMMARY (ISS, STEEL CABLES, 30 KSI STRESS)

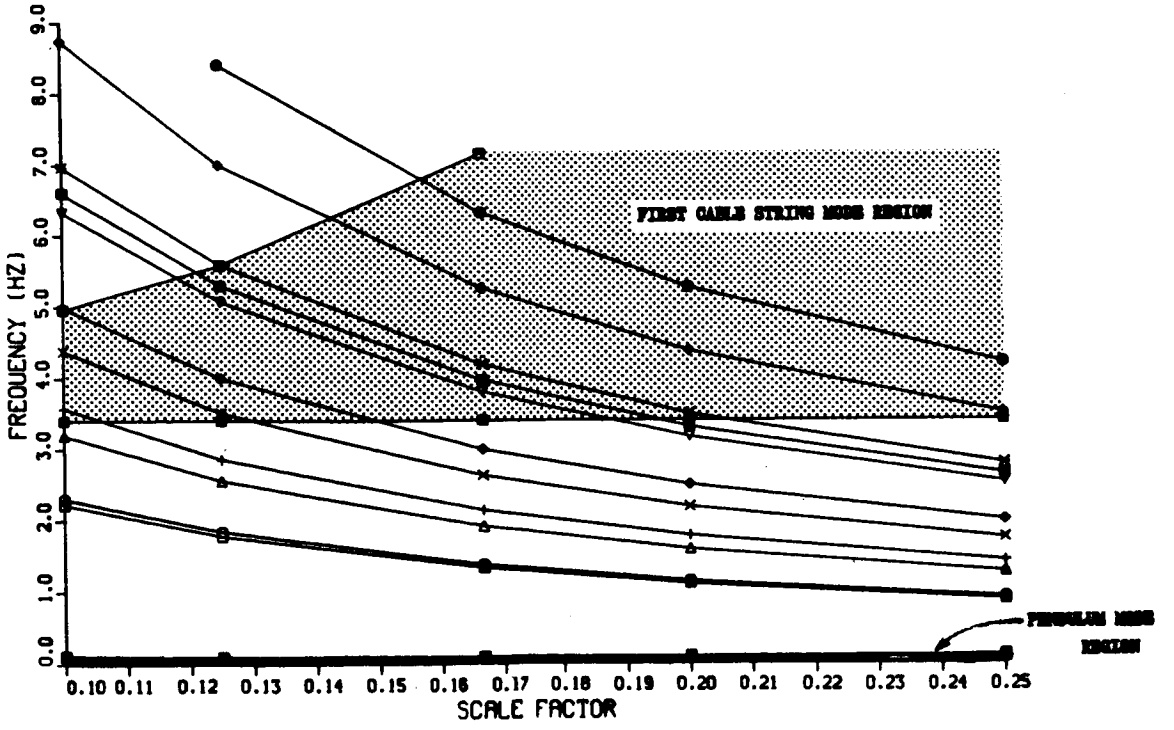

FIGURE 3.3.5.5-6. SUSPENSION INTERACTION SUMMARY (ISS, KEVLAR CABLES, 20 KSI STRESS)

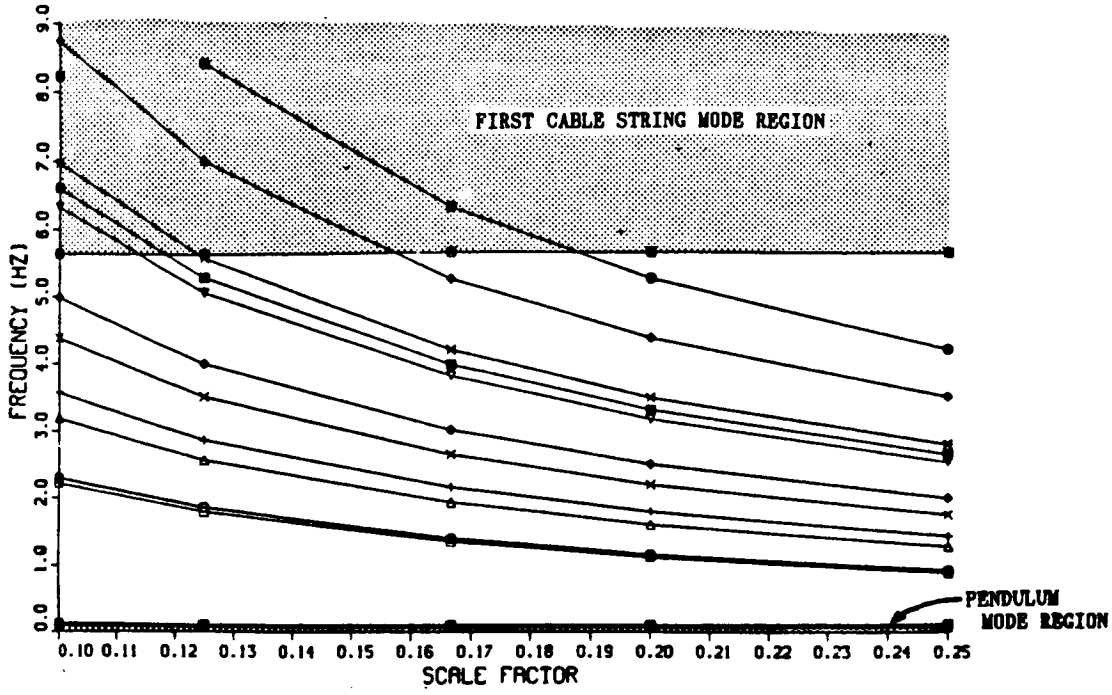

FIGURE 3.3.5.5-7. SUSPENSION INTERACTION SUMMARY (ISS, KEVLAR CABLES, 55 KSI STRESS)

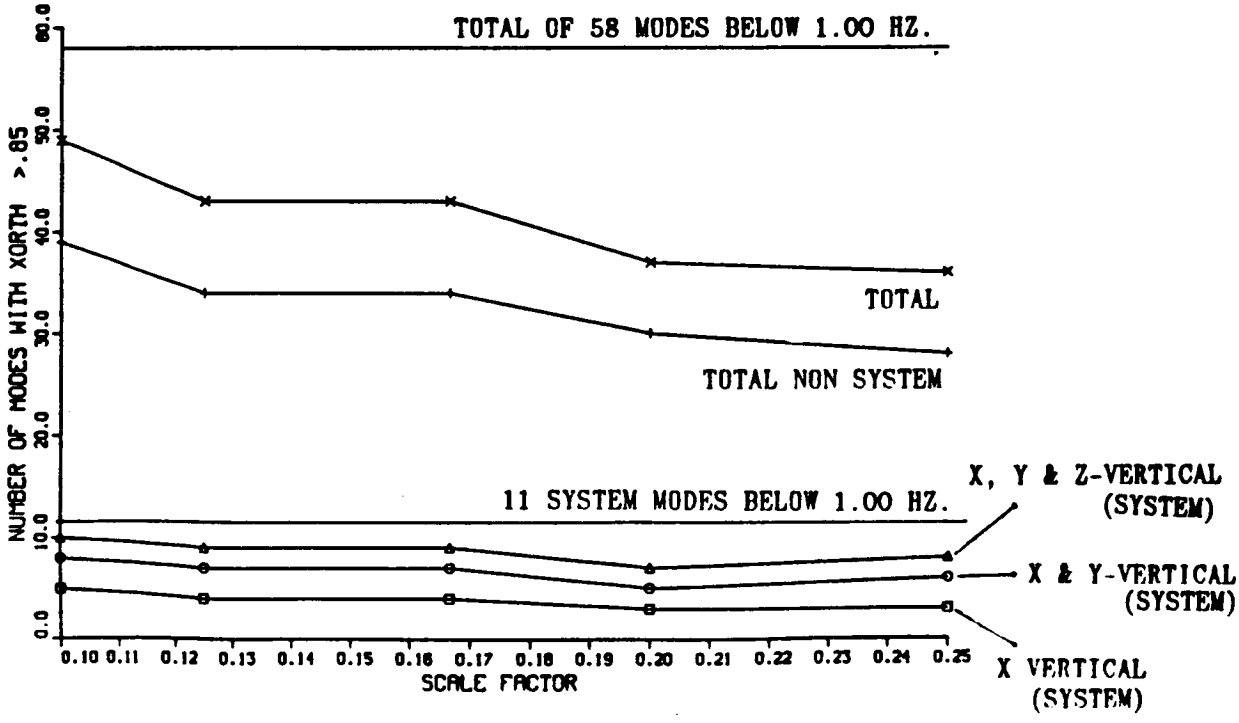

FIGURE 3.3.5.5-8. TESTABLE MODE SUMMARY (ISS)

modes or modes with low modal mass) 31 can be resolved at 1/4 scale and 39 can at 1/10 scale. Of the total of 58 modes below 1 Hz, 39 can be resolved at 1/4 scale and 49 at 1/10 scale. Overall, these results show a trend toward less suspension system interaction at lower scales.

3.4 SUMMARY OF DYNAMIC ANALYSIS RESULTS

Overall, the suspension interaction analysis trade results do not indicate a strong preference for a particular scale factor for the model. The suspension system interacts with different modes (and often in different ways) at every model scale factor. The analyses yielded insights into techniques for minimizing preloads in the truss structure, suspending the model, designing the shadow structure and cables, and assessing the constraints imposed by the size of the test facility. However, the analyses also provided insights into a few potentially serious problems in testing the scale model and in correlating the test results. A summary of the dynamic and suspension analysis results that might impact the choice of the model scale factor is presented in Section 5.2.

As far as the design of the suspension system, the analysis results show that there is not enough room to use soft cables, that the shadow structure should be attached to the LSL ceiling, and that a minimum of 35 and 65 cables are required for the Step-2 and ISS configurations, respectively. Kevlar cables may be required to reduce both weight and the potential for cable string mode interactions. The complexity of the suspension system and the amount of gravity preload introduced in the structure can be reduced by suspending the model by the large rigid masses and all flexible appendages, as opposed to by the truss joints.

The results from both the Step-2 and ISS models indicate a slight downward trend in suspension system interaction problems as the scale factor is decreased. Testing in all three orientations appears to be necessary for the ISS configuration, and is recommended for the Step-2 build-up stage configuration. However, because of their interaction with the suspension system, a number of modes could not be resolved at any of the scale factors studied. Given that the analysis only compared analytical data with

analytical data (as opposed to test data), the importance of testing these modes should be weighed against the benefits of a more advanced suspension system.

Aside from these problems, the tests are likely to be very challenging. In order to be able to correlate test data with analytical predictions, avoid over-stressing the structure, and reduce the weight of the cables, it will be necessary to tune the cables to prescribed levels of tension. This is a potentially difficult, iterative procedure in that the adjustment of the tension in one cable affects the level of tension in all the other cables. During the reduction of the test data, it may be difficult to sort out the extra suspension system modes from any "unmodeled" modes discovered during testing. This problem places an increased dependence on the ability of the analyst to accurately model the interactions of the suspension system.

4.0 SCALE MODEL COMPONENT DESIGN, MANUFACTURING, AND COST

This chapter documents the design, manufacturing and costing analyses for the scale model. The components of the ISS and Growth Space Station configurations are studied, ranging in size from 1/4 to 1/10 scale. Section 4.1 discusses the replication or simulation of scale model components. Section 4.2 presents some of the guidelines used in the design of the scale model. Section 4.3 presents an itemized breakdown of the design assumptions made for each component. Drawings, material specifications, and dimensions are also included. In a similar fashion, Sections 4.4 and 4.5 present the manufacturing and cost data, respectively. The latter part of Section 4.5 combines the component cost data to yield ROM costs for the collection of Space Station components required to construct scale models of the ISS and/or Growth configurations. Four different scale model options are presented, with varying degrees of component replication.

4.1 REPLICATIONS VERSUS SIMULATION

Replication, the process of geometrically scaling all individual components of a structure, is theoretically the "best" way to build a scale model, since all the dimensionless static and dynamic ratios are preserved. In addition to those mentioned in Chapter 2, many difficulties are encountered in practice, especially when the limits of current fabrication and machining technology are reached. Near this point, the cost of building replica, scaled hardware increases greatly. Tolerances, which must also be scaled if the model is to remain consistent, become so small that numerous parts must be fabricated to obtain a few, or even one, acceptable part. This high scrap rate is a major contributor to the associated high manufacturing costs. An additional shortcoming of replica scaling is the increase in model fragility with respect to non-scaled loads (see Section 2.1). One of the principal benefits of replication lies in the inability to anticipate every future use of the model. Replication of all the components theoretically strengthens the validity of future tests, which may involve questions (and require the preservation of dimensionless ratios) that are unrelated to the original motivation for the scale model.

Simulation, the process of duplicating only those characteristics which are important to the dynamic behavior, can be used to lower the scrap rate and thereby reduce cost. Conscious attempts can be made to avoid the problems associated with replicating extremely small components by designing parts which are less sensitive to tolerances. The difficulty involved in simulation lies in the selection of the dimensionless ratios to be preserved. Both anticipated and unanticipated behavior can be simulated, provided that the unanticipated behavior is governed by the same dimensionless ratios. If one of the primary dimensionless ratios governing a certain type of unanticipated behavior is not scaled properly, the interpretation of the model test results will be muddled. For example, if a truss tube is simulated as an axial element only, and susbsequent test work indicates that the influence of the tube bending is important, the scale model test results may not be correlated with the full-scale on-orbit test data. Sections 2.2 and 2.3 include a discussion of the truss tube and joint parameters which need to be properly scaled, ranked in order of importance.

The analyses in the following sections compare the cost and difficulty of designing and manufacturing both simulated and replicated scale model components. These costs must be traded against the fidelity and usefulness of the scale model. Given that all of the scale model components can be changed-out, it may be desirable to consider the option of converting from a set of simulated components to replicated ones during the life of the scale model program.

4.2 DESIGN CRITERIA AND ASSUMPTIONS

The goal in designing the scale model components is to create a model of the Space Station which emulates the dynamic behavior of the full-scale Space Station. Guidelines used in the design process are summarized as follows:

1. The dynamic characteristics of sub-scale components are derived from scaling laws presented in Section 2.1. These characteristics include materials, dimensions, mass, mass and area moments of inertia, stiffness, and frequency. Thus, all dimensions of sub-scale components are linearly

scaled from those of the full-scale.

2. To achieve low cost, the thicknesses of sub-scale components are maintained at standard manufacturing units in cases where the thickness dimension does not affect the overall dynamic behavior of the component.

3. Additional masses, necessary to replicate component inertial properties, are added to the respective components as internal structure and concentrated masses. The locations of the concentrated masses are adjustable, permitting the inertial properties of the individual components to be finely tuned, or altered to accomodate future design changes.

4. The module internal structure design minimizes local vibrations in the frequency range of interest.

5. Components are designed using materials which are indicated in Table 4.2-1. Aluminum, the material proposed for most full-scale components, was considered for all of the components in this table as a cost-saving alternative. Fiberglass is considered as an option for habitat modules because of its light weight and reasonable cost, and graphite-epoxy is considered for the strut tubes in an effort to replicate the full-scale design.

6. Components are simulated and/or replicated depending on the role of that particular component in the dynamic response of the model. Joint fittings and truss tubes, which dominate the structural response, are replicated as closely as possible. Simulated designs are also studied for comparison. Other components which behave like lumped masses, such as the payloads and modules, are simulated. Light appendages, such as the solar arrays and radiators, are simulated in terms of cantilever frequency, modal mass, and inertia distribution in order to reduce complexity and cost. Table 4.2-2 summarizes the modeling method for all of the components considered in this study.

TABLE 4.2-1: Material Options of Scale Components

			Graphite Epoxy	
	Aluminum	Fiberglass	P-55	P-75
Habitats	x	x		
Subsystems	x			
Rotary Joints	x			
Tubing	x		x	x
Nodal Fittings	x			

TABLE 4.2-2: Modeling Method of Components

Components	Simulation	Near Replication
Habitats	x	
Subsystems	x	
Rotary Joints		x
Tubing	x	x
Nodal Joint & Fittings	x	x

4.3 DOCUMENTATION OF DESIGN

This section presents details of the design process as they relate to scaled components of the configurations studied under this contract. The discussion is divided into sections for each of five related groups: habitats (4.3.1), subsystems (4.3.2), rotary joints (4.3.3), truss tubes (4.3.4), and nodal joints and fittings (4.3.5). In each of these sections, materials, replication/simulation, and dimensional details are presented along with an overview of the design processes. The designs and design criteria resulting from this effort were provided to vendors for cost quotes.

4.3.1 Habitat Module Design

The scaled habitat modules are designed using aluminum and fiberglass materials. Since the characteristic natural frequencies of the modules are substantially higher than the fundamental frequencies of the integrated Space Station , they are modeled as rigid bodies with replically scaled masses and inertias.

The outside dimensions of the habitats are scaled according to the scaling laws in Section 2.1. To determine the thicknesses which satisfy the scaled inertial properties for each of the modules, an iterative procedure is employed:

1) An initial habitat wall thickness is assumed.
2) Mass and inertial properties of the habitat are calculated based on this assumption.
3) The values calculated in step 2 are subtracted from the corresponding theoretical values (dictated by the scaling laws in Section 2.1).
4) Differences calculated in step 3 are used in the following manner to determine the dimensions of the internal structure: a. Total mass discrepancy dictates interior structural disk thickness, b. Inertial discrepancies dictate disk inner radii (outside radii are set equal to the inner radius of the habitat) and separation distance.

5) Values calculated in step 4 are examined for feasibility, resulting in further iteration or acceptance of the values from the last iteration.

Figures 4.3.1-1 to 4.3.1-4 illustrate scaled designs of the MPL, HSO, ESA modules (they have nearly the same dimensions and are modeled the same for commonality) the JEM, node/airlock, and tunnel, respectively. Figure 4.3.1-5 illustrates the typical internal structure for a scaled module. Mass and inertial properties of the scaled modules are provided in Tables 4.3.1-1 to 4.3.1-4. Tables 4.3.1-5 to 4.3.1-14 provide typical overall dimensions and thicknesses of the scaled modules. These data were provided to the vendors contacted for cost estimation.

4.3.2 Design of Appendage Subsystems

The complexity of the design of the appendage subsystems (e.g. the slender member, joint dominated, solar array truss) would be very costly to replicate. It is assumed that the smaller details of these particular designs are incidental to the dynamics of the fundamental space station modes, and thus these components are modeled using simulators. These subsystems include radiators, solar arrays, and solar dynamic systems and are designed using aluminum. Each of these components is designed to simulate the frequency, mass and inertia properties derived from the replica scaling laws presented in Section 2.1. The radiator and solar array models consist primarily of straight beams modified by the distribution of movable rings along the beam to satisfy mass and inertia replication requirements. In this manner, the frequencies of the subsystems may be altered without adjusting the stiffness of the beam. The solar dynamic system models consist primarily of lumped masses (with various cosmetic features added) which are positioned in such a way that scaled inertial properties are replicated.

In order to avoid significant air damping effects, the thin surfaces of these subsystems (i.e., solar array panels, etc.) are simulated by open-grid structures which have little effect on the respective inertial properties. In addition, all edges are rounded in order to reduce the generation of vortices.

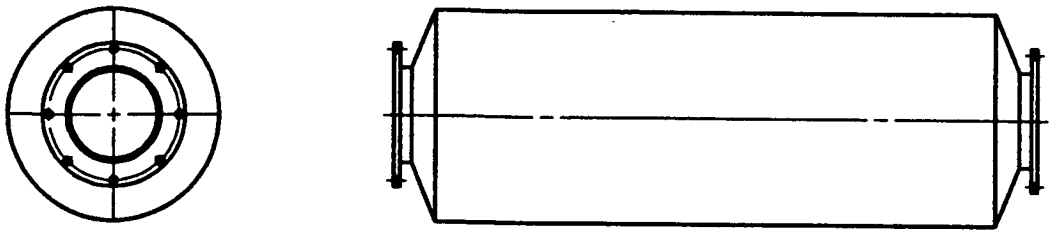

FIGURE 4.3.1-1: A TYPICAL MPL/HSO/ESA SCALED MODULE

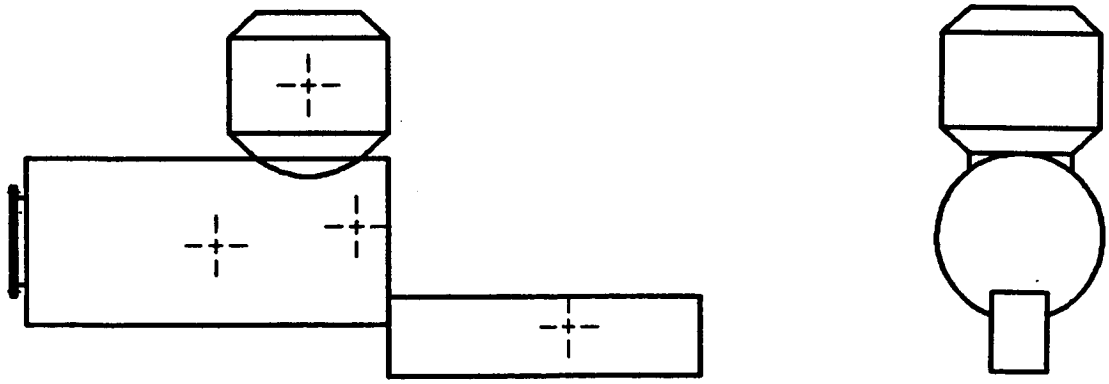

FIGURE 4.3.1-2: A TYPICAL JEM SCALED MODULE

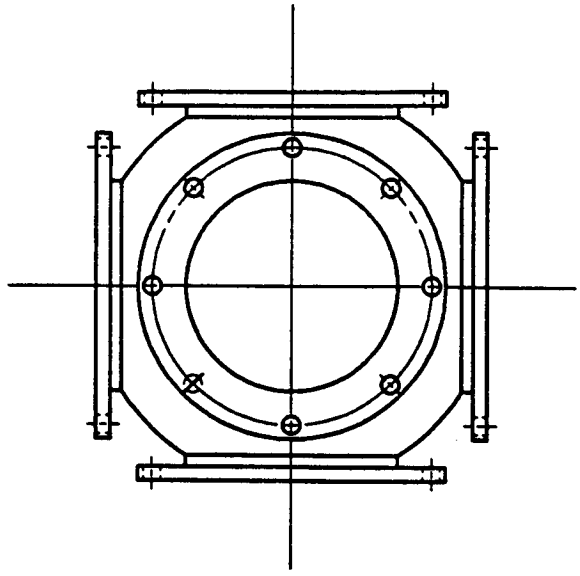

FIGURE 4.3.1-3: A TYPICAL SPHERICAL NODE SCALED MODULE

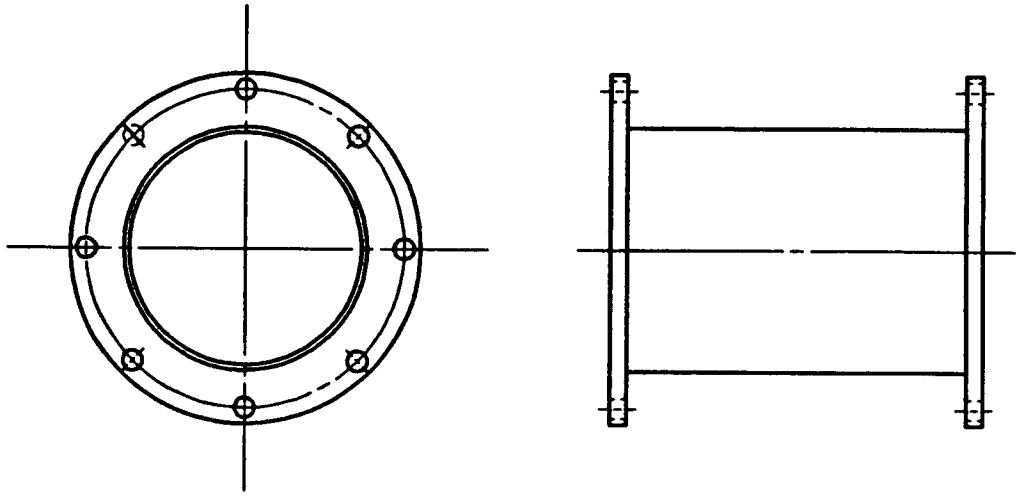

FIGURE 4.3.1-4: A TYPICAL TUNNEL SCALED MODULE

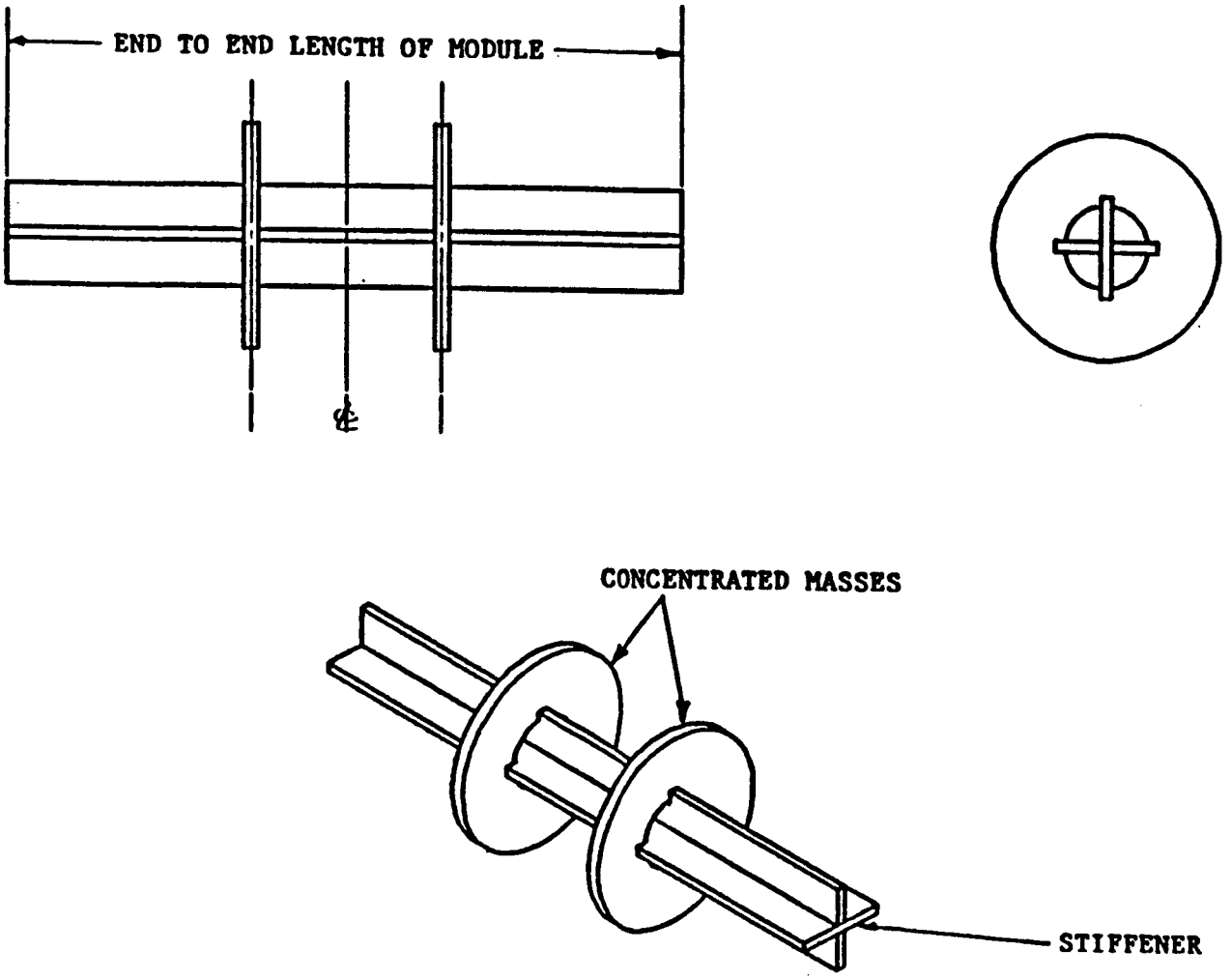

FIGURE 4.3.1-5: A TYPICAL INTERNAL STRUCTURE OF A SCALE MODULE

TABLE 4.3.1-1: MASS AND INERTIAL PROPERTIES OF MPL SCALED MODULES (UNITS ARE IN LBS AND INCHES)

	SCALE FACTOR					
	1/1	1/4	1/5	1/6	1/8	1/10
MASS	54,400	850	435	252	106	54
Ixx*	255,000,000	249,000	81,500	32,700	7,770	2,550
Iyy*	745,000,000	728,000	238,000	95,800	22,700	7,450

* Ixx and Iyy denote moments of inertia about revolutionary and normal axes, respectively.

TABLE 4.3.1-2: MASS AND INERTIAL PROPERTIES OF ESA SCALED MODULES (UNITS ARE IN LBS AND INCHES)

	SCALE FACTOR					
	1/1	1/4	1/5	1/6	1/8	1/10
MASS	46,700	730	374	216	93	47
Ixx*	270,000,000	264,000	86,500	34,700	8,250	2,700
Iyy*	791,000,000	772,000	253,000	102,000	24,100	7,910

* Ixx and Iyy denote moments of inertia about revolutionary and normal axes, respectively.

TABLE 4.3.1-3: MASS AND INERTIAL PROPERTIES OF ESA SCALED MODULES (UNITS ARE IN LBS AND INCHES)

	SCALE FACTOR					
	1/1	1/4	1/5	1/6	1/8	1/10
MASS	46,300	724	371	214	91	46
Ixx*	241,000,000	236,000	77,300	31,100	7,370	2,410
Iyy*	707,000,000	691,000	226,000	90,900	21,600	7,070

* Ixx and Iyy denote moments of inertia about revolutionary and normal axes, respectively.

TABLE 4.3.1-4: MASS AND INERTIAL PROPERTIES OF JEM SCALED MODULES (UNITS ARE IN LBS AND INCHES)

	SCALE FACTOR					
	1/1	1/4	1/5	1/6	1/8	1/10
MASS	60,000	938	480	278	117	60
Ixx*	502,200,000	490,000	161,000	64,600	15,300	5,022
Iyy*	1,470,000,000	1,440,000	470,000	189,000	44,900	14,700
Izz*	1,190,000,000	1,160,000	381,000	153,000	36,300	11,900

* Ixx, Iyy and Ixx denote moments of inertia about revolutionary and two normal axes, respectively.

TABLE 4.3.1-6: MASS AND INERTIAL PROPERTIES OF SPHERICAL AIRLOCK SCALED MODULES (UNITS ARE IN LBS AND INCHES)

	SCALE FACTOR					
	1/1	1/4	1/5	1/6	1/8	1/10
MASS	7,850	123	63	36	15	8
I*	39,400,000	38,400	12,600	5,060	1,200	394

* Moment of inertia I is the same for all three orthogonal axes.

TABLE 4.3.1-5: MASS AND INERTIAL PROPERTIES OF SPHERICAL NODE SCALED MODULES (UNITS ARE IN LBS AND INCHES)

	SCALE FACTOR					
	1/1	1/4	1/5	1/6	1/8	1/10
MASS	5,530	87	44	26	11	55
I*	27,600,000	27,000	8,830	3,550	842	276

* Moment of inertia I is the same for all three orthogonal axes.

TABLE 4.3.1-7: MASS AND INERTIAL PROPERTIES OF TUNNEL SCALED MODULES (UNITS ARE IN LBS AND INCHES)

	SCALE FACTOR					
	1/1	1/4	1/5	1/6	1/8	1/10
MASS	1,420	22	11	7	3	1
Ixx*	-	-	-	-	-	-
Iyy**	2,050,000	2,000	655	263	63	21

* Ixx is not provided in DR-02 report.
** Moment of inertia I is the same for all three orthogonal axes.

TABLE 4.3.1-8: OVERALL DIMENSIONS OF MPL/HSO/ESA SCALE MODULES (units are in inches)

DIMENSIONS	SCALE FACTOR					
	1/1	1/4	1/5	1/6	1/8	1/10
End-End Length "A"	534	134	107	89	67	54
Diameter "B"	175	44	35	29	25	18
Cyl. Length "C"	464	116	93	78	58	46

TABLE 4.3.1-9: OVERALL DIMENSIONS OF JEM SCALE MODULES (Units are in inches)

SCALE FACTOR	LENGTH AND DIA. OR HEIGHT/WIDTH OF SCALE MODULES			OVERALL HEIGHT OF JEM
	PM L x D	ELM L x D	EF L x H x W	
1/1	369 x 165	146 x 158	313 x 79 x 55	362
1/4	90 x 41	36 x 40	78 x 20 x 14	90
1/5	72 x 33	29 x 32	63 x 16 x 11	72
1/6	60 x 28	24 x 26	52 x 13 x 9	60
1/8	45 x 21	18 x 20	39 x 10 x 7	45
1/10	37 x 17	15 x 16	31 x 9 x 6	36

TABLE 4.3.1-10: OVERALL DIMENSIONS OF SPHERICAL SCALE MODULES
(Units are in inches)

DIMENSIONS	SCALE FACTOR 1/1	1/4	1/5	1/6	1/8	1/10
End-End Length "A"	132	34	28	23	17	14
Spherical Dia. "B"	70	18	14	12	9	7

TABLE 4.3.1-11: OVERALL DIMENSIONS OF TUNNEL MODULES
(Units are in inches)

DIMENSIONS	SCALE FACTOR 1/1	1/4	1/5	1/6	1/8	1/10
Length "A"	132	34	28	23	17	14
Diameter "B"	70	18	14	12	9	7

TABLE 4.3.1-12: TYPICAL THICKNESS OF MPL/HSO/ESA SCALE MODULES
(Units are in inches)

MATERIALS	SCALE FACTOR 1/4	1/5	1/6	1/8	1/10
Aluminum	0.1	0.08	0.063	0.05	0.04
Fiberglass	3/16	5/32	1/8	3/32	1/16

TABLE 4.3.1-13: TYPICAL THICKNESSES OF SPHERICAL SCALE MODULES
(Units are in inches)

	SCALE FACTOR				
MATERIALS	1/4	1/5	1/6	1/8	1/10
Aluminum	0.1	0.09	0.08	0.032	0.032
Fiberglass	3/16	1/8	1/8	3.64	1/16

TABLE 4.3.1-14: TYPICAL THICKNESSES OF TUNNEL MODULES
(Units are in inches)

	SCALE FACTOR				
MATERIALS	1/4	1/5	1/6	1/8	1/10
Aluminum	0.09	0.09	0.063	0.05	0.032
Fiberglass	3/16	1/8	1/8	3/32	1/16

Figures 4.3.2-1 to 4.3.2-3 illustrate the subsystem scaled models and Tables 4.3.2-1 to 4.3.2-6 provide the overall dimensions and mass and inertial properties of the scaled components. This data was provided to the vendors for cost estimation.

4.3.3 Alpha and Beta Rotary Joint Desgin

The scaled rotary joint units were designed by ABLE Engineering Co. based on replically scaled dimensions, masses, and inertias. AEC-ABLE has previously manufactured fifth and half scale operational scale models of the Alpha joint for static testing as part of the Space Station Phase B program. The same fabrication methods utilized for these existing components are proposed for the scale model joints in this study. These aluminum components are constructed primarily with off-the-shelf materials which are machined using standard tools and methods. The motor systems of the alpha joints are simulated as lumped masses due to the impracticality of replically scaling them. The beta joints (also referred to as universal joints) are designed to look like half of an alpha joint.

4.3.4 Truss Tube Design

Scale model truss tubes are designed using aluminum, graphite epoxy P-55, or graphite epoxy P-75 materials. The Space Station requirements baseline a 40 million psi modulus tube with a 60 thousandths wall, but no particular Gr/Ep layup is specified. The Space Station Phase B contractors have had to either increase the wall thickness or use Aluminum Clad tubes in order to meet the modulus target. Thus, the replication of a particular tube is carried out to meet the proper modulus and weight, regardless of the layup. The outside diameters of the tubes are scaled according to Section 2.1, and the thicknesses of the tubes satisfy the requirements dictated by the replication of the axial stiffness. The aluminum tubes are sized using standard stock, when possible. Table 4.3.4-1 provides the axial stiffness properties for the tubes and sizing data for the three tube designs considered. The axial stiffness targets and sizing data were provided to vendors for estimation of the cost and feasibility of manufacturing.

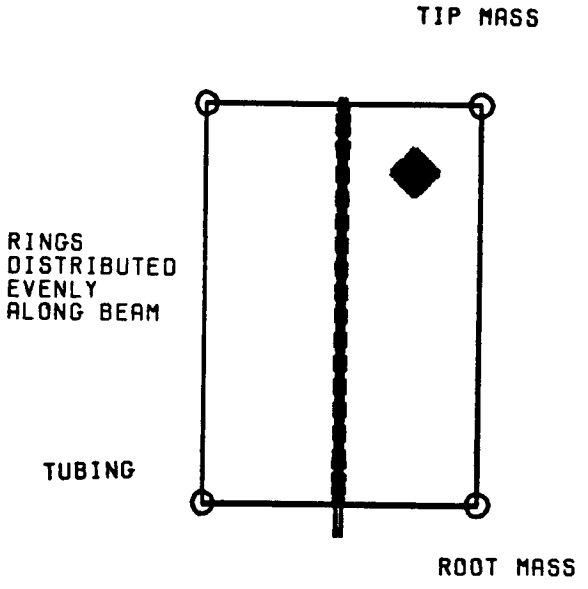

FIGURE 4.3.2-1:
SOLAR ARRAY SCALED COMPONENT

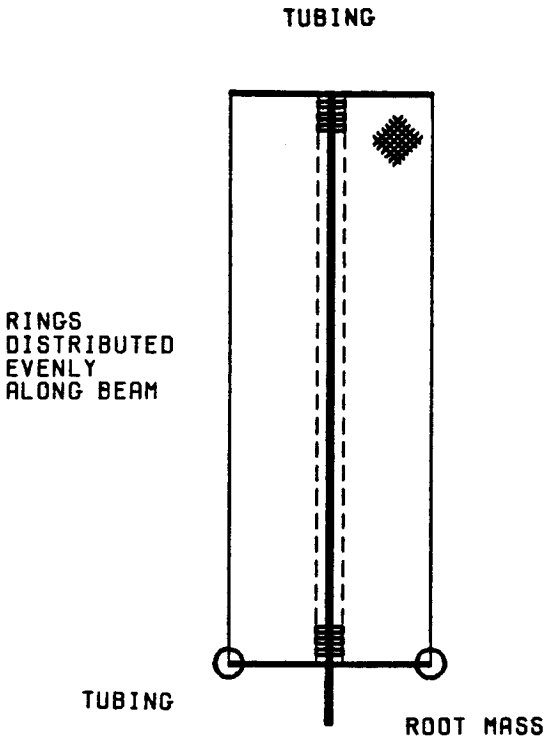

FIGURE 4.3.2-2:
RADIATOR SCALED COMPONENT

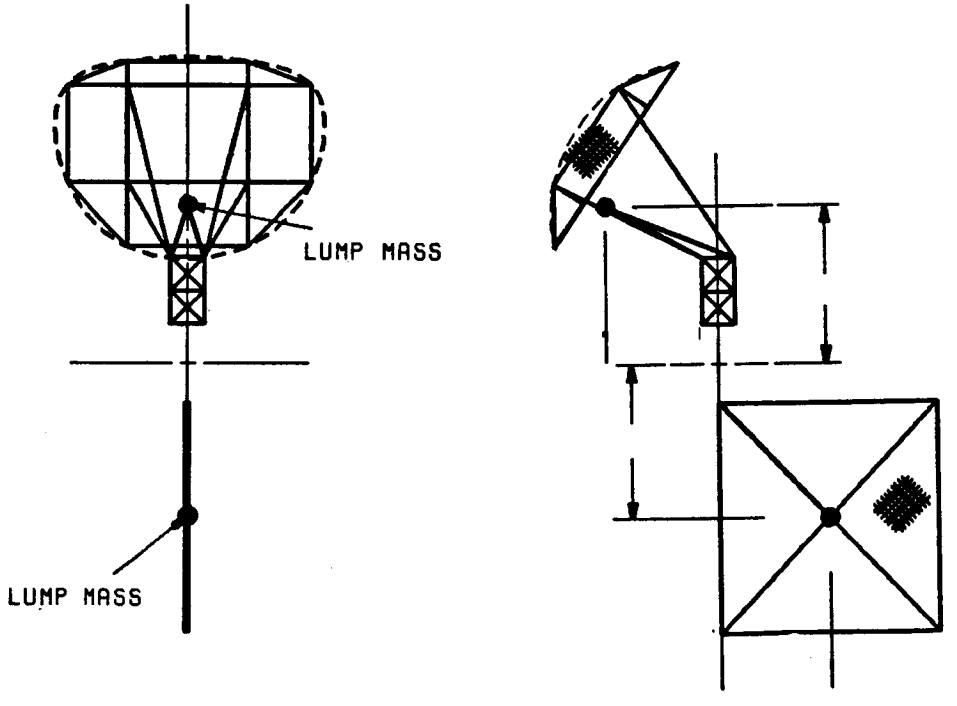

FIGURE 4.3.2-3: SOLAR DYNAMIC SYSTEM SCALED COMPONENT

TABLE 4.3.2-1: MASS AND INERTIAL PROPERTIES OF RADIATOR SCALE COMPONENTS (UNITS ARE IN LBS AND SLUG-FT^2)

NOMENCLATURE	SCALE FACTOR 1/1	1/4	1/5	1/6	1/8	1/10
Mass	1,700	27	14	8	3	2
Ixx*	82,600	81	26	11	3	0.8
Iyy*	82,000	80	26	11	3	0.8
Izz*	625	0.6	0.2	0.08	0.02	0.006

* Izz is the moment of inertia about the revolutionary axis. Ixx and Iyy are about the two orthogonal axes that are normal to the zz axis.

TABLE 4.3.2-2: MASS AND INERTIAL PROPERTIES OF SOLAR ARRAY SCALE COMPONENTS (UNITS ARE IN LBS AND SLUG-FT^2)

NOMENCLATURE	SCALE FACTOR 1/1	1/4	1/5	1/6	1/8	1/10
Mass	922	14	7	4	2	1
Ixx*	40,500	40	13	5	1	0.4
Iyy*	38,000	37	12	5	1	0.4
Izz*	2,700	3	0.8	0.3	0.08	0.03

* Izz is the moment of inertia about the revolutionary axis. Ixx and Iyy are about the two orthogonal axes that are normal to the zz axis.

TABLE 4.3.2-3: MASS AND INERTIAL PROPERTIES OF SOLAR DYNAMIC SYSTEM SCALED COMPONENTS (UNITS ARE IN LBS AND INCHES)

NOMENCLATURE	SCALE FACTOR 1/1	1/4	1/5	1/6	1/8	1/10
Mass	9287	145	74	43	18	9
Ixx*	1.5×10^{9}	1.4×10^{6}	4.7×10^{5}	1.9×10^{5}	4.5×10^{4}	1.5×10^{4}
Iyy*	1.9×10^{9}	1.9×10^{6}	6.1×10^{5}	2.4×10^{5}	5.8×10^{4}	1.9×10^{4}
Izz*	7.4×10^{8}	7.2×10^{5}	2.4×10^{5}	9.5×10^{4}	2.2×10^{4}	7.4×10^{3}

* Ixx is the moment of inertia about the revolutionary axis. Ixx and Iyy are about the two orthogonal axes that are normal to the zz axis.

TABLE 4.3.2-4: SIZING DATA FOR RADIATOR SCALE COMPONENTS
(Dimensions are in inches)

	SCALE FACTOR					
DIMENSIONS	1/1	1/4	1/5	1/6	1/8	1/10
Beam Length	810	202	162	135	101	81
Beam Diameter*		1.25	.875	.75	.5	.375
Beam Thickness*		.035	.065	.035	.049	.035
Radiator Width	286	72	57	48	36	29

TABLE 4.3.2-5: SIZING DATA FOR SOLAR ARRAY SCALE COMPONENTS
(UNITS ARE IN INCHES)

	SCALE FACTOR					
DIMENSIONS	1/1	1/4	1/5	1/6	1/8	1/10
Beam Length	623	156	125	104	78	62
Beam Diameter*		1	.625	.25	.375	.3125
Beam Thickness*		.031	.065	.065	.049	.035
SA Width	390	97	78	65	49	39

* Standard size dimensions of ALCOA Aluminum products.

TABLE 4.3.2-6: OVERALL DIMENSIONS FOR SOLAR DYNAMIC SYSTEM SCALE COMPONENTS
(DIMENSIONS ARE IN INCHES)

	SCALE FACTOR					
NOMENCLATURE	1/1	1/4	1/5	1/6	1/8	1/10
Solar Section						
Major Axis "A"	616	154	123	103	77	62
Minor Axis "B"	540	135	108	90	68	54
Depth "C"	90	23	18	15	11	9
Rad Section						
Side "D"	538	135	108	90	67	54
Lump Mass						
"E"		95	77	64	47	38
"F"		70	57	47	35	28

TABLE 4.3.4-1: AXIAL STIFFNESS PROPERTIES AND SIZING DATA OF SCALED TUBING (UNITS ARE IN LBS AND INCHES)

	SCALE FACTOR					
NOMENCLATURE	1/1	1/4	1/5	1/6	1/8	1/10
Axial Stiffness EA	1,508,000	94,000	60,300	42,000	24,000	15,000
Long. Length	197	50	40	33	25	20
Diag. Length	279	70	56	47	35	28
Diameter	2	.5	.4	.33	.25	.2
Thickness	.06					
Thickness (T-300)		.032	.026	.021	.016	.013
Thickness (P75)		.015	.012	.01	.008	.006
Diameter* (Al)		1/2	3/8	5/16	1/4	3/16
Thickness* (Al)		.065	.058	.049	.035	.035

* Standard Size Dimensions for Aluminum products.

4.3.5 Design of Nodal Joints and Fittings

Replica scaling was attempted for the candidate LaRC and Star-Net joint designs. However, it should be noted that these joint designs incorporate components which are difficult to fabricate and machine even at full-scale, due to their small sizes and tight tolerances. At sub-scale, the task of producing these joints becomes even more difficult. Both of the designs require nearly perfect mating of the interfaces in order to insure a high stiffness across the joint and the predictability of component preloads. The LaRC joint consists of two half-moon interfaces at the perimeter. The Star-Net design has four wedging interfaces in series along the load path, requiring a high preload for proper performance. Because of these multiple interfaces, the overall preload in the joint becomes more unpredictable as scale decreases.

ABLE Engineering has designed and developed a different type of nodal joint that is being considered a candidate for use in the full-scale space station. This joint is basically a latching mechanism rigidly connecting a bolt-head to a mating slot. In the Space Station candidate version of this design, the joint can be driven to the locked position using a built in "astronaut friendly" spring-loaded ratchet mechanism. For the scale model joints, this ratcheting mechanism is removed and the joint is manually placed in the locked position with no loss of structural integrity. There are no critical tolerance areas in the AEC-ABLE design, making it more amenable to sub-scale fabrication. For this reason, the AEC-ABLE joint serves as a good example of a simulated joint for the purposes of this study.

Drawings of these three joints, including the specification of tolerances, were provided to vendors to obtain cost estimates and research manufacturing techniques. Vendors were asked to quote the exact replica designs of the three joints according to their manufacturing ability.

4.4 FABRICATION PROCESSES

Design drawings of scale components were provided to outside vendors

for quotes. Fabrication methods which vary between vendors are described in the following sections.

4.4.1 Fabrication of Habitat Modules

Scaled aluminum habitat modules are composed of sections which are rolled and welded using automated tools. Some sections of these modules are bolted or hinged to provide access to the interior of the modules. Internal stiffeners are bolted to the shell and internal weights are bolted to the stiffeners at nominal locations, permitting the adjustment of their position, per Section 4.3.

Fiberglass habitats were quoted by AEC-ABLE Engineering and Toerge Design. The AEC-ABLE quotation is based on sections of the units being cast from female molds and bolted together to provide access to the module interior. A similar fabrication method is assumed by Toerge Design, except that a male mold is used in forming habitat sections. The internal structure of both designs is composed of aluminum and bolted to the shells. One difference between the two techniques is that the female mold provides components with smooth interior and exterior surfaces, whereas the male molds provide smooth exterior surfaces only. The cost for the female molding process is higher.

4.4.2 Fabrication of Appendage Subsystems

Quotes for the various subsystems were provided by ABLE Engineering. In this quote, standard aluminum beams are used for the radiators and solar arrays. Adjustable weights, rings, and cross beams are bolted to main beams. Plastic monofilament wire mesh is used to model the surface area. For the solar dynamic system, lumped masses and a parabolic mesh are attached to the appropriate beta (universal) joint by light, rigid truss work.

4.4.3 Fabrication of Alpha and Beta Rotary Joints

As mentioned previously, AEC-ABLE has previously manufactured fifth and half scale operational models of the Alpha joint for static testing in the

Space Station Phase B program. The same manufacturing methods are proposed for this study. Standard machining techniques and tolerances are used.

4.4.4 Fabrication of Truss Tubes

The aluminum tubes are all cut from standard ALCOA stock with the exception of the 1/10 scale tubes which must be ordered specially. The graphite epoxy tubes are manufactured using graphite fiber tape or sheets pre-impregnated with epoxy resin. The pre-preg is rolled around a steel mandrel and covered with peel ply, bleeder ply, and shrink tape before being cured in the autoclave. A uniaxial fiber layup is used for the P-55 tubes , while the fiber is slightly skewed from the uniaxial direction for the P-75 tubes. This is done to to reduce micro-cracking and to increase the hoop strength. When the curing process is complete, the peel ply and bleeder are removed and the tube is released from the mandrel. An epoxy layer can be glazed over the tubes to help reduce micro-cracking and provide a smooth finish against abrasion. The ply thicknesses were sized in order to provide a minimum of two ply layers in each tube wall. The fabrication data for the composite tubes differs among the vendors and is summarized in Table 4.4.4-1.

4.4.5 Fabrication of Nodal Joints and Fittings

The LaRC and Star-Net joints were quoted as replicas of the full-scale design by AEC-ABLE. The tolerances are linearly scaled from the 3.0 mil full-scale tolerance, resulting in 0.8 mil tolerances for the 1/4 scale model, and 0.5 mil tolerances for 1/5 scale. The LaRC and Star-Net joint fittings are numerically machined. The less tolerance-sensitive AEC-ABLE joints and fittings are fabricated using a numerical screw machine according to standard machining techniques.

4.5 SCALE MODEL COST

This section documents the cost data received from the vendors for ISS and Growth Space Station model components ranging from 1/10 to 1/4 scale. Vendors were asked to quote cost for components at scales (and therefore

Table 4.4.4-1: Fabrication Data for Graphite Tubing

Vendor: ART

G/E Type	Tape Thkness (mil)	Tolerance				
		Tape Thkness (mil)	Dia. (mil)	Length (mil)	Fiber Alignment (deg.)	Epoxy Layer (mil)
P-55						
All Scales	5	N/A	2	30	5	1
P-75						
1/4 Scale	4.5	.5	2	30	5	.5
Other Scales	2.5	.5	2	30	5	.5

Vendor: Lamiglas

G/E Type	Tape Thkness (mil)	Tolerance		
		Dia. (mil)	Length (mil)	Fiber Alignment (mil/ft)
P-55				
All Scales	7.5	1	1	16
P-75				
All Scales	2.5	1	1	16

tolerances) within the limits of their manufacturing capability and expertise, based on the drawings and specifications provided. The cost estimates presented in this section are unburdened. More specifically, the costs do not reflect the engineering work required to develop the design and generate the drawings, nor do they include any assembly work other then for each components as it is broken out in this study. The costs for the system integration and fees are also not included.

4.5.1 Vendor Data

Cost quotations were provided by four independent vendors for the fabrication of various scale model components. Information regarding these vendors and the types of data solicited from them are contained in Table 4.5.1-1.

4.5.2 Costing Assumptions and Data

Total costs presented in this section are based on the component quantities provided in Table 4.5.2-1 for the ISS and Growth configurations. In the graphs of cost presented in this section, two trends are prevalent. When the cost increases for larger scales, the production costs are driven by the volume of material required. When the opposite is observed, the costs are driven by labor-intensive processes, such as machining, or quality assurance, such as the scrap rate necessary to produce joints to tight tolerances. The following paragraphs present the cost assumptions specifcally related to each individual component.

4.5.2.1 Habitats

The production costs of the habitat modules fabricated of aluminum or fiberglass are evaluated. The cost for the first fiberglass habitat module includes costs associated with the fabrication of the mold used in the production of all subsequent modules. The costs for these subsequent units are therefore lower than the first. The aluminum habitats are all costed identically.

TABLE 4.5.1-1: Vendor Information

Components	Material	VENDOR			
		ABLE(1)	TOERGE(2)	ART(3)	LAMIGLASS(4)
Habitat Modules	Aluminum	x			
	Fiberglass	x	x		
Subsystems	Aluminum	x			
Rotary Joints	Aluminum	x			
Tubing	Aluminum	x			
	Gr/Ep, P-55			x	x
	Gr/Ep, P-75			x	x
Nodal Joints & Fitting	Aluminum	x			

VENDOR ADDRESS LIST:

(1) AEC-ABLE ENGINEERING COMPANY
5790 Thornwood Dr.,
Goleta, CA 93117
Mr. Michael Everman

(2) TOERGE DESIGN
1136 1/2 N. Pacific Ave,
Glendale, CA 91202
Mr. Fred L. Toerge

(3) ADVANCED REINFORCED TUBING
P.O. Box 3147
Carson City, NV 89702
Mr. Jim Fisher, President

(4) Lamiglas
P.O. Box U
Woodland, Washington 98674
Mr. Dick Posey

TABLE 4.5.2-1: Quantities of Components in ISS and Growth Space Station Configuration

Components	ISS	Growth
Habitats		
MPL/ESA/HSO	3	3
JEM	1	1
Nodes/Airlocks	6	6
Subsystems		
Rotary Radiators	4	4
Beta Radiators	2	2
Solar Arrays	4	4
Solar Dyn. Sys	2	12
Rotary Joints		
Alpha Joints	2	2
Universal Joints	10	24
Tubing		
Longerons	816	1120
Diagonals	510	619
Nodes	408	580
Joint Fittings	2652	3770

Costs for each of the habitat scale modules as a function of the scale factor are provided in Tables 4.5.2.1-1 through 4.5.2.1-3. The first of these tables presents unit costs for the habitats fabricated using fiberglass materials, based on the data provided by two different vendors. Total costs for all the habitats required in the ISS or Growth configurations, based on data in the previous table, are presented in Table 4.5.2.1-2. The third table contains analogous data for the aluminum modules. In Figure 4.5.2.1-1, these total costs are plotted against scale factor.

4.5.2.2 Subsystems and Rotary Joints

Several assumptions were incorporated into the cost estimates for the subsystems and rotary joints. The costs for solar dynamic systems include the engines and power conditioning units. The cost of the alpha joint motor system is provided separately. Universal joints were designed as half of the alpha joint. Therefore, costs for the second alpha joint and all universal joints are recurring.

Individual costs for each of the subsystems are provided in Table 4.5.2.2-1 as well as the subtotals for the ISS and Growth configurations. Cost estimates for the alpha joint motor system are detailed in Table 4.5.2.2-2. Figure 4.5.2.2-1 presents the total cost of the subsystems and rotary joints versus scale factor for the ISS and Growth configurations.

4.5.2.3 Truss Tubes

Costs were obtained for the three truss tube types, two using graphite epoxy and one using aluminum 6061-T6. The cost of the composite tubes is dominated by the scrap rate, which increases for the smaller scales. The scrap rates (and costs) for the tubes made with the P-75 material are higher than for those for the tubes made with the P-55 material. Special tooling is required for both composites considered, but the cost of such tooling is negligible when compared with the scrap rate surcharge. Cost figures presented in this section include 10% spares.

TABLE 4.5.2.1-1: PER-UNIT COST FOR FIBERGLASS HABITATION MODULES

ABLE DATA

	0.1	0.125	0.167	0.2	0.25
COMPONENT	FIBERGLASS	FIBERGLASS	FIBERGLASS	FIBERGLASS	FIBERGLASS
MPL/ESA/HSO	12161	14910	15550	16227	18117
Recurring	7505	8490	9757	10256	11406
JEM	16050	16545	17610	18417	19101
Recurring	7650	8085	8370	9177	9861
TUNNEL	7920	8738	9038	9345	9615
Recurring	4170	3938	4238	4545	4815
NODE/AIRLOCK	8201	8633	9188	8428	11153
Recurring	4241	4673	5258	5496	7193

TOERGE DATA

	0.1	0.125	0.167	0.2	0.25
COMPONENT	FIBERGLASS	FIBERGLASS	FIBERGLASS	FIBERGLASS	FIBERGLASS
MPL/ESA/HSO	3200	5000	8010	10180	18750
Recurring	1075	1665	2675	3390	6250
JEM	4200	6250	10000	12730	23450
Recurring	1500	2600	3700	4250	7800
TUNNEL	665	1025	1350	1600	2500
Recurring	225	340	450	600	850
NODE/AIRLOCK	3500	3950	4700	7000	9850
Recurring	1200	1315	1565	2335	3280

TABLE 4.5.2.1-2: UNBURDENED COST ESTIMATES FOR HABITATION SYSTEM FOR ISS AND GROWTH CONFIGURATIONS (FIBERGLASS)

			0.1	0.125	0.167	0.2	0.25
VENDOR	COMPONENT	QNTY	FIBERGLASS	FIBERGLASS	FIBERGLASS	FIBERGLASS	FIBERGLASS
ABLE	MPL/HSO/ESA	3	27171	31890	35064	36739	40929
	JEM	1	16050	16545	17610	18417	19101
	TUNNEL	2	12090	12676	13276	13890	14430
	NODE	6	29406	31998	35328	35908	47118
	TOTAL		84717	93109	101278	104954	121578
TOERGE	MPL/HSO/ESA	3	5907	9163	14696	18656	34375
	JEM	1	4620	6875	11000	14003	25795
	TUNNEL	2	979	1502	1980	2422	3685
	NODE	6	10450	11577	13778	20543	28875
	TOTAL		21956	29117	41454	55624	92730

TABLE 4.5.2.1-3: UNBURDENED COST ESTIMATES FOR HABITATION SYSTEM FOR ISS AND GROWTH CONFIGURATIONS (ALUMINUM 6061-T6)

			0.1	0.125	0.167	0.2	0.25
VENDOR	COMPONENT	QNTY	6061-T6	6061-T6	6061-T6	6061-T6	6061-T6
ABLE	MPL	1	6000	7500	9000	10500	11250
	HSO	1	6160	7750	10125	11625	12375
	ESO	1	6320	8122	10250	11750	13250
	JEM	1	14625	16510	18000	21000	22500
	TUNNEL	2	4500	6000	6750	7500	8250
	NODE	4	24000	27000	33000	36000	45000
	AIRLOCK	2	12000	13500	16500	18000	22500
	TOTAL		73605	86382	103625	116375	135125

FIGURE 4.5.2.1-1: COST ESTIMATES FOR HABITATION SET, ISS AND GROWTH CONFIGURATIONS

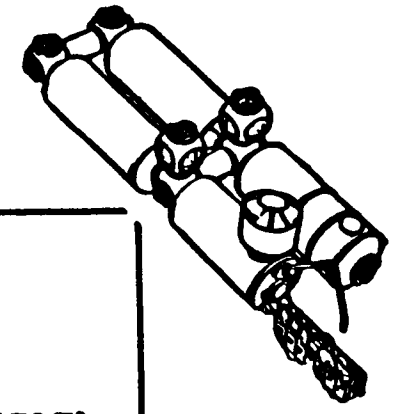

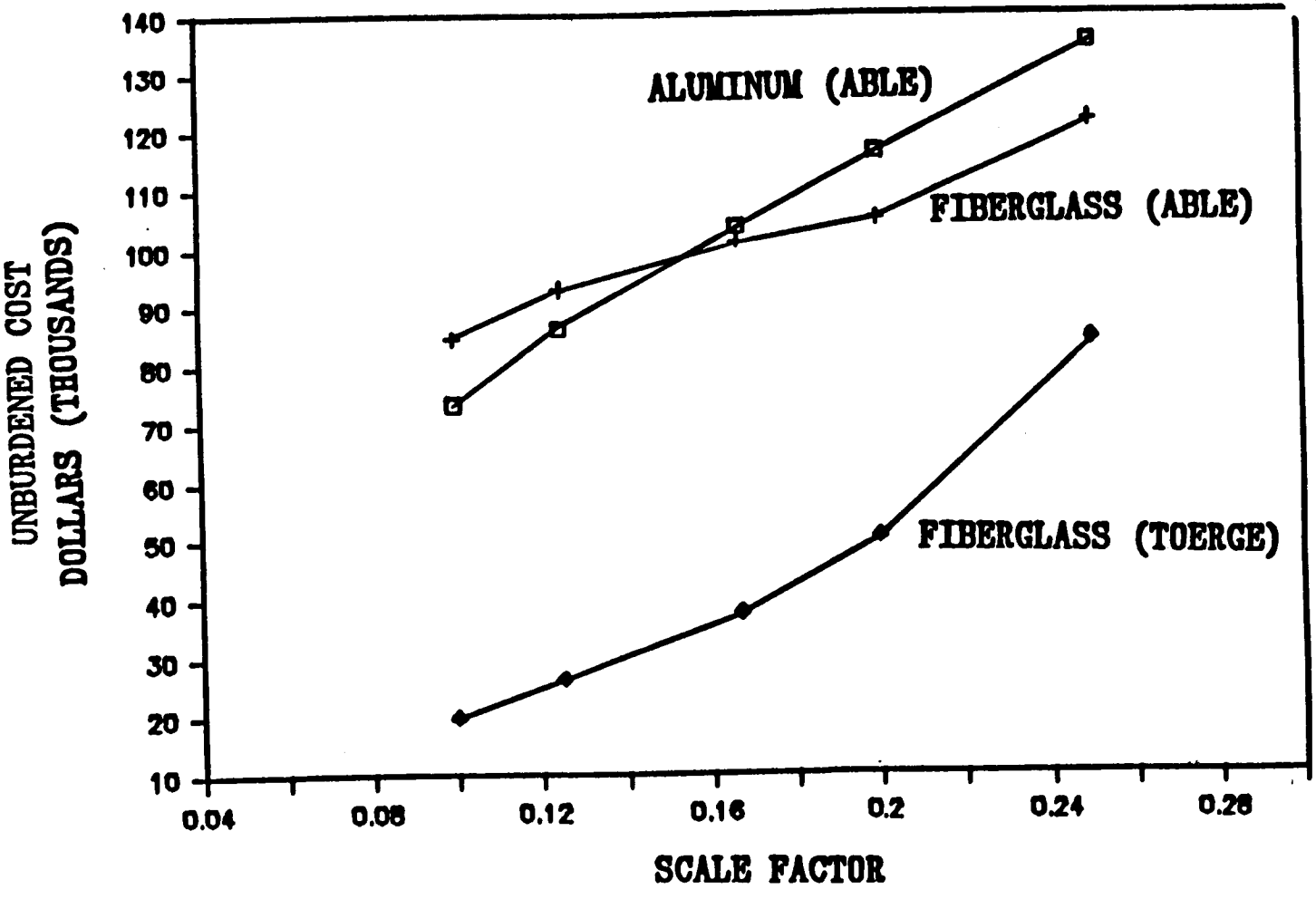

TABLE 4.5.2.2-1: UNBURDENED COST ESTIMATE FOR SUBSYSTEMS/ROTARY JOINTS FOR ISS AND GROWTH CONFIGURATIONS (ALUMINUM 6061-T6)

ISS CONFIGURATION

		0.1	0.125	0.167	0.2	0.25
COMPONENT	QNTY	6061-T6	6061-T6	6061-T6	6061-T6	6061-T6
SOLAR ARRAY	1	1474	1482	1497	1523	1560
	4	5896	5928	5988	6092	6240
RADIATOR	1	1080	1106	1280	1525	1610
(ROTARY+BETA)	6	6480	6636	7680	9150	9660
SOLAR DYN SYS*	1	3258	3495	3815	4215	4440
(SOLR+RADTR)	2	6516	6990	7630	8430	8880
ALPHA JOINT**	1	17350	17425	17109	16944	17367
	2	28480	28715	28104	27860	28706
UNIV. JOINT	1	9322	9517	9652	9874	10379
	10	93220	95170	96520	98740	103790
TOTAL (ISS)		140592	143439	145922	150272	157276

GROWTH CONFIGURATION
(Add 12 more solar dynamic systems and universal joints)

UNIVERSAL JOINTS	12	111864	114204	115824	118488	124548
SOLAR DYN SYS	12	39096	41940	45780	50580	53280
TOTAL (GROWTH)		291552	299583	307526	319340	335104

* ENGINE/POWER CONDITIONER UNIT INCLUDED
** MOTOR COST IS QUOTED SEPERATELY

TABLE 4.5.2.2-2: UNBURDENED COST ESTIMATE FOR ALPHA JOINT MOTOR SYSTEM

		0.1	0.125	0.167	0.2	0.25
COMPONENT	QNTY	6061-T6	6061-T6	6061-T6	6061-T6	6061-T6
MOTOR SYSTEM	1	1300	1400	1875	2250	2500

FIGURE 4.5.2.2-1: COST ESTIMATES FOR SUBSYSTEMS AND ROTARY JOINTS, ISS AND GROWTH CONFIGURATIONS

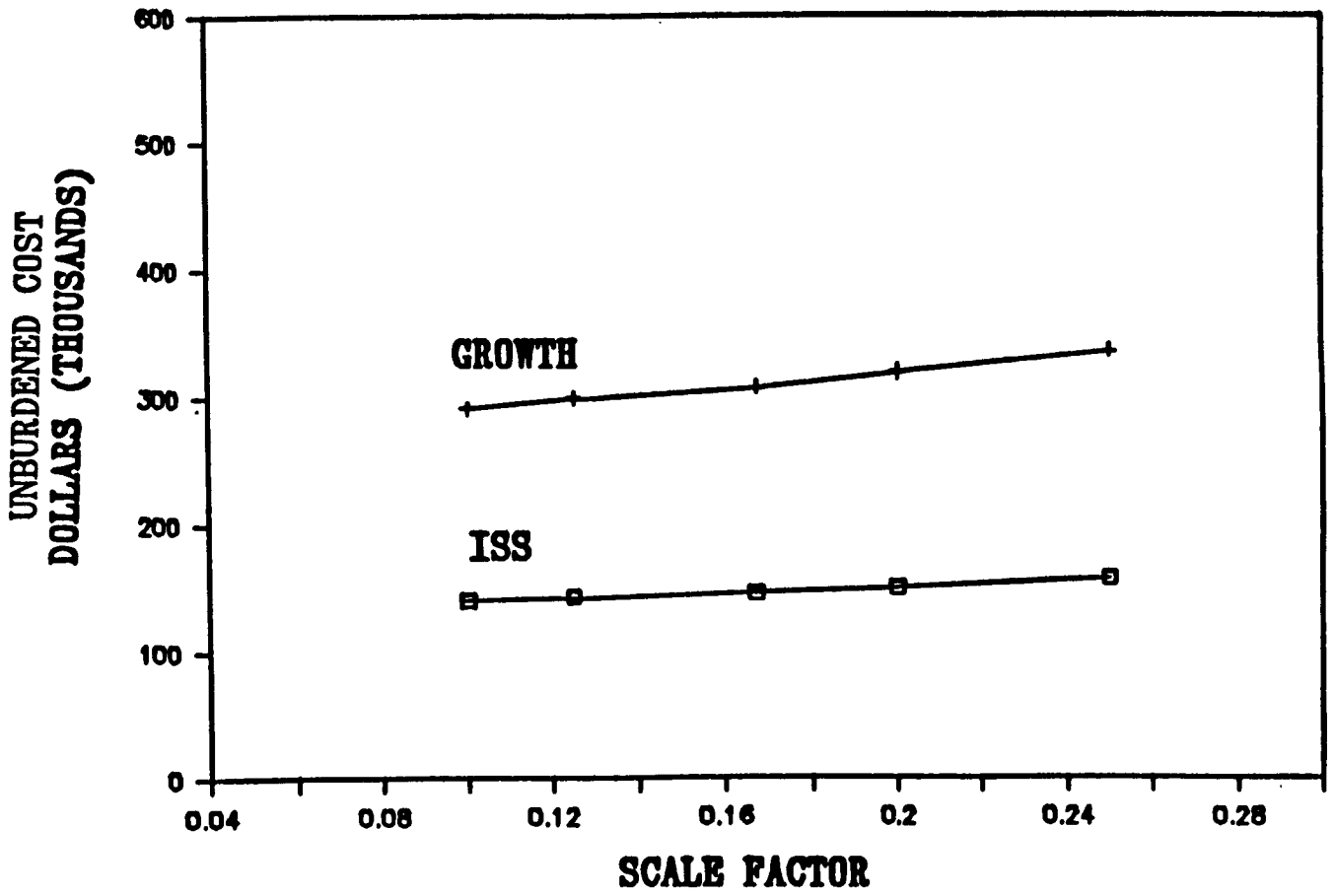

The costs for the truss tubes are listed in Tables 4.5.2.3-1 and 4.5.2.3-2. The cost estimates for the graphite epoxy tubes are plotted versus the scale factor in Figure 4.5.2.3-1 for the ISS configuration. In Figure 4.5.2.3-2, the cost estimates for the Aluminum and selected graphite epoxy tubes are plotted for the ISS configuration. The cost curve for the 1/10 scale aluminum tubes rises slightly due to the fact that they must be special-ordered. The wide variation in the cost estimates for the P75 tubes is attributed to the inexperience of industry in using the relatively new P75 material in applications involving very thin sections.

4.5.2.4 Nodal Joints and Fittings

A number of vendors and machine shops were contacted for various parts of each joint design. Those with the better fabrication methods and experience were included in forming the cost estimates. Although quotes were requested for all scales investigated, all vendors contacted refused to estimate the cost of producing replically scaled LaRC and Star-Net joints at sizes smaller than 1/5 scale on a fixed-price contract basis. This is primarily due to the extremely tight tolerances on small-scale joints (full-scale tolerance for the LaRC joint is 3.0 mils). Cost quotes increase sharply from full-scale to 1/5 scale because of this tolerance sensitivity. Joints proposed by AEC-ABLE are quoted for the range from 1/4 to 1/8 scale. For this joint design, cost decreases from full-scale to 1/5 scale, and increases for smaller scales due to the tight tolerances and fine threads of miniature-size fasteners. All costs quoted in this section include 5% spares and assume an average of 6.5 fittings per nodal joint.

The cost estimates for the individual nodal joints and fittings, together with the total cost for the ISS and Growth configurations, are provided in Table 4.5.2.4-1. Additionally, the per-item costs for the LaRC joint are presented in this table. The total costs for the three different joint designs for ISS and Growth configurations are illustrated in Figures 4.5.2.4-1 and 4.5.2.4-2, respectively.

TABLE 4.5.2.3-1: UNBURDENED COST ESTIMATES FOR TUBING FOR ISS CONFIGURATION

VENDOR	MATERIAL	0.1	0.125	0.167	0.2	0.25
ABLE	ALUMINUM	2420	1600	1940	2725	3400
ART	GR/EP, T-300	17815	24884	44678	58012	106045
	GR/EP, P75	104832	132812	176676	284250	298678
LAMIGLASS	GR/EP, T-300		18717	33225	44625	76975
	GR/EP, P75	195604	476610	621027	1109913	1830538

TABLE 4.5.2.3-2: UNBURDENED COST ESTIMATE FOR TUBING FOR GROWTH CONFIGURATION

VENDOR	MATERIAL	0.1	0.125	0.167	0.2	0.25
ABLE	ALUMINUM	3172	2090	2544	3569	4456
ART	GR/EP, T-300	23023	30656	56045	67565	134995
	GR/EP, P75	135239	171327	227912	366682	385295
LAMIGLASS	GR/EP, T-300		24316	43164	58083	100042

FIGURE 4.5.2.3-1: COST ESTIMATES FOR GRAPHITE EPOXY TUBING, ISS CONFIGURATION

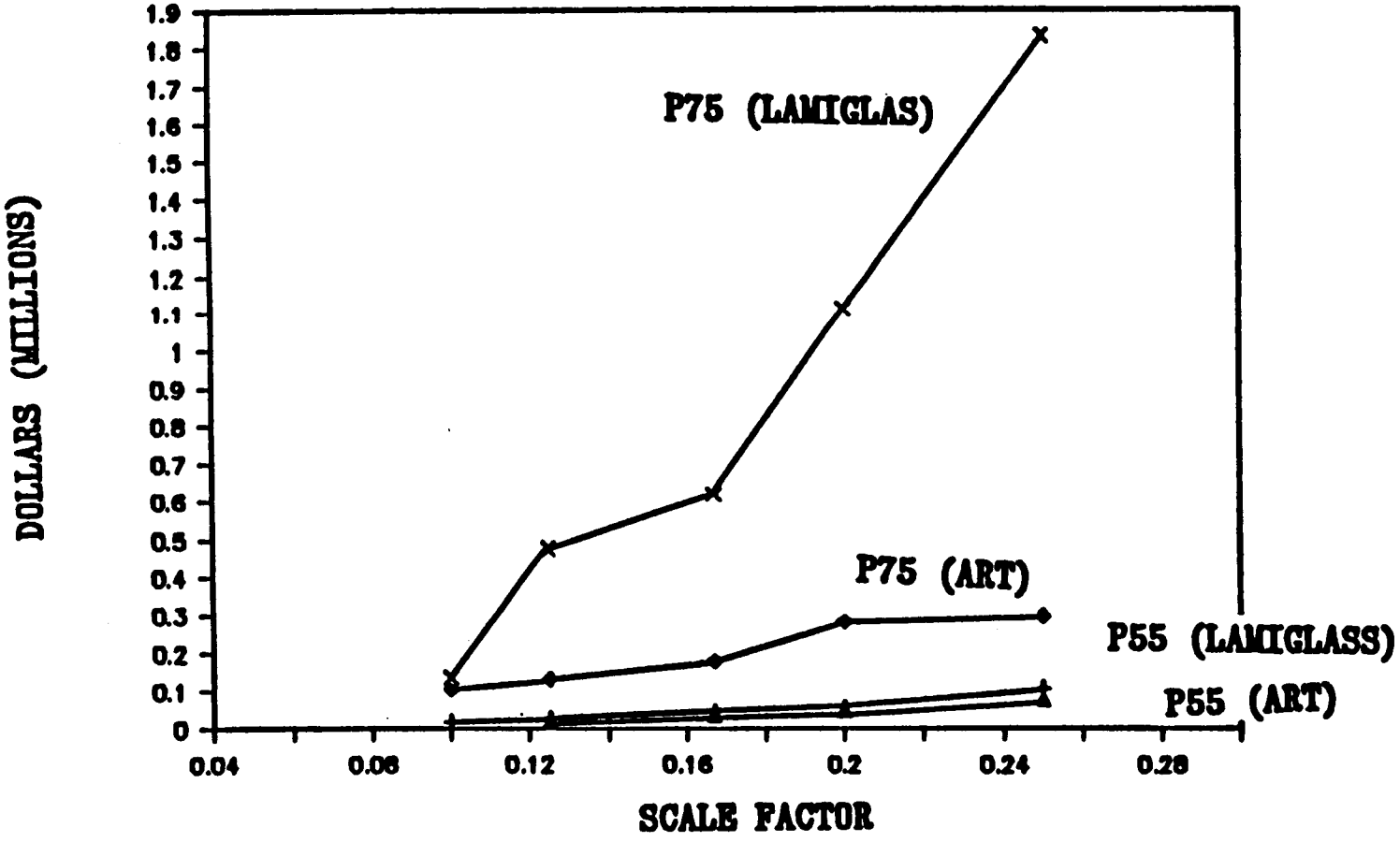

UNBURDENED COST

FIGURE 4.5.2.3-2: COST ESTIMATES FOR ALUMINUM AND SELECTED GR/EP TUBING, ISS CONFIGURATION

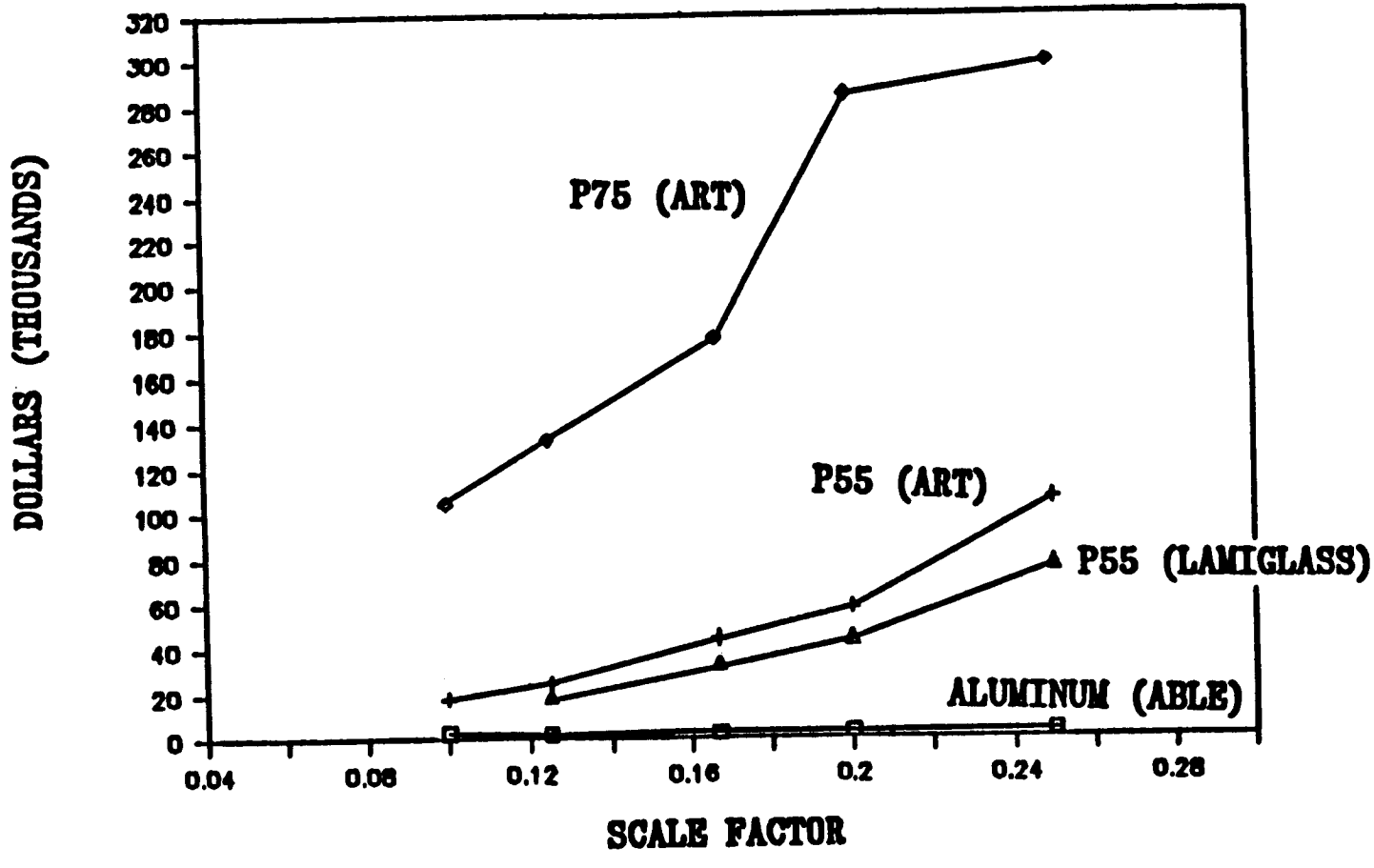

UNBURDENED COST

TABLE 4.5.2.4-1: UNBURDENED COST ESTIMATES FOR JOINT/FITTING FOR ISS AND GROWTH CONFIGURATIONS

JOINT DESIGN		0.125	0.167	0.2	0.25	1
LANGLEY	per 1 node			1189	849	340
	per 1 fitting			1646	1176	470
	per nodal joint*			11886	8490	3396
	Total ISS**			5091962	3637116	1454846
	Total Growth**			6988968	4992120	1996848
STAR-NET	per nodal joint*			6956	4968	1987
	Total ISS**			2979950	2128291	851231
	Total Growth**			4090128	2921184	1168356
ABLE	per nodal joint*	3580	2186	1197	1229	1822
	Total ISS**	1533672	936482	512795	526504	780545
	Total Growth**	2105040	1285368	703836	722652	1071336

* ONE NODAL JOINT INCLUDES ONE NODE AND 6.5 FITTINS IN AVERAGE
** INCLUDE 5% SPARES

FIGURE 4.5.2.4-1: COST ESTIMATES FOR NODAL JOINTS AND FITTINGS, ISS CONFIGURATION

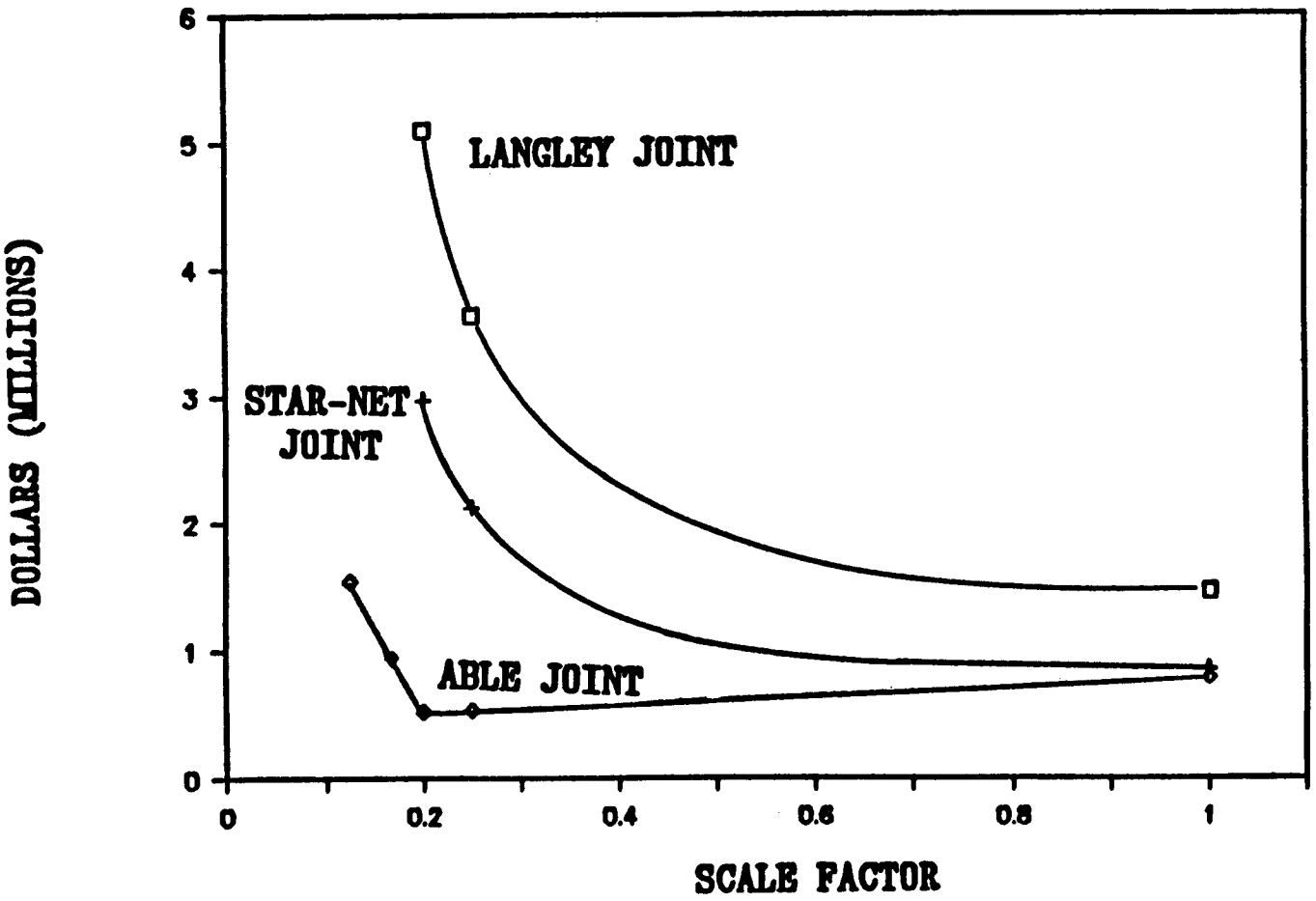

UNBURDENED COST

FIGURE 4.5.2.4-2: COST ESTIMATES FOR NODAL JOINTS AND FITTINGS, GROWTH CONFIGURATION

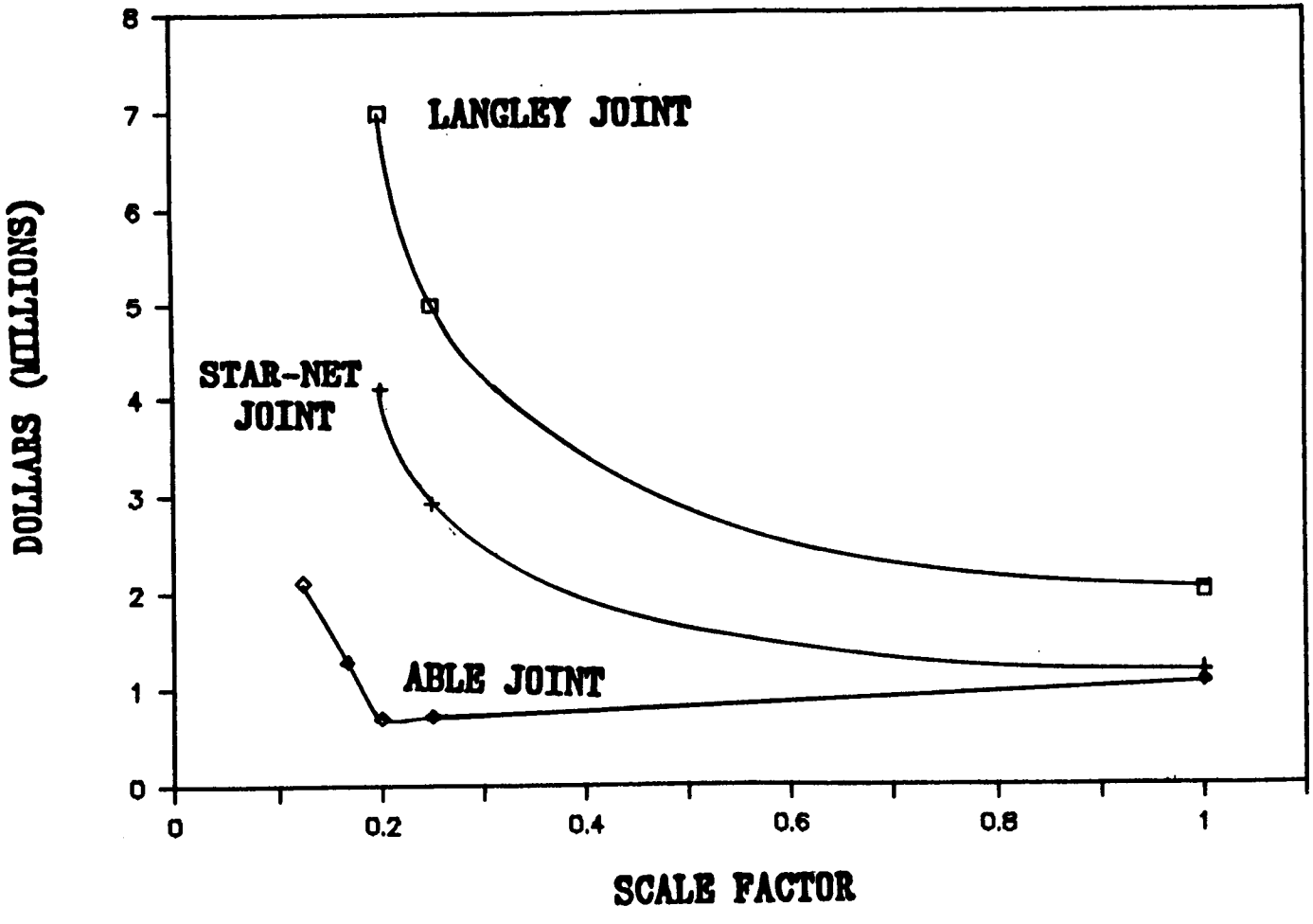

UNBURDENED COST

4.5.3 Cost Analysis

In order to assimilate all of the raw cost data at the system level, four model packages have been formed, each possessing different combinations of the components whose costs are estimated in Section 4.5.4. Each of these models incorporates fiberglass habitats and aluminum subsystem simulators (detailed in previous sections of this report), but the type of joint and material used in the truss tubes is varied between models. The packages are presented in decreasing order of component replication. In cases where several different cost estimates were obtained for the same component, the least expensive option was assumed. The cost data for each of these models is presented in tabular form in Tables 4.5.3-1 and 4.5.3-2 for the ISS and Growth configurations, respectively. These space station models are described as follows:

1. The Near-Replica model consists of replicated LaRC joints and P-75 graphite epoxy tubes. This model is only available in the 1/4 and 1/5 scale sizes because of the limitations imposed by joint fabrication considerations. Figure 4.5.3-1 illustrates the total cost of the Near-Replica model in graphical form for the ISS configuration. The cost for the Growth configuration, while not presented in graphical form, is listed in Table 4.5.3-2.

2. The Star-Net model consists of replicated Star-Net joints and P-55 graphite epoxy tubes. It is available only in the 1/4 and 1/5 scale sizes because of limitations imposed by joint fabrication considerations. Figure 4.5.3-2 illustrates the total cost of the Star-Net model for the ISS configuration. Cost data for the Growth configuration is also presented in the Table.

3. The Simulated model incorporates AEC-ABLE joints and P-55 graphite epoxy tubes in a space station model which is available in sizes ranging from 1/8 to 1/4 scale. Figure 4.5.3-3 illustrates the total cost of the Simulated model for the ISS configuration. Growth configuration costs are in Table 4.5.3-2.

TABLE 4.5.3-1: SUMMARY OF COST ESTIMATE FOR SPACE STATION MODEL

ISS CONFIGURATION

ITEM	DESCRIPTION	COST IN MILLIONS 1/10	1/8	1/6	1/5	1/4
1	LANGLEY JOINTS				5.09	3.64
2	STAR-NET JOINTS				2.98	2.13
3	ABLE JOINTS		1.53	0.94	0.51	0.53
4	ALTBNG+SUBSYS+HABSYS		0.19	0.21	0.22	0.27
5	P55TBNG+SUBSYS+HABSYS		0.21	0.24	0.27	0.34
6	P75TBNG+SUBSYS+HABSYS				0.51	0.56
1 + 6	NEAR REPLICA				5.6	4.2
2 + 5	STAR-NET				3.25	2.47
3 + 5	SIMULATED		1.74	1.17	0.78	0.87
3 + 4	SIMULATED-AL		1.72	1.14	0.74	0.79

TABLE 4.5.3-2: SUMMARY OF COST ESTIMATE FOR SPACE STATION MODEL

GROWTH CONFIGURATION

ITEM	DESCRIPTION	COST IN MILLIONS 1/10	1/8	1/6	1/5	1/4
1	LANGLEY JOINTS				6.99	4.99
2	STAR-NET JOINTS				4.09	2.92
3	ABLE JOINTS		2.11	1.29	0.7	0.72
4	ALTBNG+SUBSYS+HABSYS		0.46	0.48	0.51	0.57
5	P55TBNG+SUBSYS+HABSYS		0.48	0.52	0.57	0.67
6	P75TBNG+SUBSYS+HABSYS				0.88	0.95
1 + 6	NEAR REPLICA				7.87	5.94
2 + 5	STAR-NET				4.66	3.59
3 + 5	SIMULATED		2.59	1.81	1.27	1.39
3 + 4	SIMULATED-AL		2.57	1.77	1.21	1.29

FIGURE 4.5.3-1: COST ESTIMATES FOR NEAR-REPLICA MODEL, ISS CONFIGURATION

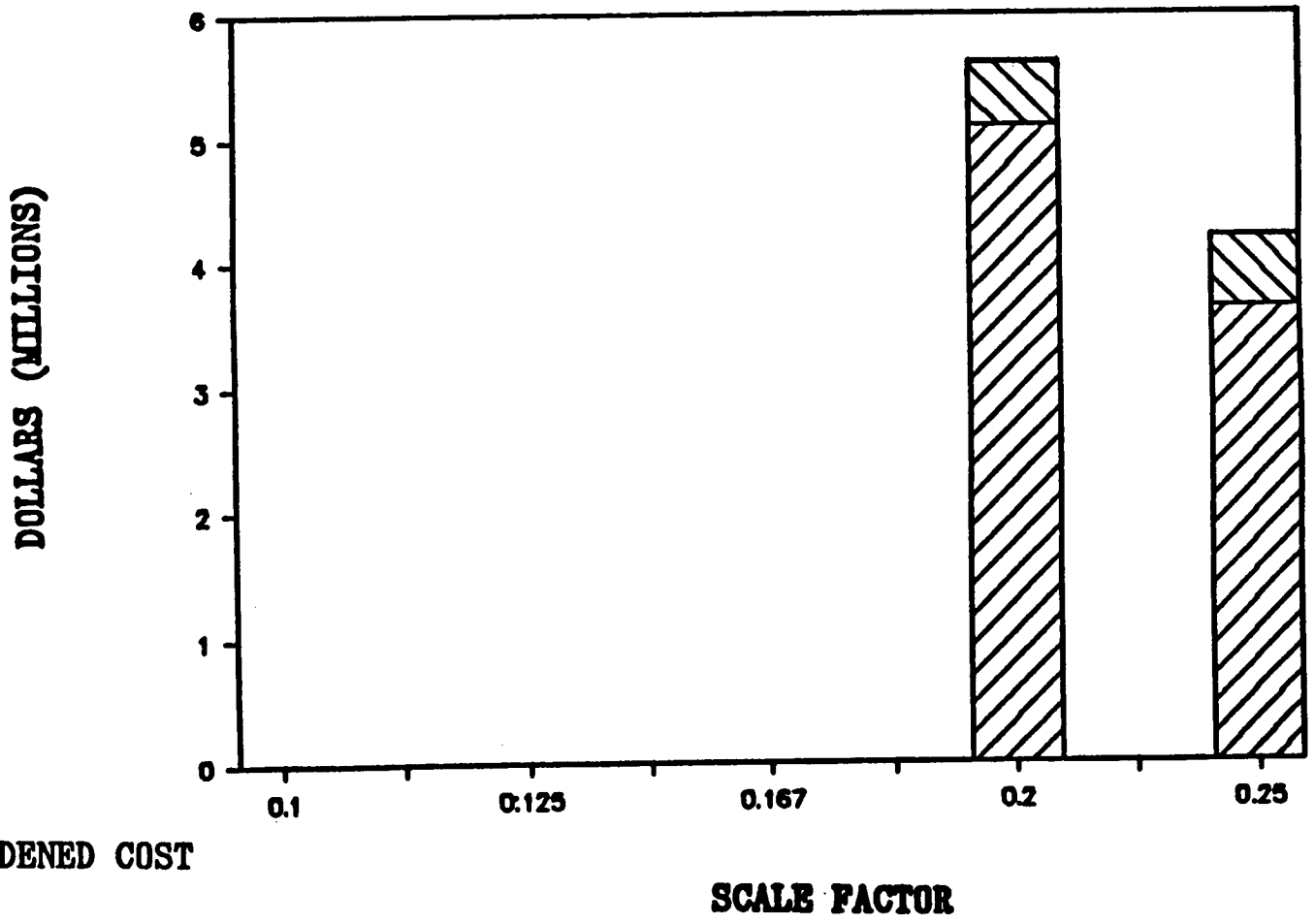

FIGURE 4.5.3-2: COST ESTIMATES FOR STAR-NET MODEL, ISS CONFIGURATION

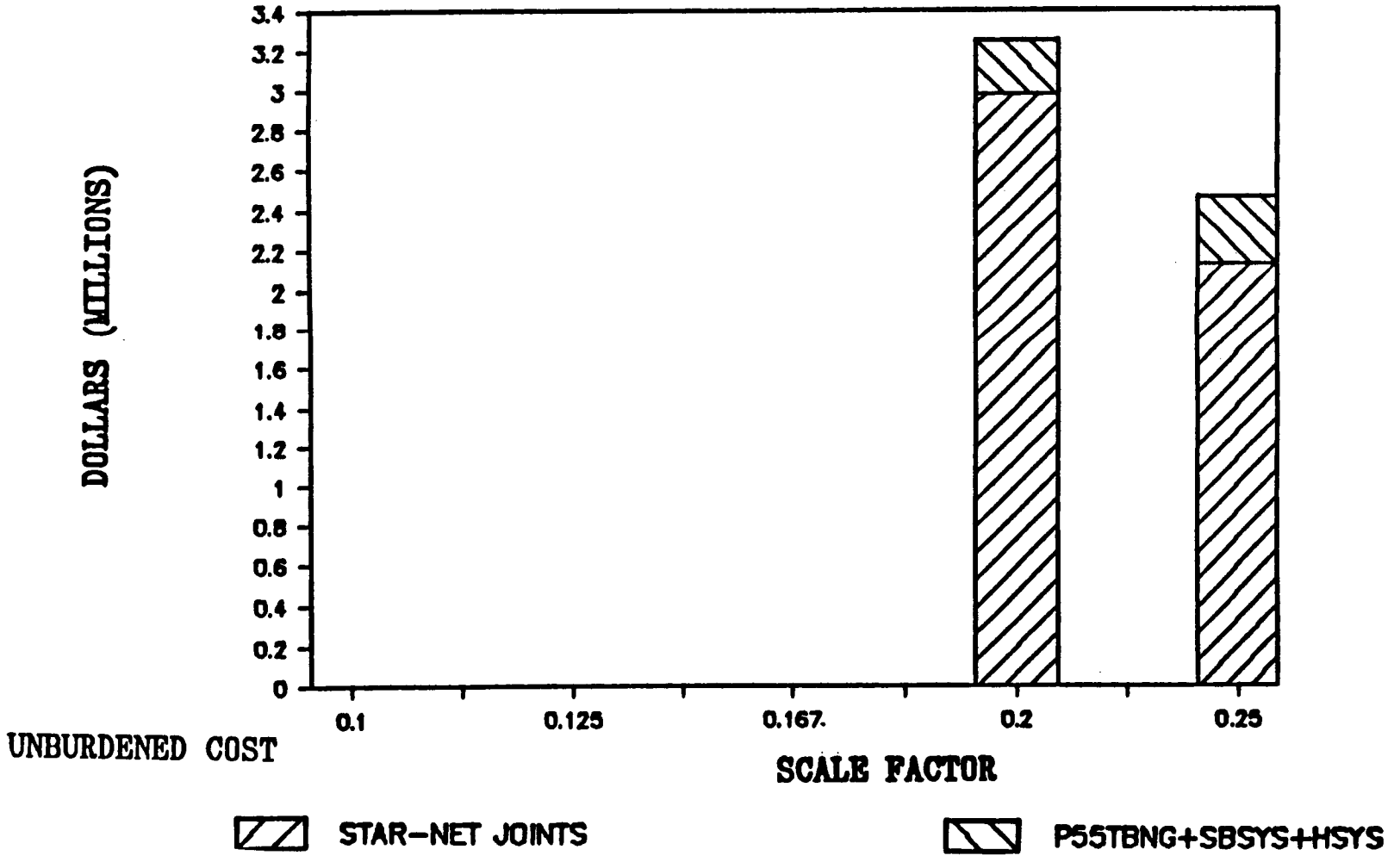

FIGURE 4.5.3-3: COST ESTIMATES FOR SIMULATED MODEL, ISS CONFIGURATION

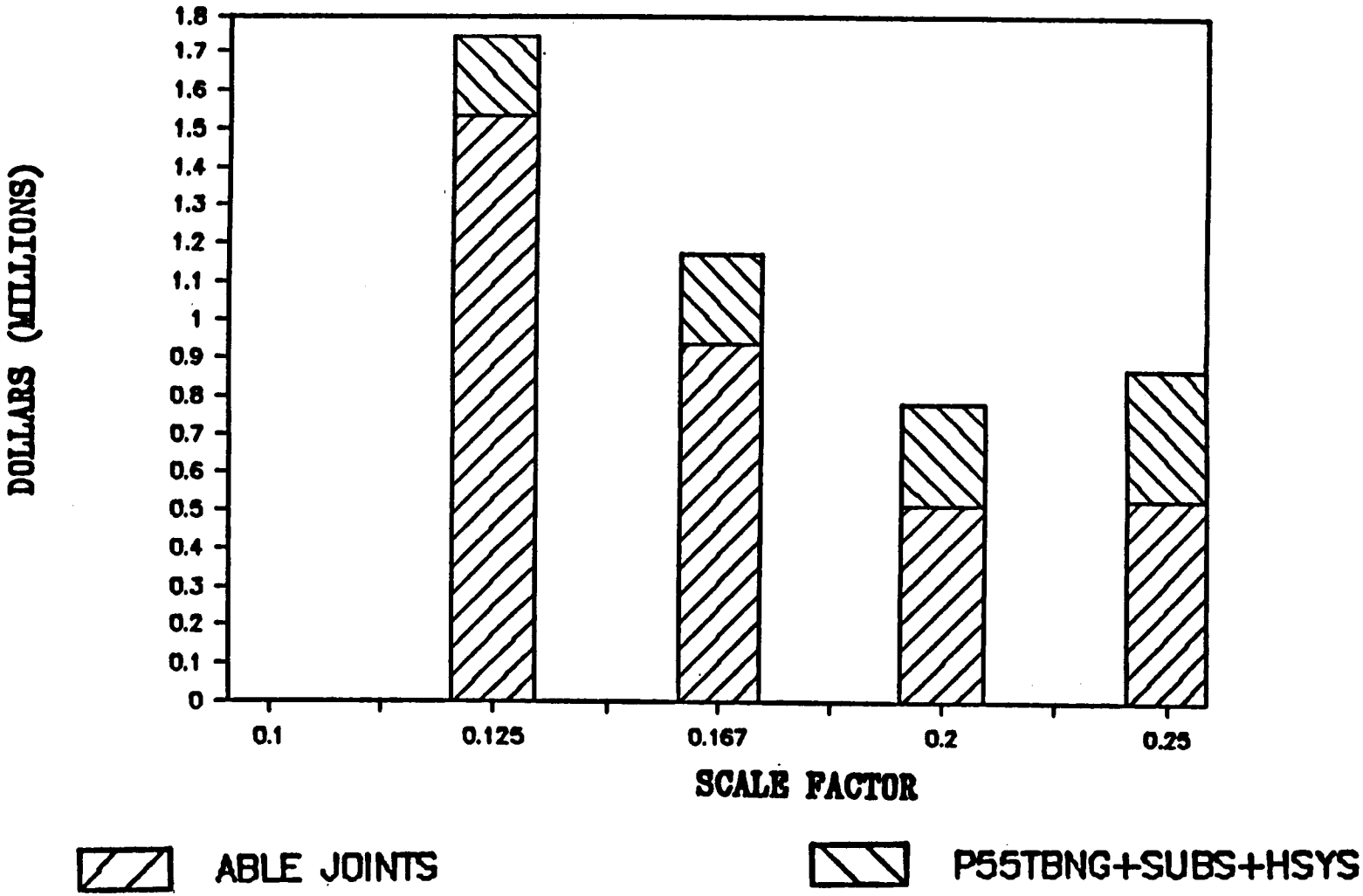

UNBURDENED COST

4. The Simulated-Al model, combining AEC-ABLE joints and aluminum tubes with the other components listed above, is available in sizes ranging from 1/8 through 1/4 scale , inclusive. Figure 4.5.3-4 illustrates the total cost of the Simulated-Al model for the ISS configuration, while the Growth configuration costs are contained in Table 4.5.3-2.

Figure 4.5.3-5 shows the relative cost of the first three models at the available scale factors for both the ISS and Growth configurations. The Simulated-Al model cost is not plotted because the cost difference between the Simulated and Simulated-Al models would make the curves nearly coincident at the chosen plot scale.

The salient points of Figures 4.5.3-1 to 4.5.3-5 are summarized as follows:

1. The Near-Replica model configuration is the most expensive, followed by the Star-Net model. Both the Simulated and Simulated-Al models cost substantially less than the first two, with the Simulated-Al version only slightly less expensive than the Simulated.

2. In general, the cost of any of the scale models discussed above increases with smaller scales because of the joint fabrictation costs. The minor exception to this is noted in the slight decrease in cost of the Simulated and Simulated-Al models between 1/4 and 1/5 scales. This is due to the relative tolerance insensitivity of the AEC-ABLE joint design.

3. The cost of the joints dominates the total cost of any of the scale models. Although the cost for the graphite epoxy tubes is higher than the cost for the aluminum tubes, the difference is found to be negligible when factored into the total cost of any of the four options presented. The cost difference between the Simulated and Simulated-Al models does not offset the increased weight penalty associated with the use of aluminum tubes.

4. The fraction of the total cost attributable to the nodal joints and fittings decreases as more model components are simulated rather than replicated. For example, 90% of the total price of the 1/5 scale Near-replica model is attributed to the joints and fittings. For the 1/4

FIGURE 4.5.3-4: COST ESTIMATES FOR SIMULATED-AL MODEL, ISS CONFIGURATION

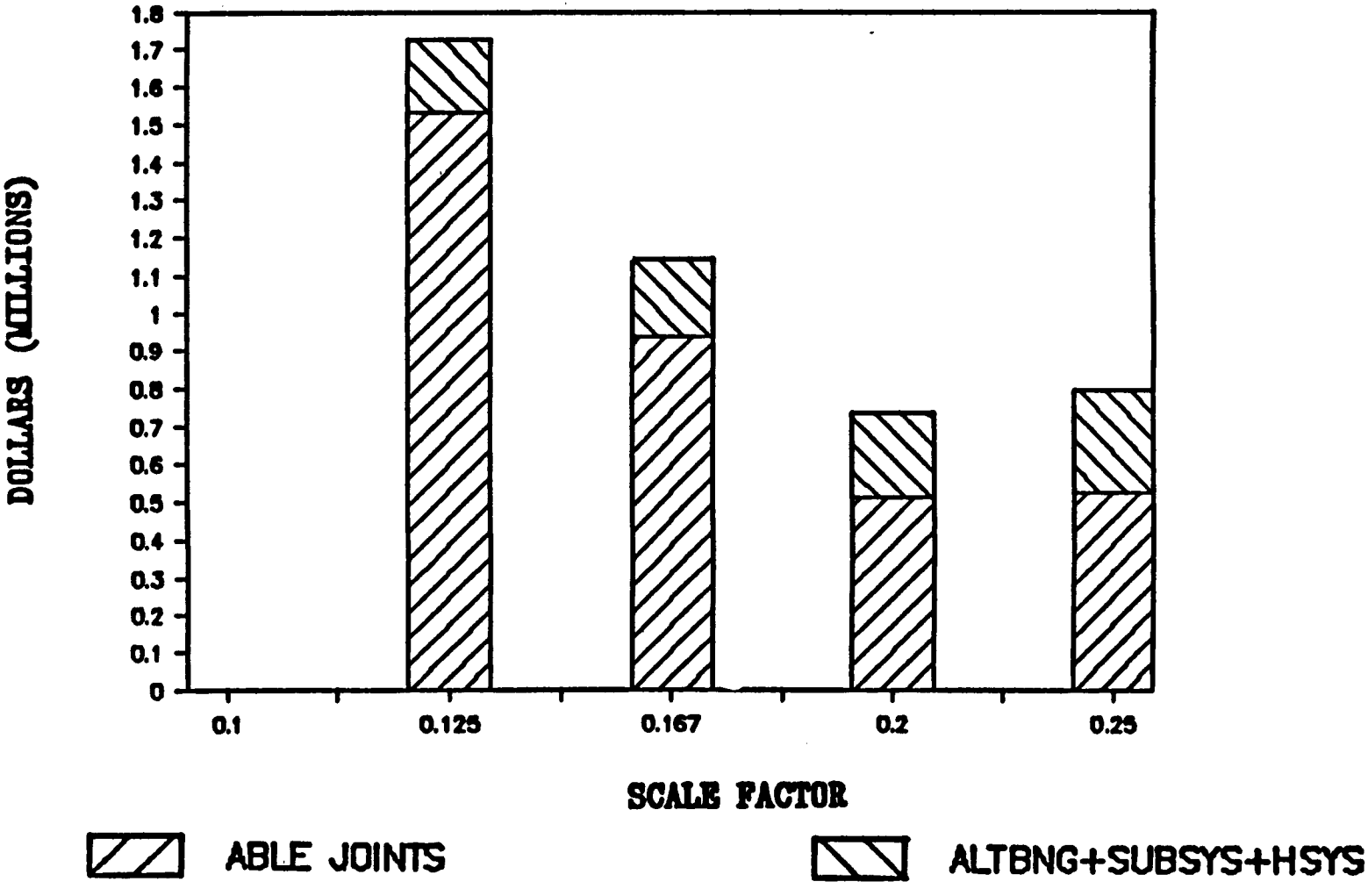

FIGURE 4.5.3-5: COST ESTIMATES FOR NEAR-REPLICA, STAR-NET AND SIMULATED MODELS, ISS AND GROWTH CONFIGURATION

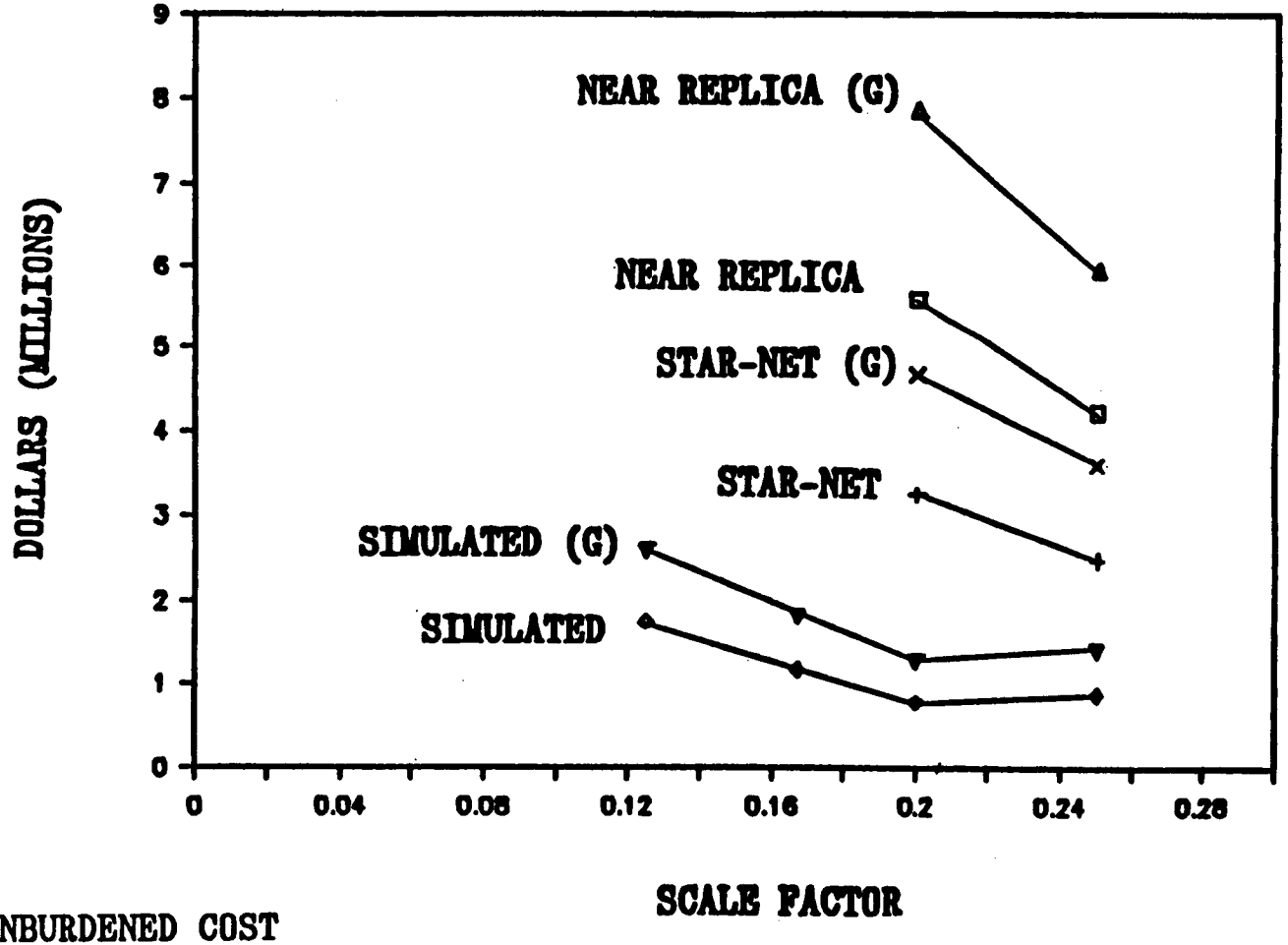

UNBURDENED COST

scale Simulated model, only 65% of the total price is quoted for the joint components.

The cost estimates presented in this section reflect only the costs of producing the components associated with the scale models of the space station configurations studied. The labor-intensive process of assembly is not included, but is expected to be similar for each of the options presented. This is because the process is dominated by truss assembly involving tube/joint and joint/node connections. There are the same number interfaces to be joined, regardless of the scale of the model.

4.6 SUMMARY OF DESIGN, FABRICATION, AND COST DATA

Data presented in this section form the basis for the preliminary design and costing of the space station scale model. Modules with sufficiently high fundamental vibration frequencies were designed as simulated units, in an effort to maintain low cost. These simulators were designed such that dynamic characteristics of the modules were replicated according to the scaling laws presented in Section 2.1. A similar philosophy was adopted for the design of the simulated solar arrays, thermal radiators, and truss tubes. Three types of joints and fittings, found to be the most expensive components in the model, were replicated by linearly scaling all dimensions, including tolerances. The costs of the individual parts mentioned above were estimated by vendors experienced in the fabrication of similar items. From these cost estimates, four combinations of replicated and simulated components were constructed and ranked according to cost. A summary of the design, manufacturing, and cost results that impact the choice of the model scale factor is presented in Section 5.3.

5.0 SUMMARY

This chapter summarizes the results of the analyses and trade studies on scaling and joint effects (2.0), dynamic analyses and suspension interaction (3.0), and manufacturing and cost (4.0). Some of the potential problems in constructing and testing the scale model are reviewed. The results are combined in a system-level analysis to form a basis for recommending the model scale factor.

5.1 SCALING SUMMARY

This section summarizes the application of the replica scaling laws to simplified theoretical joint and truss tube models and the practical interpretation of the results for the specific case of a Space Station scale model. Included are unscaled effects which cannot practically be changed in the test environment such as gravity, air, handling effects, and the building size. The suspension effects are summarized in the next section.

5.1.1 Scaling of Stiffness

Three observations were made regarding the scaling of the joint and tube stiffnesses:

- In modeling the truss tube properties, the only significant parameter to match is the extensional stiffness of the tube, as the tubes are slender and exhibit little bending.

- The stiffness of the joint/tube/joint strut is insensitive to the joint stiffness because the tube is relatively flexible. However, in areas where local load effects are important (i.e. module interconnects), more replication may be required.

- The gravity preload in the joints due to (only) the truss weight is a small fraction of the mechanical preload. However, the utility trays should be suspended independently since the gravity preload grows to a significant

fraction of the mechanical preload if the utility tray weight is supported by the truss.

Table 5.1.1-1 summarizes the practical significance of the different factors discussed in Chapter 2. In general, the material used and the suspension system contribute to the stiffness as first order effects while the joint dynamics, gravity preloads, and airloads are at worst second order effects. Note that joint effects drive one to select a large scale factor while the gravity effects tend to drive the selection to a smaller scale factor. Based on the results of Chapter 2, correctly scaling the stiffness, and thereby obtaining mode and frequency data, appears to be an achievable goal.

5.1.2 Scaling of Damping

Several observations were made regarding the scaling of damping in the structure:

- The damping in the joints can probably be matched if perfect replica scaling is employed, including scaled tolerances. The practical feasibility of attaining this precision in 1/10 to 1/4 scale is low.

- The influence of the gravity loads and torques on the joint damping is uncertain.

- The suspension system can act as a series of tuned-mass dynamic absorbers, significantly increasing the apparent damping in the model.

Table 5.1.2-1 summarizes the importance of several factors on the difficulty of obtaining damping data from the scale model. The difficulty of manufacturing joints to the required tolerances and the presence of external energy dissipation mechanisms that may provide the same order of damping contribute to the conclusion that scaling the damping is probably not achievable in practice for the range of scale factors considered.

TABLE 5.1.1-1 PRACTICAL SIGNIFICANCE OF REPLICA SCALING LAWS FOR STIFFNESS

	MATERIAL	JOINTS	AIR	GRAVITY	SUSPENSION
RELATIVE IMPORTANCE	●	◓	O	◓	●
ORDER OF SIGNIFICANCE	1	10^{-1}	10^{-3}	10^{-1}	1
INFLUENCE ON SCALE FACTOR	-	↑	-	↓	(see 5.2)
ACHIEVABLE IN PRACTICE	YES	YES	-	YES	(see 5.2)

o BASED ON THESE CONSIDERATIONS, CAN PROBABLY SCALE STIFFNESS

TABLE 5.1.2-1 PRACTICAL SIGNIFICANCE OF REPLICA SCALING LAWS FOR DAMPING

	MATERIAL	JOINTS	AIR	GRAVITY	SUSPENSION
RELATIVE IMPORTANCE	●	●	◒	◒	●
ORDER OF SIGNIFICANCE	10^{-3}	10^{-2} ?	10^{-4}	?	10^{-2} !
INFLUENCE ON SCALE FACTOR	-	↑	-	↓	↑
ACHIEVABLE IN PRACTICE	YES	NO	-	?	NO

- BASED ON THESE CONSIDERATIONS, PROBABLY CANNOT SCALE DAMPING:
  1) DAMPING DOMINATED BY JOINTS WHICH ARE HARD TO SCALE
  2) HAVE SUSPENSION DAMPING EFFECTS WHICH ARE OF THE SAME MAGNITUDE AND ARE UNIQUE TO THE 1G TEST CONDITIONS

5.1.3 Other Unscaled Effects

Many of the unscaled effects discussed in Section 2.1 drive the selection of the scale factor toward smaller scales:

- Testing a 1/10 scale model in 1-g is comparable to testing the full-scale Space Station in 0.1-g. Thus, as the scale factor of the model is reduced, the test conditions asymptotically approach those of the zero-gravity on-orbit environment.

- The margin of safety against buckling while suspended in 1-g improves since the ratio of Pgravity/Pcr scales linearly with the scale factor.

- The ratio of the frequency of the first system mode of the model to the frequency of the pendulum modes increases for smaller scales (because the fixed size of the building permits longer cables for smaller scales).

- In terms of handling, the weight and volume decrease dramatically as the scale factor is reduced.

Other effects tended to favor the selection of a larger scale factor:

- The traceability of the results from the scale model to the full-scale Space Station is enhanced.

- In terms of handling, the risk of fracture due to impact loads and the fragility of thin sections favors larger scales.

- The cost of miniaturizing added hardware and mechanisms (i.e. payload gimbals, control devices, MRMS, etc.) increases with smaller scales.

- The percentage of the parasitic test equipment weight is reduced for larger scales.

Figure 5.1.3-1 illustrates the variation of some of these effects with the scale factor. The curves are normalized so that all the effects measure

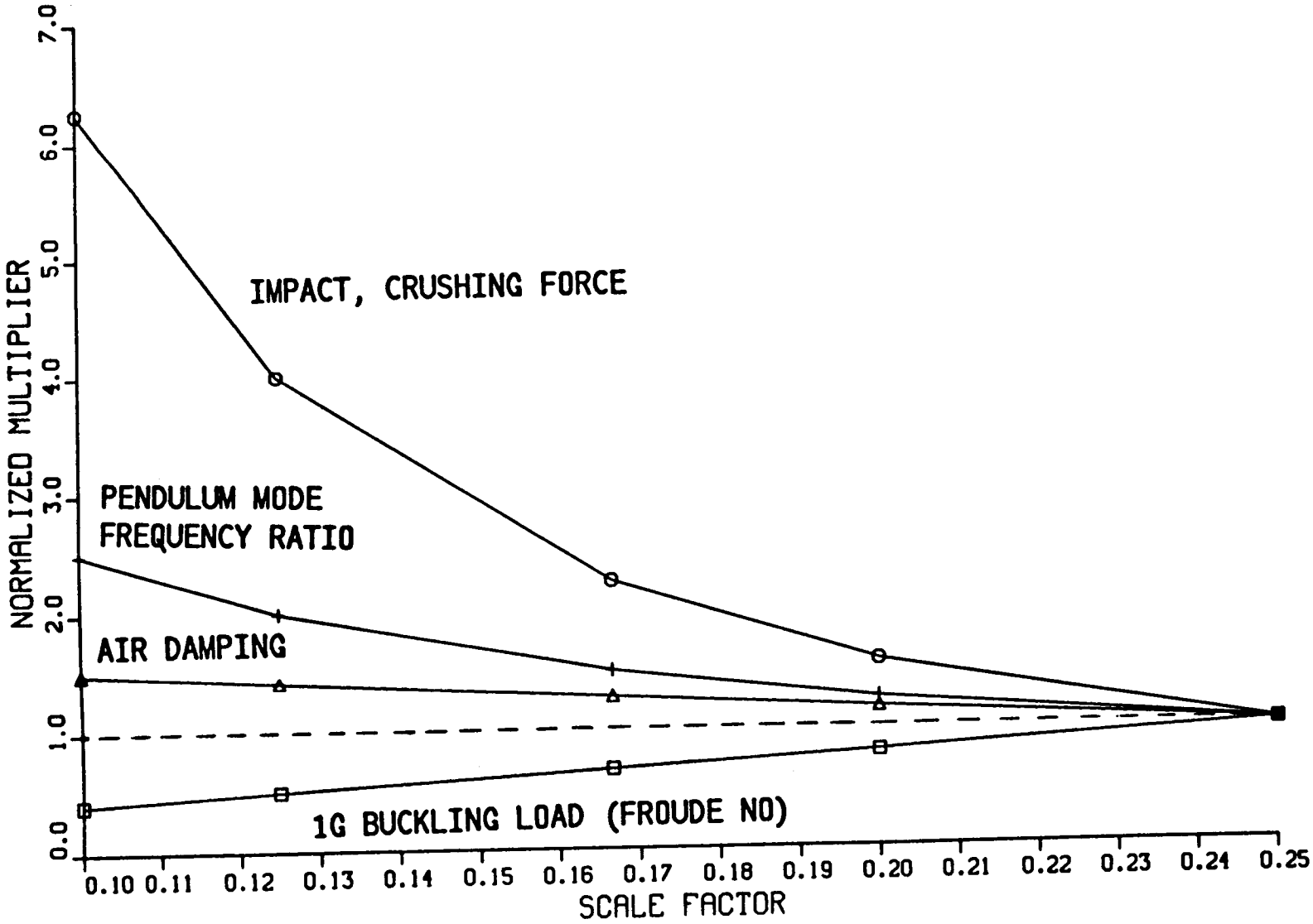

FIGURE 5.1.3-1 VARIATION IN UNSCALED EFFECTS VS. SCALE FACTOR

unity at 1/4 scale. Note that theoretically there is little variation in the undesirable air damping effects with scale factor.

5.2 SUSPENSION INTERACTION TRADE SUMMARY

This section summarizes the results of analyses which evaluated the ability of the suspended scale model to emulate the dynamic behavior of the full-scale free-free Space Station. The suspension system can interact with the model in a number of ways (Section 3.3), to the detriment of the tests being conducted. The suspension analysis results also provide insight into some potential problems in testing the scale model and in correlating the results.

Several conclusion and insights into the design of the suspension system can be inferred from the analyses:

- It is highly desirable to suspend the model by the large rigid masses and at all flexible appendages. This offloads over 95% of the weight of the Space Station from the truss. This practice minimizes both the gravity preload in the joints and the pendulum mode interactions. For the configurations analyzed, a buckling margin of safety of at least 2.0 and little sag can be achieved by suspending the Step-2 and ISS by 35 and 65 cables, respectively. Only two cables were required to support each of the radiators and solar arrays.

- There is insufficient height available in the LSL to permit the use soft (low spring-rate) cables without incurring high strain rates and damping levels. Fortunately, most of the system modes are planar, but in order to resolve these modes using a hard suspension system, the models will have to be tested in all 3 planar orientations. This may not be necessary if an active suspension system is employed.

- It is desirable to anchor the shadow structure to the LSL ceiling in order to minimize the dynamic interaction.

- Dynamically, there is a slight preference for smaller scales. The frequency errors increased noticeably from 1/5 to 1/4 scale, but decreased only slightly from 1/5 to 1/10 scale. This is shown in Figures 5.2-1 and 5.2-2, which compare the absolute value of the frequency error between the suspended and free-free modes. The table in each plot lists the orientation of the model in the LSL (x, y, or z-axis vertical) which provides the best data. The mode shape and modal mass distribution errors also decreased slightly with decreasing scale factor. Figure 5.2-3 summarizes the number of modes which could be obtained with confidence as a function of scale factor.

- In several cases, some modes could not be resolved at any of the scale factors between 1/10 and 1/4 scale; largely because they are characterized by motion in all three planes. Figure 5.2-3 shows that over the range from 1/4 to 1/10 scale, an ISS Station model could theoretically match 7 to 10 out of 11 free-free system modes, and 39 to 49 out of a total of 58 free-free modes below 1 Hz on the full-scale article. Similarly, the Step-2 build-up stage could match 9-11 out of 11 free-free system modes and 70 to 72 out of a total of 75 free-free modes below 1 Hz on the full-scale article. It is important to note that these analyses compare analytical data with analytical data (as opposed to test data) and thus are not conservative.

The analyses also revealed a number of potential problems regarding the suspension system:

- The cables must be "tuned" to a prescribed stress level in order to avoid preloading or over-stressing the structure, minimize the weight of the cables, and provide a common basis for correlating analytical and test data. Tuning the cables is a potentially difficult, iterative procedure. Additional safety cables are recommended when hoisting the model, since all the cables will be untuned at that point.

- There is a strong potential for a cable "string" mode interaction problem whereby the cables function as vibration absorbers. This could have a strong effect on damping test results and a smaller effect on the frequency and mode shape test results.

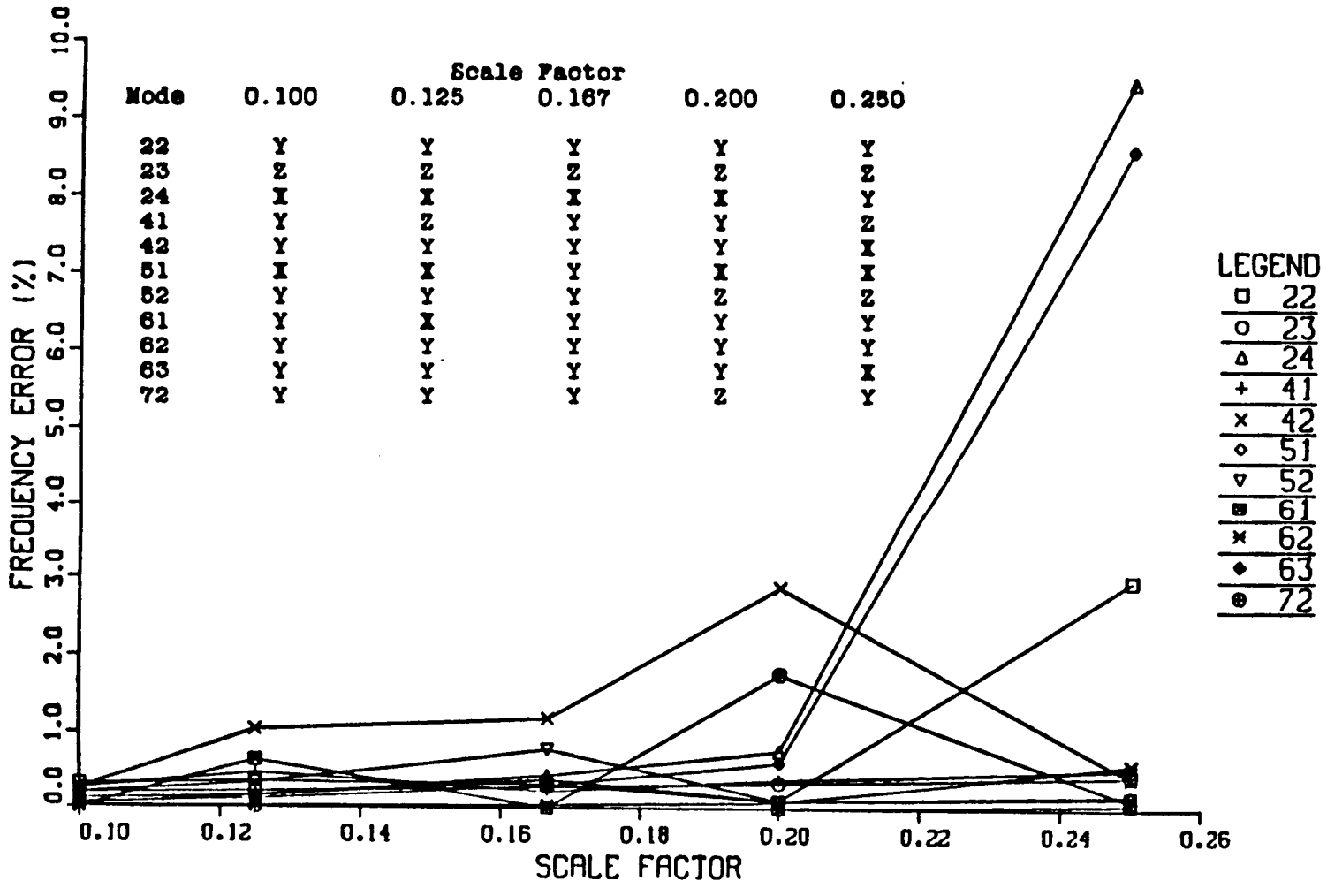

(ABSOLUTE VALUE OF FREQUENCY ERROR BETWEEN SUSPENDED & FREE-FREE MODES)

FIGURE 5.2-1 FREQUENCY ERROR SUMMARY - STEP-2 BUILD-UP STAGE

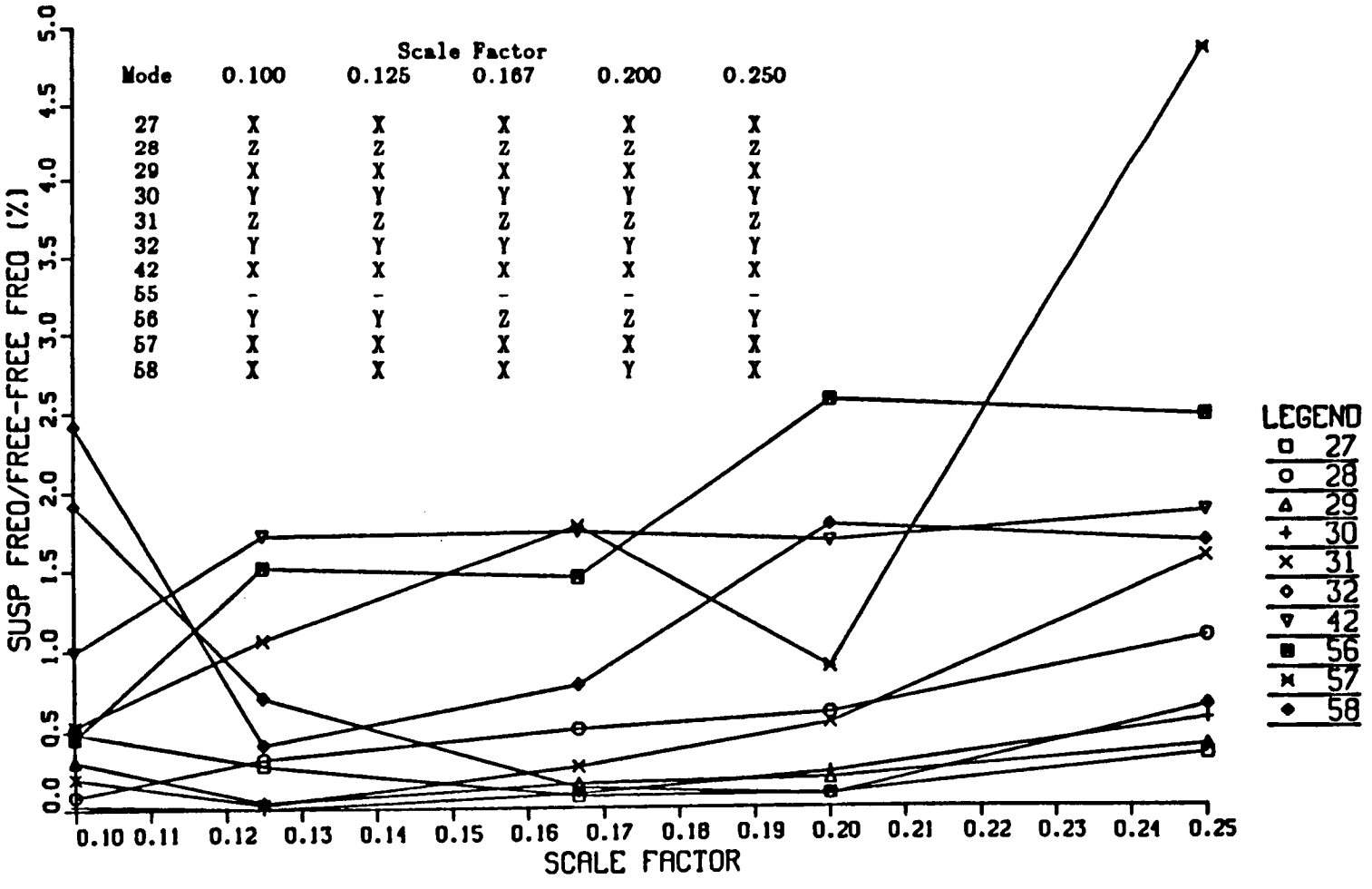

(ABSOLUTE VALUE OF FREQUENCY ERROR BETWEEN SUSPENDED & FREE-FREE MODES)

FIGURE 5.2-2 FREQUENCY ERROR SUMMARY - ISS SPACE STATION

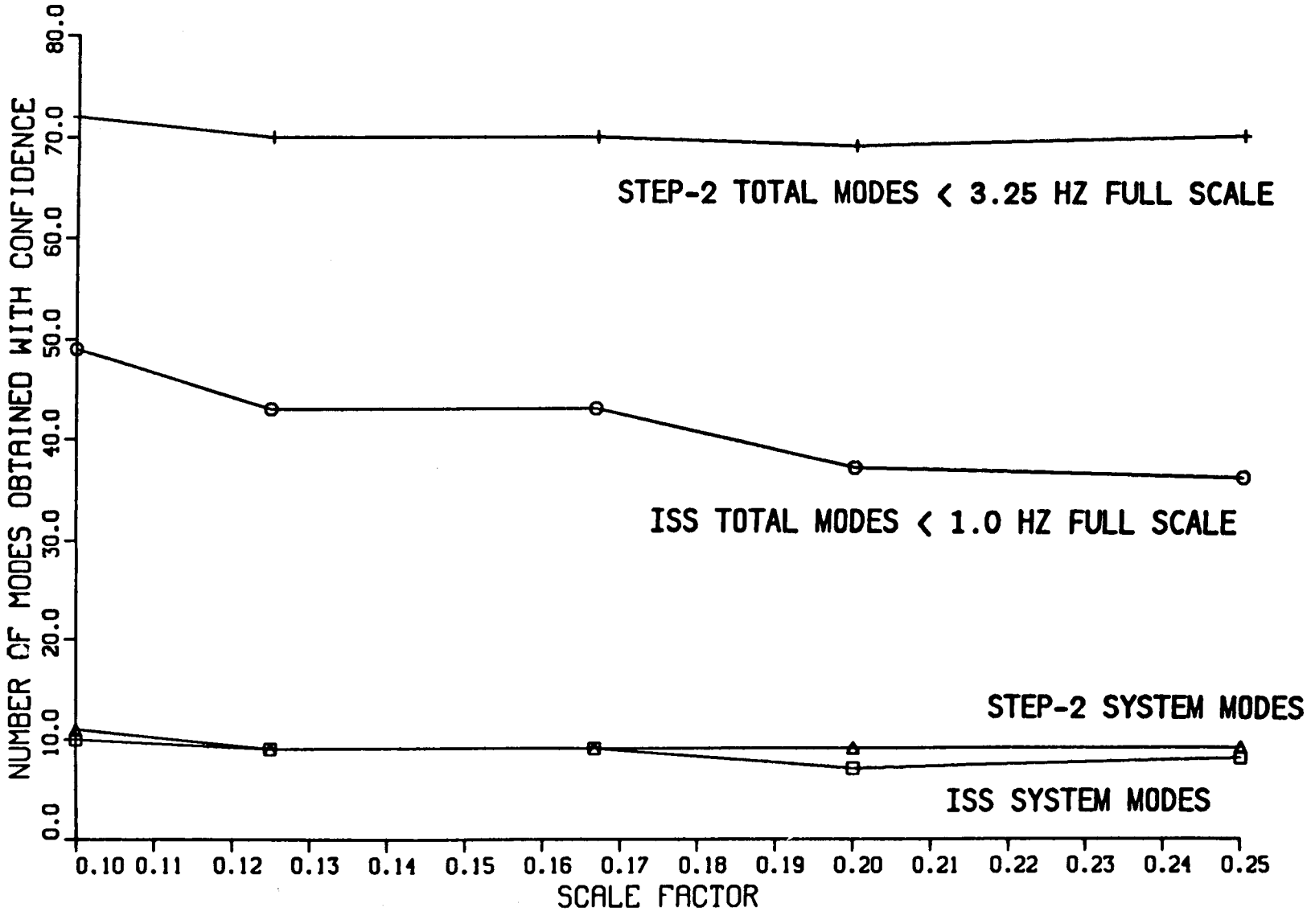

FIGURE 5.2-3 SUSPENSION INTERACTION TRADE SUMMARY

NUMBER OF MODES WITH X-ORTHOGONALITY > .85 WHEN COMPARED WITH FREE-FREE MODES

- There is a potential cable weight problem. The weight of the cables alone (excluding fixtures or turnbuckles) comprises 5% of the total ISS model weight. Kevlar materials may be required to reduce weight and the potential for string mode interactions.

- In the analyses that compared the suspended and free-free modes, a large number of "spurious" modes were found. These are modes which do not correlate with any of the free-free system modes - they typically represent free-free modes in the other two test planes which are coupled with the suspension system. These spurious modes can be predicted by including the dynamics of the suspension system in the model. However, when the scale model is tested and "unmodeled" modes are discovered, it may be very difficult to determine whether the "unmodeled" mode is a spurious mode or a bona fide Space Station mode. Thus, the interaction of of the suspension system complicates the interpretation of test data and places an increased dependence on the ability of the analyst to accurately model all the suspension system interactions.

Overall, the suspension analysis trade results do not identify an overwhelming preference for a particular scale factor for the model. The suspension system interacted with different modes and often in different ways for each scale factor analyzed. The suspension analysis results also provide insight into some potentially serious problems in testing the scale model and in correlating the results. Many of the suspension interaction problems may be reduced by employing a more advanced, passive or active suspension system.

5.3 SUMMARY OF MANUFACTURING AND COST TRADES

This section summarizes the results of the manufacturing and cost trades detailed in Chapter 4. The replication vs. simulation trade results are presented along with the unburdened cost for the components. The cost estimates are based on the cost of parts, tooling, labor and and material using drawings provided by the customer. Thus, the costs presented do not reflect the design and engineering work to create the drawings, any assembly

work other than for the components as they are broken out, nor any profits or fees. In the case of the joints and tubes, both simulated and replicated costs are shown for comparison.

Vendors were provided drawings of the components and asked to quote costs at scales (and therefore tolerances) within their manufacturing capability. The components were designed to conform to the scaling laws detailed in Chapter 2. All of the items except for the joints and tubes could be simulated. Three joints designs were included. They are the LaRC joint, the Star-Net joint, and the AEC-ABLE joint. For the purposes of this study, the LaRC joint and Star-Net joints are viewed as candidate Space Station joints. The AEC-ABLE joint serves as a representative simulated joint, because its design is much less dependent on tolerances (at this writing, the AEC-ABLE joint is also undergoing evaluation as a candidate Space Station joint). The following quotes were obtained from a number of vendors:

- Replicated joints - 1/5 through 1/4 scale
- Simulated joints - 1/8 through 1/4 scale
- Near-Replica tubes - 1/10 through 1/4 scale
- Simulated tubes - 1/10 through 1/4 scale
- All other components simulated - 1/10 through 1/4 scale

Several conclusions can be drawn from the cost analysis:

- Total cost increases with decreasing scale factor.
- Total cost increases with the degree of replication.
- Joint costs dominate the cost of the scale model.
- Replicated component costs are tolerance-driven.
- Simulated component costs are primarily bulk-material driven.
- The cost differential between Aluminum and P55 tubes is neglible when compared to the total cost.
- The large deviation in cost quotes received for the P75 (near replica) tubes indicates that the industry has less experience with this material, especially when compared to the low deviation in costs for the P55 tubes.

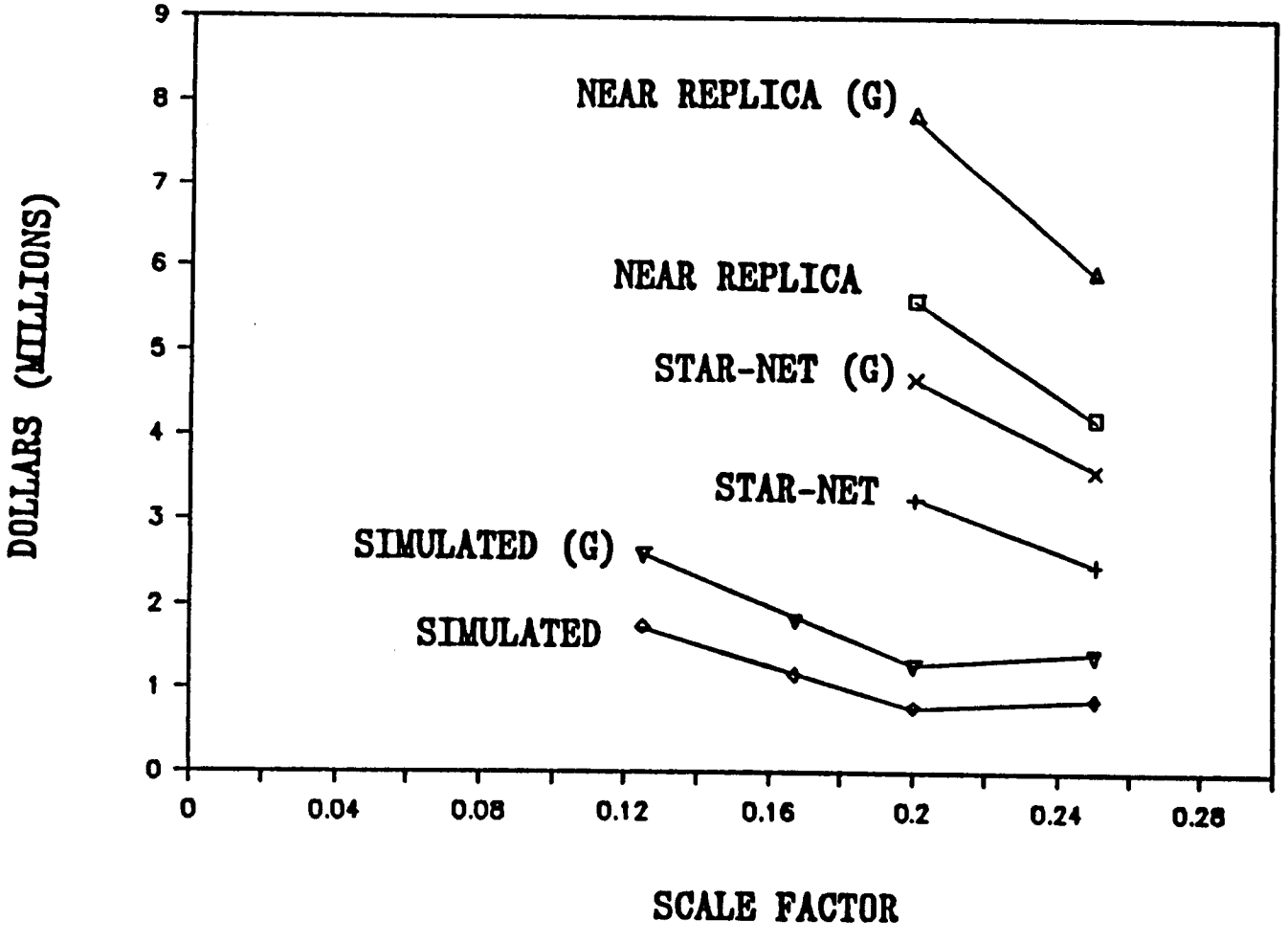

FIGURE 5.3-1 UNBURDENED COST ESTIMATES FOR SPACE STATION SCALE MODELS, ISS AND GROWTH CONFIGURATIONS

Total cost estimates for three different models with varying degree of replication are shown in Figure 5.3-1. Two sets of three curves are shown corresponding to the ISS and Growth Space Station configurations. The Near Replica model includes LaRC joints and tubes which are replica except that all the plies are longitudinal. The Star-Net model includes Star-Net joints and simulated tubes made of P55 material. The Simulated model employs AEC-ABLE joints and tubes made with P55 material. All of the other subsystem components are simulated and the costs are based on the lowest quote received from the vendors.

Overall, the cost estimates in Figure 5.3-1 illustrate three major conclusions. The first is that replicated joints were only quoted by the vendors at 1/5 and 1/4 scale, with the 1/5 scale cost being dramatically higher. The second is that the cost of the model with simulated components is relatively independent of the scale factor (within the ROM accuracy of the cost quotes in this study). Finally, the results show the significant savings that can be incurred by using simulated joints.

5.4 RECOMMENDATIONS FOR THE SCALE MODEL SCALE FACTOR

Based on the foregoing trade results, the cost of small replica models could be prohibitive. The dynamic analyses and the accompanying concerns regarding test data quality favor smaller scales. The need to show traceability to the full-scale Space Station design favors larger scales. Accurate representation of the flight article is desirable in light of the requirements of anticipated and as yet unanticipated tests, in order to maximize the utility of the model. Given the trade study conclusions summarized in the previous sections, separate scale factor recommendations are made for three scale models exhibiting varying degrees of cost and replication. They are, in decreasing order of cost and replication:

1) Replica Model
   - Cost considerations favor a 1/4 scale model
   - Dynamic considerations favor a 1/5 scale model

2) Simulated Model with an Option for Later Replication
   - Recommend a 1/5 scale model

3) Fully Simulated Model
   - Comparatively low sensitivity to scale factor

For the replica model (1), the cost of the 1/4 scale model is lower, but the dynamic analysis results indicate that a 1/4 scale model is very sensitive to suspension interactions and larger gravity loads. Thus, a 1/5 scale model is recommended unless a more sophisticated suspension system is employed.

Option (3) represents a low-cost option for constructing a simulated model. Fully simulated models can be constructed for half the cost (or less) of the replicated models. Because the analytical and cost results did not overwhelmingly favor a particular scale factor for the simulated model, a practical middle range from 1/8 to 1/5 scale is recommended. This range avoids the dynamic suspension complications at 1/4 scale as well as the fragility problems at 1/10 scale.

Given that the Space Station joints are still under development, it may be prudent to initiate the scale model program using a model with simulated joints and then replace the joints at a later date once the design of the Space Station joint design is frozen. By constructing a 1/5 scale model, it is possible to convert to replicated joints if necessary. If the scale model is to be used as a proof-testbed for the checkout of orbital modifications and experiments, the conversion to replica joints can be made years into the scale model program. If the behavior of the actual Space Station joint is very linear, a replicated joint may never be required. Thus, option (2) results in a 50% cost reduction without eliminating the option for later replication. Given the challenging schedule of the proposed Scale Model program, this option permits the commencement of testing without delays caused by changes in the Space Station joint design. Thus, a 1/5 scale model with simulated joints is recommended by the investigators in this study.

6.0 RECOMMENDATIONS FOR FURTHER STUDY

During the course of this study, a number of important issues were identified that need to be addressed in the scale model program. Given the desire to complete the scale model ground testing prior to the Space Station critical design review, these issues should be addressed in a timely manner.

Areas recommended for further study are:

1) Static and dynamic testing of candidate full-scale Space Station joints and interconnects to determine their stiffness, damping, preload, and dynamic characteristics over the range of operational loads. This activity would provide valuable information on the level of difficulty involved in designing and scaling the model, the amount of replication required, and the cost.

2) Use the data obtained during (1) to develop realistic simulated joint designs for the scale model. Fabricate prototype simulated joints and test them to verify that they exhibit the desired dynamic behavior. The potential cost savings obtained through the use of simulated joints warrants their further study.

3) Conduct a pre-test analysis of the candidate test configurations. The analyses in the present study examined the effects of the suspension system and the replica scaling laws on the selection of the scale factor. A similar analysis needs to be conducted to evaluate the issues associated with testing the model at scaled force (and therefore response) levels, the weight of the test equipment, and the location of actuators and sensors. This analysis should also include further detailed study of the dynamic and suspension problems outlined in Section 3.5., (e.g., cable string mode interaction, cable tuning, etc.).

4) Investigate options for substructured testing and synthesis of the scale model. Determine the level of difficulty of testing the full-scale Space Station in this manner and compare it with the level difficulty of testing scale models for the specific case of the Space Station. Explore test plans for the full-scale Space Station and investigate the role of the Space Station scale model in validating substructured testing procedures using scale model components and subsequently the fully mated scale model structure.

5) Investigate the use of more advanced suspension systems with the scale model. Consider both passive and active suspension techniques. Evaluate the amount of further development required before these techniques can be implemented.

6) Evaluate the impact of the lastest Space Station design changes on the previous recommendations for the model scale factor and the scale model test program.

REFERENCES

1. Housner, J.M., "Space Station Focused Technology Review - Replica Scale Model Studies", presented at the Space Station Structures TIP meeting at Marshall Space Flight Center, June 24, 1986.

2. Herr, R.W., "Some Cable Suspension Systems and Their Effects on the Flexural Frequencies of Slender Aerospace Structures", NASA TN D-7693, Sept. 1974.

3. Housner, J.M., and Belvin, W.K., "Dynamic Response and Collapse of Slender Guyed Booms for Space Application", Journal of Spacecraft and Rockets, Vol. 23, No. 1, Jan.-Feb. 1986, p.88.

4. Brooks, G.W., "The Results of a Limited Study of Approaches to the Design, Fabrication, and Testing of a Dynamic Model of the NASA IOC Space Station", NASA CR-178276, NASA/LaRC, Aug. 1985.

5. Ashley, H., "Some Considerations on Earthbound Dynamic Testing of Large Space Structures", AIAA 27th Structures, Structural Dynamics, and Materials Conference, April 1986.

6. Bisplinghoff, R. L., Ashley, H. and Halfman, R. L., Aeroelasticity, Addison-Wesley Publishing Company, Inc., Cambridge, MA, Feb. 1955, Chapter 11.

7. Timonshenko, S., and Young, D.H., Advanced Dynamics, McGraw Hill Book Co, Inc., New York, NY, 1948, p 249.

8. Whetstone, W. D., "EISI-EAL Engineering Analysis Language Reference Manual", EISI-EAL System Level 20.1, Volume 1: General Rules and Utility Processors. Engineering Information Systems, Inc., San Jose, CA, July 1983.

APPENDIX A

DRAWINGS OF SCALE MODELS SUSPENDED IN THE LSL

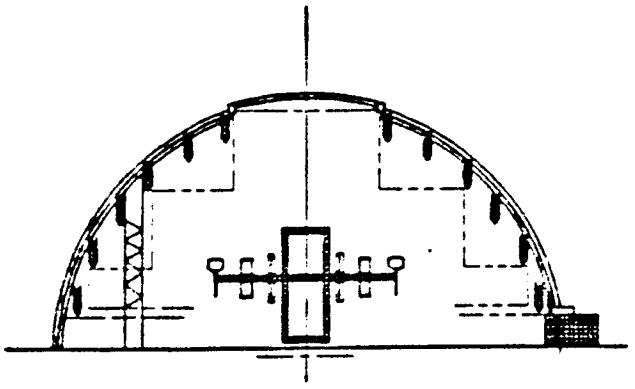

FIGURE A-1
FIFTH SCALE ISS MODEL
IN VERTICAL ORIENTATION

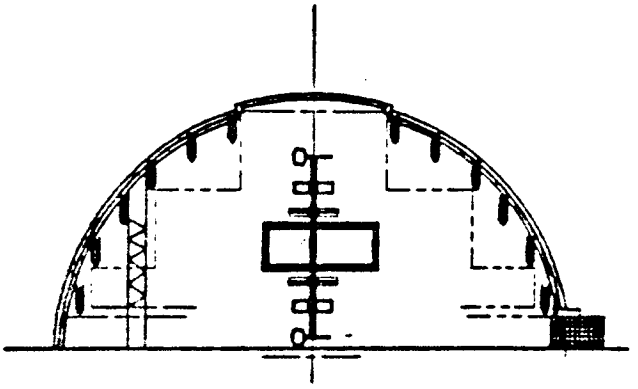

FIGURE A-2
FIFTH SCALE ISS MODEL
IN HORIZONTAL ORIENTATION

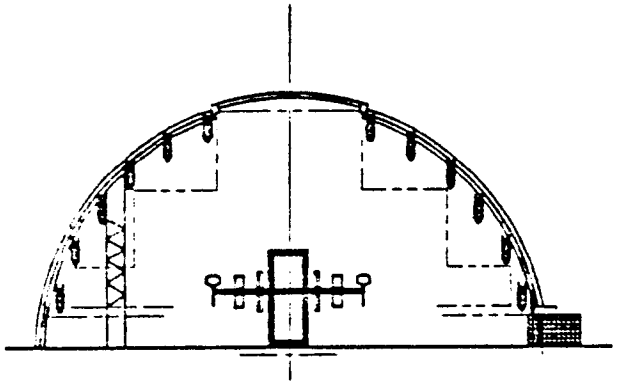

FIGURE A-3
SIXTH SCALE ISS MODEL
IN HORIZONTAL ORIENTATION

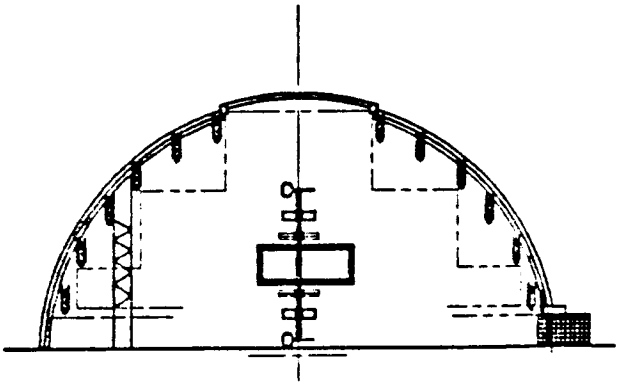

FIGURE A-4
SIXTH SCALE ISS MODEL
IN VERTICAL ORIENTATION

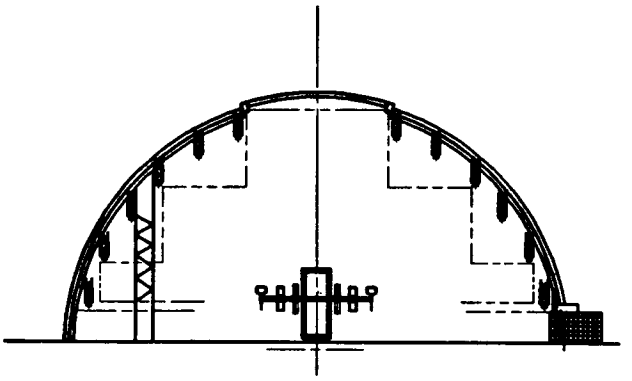

FIGURE A-5
EIGHTH SCALE ISS MODEL
IN HORIZONTAL ORIENTATION

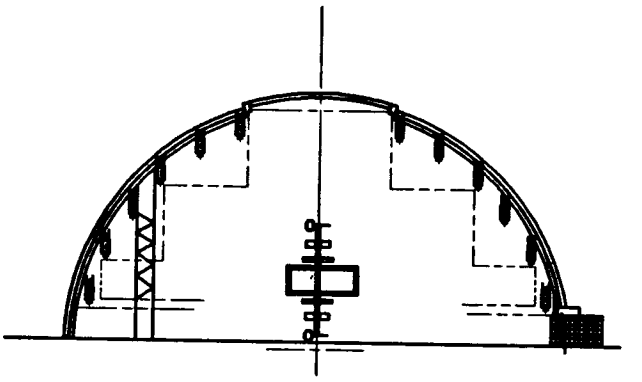

FIGURE A-6
EIGHTH SCALE ISS MODEL
IN VERTICAL ORIENTATION

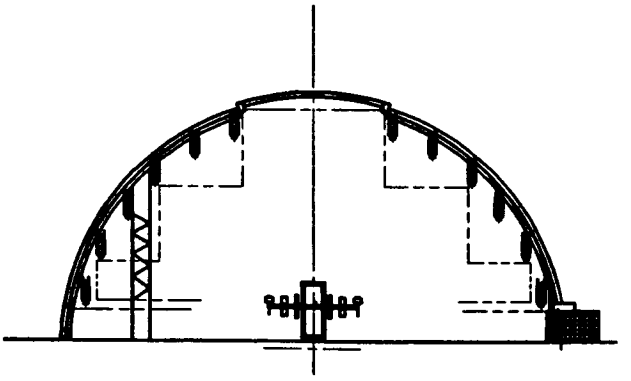

FIGURE A-7
TENTH SCALE ISS MODEL
IN HORIZONTAL ORIENTATION

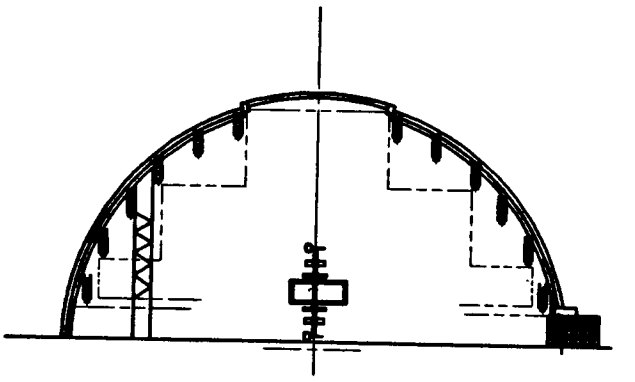

FIGURE A-8
TENTH SCALE ISS MODEL
IN VERTICAL ORIENTATION

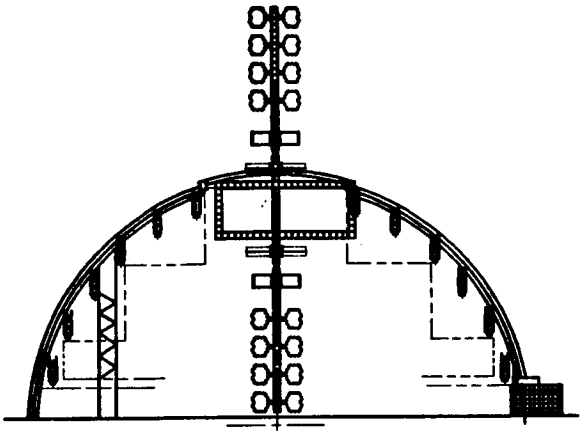

FIGURE A-9
QUARTER SCALE GROWTH MODEL
IN VERTICAL ORIENTATION

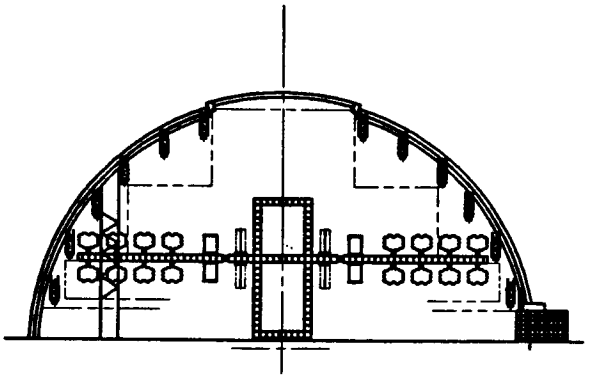

FIGURE A-10
QUARTER SCALE GROWTH MODEL
IN HORIZONTAL ORIENTATION

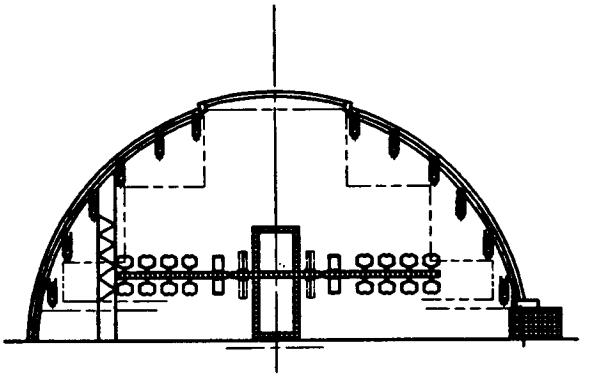

FIGURE A-11
FIFTH SCALE GROWTH MODEL
IN HORIZONTAL ORIENTATION

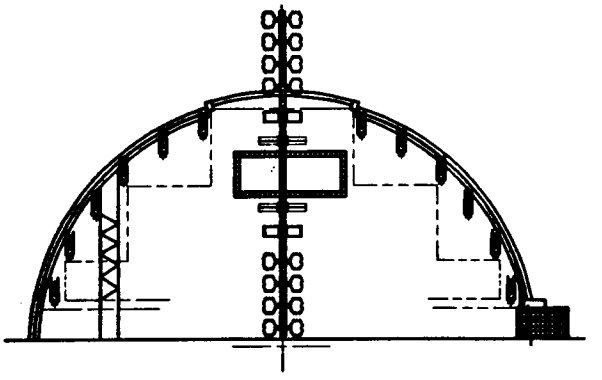

FIGURE A-12
FIFTH SCALE GROWTH MODEL
IN VERTICAL ORIENTATION

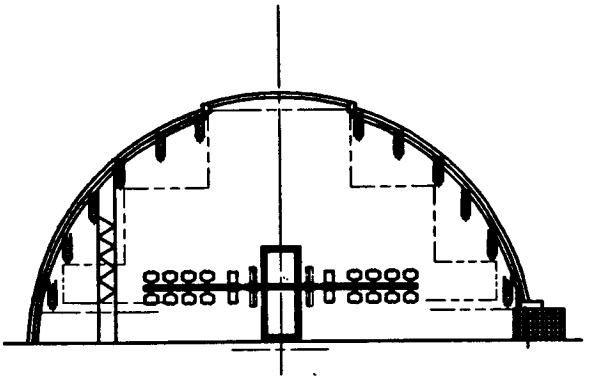

FIGURE A-13
SIXTH SCALE GROWTH MODEL
IN HORIZONTAL ORIENTATION

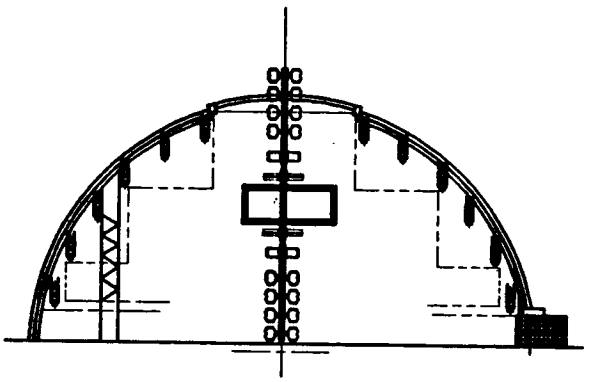

FIGURE A-14
SIXTH SCALE GROWTH MODEL
IN VERTICAL ORIENTATION

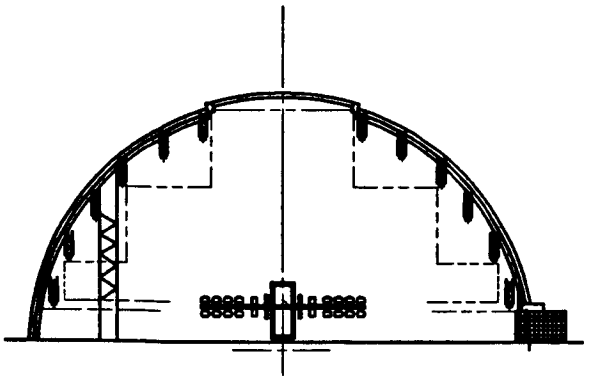

FIGURE A-15
TENTH SCALE GROWTH MODEL
IN HORIZONTAL ORIENTATION

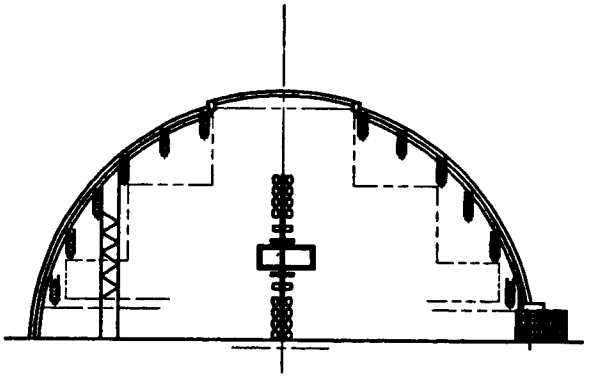

FIGURE A-16
TENTH SCALE GROWTH MODEL
IN VERTICAL ORIENTATION

APPENDIX B

SAMPLE LISTING OF EAL RUNSTREAM FOR ISS MODEL SUSPENDED IN LSL BY CABLES

```
*XQT AUS
$$$$$$$$$$$$$$$$$$$$$$$$$$$$$$$$$$$$$$$$$$$$$$$$$$$$$$
$ USER INPUT SECTION
!SL=.25                 $ LENGTH SCALE FACTOR
!AFD=1.0                $ DISTANCE ABOVE LSL FLOOR
!NVA=1                  $ AXIS POINTING TOWARD CEILING
!NHN=57                 $ NO. OF CABLES/HANGING NODES
!SIGW=10000.0           $MAXIMUM WORKING STRESS FOR CABLES
!RHOC=0.3/386.          $DENSITY OF CABLE MATERIAL
!ECAB=3.E+07            $MODULUS OF CABLE MATERIAL
TABLE(NI=1, NJ="NHN", TYPE=0): SUSP NODS 1 1     $ NODE NOS. AT END OF CABLES
J=1,"NHN"
510: 511: 512: 525: 528          $ VISIBLE MODULE NODES + LOGISTICS + JEM TURRET
526: 527                         $AIRLOCKS (2)
529:530:531:533:534: 532         $AVIONICS MODULES + 1 RCS MODULE
537:539:541:538       $540       $MODULAR EQUIPMENT
543:544:545:546                  $MODULAR EQUIPMENT
$550      $549                    $ALPHA ROTARY JOINT
460:553:555: 459        $554     $MODULAR EQUIPMENT
557                   $556       $SOLAR DYNAMICS
558:560:561        $559          $OTHER ALPHA GIMBAL ITEMS (TABLE 5.0-5)
562:563:564:565:567  $566        $PAYLOADS AND SERVICE FACILITY
440:446:452:458:438:444:450:456  $SOLAR ARRAYS
466:472:478:484:464:470:476:482  $RADIATORS
10                               $MOBILE SERVICE CENTER
433:434                          $SOLAR BETA
222:153:318:365                  $ ADDED NODES TO KEEL TRUSS 9/25
$$$$$$$$$$$$$$$$$$$$$$$$$$$$$$$$$$$$$$$$$$$$$$$$$$$$$$
```

```
!NNT=567+NHN: !AFDN=-AFD: !NAVA=ABS(NVA): !NVAM=NAVA-1
$-----------------------------------------------
$ 6-5-86 CONFIGURATION
$ NOTE SOLAR ARRAY TORSION MODES NOT MODELED
$-----------------------------------------------
*XQT TAB
START "NNT"
$%%%%%%%%%%%%%%%%%%%%%%%%%%%%%%%%%%%%%%%%%%%%%%%%%%%%%%%%%%%%%%%%
TITLE' ISS BASELINE CONFIGURATION, FULL UP
$-----------------------------------------------
$ 6-5-86 CONFIGURATION
$ NOTE SOLAR ARRAY TORSION MODES NOT MODELED
$-----------------------------------------------
$ --- Variables used
!DL=16.4042*12.           $--LENGTH OF 1 BAY IN.
!DL2=DL/2.                $-- HALF BAY DIMENSION
!DL2N=-1.0*DL2
!SL2=SL*SL                $ NSW SCALE FACTOR
!SL3=SL*SL2               $ RMASS MASS SCALE FACTOR
!SL4=SL*SL3
!SL5=SL*SL4               $ RMASS INERTIA SCALE FACTOR
$%%%%%%%%%%%%%%%%%%%%%%%%%%%%%%%%%%%%%%%%%%%%%%%%%%%%%%%%%%%%%%%%
$
$---- EXECUTABLE RUNSTREAM ELEMENTS
$
$*********************** ************************
$%%%%%%%%%%%%%%%%%%%%%%%%%%%%%%%%%%%%%%%%%%%%%%%%%%%%%%%%
$  CREATE CON=1 FOR CABLES AUTOMATICALLY
$ CABLE NODES ARE ASSUMED TO BE NUMBERED STARTING AT 568
$ FOR CON=1 CABLES ARE CONSTRAINED AT THE LSL CEILING
*XQT U1
```

```
*XQT U1
*(1 CON1 CABL) CEND
!LINC=1
*LABEL 100
!NODN= NNT - NHN + LINC
 ZERO 1,2,3,4,5,6: "NODN"
!LCNT=NHN-LINC
!LINC=LINC+1
*JGZ (LCNT,100)
*CEND
$
$ NOW FOR CON=2 (BOTH ENDS OF CABLES CONSTRAINED)
*(1 CON2 CABL) CEND
!LINC=1
*LABEL 200
!NODZ=DS 1 "LINC" 1 (1 SUSP NODS 1 1)
!NODN= NNT - NHN + LINC
 ZERO "NAVA":"NODZ"
 ZERO 1,2,3,4,5,6: "NODN"
!LCNT=NHN-LINC
!LINC=LINC+1
*JGZ (LCNT,200)
*CEND
$
*(1 ELD CABL) LEND
!LINC=1
*LABEL 100
!NOD1=DS 1 "LINC" 1 (1 SUSP NODS 1 1)
!NOD2=NNT-NHN+LINC
 NSECT="LINC"
 "NOD1" "NOD2"
!LCNT=NHN-LINC
!LINC=LINC+1
*JGZ (LCNT,100)
*LEND
$
*(1 JLOC GEN)   EJG
*XQT AUS
TABLE(NI=1, NJ="NHN", TYPE=0): SNOD SEQ 1 1 $ LIST:  1,NHN
 DDATA=1: RJ=1,"NHN": 1
TABLE(NI=1, NJ="NHN", TYPE=0): SNOD NOS 1 1 $ NODE NOS. AT CEILING
 DDATA=1: RJ=1,"NHN": 568
TABLE(NI=1, NJ="NHN"): RSQD LSL 1 1 $ SQUARE OF LSL HEIGHT AT CENTER
 DDATA=0.: J=1,"NHN": 3.24E+06
TABLE(NI=1, NJ="NHN"): UVEC AUS 1 1 $ VECTOR OF ONES
 DDATA=0.: J=1,"NHN": 1.
$
DEFINE MMJ=MXMN JLOC 1 1
DEFINE JLM=JLOC BTAB 2 5
DEFINE SJLT=SUSP JLTR 1 1
JLOC TRAN 2 5=RTRAN(JLM)
$
DE1 $ LOCATIONS OF NODES AT END OF CABLES ON STRUCTURE
 SOURCE=JLOC BTAB 2 5: DEST=SUSP JLTR 1 1
 IS=SERIAL: ID=SERIAL: JS=SUSP NODS 1 1: JD=SNOD SEQ 1 1: EX1
 SUSP JLOC 1 1=RTRAN(SJLT)
DE1 $ X-COORDINATE VECTOR IN "SUSP JLTR"
 SOURCE=SUSP JLTR 1 1: DEST=XS
 IS=1: ID=1: JS=SERIAL: JD=SERIAL: EX1
 XS AUS 1 1=RTRAN(XS)
DE1 $ Y-COORDINATE VECTOR IN "SUSP JLTR"
 SOURCE=SUSP JLTR 1 1: DEST=YS
 IS=2: ID=1: JS=SERIAL: JD=SERIAL: EX1
 YS AUS 1 1=RTRAN(YS)
DE1 $ Z-COORDINATE VECTOR IN "SUSP JLTR"
 SOURCE=SUSP JLTR 1 1: DEST=ZS
 IS=3: ID=1: JS=SERIAL: JD=SERIAL: EX1
 ZS AUS 1 1=RTRAN(ZS)
$
$ BRANCH TO THE RUNSTREAM SEGMENT BASED ON VERTICAL AXIS
$
*JGZ,-2(NAVA AX3)
*JZ (NAVA AX2)
$
```

```
$ INITIALIZE X-AXIS VERTICAL RUNSTREAM
!AOIV='XVEC
!AOIC='XCV
!AOI='X
!AOIS='XSUS
!AOIO='XS
!O1S='YS
!O2S='ZS
!O1N=2: !O2N=3: !ANOI=1
*CALL (1 JLOC WHRS)
*JUMP COMN
$
$ INITIALIZE Y-AXIS VERTICAL RUNSTREAM
*LABEL AX2
!AOIV='YVEC
!AOIC='YCV
!AOI='Y
!AOIS='YSUS
!AOIO='YS
!O1S='XS
!O2S='ZS
!O1N=1: !O2N=3: !ANOI=2
*CALL (1 JLOC WHRS)
*JUMP COMN
$
$ INITIALIZE Z-AXIS VERTICAL RUNSTREAM
*LABEL AX3
!AOIV='ZVEC
!AOIC='ZCV
!AOI='Z
!AOIS='ZSUS
!AOIO='ZS
!O1S='YS
!O2S='XS
!O1N=2: !O2N=1: !ANOI=3
*CALL (1 JLOC WHRS)
*LABEL COMN
*EJG
$
*(1 JLOC WHRS) EJW
DEFINE CV=COR VEC 1 1
DE1 $ COORDINATE VECTOR IN "JLOC BTAB"
 SOURCE=JLOC BTAB 2 5: DEST=COR VEC 1 1
 IS="ANOI": ID=1: JS=SERIAL: JD=SERIAL: EX1
 "AOIV"=RTRAN(CV)
 W1=SRSS("O1S" "O2S") $ RADIAL DISTANCE AWAY FROM CENTER OF LSL
 RSQD DIST 1 1=SQUARE(W1)
DEFINE RL=RSQD LSL 1 1
DEFINE RD=RSQD DIST 1 1
 W1=SUM(RL -1. RD)
 W1=SQRT(W1) $ HEIGHT OF LSL AT A GIVEN RADIAL DISTANCE FROM CENTER
 "AOI"=SUM(W1 "AFDN" UVEC) $ ACCOUNT FOR FLOOR CLEARANCE
*XQT AUS
 MXMN JLOC 1 1=MM1("AOIV")
!MXV=DS 1 1 1 (1 MXMN JLOC 1 1) $ MAXIMUM COORDINATE
!MNV=DS 2 1 1 (1 MXMN JLOC 1 1) $ MINIMUM COORDINATE
*JLZ (NVA NEGA) $ BEGIN +AXIS UPWARD SEGMENT
 "AOIS"=SUM("AOI" "MNV" UVEC) $ CEILING COORDINATE AT GIVEN RADIAL DISTANCE
*JUMP COMP
*LABEL NEGA    $ BEGIN -AXIS UPWARD SEGMENT
!MXVN=-MXV
 "AOI"=SUM("AOI" "MXVN" UVEC)
 "AOIS"=UNION(-1. "AOI") $ CEILING COORDINATE AT GIVEN RADIAL DISTANCE
*LABEL COMP
!VSKP=ANOI-1*NNT+567
 DEFINE JLT=JLOC TRAN 2 5
 DEFINE SJL=SUSP JLOC 1 1
TABLE(NI="NNT",NJ=3): CJLT $ FORM MODIFIED "JLOC BTAB"
 TRANSFER(SOURCE=JLT)
 TRANSFER(SOURCE=SJL,DBASE=567,DSKIP=567,ILIM="NHN",JLIM=3)
 TRANSFER(SOURCE="AOIS",DBASE="VSKP",DSKIP=567,OPERATION=XSUM)
 JLOC BTAB 2 5=RTRAN(CJLT)
 W1=SUM("AOIS" -1. "AOIO")
 CABL LENG 1 1=ABS(W1) $ LENGTH OF CABLES
```

```
*EJW
$
*(1 BC INIT) EBI $ INITIALIZES "BC BTAB" TO 1.
*XQT AUS
TABLE (NI=6, NJ="NHN"): BC BTAB 2 11
 I=1 2: DDATA=0. 0.: J=1,"NHN": 1. 1.
*XQT TAB
*EBI
$--- NODE GENERATION ROUTINE
*(1 GEN NODE)    EGN
!J=NS-1          $---MODIFICATION FOR 1 NODE
!NJ=NB+1         $-- NO. OF JOINTS
!AB=FLOAT(NB)
!YE=DL*AB+Y            $--END POINT OF TRUSS
!Z1=Z+DL2              $--- POINTS OF TRUSS
!Z2=Z-DL2
!X1=X+DL2
!X2=X-DL2
MOD="J"
 1 "X1" "Y" "Z1" "X1" "YE" "Z1" "NJ" 4
 2 "X1" "Y" "Z2" "X1" "YE" "Z2" "NJ" 4
 3 "X2" "Y" "Z2" "X2" "YE" "Z2" "NJ" 4
 4 "X2" "Y" "Z1" "X2" "YE" "Z1" "NJ" 4
*EGN
$
$---- ELEMENT GENERATION ROUTINES
*(1 ELD A)       EEA     $--- CASE A
!J=NS-1                  $--- JOINT MODIFICATION NO.
!NB2=NB-NB1
!NB3=NB+1
MOD JOINT="J"
 1 5 1 "NB" 4 1             $-- LONGERON
 1 2 2 4 "NB3" 4            $-- BATTEN
 1 3 1 1 "NB3" 4            $-- INNER DIAG.
 2 7 1 1 "NB1" 8            $-- DIAGONALS
 7 10 1 1 "NB2" 8
 4 7 1 1 "NB1" 8    :7 12 1 1 "NB2" 8
 4 5 1 1 "NB1" 8    :5 12 1 1 "NB2" 8
 2 5 1 1 "NB1" 8    :5 10 1 1 "NB2" 8
*EEA
$
*(1 ELD B)       EEB     $--- CASE B
!J=NS-1                  $--- JOINT MODIFICATION NO.
!NB2=NB-NB1
!NB3=NB+1
MOD JOINT="J"
 1 5 1 "NB" 4 1             $-- LONGERON
 1 2 2 4 "NB3" 4            $-- BATTEN
 1 3 1 1 "NB3" 4            $-- INNER DIAG.
 3 6 1 1 "NB1" 8            $-- DIAGONALS
 6 11 1 1 "NB2" 8
 3 8 1 1 "NB1" 8    :8 11 1 1 "NB2" 8
 1 8 1 1 "NB1" 8    :8 9 1 1 "NB2" 8
 1 6 1 1 "NB1" 8    :6 9 1 1 "NB2" 8
*EEB
$
*(1 ELD C)       EEC     $--- CASE C
!J=NS-1                  $--- JOINT MODIFICATION NO.
!NB2=NB-NB1
!NB3=NB+1
MOD JOINT="J"
 1 5 1 "NB" 4 1             $-- LONGERON
 1 2 2 4 "NB3" 4            $-- BATTEN
 2 4 1 1 "NB3" 4            $-- INNER DIAG.
 3 6 1 1 "NB1" 8            $-- DIAGONALS
 6 11 1 1 "NB2" 8
 3 8 1 1 "NB1" 8    :8 11 1 1 "NB2" 8
 1 8 1 1 "NB1" 8    :8 9 1 1 "NB2" 8
 1 6 1 1 "NB1" 8    :6 9 1 1 "NB2" 8
*EEC
$$$$$$$$$$$$$$$$$$$$$$$$$$$$$$$$$$$$$$$$$$$$$$$$$$$$$$$$$$$$$$$$$$$$$$$$$
$
$                  START OF RUNSTREAM
$
```

```
$$$$$$$$$$$$$$$$$$$$$$$$$$$$$$$$$$$$$$$$$$$$$$$$$$$$$$$$$$$$$$$$$$$$$$$$
*XQT TAB
$
BB
 1 1.+7            $--- RIGID JOINT CONNECTIONS FOR ALPHA JOINT
 0. 1.+7
 0. 0. 1.+7
 0. 0. 0. 1.+7
 0. 0. 0. 0. 1.+7
 0. 0. 0. 0. 0. 1.+7
$
*CALL (1 BC INIT)
$
ALTREF
 2 1 0. 2 0. 3 0. 0. 0. 0.     $--- CENTER OF Y-AXIS TRUSS
 3 1 -90. 2 0. 3 0. 0. 0. 0.   $-- VERTICAL TRUSS
 4 3 90. 2 0. 3 0. 0. 0. 0.    $-- X-AXIS TRUSS
$
MATC
 1 3.4E+07 .28 0.0  $ MASSLESS GR/EP TUBES  15% JOINT KNOCKDOWN
 2 1.E+07 .3 0.0    $ MASSLESS ALUMINUM
 3 4.E+09 .28 0.0   $ MASSLESS PSEUDO-RIGID BEAMS
 4 3.4E+07 .28  0.0 $ ROTARY JOINT TUBES 2" O.D., .330 WALLS
 5 "ECAB" .30 0.0   $ CABLES FOR SUSPENSION
$
$      ************************************************
$                      JLOC
$      ************************************************
$
JLOC
!NS=1       $--- START NODE
!NB=8      $--- NO. OF BAY
!Y=-17.5*DL      $--- START DISTANCE IN Y AXIS
!X=0.0           $---X-AXIS OFFSET
!Z=0.0            $---Z-AXIS OFFSET
NREF=2
*CALL (1 GEN NODE)           $---PORT TRANSVERSE BOOM OUTBOARD OF ROT. JT.
!NS=37    :!NB=17    :!Y=-8.5*DL
*CALL (1 GEN NODE)            $---CENTER TRANSVERSE BOOM
!NS=109   :!NB=8    :!Y=9.5*DL
*CALL (1 GEN NODE)           $--- STBD TRANSVERSE BOOM OUTBOARD OF ROT. JT.
!NS=181   :!NB=7   :!Z=-9.*DL   :!Y=-2.5*DL  $-- UPPER BOOM
*CALL (1 GEN NODE)
!NS=385   :!NB=5   :!Z=12.*DL   :!Y=-2.5*DL  $--- LOWER BOOM
*CALL (1 GEN NODE)
$
$---- MODULE BOOM AND CROSS TIES
!NS=241   :!NB=1   :!Z=0.   :!Y=1.5*DL
!X=-4.*DL             $--- EXTRA NODES WILL BE OVERWRITTEN (425-432)
NREF=4
*CALL (1 GEN NODE)
!NS=285   :!NB=1   :!X=4.*DL
*CALL (1 GEN NODE)
NREF=2
!NS=245   :!NB=9   :!Y=-4.5*DL   :!X=-3.*DL
*CALL (1 GEN NODE)
$
$--------KEELS
NREF=3
!NS=145   :!NB=8   :!Z=-4.*DL   :!Y=1.5*DL    $--PORT UPPER KEEL
!X=0.
*CALL (1 GEN NODE)
!NS=213   :!NB=6   :!Z=4.*DL        $--STBD UPPER KEEL
*CALL (1 GEN NODE)
!NS=289   :!NB=11   :!Z=4.*DL   :!Y=-12.5*DL    $-- STBD LOWER KEEL
*CALL (1 GEN NODE)
!NS=337   :!NB=11   :!Z=-4.*DL                  $--- PORT LOWER KEEL
*CALL (1 GEN NODE)
$
$--------------****** MORE NODE TO BE ADDED IN THIS AREA *******
MOD=0
$--------JOINTS FOR TRANSVERSE BOOM ALPHA JOINT CONNECTION
$--- ASSUME DIAMETER=160" OR .81 X BAY LENGTH
NREF=2   :!DL4=DL*0.4064   :!DL4M=-DL4          $-- RADIUS OF ALPHA JOINTS
```

```
!Y=9.*DL                    $--STBD TRANSVERSE BOOM, NODES ON CENTER SIDE
409 "DL4" "Y" 0.   :410 0. "Y" "DL4M"
411 "DL4M" "Y" 0.   : 412 0. "Y" "DL4"
MOD=4               $------NODES ON BOOM SIDE
409 "DL4" "Y" 0.   :410 0. "Y" "DL4M"
411 "DL4M" "Y" 0.   : 412 0. "Y" "DL4"
!Y=-9.*DL                    $---- PORT TRANSVERSE BOOM, NODES ON BOOM SIDE
MOD=8
409 "DL4" "Y" 0.   :410 0. "Y" "DL4M"
411 "DL4M" "Y" 0.   : 412 0. "Y" "DL4"
MOD=12                      $--- NODES NEAR CENTER SIDE
409 "DL4" "Y" 0.   :410 0. "Y" "DL4M"
411 "DL4M" "Y" 0.   : 412 0. "Y" "DL4"
MOD=0
$
$ .1 HZ SOLAR ARRAYS
$
MOD=432
!Y=2205.0
!YN=-1.0*Y
!Z=DL2+567.6
!ZN=-1.0*Z
1 0. "YN" 0.
2 0. "Y"  0.
3 0. "YN" "DL2"    0. "YN" "Z" 6 1
9 0. "YN" "DL2N"   0. "YN" "ZN" 6 1
15 0. "Y" "DL2"    0. "Y"  "Z"  6 1
21 0. "Y"  "DL2N" 0. "Y"  "ZN" 6 1
$
$ RADIATORS
$
MOD=458
!Y=1310.0
!YN=-1.0*Y
!Z=DL2+787.4
!ZN=-1.0*Z
1 0. "YN" 0.
2 0. "Y"  0.
3 0. "YN" "DL2"    0. "YN" "Z" 6 1
9 0. "YN" "DL2N"   0. "YN" "ZN" 6 1
15 0. "Y" "DL2"    0. "Y"  "Z"  6 1
21 0. "Y"  "DL2N" 0. "Y"  "ZN" 6 1
$
$ESS RADIATORS
$
MOD=484
!Y=1968.0
!YN=-1.0*Y
!X=DL2+600.0
!XN=-1.0*X
1 0. "YN" 0.
2 0. "Y"  0.
3 "DL2N" "Y" 0.    "XN" "Y"  0.  6 1
9 "DL2N" "YN" 0.   "XN" "YN"  0. 6 1
MOD=0
$
$
$ MODULES, NODES AND TUNNELS
$
MOD=498
1 -866.6 0. -245.28:       2 -721.7 0. -245.28:       3 -615.4 0. -245.28
4 -509.1 0. -245.28:       5 -364.2 0. -245.28:       6 -295.3 0. -245.28
7 -226.4 0. -245.28:       8 -75.4 0. -245.28:        9 40.6 0. -245.28
10 156.6 0. -245.28:       11 307.6 0. -245.28:       12 376.5 0. -245.28
13 376.5 -143.9 -245.28:   14 376.5 -287.8 -245.28:   15 307.6 -287.8 -245.28
16 156.6 -287.8 -245.28:   17 40.6 -287.8 -245.28:    18 -75.4 -287.8 -245.28
19 -226.4 -287.8 -245.28:  20 -295.3 -287.8 -245.28:  21 -295.3 -143.9 -245.28
22 -364.2 -287.8 -245.28:  23 -567.2 -287.8 -245.28:  24 -689.0 -287.8 -245.28
25 -781.5 -287.8 -245.28:  26 -1139.8 -287.8 -245.28: 27 -689.0 -287.8 -407.7
28 -295.3 0.0 -432.0:      29 -295.3 -287.8 -432.0:   30 -295.3 -287.8  19.0
MOD=0
$
$
$ MODULAR EQUIPMENT (FROM TABLE 5.0-4)
```

```
$
MOD=528
1 0.0 787.0 -1772.0  $AVIONICS MODULE FOOSO4U09
2 0.0 -787.0 -1772.0 $AVIONICS MOD    FOOPO4U09
3 0.0 0.0 -1772.0    $AVIONICS MOD    FOOSOOU09
4 0.0 787.0 0.0      $AVIONICS MOD    FOOSO4DOO
5 0.0 0.0 2362.0     $AVIONICS MOD    FOOSOOD12
6 0.0 -984.0 -1181.   $RCS MODULE FOOSO4U06
9 0.0  984.0 -1181.  $RCS MODULE FOOPO4U06
10 0.0 -984.0 0.0    $GN&C/DMS MOD FOOPO5DOO
11 0.0 -787.0 0.0    $HR&T MOD FOOPO4DOO
12 0.0 -197.0 0.0    $FMAD MOD FOOPO1DOO
13 -591.0 -394.0 0.0 $AVIONICS MOD AO3PO2DOO
15 0.0 984.0 1181.0  $RCS MODULE FOOSO4DO6
16 0.0 -984.0 1181.0 $RCS MODULE FOOPO4DO6
17 0.0 801.0 2165.0  $C&T MODULE FOOSO4D11
18 0.0 -801.0 2165.0 $C&T MODULE FOOPO4D11
21 0.0 1771.0 0.0    $ALPHA ROTARY + STRUCTURE (1/2) (STBD)
22 0.0 -1771.0 0.0   $ALPHA ROTARY + STRUCTURE (1/2) (PORT)
25 0.0 0.0 0.0       $FMAD MODULE FOOSOODOO
26 -150.0 -1181.0 2.0   $NAV BASE FOOPO6DOO
27 161.0 984.0 -1742.0  $TDRSS ANTENNA + SUPT
$
$  PORT ALPHA GIMBAL ITEMS
$
MOD=0
556 0.0 -3387.0 0.0    $BETA GIMBAL FOOP17DOO
557 51.2 -3387.0 13.0  $SOLAR DYNAMIC MODULE
558 0.0 -1968.0 0.0    $ESS MODULE FOOP1ODOO
$
$  STARBOARD ALPHA GIMBAL ITEMS
$
MOD=0
559 0.0 3387.0 0.0     $BETA GIMBAL FOOS17DOO
560 51.2 3387.0 0.0    $SOLAR DYNAMIC MODULE
561 0.0 1968.0 0.0     $ESS MODULE FOOS1ODOO
$
$ PAYLOADS AND SERVICE FACILITY (TABLE 5.0-7)
$
MOD=0
562 0.0 0.0 -1942.0    $SAAX 0115
563 -190.0 -347.0  -1772.0  $TDMX 2011
564 0.0 0.0 2558.0     $SAAX 4006
565 0.0 0.0 -1476.0    $SERVICE FACILITY
566 0.0 -757.0 -394.0  $P/L SUPT- KEEL P/L'S
567 0.0 197.0 2481.0   $P/L SUPT- SAAX 0250
$
$   EXTRA NODES (ZERO OUT IN CON=1)
535 0. 0. 0.
536 0. 0. 0.
542 0. 0. 0.
547 0. 0. 0.
548 0. 0. 0.
551 0. 0. 0.
552 0. 0. 0.
$
MREF
FORMAT=2
1 1 6000. 6. 6000.
$
$%%%%%%%%%%%%%%%%%%%%%%%%%%%%%%%%%%%%%%%%%%%%%%%%%%%%%%%%%%%%%%%%%%%%%%%%%%%%%%%%
CON=1  $ CONSTRAINING THE CABLE ATTACHMENTS AT SUPPORT
$         ROTATIONAL CONSTRAINTS ARE UNAFFECTED BECAUSE E23 HAS NO
$         ROTATIONAL (BEAM) STIFFNESSES AND IKG2=1 IN KG
*CALL (1 CON1 CABL)
$
CON=2  $ CONSTRAINING THE CABLE ATTACHMENTS AT SUPPORT & STRUCTURE
*CALL (1 CON2 CABL)
$%%%%%%%%%%%%%%%%%%%%%%%%%%%%%%%%%%%%%%%%%%%%%%%%%%%%%%%%%%%%%%%%%%%%%%%%%%%%%%%%
BA  $ E21 PROPERTIES
$
!RO=1.154*SL
TUBE 1 0.0 "RO"         $.1 HZ  SOLAR ARRAY
!RO=1.804*SL
```

```
TUBE 2 0.0 "RO"          $.11 HZ RADIATOR
!RO=0.961*SL
TUBE 3 0.0 "RO"          $.11 HZ ESS RADIATOR
TUBE 4 9.0 10.0          $ PSEUDO-RIGID LINKS
!RI=83.0*SL: !RO=87.5*SL
TUBE 5 "RI" "RO"         $ MODULES
!RI=70.0*SL: !RO=87.5*SL
TUBE 6 "RI" "RO"         $ NODES AND AIRLOCKS
!RI=0.94*SL: !RO=1.0*SL
TUBE 7 "RI" "RO"         $TRUSS STRUTS 2"OD, .06 WALL
!RI=0.67*SL: !RO=1.0*SL
TUBE 8 "RI" "RO"         $ROTARY JOINT TRUSS STRUTS
$
NSW
$
!VM=.00428*SL2*386.0
1, "VM"                  $.1 HZ SOLAR ARRAYS   (LB/IN)
!VM=.0056*SL2*386.0
2, "VM"                  $.11 HZ RADIATORS
!VM=.00134*SL2*386.0
3, "VM"                  $.11 HZ ESS RADIATORS
!VM=.000603*SL2*386.0
4, "VM"                  $ STRUCTURE AND UTILITIES LUMPED TOGETHER
$ ***************************************************
RMASS
$***************************************************
$ THESE ARE GLOBAL
!P=2.588E-03*SL3
!Q=12.0*SL5
$SET SCALE FACTORS
CM "P","Q"  $CONVERT FROM LBS AND SLUG*FT**2 TO SNAILS AND SNAIL*IN**2
$
$  MODULES
$
505 46372.0 .5208+05 .1525+06 .1525+06  $HSD MODULE
507 54351.0 .5491+05 .1607+06 .1607+06  $MPL (U.S. LAB) LAB MODULE
501 46738.0 .5827+05 .1705+06 .1704+06  $ESA MODULE
521 34611.0 0.0      0.0      0.0       $JEM MODULE (PRESSURIZED)
522 0.0     .1084+06 .3172+06 .2569+06  $JEM MODULE (INERTIAS AT C.G.)
525 14769.1 0.0      0.0      0.0       $JEM MODULE (ELM)
524 16753.3 0.0      0.0      0.0       $JEM MODULE (EF BOOM)
528 35583.0 .1298+06 .1298+06 .4436+05  $LOGISTICS MODULE
527 7853.0  .8491+04 .8491+04 .8491+04  $AIRLOCK 1
REPEAT 2,2
510 5534.0  .5984+04 .5984+04 .5984+04  $NODES, FWD
REPEAT 2,14
504 7538.0  .8151+04 .8151+04 .8151+04  $NODES, AFT
REPEAT 2,8
511 1422.0  .4416+03 0.0      .4416E+03 $TUNNELS
526 6812.0  .7366+04 .7366+04 .7366+04  $AIRLOCK 2
$
$ MODULAR EQUIPMENT (FROM TABLE 5.0-4)
$
MOD=528
1 1373.0 .101+04 .506+03 .506+03        $AVIONICS MODULE FOOSO4U09
2 993.0  .732+03 .366+03 .366+03        $AVIONICS MOD    FOOPO4U09
3 2055.0 .757+03 .757+03 .152+04        $AVIONICS MOD    FOOSOOU09
4 2456.0 .905+03 .181+04 .905+03        $AVIONICS MOD    FOOSO4DOO
5 2105.0 .776+03 .155+04 .776+03        $AVIONICS MOD    FOOSOOD12
REPEAT 2,3
6 3088.0 .114+04 .228+04 .114+04        $RCS MODULE FOOSO4UO6, PO4UO6
10 5040.0 .372+04 .186+04 .186+04       $GN&C/DMS MOD FOOPO5DOO
11 2230.0 .822+03 .164+04 .822+03       $HR&T MOD FOOPO4DOO
12 3547.0 .131+04 .262+04 .131+04       $FMAD MOD FOOPO1DOO
13 1132.0 .417+03 .834+03 .417+03       $AVIONICS MOD AO3PO2DOO
REPEAT 2,1
15 3088.0 .114+04 .228+04 .114+04       $RCS MODULE FOOSO4DO6, PO4DO6
17 1026.0 .0000   .0000   .0000         $C&T MODULE FOOSO4D11
18 1013.0 .0000   .0000   .0000         $C&T MODULE FOOPO4D11
REPEAT 2,1
21 725.0  .171+03 .271+03 .171+03       $ALPHA ROTARY + STRUCTURE (1/2)
10 8000.0 .1115+05 .5576+05 .5576+05    $MOBILE SERVICE CENTER (MRMS)
25 3396.0 .125+04  .250+04 .125+04      $FMAD MODULE FOOSOODOO
26 723.0  .533+03  .267+03 .267+03      $NAV BASE FOOPO6DOO
```

```
27 1302.0 .0000    .0000   .0000       $TDRSS ANTENNA + SUPT
MOD=0
237 194.0  .0000   .0000   .0000        $ANTENNA F00S04U07
460 1216.0 .439+03 .878+03 .439+03      $RADIATOR ROTARY MOD F00S07D00
166 181.0  .0000   .0000   .0000        $ANTENNA F00P04U07
459 1191.0 .439+03  .878+03  .439+03    $RADIATOR ROTARY MOD F00P07D00
470 0. 100. 0. 0.0                      $RADIATOR  SMALL IXX
464 0. 100. 0. 0.0                      $RADIATOR IXX
476 0. 100. 0. 0.0                      $RADIATOR IXX
482 0. 100. 0. 0.0                      $RADIATOR IXX
459 0. 0. 0. 1294.6                     $RADIATOR IZZ
460 0. 0. 0. 1294.6                     $RADIATOR IZZ
$
$  PORT ALPHA GIMBAL ITEMS
$
MOD=0
556 2489.0 .917+03 .184+04 .917+03        $BETA GIMBAL F00P17D00
557 9287.0 .31723+06 .40985+06 .15842+06  $SOLAR DYNAMIC MODULE
433 1830.0 .675+03 .135+04 .675+03        $BETA GIMBAL F00P11D00
558 4442.0 .327+04 .1702+05 .1637+05      $ESS MODULE F00P10D00
550 725.0  .171+03 .271+03 .171+03        $ALPHA GIMBAL + SUPT STRUCT (1/2)
444 0. 100. 0. 0.0                       $SOLAR ARRAY SMALL IXX
438 0. 100. 0. 0.0                       $SOLAR ARRAY SMALL IXX
433 0. 0. 0. 5386.5                      $SOLAR ARRAY IZZ
485 0. 127.0 0. 0.                        $ESS RADIATOR IXX ONLY
$
$  STARBOARD ALPHA GIMBAL ITEMS
$
MOD=0
559 2489.0 .917+03 .184+04 .917+03        $BETA GIMBAL F00S17D00
560 9287.0 .31723+06 .40985+06 .15842+06  $SOLAR DYNAMIC MODULE
434 1830.0 .675+03 .135+04 .675+03        $BETA GIMBAL F00S11D00
561 4442.0 .327+04 .1702+05 .1637+05      $ESS MODULE F00S10D00
549 725.0  .171+03 .271+03 .171+03        $ALPHA GIMBAL + SUPT STRUCT (1/2)
456 0. 100. 0. 0.0                        $SOLAR ARRAY SMALL IXX
450 0. 100. 0. 0.0                        $SOLAR ARRAY SMALL IXX
434 0. 0. 0. 5386.5                       $SOLAR ARRAY IZZ
486 0. 127.0 0. 0.                        $ESS RADIATOR IXX ONLY
$
$ PAYLOADS AND SERVICE FACILITY (TABLE 5.0-7)
$
MOD=0
562 7700.0 .830+04 .830+04 .711+04        $SAAX 0115
563 1545.0 .000    .100+04 .100+04        $TDMX 2011
564 2250.0 .353+04 .353+04 .000           $SAAX 4006
565 31100.0 .220+07 .400+06 .430+06       $SERVICE FACILITY
562 4828.0 .261+04 .261+04 .261+04        $P/L SUPT- SAAX 0115
563 1664.0 .898+03 .898+03 .898+03        $P/L SUPT- TDMX 2011
566 1664.0 .898+03 .898+03 .898+03        $P/L SUPT- KEEL P/L'S
567 1734.0 .898+03 .898+03 .898+03        $P/L SUPT- SAAX 0250
564 1664.0 .898+03 .898+03 .898+03        $P/L SUPT- SAAX 4006
$
$
$%%%%%%%%%%%%%%%%%%%%%%%%%%%%%%%%%%%%%%%%%%%%%%%%%%%%%%%%%%%%%%%%%%%%
$
$ Scale the JLOC array for dimensional similarity
$
*XQT AUS
 DEFINE X=JLOC BTAB 2 5
 Y=UNION("SL" X)
 JLOC BTAB 2 5= UNION(Y)
$
*CALL (1 JLOC GEN)
$%%%%%%%%%%%%%%%%%%%%%%%%%%%%%%%%%%%%%%%%%%%%%%%%%%%%%%%%%%%%%%%%%%%%
$ $$$$$$$$$$$$$$$$$$$$$$$$$$$$$$$$$$$$$$$$$$$$$$$$$$$$$$$$$$$$$$
$                  START OF ELEMENT DEFINITIONS
$ $$$$$$$$$$$$$$$$$$$$$$$$$$$$$$$$$$$$$$$$$$$$$$$$$$$$$$$$$$$$$$$
*XQT ELD
$%%%%%%%%%%%%%%%%%%%%%%%%%%%%%%%%%%%%%%%%%%%%%%%%%%%%%%%%%%%%%%%%
$
$             ********** E23 ELEMENTS *********
E23
$
GROUP 1 ' CABLES FROM LSL TO SCALE MODEL STRUCTURE
```

```
 NMAT=5
*CALL (1 ELD CABL)
$%%%%%%%%%%%%%%%%%%%%%%%%%%%%%%%%%%%%%%%%%%%%%%%%%%%%%%%%%%%%%%%%%%%%%%%%%%%%%%%%
$
$              ********** E21 ELEMENTS *********
E21
$
GROUP 1'PORT OUTER TRANSVERSE BOOM
$
NNSW=4: NMAT=1: NSEC=7
!NS=1   :!NB=8 .. :!NB1=4        $--PORT OUTER TRANSVERSE BOOM
*CALL (1 ELD B)
$
GROUP 2' CENTER TRANSVERSE BOOM
$
!NS=37   :!NB=17   :!NB1=9     $ CENTER TRANSVERSE BOOM
*CALL (1 ELD A)
$
GROUP 3' STBD OUTER TRANSVERSE BOOM
$
!NS=109   :!NB=8   :!NB1=4         $---STBD OUTER TRANSVERSE BOOM
*CALL (1 ELD A)
$
GROUP 4' TOP VERTICAL AND HORIZONTAL
$
!NS=145   :!NB=8   :!NB1=4       $-- PORT UPPER KEEL
*CALL (1 ELD B)
!NS=181   :!NB=7   :!NB1=4       $--UPPER BOOM
*CALL (1 ELD A)
!NS=213   :!NB=6   :!NB1=3       $--- STBD UPPER KEEL
*CALL (1 ELD A)
$---------- ADD CONNECTING ELEMENTS HERE ********************
MOD JOINT=0
54 146   :55 147   :58 145   :59 148       $-- PORT VERT TO HORIZ
54 145   :59 147   :58 148   :146 55
86 214   :87 215   :90 213   :91 216      $-- STBD VERT TO HORIZ
90 214   :87 216   :90 216   :214 87
173 181   :176 183   :177 182   :180 184     $--PORT VERT TO TOP
173 182   :180 183   :177 184   :176 181
205 238   :208 239   :209 237   :212 240      $-- STBD VERT TO TOP
238 209   :240 208   :212 237   :205 239
$
GROUP 5' MODULE BOOM
$
!NS=245   :!NB=9   :!NB1=5        $--- MODULE BOOM
*CALL (1 ELD B)
$----------ADD CONNECTING ELEMENTS HERE  *****************
MOD JOINT=0
242 55   :244 60   :242 60   :244 55      $---PORT CROSS TIE
242 59   :241 60   :243 55   :244 56
241 249   :242 250   :243  246   :244 245
242 246   :249 244   :246 244   :249 242
241 242 2 4
91 286   :92 285   :87 287   :88 288        $--- STBD CROSS TIE
87 286   :92 288   :91 285   :287 88
286 282   :285 281   :287 278   :288 277
286 278   :288 281   :285 282   :277 287
285 286 2 4
$
GROUP 6 ' LOWER BOOM AND KEELS
$
!NS=289   :!NB=11   :!NB1=6   $---STBD LOWER KEEL
*CALL (1 ELD B)
!NS=337   :!NB=11   :!NB1=6     $--- PORT LOWER KEEL
*CALL (1 ELD B)
!NS=385   :!NB=5   :!NB1=3      $---- LOWER BOOM
*CALL (1 ELD C)
$---- ADD CONNECTING ELEMENTS HERE *********************
$
MOD JOINT=0
385 341   :340 387   :386 344   :337 388      $--PORT BOOM TO KEEL
386 341   :387 344   :385 337   :388 340
294 406   :295 407   :290 405   :291 408       $-- STBD BOOM TO KEEL
290 406   :295 408   :407 294   :291 405
```

```
335 92  :333 85  :336 89  :88  334          $-- STBD  KEEL TO BOOM
333 89  :334 85  :336 92  :335 88
381 57  :384 60  :382 53  :383 56           $-- PORT KEEL TO BOOM
382 57  :384 56  :381 60  :53 383
$
GROUP 7' ALPHA JOINT ELEMENTS
$
NSEC=1: NNSW=0: NMAT=4: NSEC=8
MOD JOINT=0        $---STBD BOOM, CENTER SIDE
107 410  :106 410  :106 409  :105 409  :105 412  :108 412
108 411  :107 411
MOD JOINT=4          $--- STBD BOOM, BOOM SIDE
107 410  :106 410  :106 409  :105 409  :105 412  :108 412
108 411  :107 411
MOD JOINT=0            $--- PORT BOOM, BOOM SIDE
35 418  :34 418  :34 417  :33 417  :33 420  :36 420
36 419  :35 419
MOD JOINT=4               $--- PORT BOOM, CENTER SIDE
35 418  :34 418  :34 417  :33 417  :33 420  :36 420
36 419  :35 419
$
$              ******** OTHER E21 ELEMENTS *********
MOD GROUP=7
MOD JOINT=0
$
GROUP 1' SOLAR ARRAYS
$
NMAT=2: NSEC=1: NNSW=1: NREF=1
435 436 1 5 4 6
NMAT=3: NSEC=4: NNSW=0: NREF=1
28 435: 435 25: 26 441: 441 27
26 433: 27 433: 28 433: 25 433: 433 441: 433 435
120 447: 447 117: 118 453: 453 119
118 434: 119 434: 120 434: 117 434: 434 453: 434 447
$
GROUP 2' RADIATORS
$
NMAT=2: NSEC=2: NNSW=2: NREF=1
461 462 1 5 4 6
NMAT=3: NSEC=4: NNSW=0: NREF=1
48 461: 461 45: 46 467: 467 47
46 459: 47 459: 48 459: 45 459: 459 467: 459 461
100 473: 473 97: 98 479: 479 99
98 460: 99 460: 100 460: 97 460: 460 479: 460 473
$
GROUP 3' ESS RADIATORS
$
NMAT=2: NSEC=3: NNSW=3: NREF=1
487 488 1 5 2 6
NMAT=3: NSEC=4: NNSW=0: NREF=1
35 493: 493 36: 33 34
34 485: 35 485: 36 485: 33 485: 485 493
111 487: 487 112: 109 110
110 486: 111 486: 112 486: 109 486: 486 487
$
GROUP 4' PSEUDO-RIGID LINKS
$
NMAT=3: NSEC=4: NNSW=0: NREF=1
$ RIGIDIZE THE PLANE OF THE ROTOR IN ROTARY JOINT
409 410 1 3 1: 413 414 1 3 1: 412 409: 416 413
417 418 1 3 1: 421 422 1 3 1: 420 417: 424 421
$
GROUP 5' MODULES, NODES, AND AIRLOCKS
$
NMAT=2: NSEC=5: NNSW=0: NREF=1
MOD JOINT=498
1 2 1 4                  $ ESA LAB MODULE
7 8 1 4                  $ U.S. LAB MODULE
15 16 1 4                $ HSO MODULE
22 23 1 4: 24 27         $ JEM MODULE
20 30                    $ LOGISTICS MODULE
NSEC=6
5 6 1 2: 11 12 1 4: 19 20: 20 22
6 21: 21 20              $ MODULE NODES
```

```
6 28: 20 29              $ AIRLOCKS
MOD JOINT=0
$
GROUP 6' MODULE-TO-TRUSS INTERCONNECTS
$
NMAT=2: NSEC=4: NNSW=0: NREF=1
267 501: 263 501: 266 502: 262 502    $ESA MODULE CONNECTION
263 522: 259 522: 262 521: 258 521    $JEM MODULE CONNECTION
75 506: 75 507: 71 506: 71 507: 74 507: 70 507  $US LAB CONNECT
71 516: 71 515: 67 516: 67 515: 70 515: 66 515  $HSO MODULE CONNECT
$
GROUP 7' MODULAR EQUIPMENT (FROM TABLE 5.0-4)
$
NMAT=3: NSEC=4: NNSW=0: NREF=1
MOD JOINT=0
529 205: 529 206: 529 207: 529 208       $AVIONICS MODULE FOOSO4U09
530 173: 530 176: 530 177: 530 180       $AVIONICS MOD    FOOPO4U09
531 189: 531 190: 531 191: 531 192       $AVIONICS MOD    FOOSOOU09
532 89: 532 90: 532 91: 532 92           $AVIONICS MOD    FOOSO4DOO
533 393: 533 394: 533 395: 533 396       $AVIONICS MOD    FOOSOOD12
534 162: 534 163: 534 166: 534 167       $RCS MODULE FOOSO4U06
537 229: 537 232: 537 233: 537 236       $RCS MODULE FOOPO4U06
538 49: 538 50: 538 54: 538 53           $GN&C/DMS MOD FOOPO5DOO
539 53: 539 54: 539 55: 539 56           $HR&T MOD FOOPO4DOO
540 69: 540 70: 540 71: 540 72           $FMAD MOD FOOPO1DOO
541 253: 541 254: 541 255: 541 256       $AVIONICS MOD AO3PO2DOO
543 313: 543 316: 543 317: 543 320       $RCS MODULE FOOSO4DO6
544 362: 544 363: 544 366: 544 367       $RCS MODULE FOOSO4DO6, PO4DO6
545 297: 545 298: 545 299: 545 300       $C&T MODULE FOOSO4D11
546 345: 546 346: 546 347: 546 348       $C&T MODULE FOOPO4D11
549 105: 549 106: 549 107: 549 108       $ALPHA ROTARY + STRUCTURE (1/2)
550 37: 550 38: 550 39: 550 40           $ALPHA ROTARY + STRUCTURE (1/2)
553 69: 553 70: 553 71: 553 72           $FMAD MODULE FOOSOODOO
554 45: 554 46: 554 49: 554 50           $NAV BASE FOOPO6DOO
555 209: 555 212: 555 237: 555 240       $TDRSS ANTENNA + SUPT
$
GROUP 8' PORT AND STBD ALPHA GIMBAL ITEMS
$
NMAT=3: NSEC=4: NNSW=0: NREF=1
MOD JOINT=0
556 1: 556 2: 556 3: 556 4               $BETA GIMBAL FOOP17DOO
557 1: 557 2: 557 3: 557 4               $SOLAR DYNAMIC MODULE
558 35: 558 36: 558 31: 558 32           $ESS MODULE FOOP10DOO
559 141: 559 142: 559 143: 559 144       $BETA GIMBAL FOOS17DOO
560 141: 560 142: 560 143: 560 144       $SOLAR DYNAMIC MODULE
561 111: 561 112: 561 115: 561 116       $ESS MODULE FOOS10DOO
$
GROUP 9' PAYLOADS AND SERVICE FACILITY (TABLE 5.0-7)
$
NMAT=3: NSEC=4: NNSW=0: NREF=1
MOD JOINT=0
562 190: 562 191: 562 194: 562 195       $SAAX 0115
563 185: 563 186: 563 187: 563 188       $TDMX 2011
564 393: 564 396: 564 397: 564 400       $SAAX 4006
565 234: 565 205: 565 197: 565 185: 565 173: 565 165 $SERVICE FACILITY
565 235: 565 208: 565 200: 565 188: 565 176: 565 168 $SERVICE FACILITY
566 145: 566 148: 566 149: 566 152       $P/L SUPT- KEEL P/L'S
567 401: 567 402: 567 403: 567 404       $P/L SUPT- SAAX 0250
$
$               E25 ELEMENTS
$
E25
MOD GROUP=0
GROUP 1' ROTARY ALPHA JOINT ROTOR CONNECTON
NSEC=1
409 413: 410 414: 411 415: 412 416
417 421: 418 422: 419 423: 420 424
$$$$$$$$$$$$$$$$$$$$$$$$$$$$$$$$$$$$$$$$$$$$$$$$$$$$$$$$$$$$$$$$$$$$$$$
*XQT E
 RESET G=386.4
*XQT EKS
*XQT SEQ
*XQT TAN
*XQT K
```

```
*XQT RSI
 RESET CON=2
$%%%%%%%%%%%%%%%%%%%%%%%%%%%%%%%%%%%%%%%%%%%%%%%%%%%%%%%%%%%%%%%%%%%%%%%%%%%%%%%%%%%%%%%%%%%%%%%%%%%%%%%%%
$                    AUTOMATIC BC INPUT
$%%%%%%%%%%%%%%%%%%%%%%%%%%%%%%%%%%%%%%%%%%%%%%%%%%%%%%%%%%%%%%%%%%%%%%%%%%%%%%%%%%%%%%%%%%%%%%%%%%%%%%%%%%
$
*XQT AUS
 MT=SUM(DEM,RMAS)
 R=RIGID(12.679,-583.231,0.0)
!NAVA=ABS(NVA)
 DEFINE R3=R AUS 1 1 "NAVA","NAVA"  $APPLIED FORCE IS WEIGHT ALONG VERT AXIS
!NVA: !NAVA
!G=-386.0*NVA/NAVA
 APPL FORC 1 2=PROD("G" MT, R3)     $GRAVITY FORCE ALONG PROPER AXIS
*XQT SSOL
 RESET CON=2                         $BOTH ENDS OF CABLES CONSTRANED
!AI1=DS 1 1 1 (1 BC BTAB 2 11)
*XQT AUS
 DEFINE RES= STAT REAC 1 2
TABLE(NI=1, NJ="NNT"): RE AUS 1 1
 TRANSFER(SOURCE=RES, ILIM=1, JLIM="NNT", SBASE="NVAM", SSKIP=5)
DE1
 SOURCE=RE AUS 1 1: DEST=REAC AUS 1 1
 IS=SERIAL: ID=SERIAL: JS=SUSP NODS 1 1: JD=SNOD SEQ 1 1: EX1
 DEFINE LENG=1 CABL LENG 1 1        $LENGTH OF CABLES
$
$ PERFORM SIMPLE OPERATIONS ON AREA VECTOR TO GET PROPER AREA RATIO VECTOR
$ WHICH DEPENDS ON THE LOAD AND THE CABLE LENGTH.
$
!PI1=DS 1 1 1 (1 REAC AUS 1 1)
!LI1=DS 1 1 1 (1 CABL LENG 1 1)
!AFAC=AI1/PI1/LI1          $A/PL
 PIAI=PROD(REAC,LENG)      $ P*L
 AIC=ABS("AFAC" PIAI)      $ FIRST CUT AT AREAS
$ *********************** NOW FIND STRESSES TO SEE IF CABLES MEET SAFETY FACTOR
 AINV=POWER(1.0 AIC, -1.0)
 SIGC=PROD(REAC,AINV)
 SIGC=ABS(SIGC)
 MXMN SIGC 1 1=MM1(SIGC)
!SIGM=DS 1 1 1 (1 MXMN SIGC 1 1)   $MAXIMUM STRESS
$***************
!AFAC=SIGM/SIGW    $CALCULATE MULTIPLIER TO BE BELOW WORKING STRESS
 CABL AREA 1 1=ABS("AFAC" AIC)     $ THESE AREAS ARE THE CABLE AREAS
$                                    REQUIRED FOR A UNIFORM SAG AT ALL CABLE
$                                    ATTACH POINTS WHILE AT THE SAME TIME
$                                    NOT EXCEEDING THE CABLE WORKING STRESS
$
$ NOW CREATE BC BTAB 2 11
$
 DEFINE PA1=CABL AREA 1 1
TABLE(NI=6, NJ="NHN"): BC BTAB 2 11
 TRANSFER(SOURCE=PA1, ILIM=1, JLIM="NHN" DSKIP=5)
 TRANSFER(SOURCE=PA1, ILIM=1, JLIM="NHN" DBASE=1 DSKIP=5)
$****************   BC BTAB 2 11 COMPLETED
$
$     CALCULATE CABLE SWAY (VIOLIN) MODES
$          F= 1/(2L)*(T/M)**0.5 , M=RHO*A , T/M= SIGMA/RHO
$
!RHOI=1./RHOC
!DUMR=RHOI/AFAC
 ROOT=SQRT("DUMR",SIGC)
 LINV=POWER(1. LENG, -1.0)
 SWAY=PROD(0.5 LINV, ROOT)
 MXMN SWAY 1 1=MM1(SWAY)
*XQT DCU
 PRINT 1 MXMN SWAY 1 1 1,3
$%%%%%%%%%%%%%%%%%%%%%%%%%%%%%%%%%%%%%%%%%%%%%%%%%%%%%%%%%%%%%%%%%%%%%%%%%%%%%%%%%%%%%%%%%%%%%%%%%%%%%%%%%%%%%%%%%%%%%%
$   NOW RUN CASE WITH PROPER CABLE AREAS
$%%%%%%%%%%%%%%%%%%%%%%%%%%%%%%%%%%%%%%%%%%%%%%%%%%%%%%%%%%%%%%%%%%%%%%%%%%%%%%%%%%%%%%%%%%%%%%%%%%%%%%%%%%%%%%%%%%%%%%
*XQT E
 RESET G=386.4
*XQT EKS
*XQT SEQ
*XQT TAN
```

```
*XQT K
*XQT RSI
 RESET CON=1
*XQT AUS
 MT=SUM(DEM,RMAS)
 !XCGL=-16.99*SL
 !YCGL=-8.15*SL
 !ZCGL=-19.13*SL
 R=RIGID("XCGL","YCGL","ZCGL")
 MR=PROD(MT,R)
 RTMR=XTY(R,MR)
!NAVA=ABS(NVA)
 DEFINE R3=R AUS 1 1 "NAVA","NAVA"
!G=-386.0*NVA/NAVA
 APPL FORC 1 1=PROD("G" MT, R3)      $GRAVITY FORCE ALONG PROPER AXIS
*XQT SSOL
 RESET CON=1
*XQT DCU
 PRINT 1 RTMR AUS
*XQT GSF
 RESET EMBED=1
 RESET CON=1
*XQT KG
 RESET IKG2=1
*XQT AUS
 K+KG=SUM(K,KG)
*XQT E4
 RESET M=MT, K=K+KG, NMODES=75, SHIFT=0.0
*XQT AUS                          $COMPUTE MODAL STRAIN ENERGY
DEFINE PHI=VIBR MODE 1 1
DEFINE K=K SPAR
KPHI=PROD(K,PHI)
PKPT=XTYDIAG(PHI,KPHI)
PKP=RTRAN(PKPT)
PKP=ABS(PKP)
*XQT U1
$-------------------------------------
$  This run computes PTMP for selected portion of model
$  User only need to enter interger vector specified the node
$  numbers and name for that portion of the model.
$-------------------------------------
$
$-------LOOP FOR COMPUTING PTMP
*(1 PTMP LOOP)  EPL
*XQT AUS
DE1
SOURCE=1 MT AUS 1 1
NI=6   :NJ="NJ"
DEST=1 "NAME"
IS=1 2 3 4 5 6
ID=1 2 3 4 5 6
JS=1 "NAME" NODE 1 1
JD=1 "NAME" NODE 1 1
EX1
DEFINE P=1 VIBR MODE 1 1
DEFINE M=1 "NAME" AUS 1 1
MP=PROD(M P)
"NAME" PTM=XTYD(P MP)
DEFINE PT="NAME" PTM 1 1
"NAME" PTMP=RTRAN(PT)
*EPL
$-----------------------------------------
$    ENTER NODE NO. FOR CHOPPING IN THIS AREA
$-----------------------------------------
!NJ=TOC,NJ(1 MT AUS 1 1)
!NAME=TBOM
*LLI(1 "NAME" NODE 1 1)
1,144,1
*CALL(1 PTMP LOOP)
!NAME=UPBK
*XQT U1
*LLI(1 "NAME" NODE 1 1)
145,240,1
*CALL(1 PTMP LOOP)
```

```
!NAME=LPBK
*XQT U1
*LLI(1 "NAME" NODE 1 1)
290,425,1
*CALL(1 PTMP LOOP)
!NAME=MODS
*XQT U1
*LLI( 1 "NAME" NODE 1 1)
499,528,1
241,289,1
*CALL(1 PTMP LOOP)
!NAME=RMAS
*XQT U1
*LLI(1 "NAME" NODE 1 1)
529,558,1: 559,561,1: 562,567,1
*CALL(1 PTMP LOOP)
!NAME=SOLA
*XQT U1
*LLI(1 "NAME" NODE 1 1)
433,458,1
*CALL(1 PTMP LOOP)
!NAME=RAD
*XQT U1
*LLI(1 "NAME" NODE 1 1)
459,498,1
*CALL(1 PTMP LOOP)
!NAME=SUSP
*XQT U1
*LLI(1 "NAME" NODE 1 1)
425,432,1: 535,536: 542: 547: 548: 551: 552
*CALL(1 PTMP LOOP)
$----COMPUTE MODAL MASS FOR COMPLETE MODEL
*XQT AUS
DEFINE P=1 VIBR MODE 1 1
PN=NORM(P)
DEFINE M=1 MT AUS 1 1
MP=PROD(M PN)
NORM PTM=XTYD(PN MP)
DEFINE N=NORM PTM 1 1
NORM PTMP=RTRAN(N)
$--------------------------------
$       Print out of report
*XQT AUS
DEFINE EV=1 VIBR EVAL 1 1
FREQ T=SQRT(.02533 EV)
DEFINE F=FREQ T
FREQ=RTRAN(F)
$     START REPORT FORMATTING
*XQT U3
RP2
FORMAT 1'(1H1/50X,5HDATE ,I6//
'1X,43HMODAL KINETIC ENERGY FOR ISSO SPACE STATION//)
FORMAT 2'(1X,17HMode  Freq  Modal,15X,21HPercent Modal Kinetic,
'1X,6HEnergy/1X,18HNo.    (HZ)   K.E.,6X,4HTBOM ,3X,4HUPBK,
'3X,4HLPBK, 3X,4HMODS,  3X,4HRMAS  3X,4HSOLA 3X,4HRADI, 3X,4HPKPE //)
FORMAT 3'(I3,2X,F5.3,2X,E10.4,7F7.1,F9.0)
DEFINE TBOM=100. 1 TBOM PTMP 1 1
DEFINE UPBK=100. 1 UPBK PTMP 1 1
DEFINE LPBK=100. 1 LPBK PTMP 1 1
DEFINE MODS=100. 1 MODS PTMP 1 1
DEFINE RMAS=100. 1 RMAS PTMP 1 1
DEFINE SOLA=100. 1 SOLA PTMP 1 1
DEFINE RAD=100. 1 RAD PTMP 1 1
DEFINE PKPE=100. 1 PKP AUS 1 1
DEFINE M=1 NORM PTMP
DEFINE F=1 FREQ AUS
LAYOUT
WRITE(ALL,1)DATE
WRITE(ALL,2)
WRITE(MAIN,3)J,F,M,TBOM,UPBK,LPBK,MODS,RMAS,SOLA,RAD,PKPE
PRODUCE REPORT
*XQT DCU
COPY 1 2 PKP AUS
$$$$$$$$$$$$$$$$$$$$$$$$$$$$$$$$$$$$$$$$$$$$$$$$$$$$$$$$$$$$$$$$$$$$$$$$$$$$
```


C-3

```
$         NOW PRINT OUT CABLE RESULTS
$      START CABLE SUMMARY TABLE FORMATTING
$$$$$$$$$$$$$$$$$$$$$$$$$$$$$$$$$$$$$$$$$$$$$$$$$$$$$$$$$$$$$$$$$$$$$$$$$$$$
*XQT AUS
TABLE(NI=1,NJ="NHN",TYPE=O): LSLN
DDATA=1: RJ=1,"NHN": 568
DE1
 SOURCE=STAT DISP 1 1: DEST=VERT DISP 1 1
 IS="NAVA": ID=1: JS=SERIAL: JD=SERIAL: EX1
DE1
 SOURCE=VERT DISP 1 1: DEST=DISP AUS 1 1
 IS=1: ID=1: JS=SUSP NODS 1 1: JD=SNOD SEQ 1 1: EX1
DISP AUS 1 1=ABS(DISP)
*XQT U3
RP2
FORMAT 1'(1H1/50X,5HDATE ,I6//
'1X,21HSUMMARY OF CABLE DATA//)
FORMAT 2'(3X,12HNode Numbers,23X,5HCable,
'20X,5HVert./1X,15HOn Mod.  On LSL,6X,6HLength,4X,4HArea,
'7X,5HForce, 7X,5HFreq.,  3X,5HDisp./23X,4H[in],4X,6H[in12]
'6X,4H[lb],8X,4H[Hz],4X,4H[in]//)
FORMAT 3'(3X,I3,6X,I3,F14.3,F8.4,3X,E11.4,2F8.2)
DEFINE MODN=SUSP NODS 1 1
DEFINE LSLN=LSLN AUS 1 1
DEFINE LENG=CABL LENG 1 1
DEFINE AREA=CABL AREA 1 1
DEFINE REAC=REAC AUS 1 1
DEFINE SWAY=SWAY AUS 1 1
DEFINE DISP=DISP AUS 1 1
LAYOUT
WRITE(ALL,1)DATE
WRITE(ALL,2)
WRITE(MAIN,3)MODN,LSLN,LENG,AREA,REAC,SWAY,DISP
PRODUCE REPORT
$ LIST ALL STRUCTURAL DISPLACMENTS GREATER THAN FAC*CABLE DISP.
*XQT DCU
!FAC=2.
!CDIS=DS 1 1 1 (1 DISP AUS 1 1)
!FILT=FAC*CDIS
FILTER="FILT"
PRINT 1 VERT DISP
PRINT 1 VERT DISP
*XQT ES
!FILTL=0.5*2159.0   $CRITICAL BUCKLING STRESS SCALES AS 1.0
 U=STAT DISP 1 1    $PRINT ALL STRESSES GREATER THAN CRITICAL/2.
 FILTER="FILTL"
 SE21=SZ
 E21
*XQT DCU
COPY 1 2 VIBR MODE
COPY 1 2 VIBR EVAL
COPY 1 2 MT   AUS
COPY 1 2 STAT DISP 1 1
COPY 1 2 DEF E21
COPY 1 2 DEF E23
COPY 1 2 DEF E25
COPY 1 2 JLOC BTAB
COPY 1 2 SUSP NODS
COPY 1 2 CABL AREA
COPY 1 2 REAC AUS
COPY 1 2 SWAY AUS
COPY 1 2 CABL LENG
COPY 1 2 RTMR AUS
*XQT EXIT
/EOF
```

APPENDIX C

MODE SHAPES OF FIRST 5 SYSTEM MODES
STEP-2 AND ISS CONFIGURATIONS

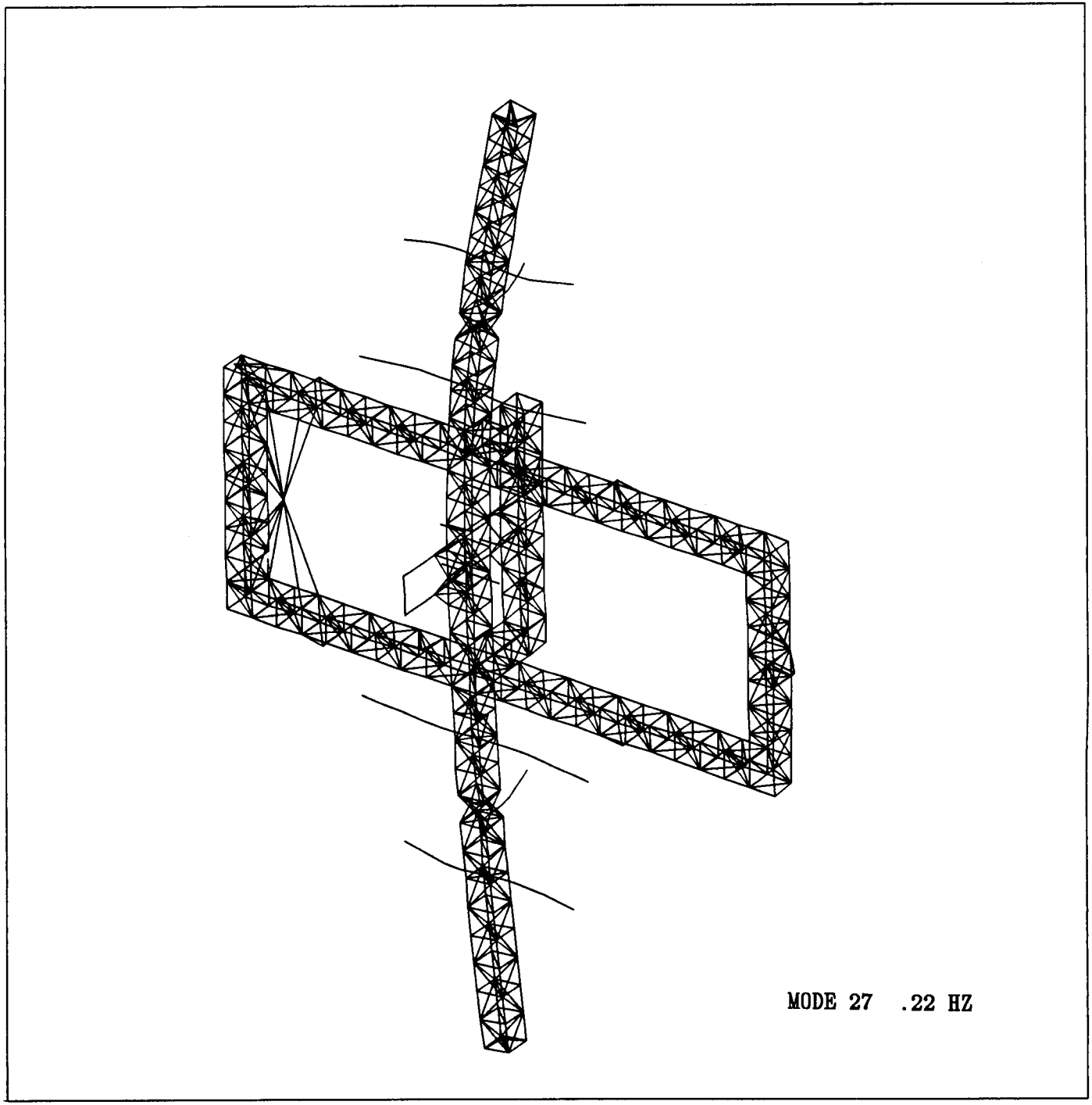
MODE 27 .22 HZ

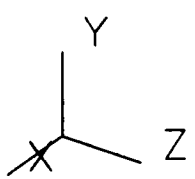
Y
Z

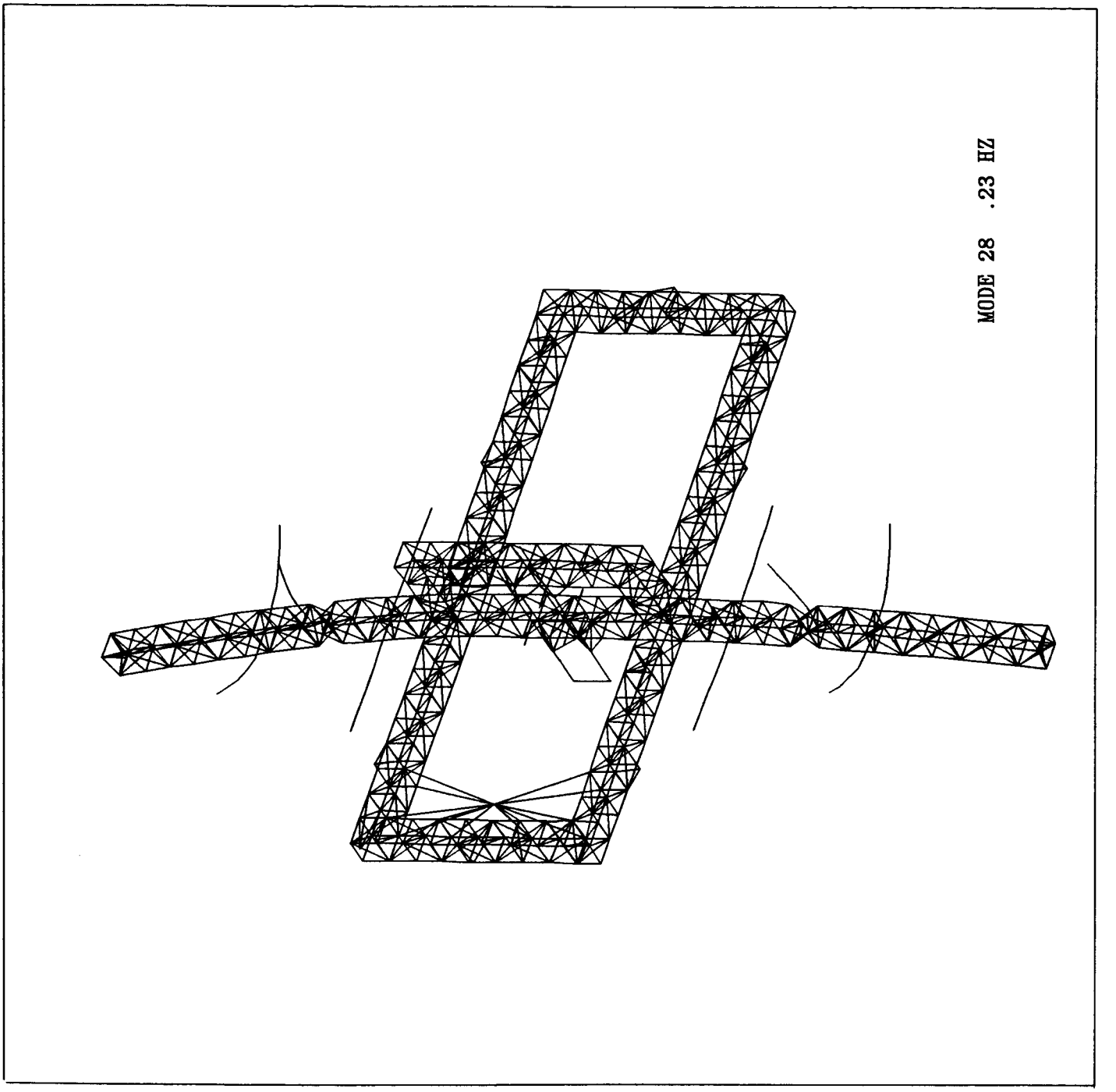
MODE 28 .23 HZ
Z
Y

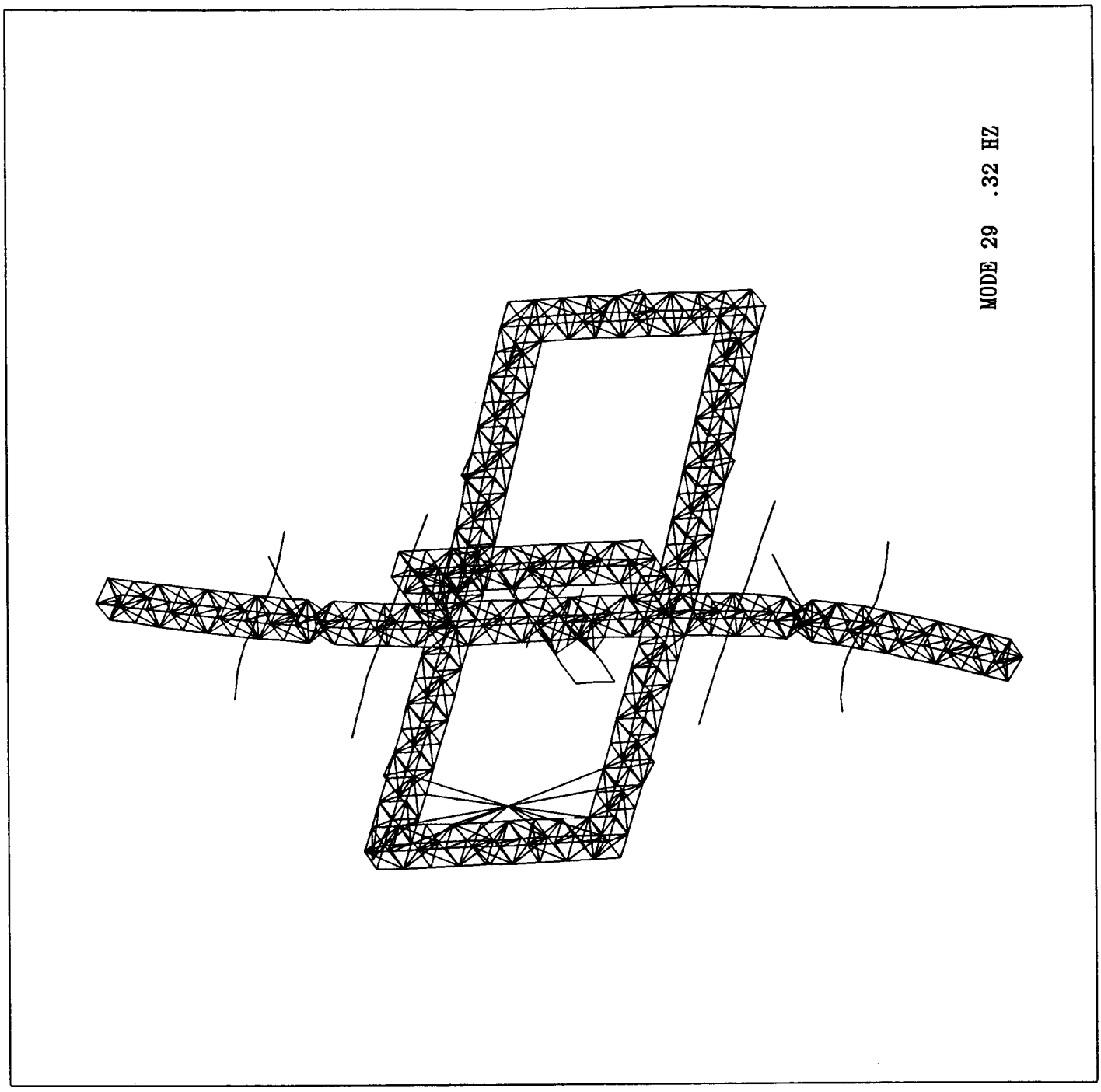
MODE 29 .32 HZ

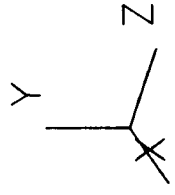
Z
Y
X

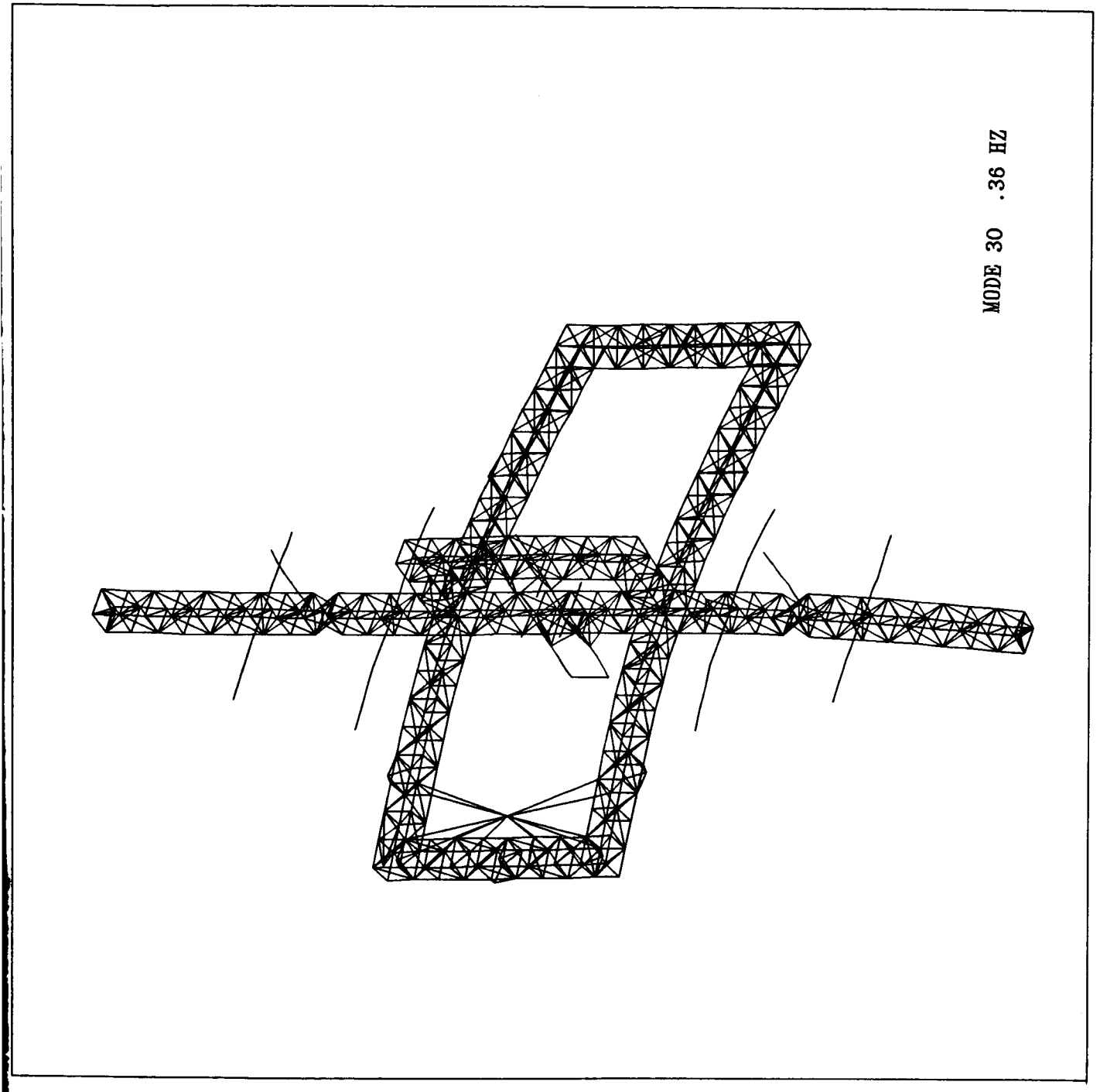
MODE 30 .36 HZ
Z
Y

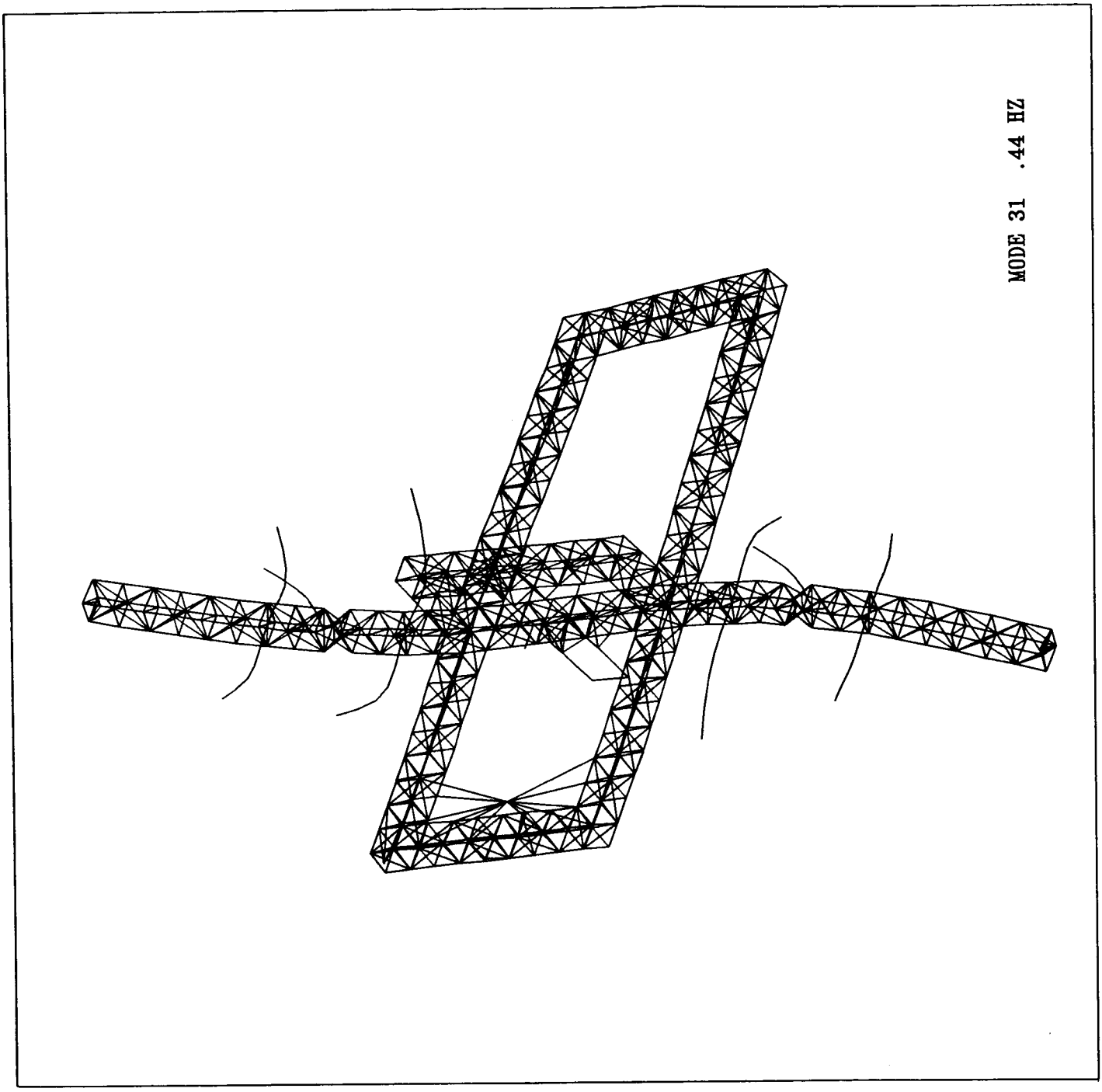
MODE 31 .44 HZ
Z
Y

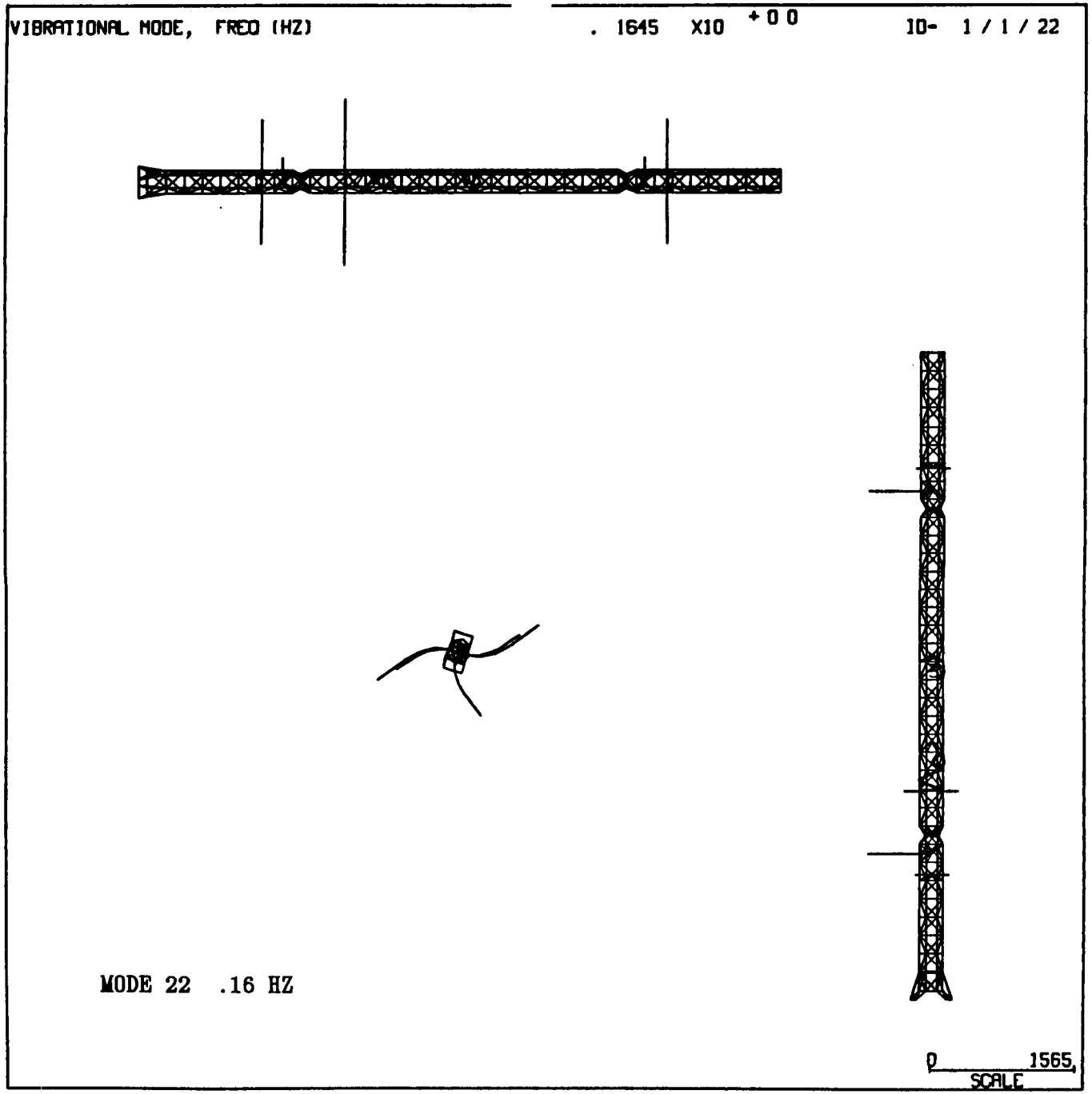
VIBRATIONAL MODE, FREQ (HZ)
. 1645 X10 +00
ID- 1 / 1 / 22
MODE 22 .16 HZ
0
1565.
SCALE

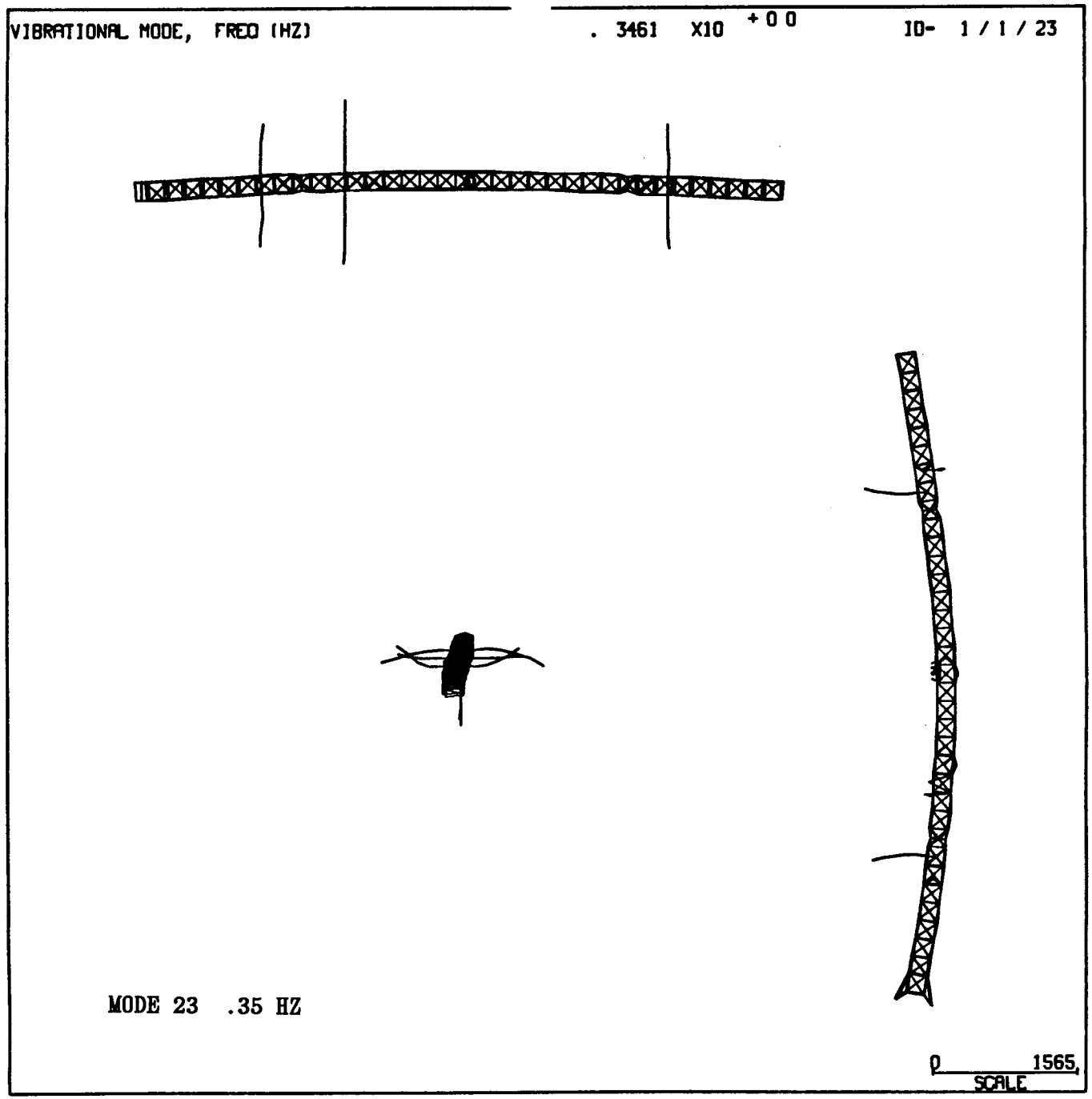
VIBRATIONAL MODE, FREQ (HZ)
. 3461 X10 +00
ID- 1 / 1 / 23
MODE 23 .35 HZ
0 1565,
SCALE

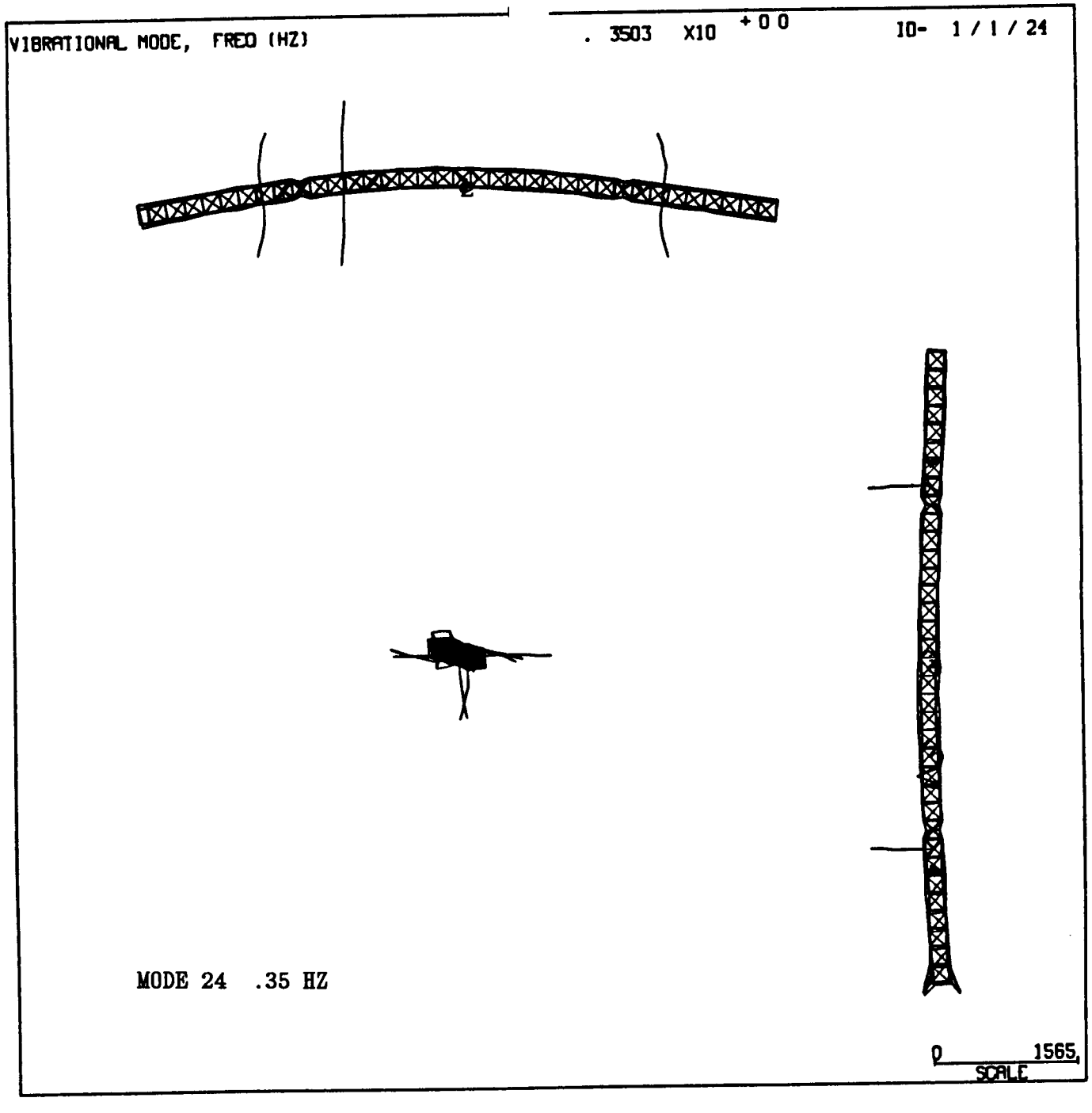
VIBRATIONAL MODE, FREQ (HZ)
. 3503 X10 +00
10- 1/1/24
MODE 24 .35 HZ
0
1565.
SCALE

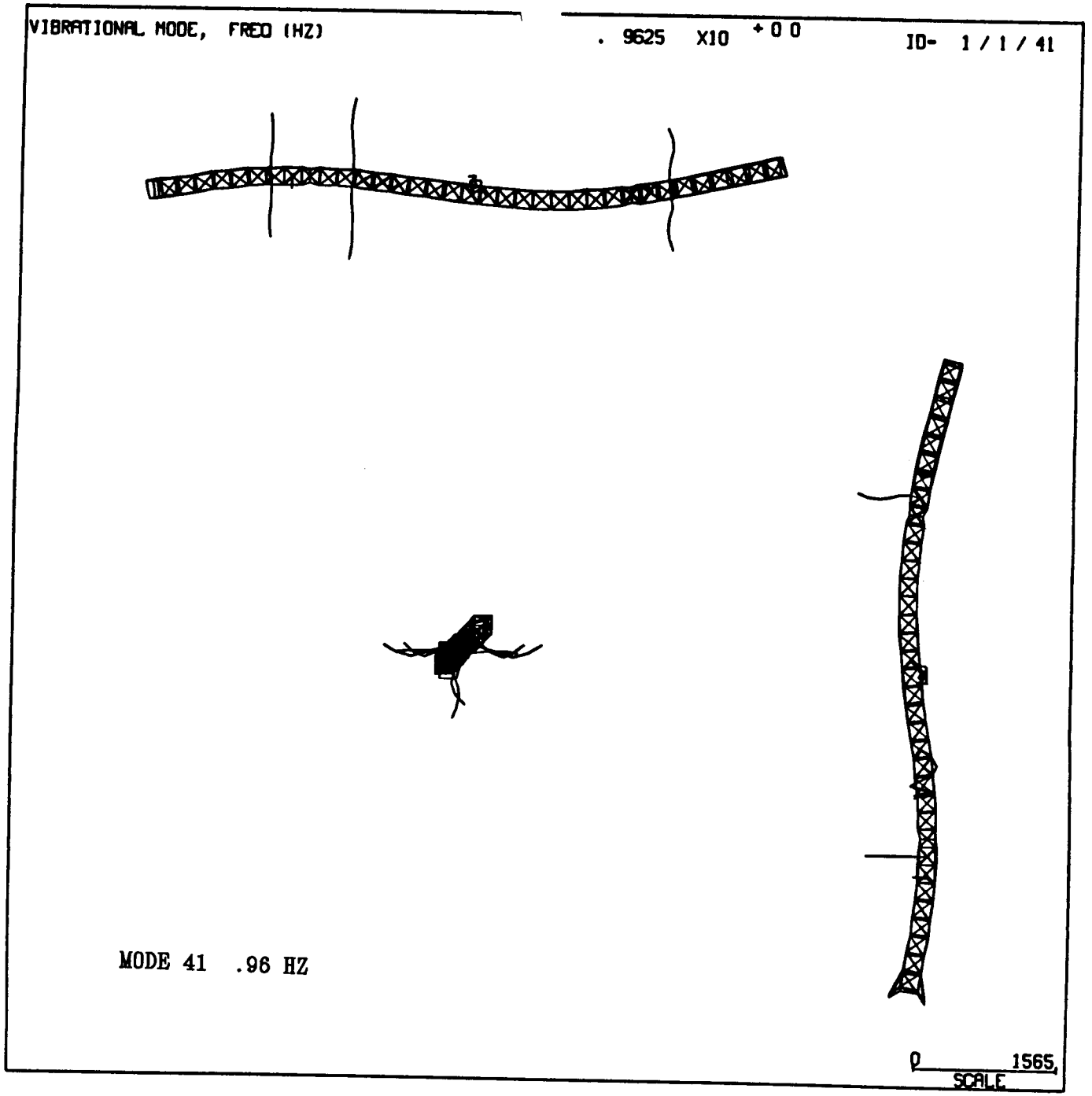
VIBRATIONAL MODE, FREQ (HZ)
. 9625 X10 + 0 0
ID- 1 / 1 / 41
MODE 41 .96 HZ
0
1565.
SCALE

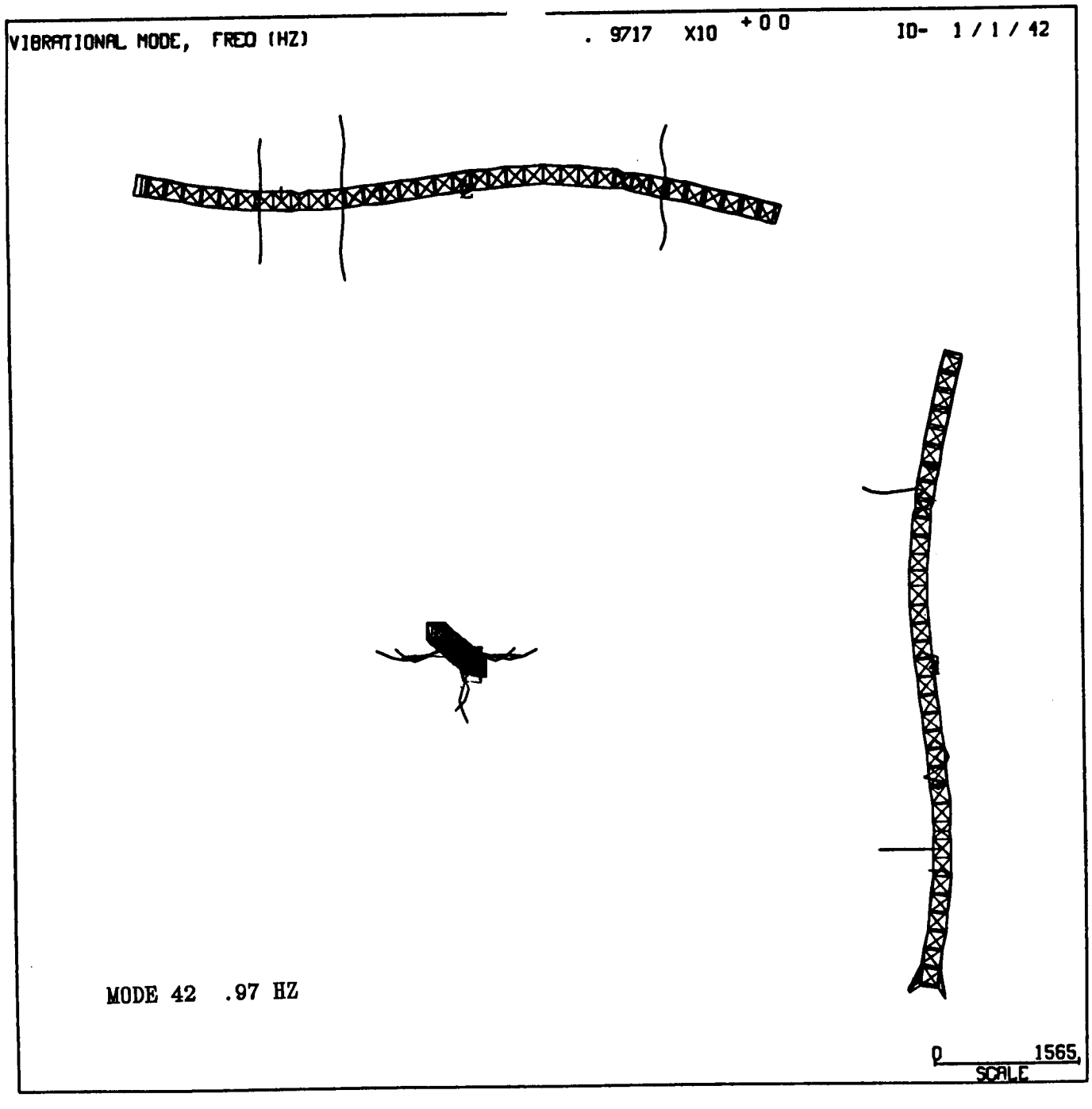
VIBRATIONAL MODE, FREQ (HZ)
. 9717 X10 +00
ID- 1/1/42
MODE 42 .97 HZ
0
1565.
SCALE

1. Report No.	2. Government Accession No.	3. Recipient's Catalog No.
NASA CR-4068		

4. Title and Subtitle	5. Report Date
Preliminary Design, Analysis, and Costing of a Dynamic Scale Model of the NASA Space Station	July 1987
	6. Performing Organization Code

7. Author(s)	8. Performing Organization Report No.
M. J. Gronet, E. D. Pinson, H. L. Voqui, E. F. Crawley, and M. R. Everman	LMSC F177633

9. Performing Organization Name and Address	10. Work Unit No.
Lockheed Missiles & Space Company, Inc. 1111 Lockheed Way Sunnyvale, California 94086	546-01-31-01
	11. Contract or Grant No. NAS1-18229

12. Sponsoring Agency Name and Address	13. Type of Report and Period Covered
National Aeronautics and Space Administration Washington, D.C. 20546	Contractor Report
	14. Sponsoring Agency Code

15. Supplementary Notes: LaRC Technical Monitors: P. McGowan, R. Letchworth. Final Report, Task 3.
M.J. Gronet, E.D. Pinson, and H.L. Voqui: Lockheed Missiles & Space Co., Inc. Sunnyvale, CA
E.F. Crawley: Massachusetts Institute of Technology, Cambridge, MA.
M.R. Everman: AEC-ABLE Engineering Co., Inc. Goleta, CA.

16. Abstract

The difficulty of testing the next generation of large flexible space structures on the ground places an emphasis on other means for validating predicted on-orbit dynamic behavior. Scale model technology represents one way of verifying analytical predictions with ground test data. This study investigates the preliminary design, scaling, and cost trades for a Space Station dynamic scale model. The scaling of nonlinear joint behavior is studied from theoretical and practical points of view. Suspension system interaction trades are conducted for the ISS Dual Keel Configuration and Build-up Stages suspended in the proposed NASA/LaRC Large Spacecraft Laboratory.

Key issues addressed are scaling laws, replication vs. simulation of components, manufacturing, suspension interactions, joint behavior, damping, articulation capability, and cost. These issues are the subject of parametric trades versus the model scale factor. The results of these detailed analyses are used to recommend scale factors for four different scale model options, each with varying degrees of replication. Potential problems in constructing and testing the scale model are identified, and recommendations for further study are outlined.

17. Key Words (Suggested by Author(s))	18. Distribution Statement
Scaling, Scale Models, Space Station Dynamic Testing, Suspension, Simulation, Replication, Joints	Unclassified - Unlimited Subject Category 39

19. Security Classif. (of this report)	20. Security Classif. (of this page)	21. No. of Pages	22. Price*
Unclassified	Unclassified	212	A10

*For sale by the National Technical Information Service, Springfield, Virginia 22161

NASA-Langley, 1987